

***u<sup>b</sup>***

# **Swab spray mass spectrometry: An electrospray-based ambient ionization technique for the analysis of surfaces**

Inauguraldissertation  
der Philosophisch-naturwissenschaftlichen Fakultät  
der Universität Bern

vorgelegt von

**Thomas Michael Muggli**

Leiter der Arbeit:

Prof. Dr. Stefan Schürch

Departement für Chemie, Biochemie und Pharmazie

Universität Bern



***u<sup>b</sup>***

# **Swab spray mass spectrometry: An electrospray-based ambient ionization technique for the analysis of surfaces**

Inauguraldissertation  
der Philosophisch-naturwissenschaftlichen Fakultät  
der Universität Bern

vorgelegt von

**Thomas Michael Muggli**

Leiter der Arbeit:

Prof. Dr. Stefan Schürch

Departement für Chemie, Biochemie und Pharmazie

Universität Bern

Von der Philosophisch-naturwissenschaftlichen Fakultät angenommen.

Bern, 28.11.2024

Der Dekan

Prof. Dr. Jean-Louis Reymond



This work is licensed under Creative Commons Attribution-NonCommercial-NoDerivatives 4.0 International <https://creativecommons.org/licenses/by-nc-nd/4.0>  
Numerous figures presented in the introduction are subject to copyright protection.

WISSEN  
SCHAFFT  
WERT.





Life can only be understood backwards; but it must be lived forwards.

*Søren Kierkegaard*



# Acknowledgments

First and foremost, I want to express my deepest gratitude to Professor Stefan Schürch for granting me the opportunity to pursue my PhD thesis within his research group. My fascination with mass spectrometry was sparked during my master's thesis, where I worked on the optimizing of a LC-MS method for gangliosides. The chance to delve deeper into my passion for electrospray-based mass spectrometry, within the research field of ambient ionization, was invaluable. Equally, I am thankful for the personal growth I experienced throughout my journey. Professor Stefan Schürch's idea to undertake a project involving ambient ionization technology was fascinating. Moreover, the possibility to work independently coupled with his generous supervision and guidance gave me an educational time that I will keep in my good memories.

A debt of gratitude is owed to Professor Gérard Hopfgartner for graciously agreeing to serve as co-referee and to review my thesis. Furthermore, I would like to thank Professor Robert Häner for serving as session chair.

Especially, I would like to extend my thanks to Claudia Bühr for her substantial and supreme technical support in the laboratory. My heartfelt appreciation goes out to all the group members including Andrea Bill, Till Vollmer, Lara Maeder, and Pia Bruni for the good company and enriching social activities during my thesis.

Furthermore, I would like to express my sincere appreciation for the essential contributions of the in-house machine shop. Their efforts were pivotal to the realization of this project. Additionally, I am profoundly grateful to Jürg Cabalzar for his expert assistance when working with instruments and software from SCIEX.

I must also extend my profound thanks to my mother for her generous support during my thesis. The accomplishment would not have been achieved without the uncompromising and continuous support of all mentioned people.



# Abstract

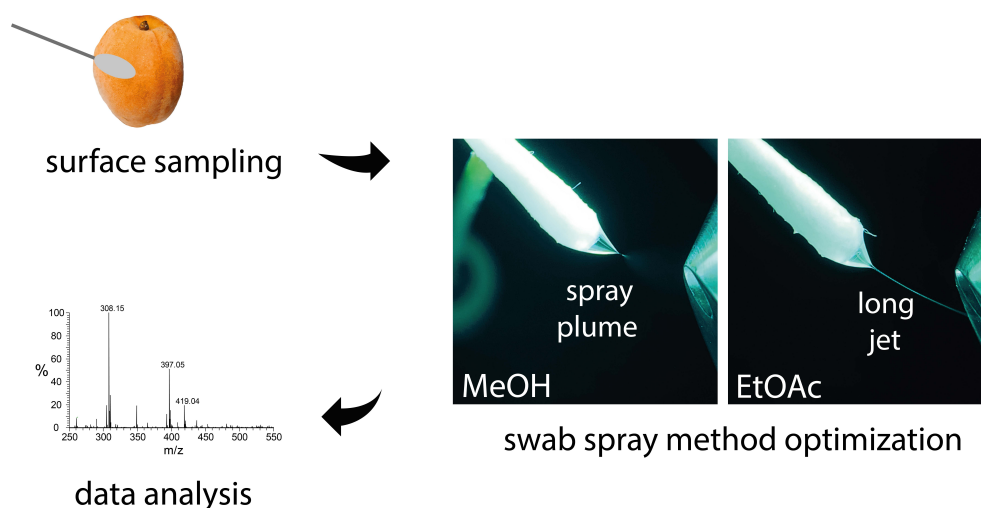
In 2004, the first ambient ionization technique, termed desorption electrospray ionization (DESI), was presented. It was the beginning of an evolution that yielded numerous ionization techniques, which allow minimization of sample preparation, permit ionization at ambient conditions, and moreover, offer the opportunity for in-situ analysis. Direct Analysis in Real Time (DART), the first plasma-based ambient ionization technique, was introduced in 2005. Ionization of a broad range of analytes was achieved using a plasma produced through corona discharge. Electrospray continued to demonstrate its versatility for ambient ionization techniques with the introduction of probe electrospray in 2007 and paper spray in 2010.

In 2015, swab spray was reported as a novel electrospray-based ambient ionization technique that merges sample collection and direct ion generation by application of solvent and high voltage directly to the swab head. Its potential has been reported in several forensic and medicinal applications, including the analysis of drugs and explosives, demonstrating that swab spray can deliver fast and reliable results while minimizing sample preparation. The use of swabs as electrospray emitters demonstrated new capabilities along with new challenges. On the one hand, swab materials must be carefully evaluated to minimize background ions and on the other hand, reproducible electrospray generation on swab tips requires diligent optimization of ion source parameters and electrospray solvent.

In the first part of this thesis, a custom-made swab spray ion source was constructed and different swab materials were extensively investigated for their suitability to act as an electrospray emitter. Copan 160C swabs with a rayon head and aluminum applicator were found to be an optimal choice. They provide low background noise, high electrospray stability, and high tolerance for organic solvents. Moreover, swab spray ion source parameters, including the distance to the counter electrode, applied electric potential, solvent capillary position, and flow rate were evaluated. The influence of electrospray solvent properties, including surface tension, viscosity, and relative permittivity was investigated using photographic observation and signal yield, in order to predict solvent behavior in swab spray. It was observed that only spray solvents with a relative permittivity higher than 25 allow the generation of a short jet. The generation of a short jet is mandatory for the formation of a spray plume

where the ionization takes place. Spray solvents with a lower relative permittivity exhibit a long jet, which is detrimental to ion formation. The influence of solvent relative permittivity in swab spray was demonstrated for the first time and results compared to paper spray and capillary-based electrospray ionization. In addition, different pulsation modes, such as the spindle mode and the dripping mode, the later occurring in spray solvents with a relative permittivity lower than 4, were examined. In the second part of the thesis, the swab spray setup was applied to rapid pesticide analysis on the surface of fruit. Pesticides were identified by their mass, isotopic pattern, and product ion spectra obtained by CAD experiments. Semi-quantitative analysis of the fungicide boscalid allowed to determine surface concentrations on a bell pepper surface. The occurrence of sodium adducts was linked to electrospray solvent composition and chemical structure of the analyte. The presence of ethyl acetate in the spray solvent was found to facilitate the formation of proton adducts. Further applications involved the analysis of skin for organic compound residues, identification of white powder, differentiation of ball point ink, and analysis of mycotoxins.

The versatility of swab spray mass spectrometry makes it invaluable for applications requiring rapid analysis of organic compounds sampled from diverse surfaces, as it allows for easy sampling and requires no sample preparation. The analysis time can be significantly reduced compared to conventional laboratory-based methods, and furthermore, it enables in-situ mass spectrometry.



Graphical Abstract

# Table of content

1	Introduction.....	1
1.1	Mass Spectrometry .....	1
1.2	Overview of Ambient Ionization Methods.....	13
1.3	The Benefits of Ambient Ionization Techniques .....	17
1.4	Pesticides.....	19
1.5	Ambient Ionization Techniques for the Analysis of Pesticides in Food Products .....	25
1.6	Swab Spray Mass Spectrometry .....	33
2	Results and Discussion .....	43
2.1	Swab Spray Ion Source Construction .....	43
2.2	Initiation of Swab Electrospray .....	46
2.3	Counter Electrode Set-up .....	49
2.4	Swab Positioning .....	50
2.5	Evaluation of Swab Material.....	52
2.6	Analyte Extraction.....	62
2.7	Solvent Effects in Swab Spray.....	66
2.8	Article: “Influence of Solvent Relative Permittivity in Swab Spray Mass Spectrometry” .....	75
2.9	Pesticide Analysis .....	93
2.10	Pesticide Analysis on Food Products.....	103
2.11	Effect of the Spray Solvent on Adduct Formation.....	107
2.12	Article: “Analysis of Pesticide Residues on Fruit Using Swab Spray Ionization Mass Spectrometry” .....	113
2.13	Comparison between Swab Spray and LC-MS.....	127
2.14	Simulated Forensic Applications .....	129
2.15	Analyte Carryover Effects .....	138
2.16	Analysis of Mycotoxins .....	141
3	Experimental .....	143

3.1	Experimental Data.....	143
4	Conclusions .....	149
5	Outlook .....	151
6	References.....	153



# Abbreviations

AChEI	Acetylcholinesterase inhibitor
APCI	Atmospheric pressure chemical ionization
ACN	Acetonitrile
BB3	Basic blue 3
BV3	Basic violet 3
BG	Background
CAD	Collisionally activated dissociation
CE	Collision energy
CEM	Chain ejection model
CRM	Charged residue model
DART	Direct analysis in real time
DBDI	Dielectric barrier discharge ionization
DEET	Diethyltoluamide
DDT	4,4'-dichlorodiphenyltrichloroethane
DESI	Desorption electrospray ionization
DMF	Dimethylformamide
EASI	Easy ambient sonic-spray ionization
EESI	Extractive electrospray ionization
EI	Electron impact ionization
ELDI	Electrospray-assisted laser desorption/ionization

ESI	Electrospray ionization
EtOAc	Ethyl acetate
EtOH	Ethanol
FA	Formic Acid
GC-MS	Gas chromatography coupled to mass spectrometry
HCD	Higher-energy collisional dissociation
IEM	Ion evaporation mode
LAESI	Laser ablation electrospray ionization I
LC-MS	Liquid chromatography coupled to mass spectrometry
LOD	Limit of Detection
LOQ	Limit of Quantitation
MALDI	Matrix assisted laser desorption ionization
MeOH	Methanol
MS	Mass spectrometry
MS <sup>2</sup>	Tandem mass spectrometry
M/Z	Mass-to-charge ratio
NL	Normalization level, indication for maximal signal intensity
PSI/PS	Paper spray ionization
PPM	Parts per million
PTFE	Polytetrafluoroethylene
SDHI	Succinate dehydrogenase inhibitor
SM	Suppression marker
XIC	Extracted Ion current





# 1 Introduction

## 1.1 Mass Spectrometry

“Mass spectrometry is a microanalytical technique that can be selectively used to detect and quantify a specific analyte” [1]. The initial step in mass spectrometry involves the generation of gas-phase ions from various states of matter such as solids, liquids, dissolved compounds, or gaseous analytes. Numerous ionization techniques exist, which are distinguished by the amount of energy that is applied to the analytes to achieve ionization. Soft ionization techniques, for instance, include electrospray ionization (ESI), matrix assisted laser desorption ionization (MALDI), and atmospheric pressure chemical ionization (APCI). The ions are generated by addition or abstraction of a proton yielding ions with an even number of electrons. Soft ionization sources mostly prevent analyte fragmentation during the ionization process. In contrast, electron impact ionization (EI) yields ions with an odd number of electrons and the high amount of energy applied often induces analyte fragmentation [1,2]. After the generation of gas-phase ions, collisionally activated dissociation (CAD) experiments can be performed before the mass-to-charge ratio is determined by the analyzer. Several types of modern mass analyzer exist, i.e., time-of-flight analyzers, transmission quadrupoles, quadrupole ion traps, Orbitraps, among others. They all offer several advantages and disadvantages. However, Orbitraps, which use a static electrostatic field between two axisymmetric electrodes for mass-depending oscillation of trapped ions, are widely applied in mass spectrometry due to their high resolving power and sensitivity [1].

### 1.1.1 The Electrospray Ionization Source

The subsequent section details the generation of droplets through a conductive capillary that emits electrospray. Following this, the ionization process, which entails transferring dissolved and charged molecules into the gas-phase, is explicated.

In electrospray ionization, a high voltage is applied to a thin, conductive capillary filled with an electrospray-compatible solvent to generate an aerosol of charged droplets. Typically, organic solvents, for example, methanol and acetonitrile, are employed as they offer low surface tension and high vapor pressure [3]. Weak acids, such as formic or acetic acid, are often added to the solvent to facilitate analyte protonation when the positive ionization mode is used [4]. The inner diameter of the capillary is typically in the range of 0.1 to 0.2 mm as its diameter affects the signal intensity [5,6]. At the tip of the spray capillary, ions are separated based on their polarity. In the positive ionization mode, the positive ions accumulate at the liquid surface on the capillary tip. Conversely, the negative ions are repelled in the opposite direction (shown in Figure 2) [7,8].

It is important to recognize that a conductive capillary operated in the positive ionization mode can promote oxidative electrochemical reactions in the spray capillary. Not only does the solvent undergo electrochemical reactions (for example, the oxidation of methanol to formaldehyde produces two protons and two electrons), but in certain cases, analyte molecules are also susceptible to oxidation. Operating an electrospray source in the negative ionization mode may enable reductive reactions. To avoid analytical pitfalls associated with electrochemical reactions, understanding the electrochemical perspective is an important prerequisite. Moreover, these reactions can be controlled by the design of the ion source, which includes capillary materials and upstream grounds. Furthermore, parameter settings such as the electric potential, solvent flow, and solvent conductivity play an important role [9–12].

At the tip of the electrospray emitter, the deformation of the liquid surface into a conical form termed as the Taylor cone, named after the British physicist Geoffrey Ingram Taylor, can be observed [13,14]. At the apex of the Taylor cone, a jet is formed, which dimension depends on viscosity, electrical resistivity, and solvent flow rate [15,16]. The jet eventually breaks up and primary parent droplets are formed (Figure 1), the sizes of which depend on the tip diameter, voltage, solvent conductivity, and flow rate [17].

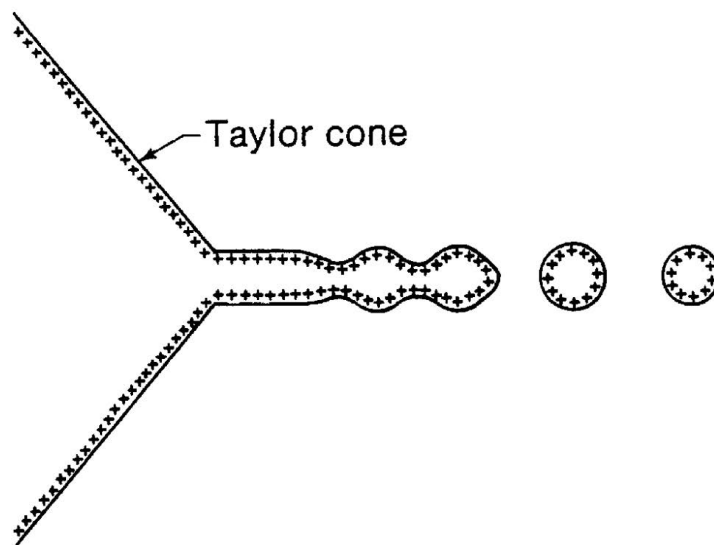


Figure 1 Emission of primary droplets at the tip of the Taylor cone using the positive ionization mode. Reprinted with permission from reference [7]. Copyright © 2000, John Wiley and Sons.

As solvent evaporation occurs, the volume of the parent droplets shrinks, which triggers asymmetrical Coulomb fission upon reaching the Rayleigh limit, resulting in the ejection of multiple progeny droplets through the formation of a Taylor cone. The Rayleigh limit is reached when the charge repulsion of the ions overcomes the surface tension of the droplets [18].

The Rayleigh equation allows to determine the coulomb instability [19]:

$$Q_{Ry} = 8\pi(\epsilon_0\gamma R^3)^{\frac{1}{2}} \quad \text{Equation 1.0}$$

$\epsilon_0$ : permittivity of the vacuum ( $8.8 \times 10^{-12} J^{-1}C^2$ )

$\gamma$ : surface tension of the solvent

R: radius of the droplet

While progeny droplets inherit approximately 10–40% of the original charge, they constitute of approximately 2–5% of the mass of the parent droplet. The proportion of mass and charge dissipation in progeny droplets is depending upon the properties of the solvent. The diameters of these progeny droplets are reduced to a mere one-tenth compared to that of the parent droplet. The progeny droplets, following further solvent evaporation, undergo Coulomb fission and generate even smaller progeny droplets. The generated cascades of solvent evaporation and ensuing coulomb fission enlarge the total droplet surfaces and diminish the volume. At the end of the ionization process gas-phase ions are formed [7,8,20–22]. To enhance the solvent evaporation rate in conventional electrospray ion sources, heater gas is introduced to improve the

ionization efficiency [23]. Figure 2 presents an overview of the processes involved in electrospray ionization.

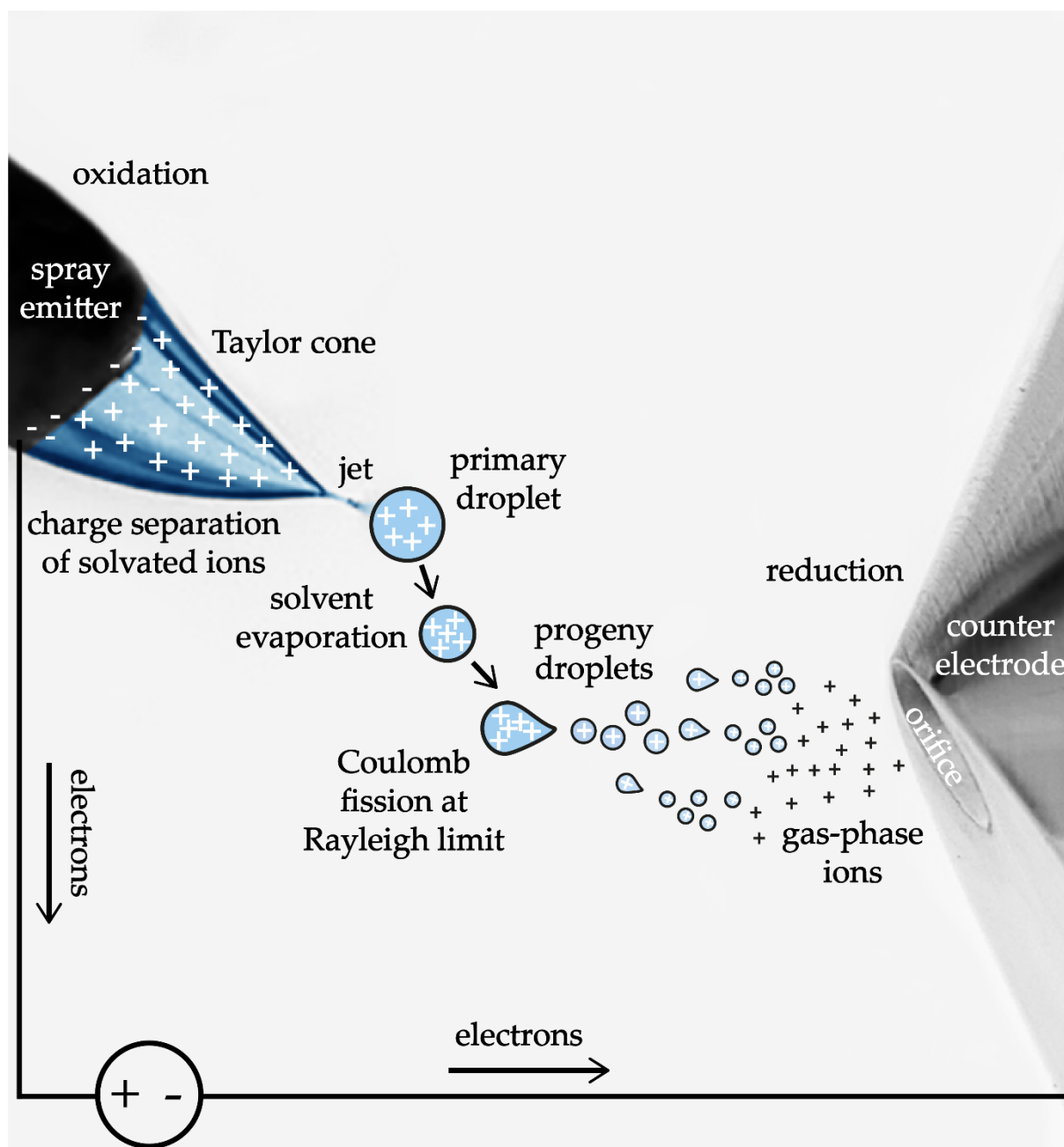


Figure 2 Overview of an electrospray ionization source operated in the positive ionization mode, including charge separation, droplet emissions, and generation of gas-phase ions.



### 1.1.2 Taylor Cone Modes

Many forms of Taylor cones exist, all of which are responsible for the emission of charged droplets [24]. Figure 3 presents an overview of different electrospray modes. Pulsating modes, depicted in the top row, include the dripping and microdripping modes, as well as the spindle and multispindle modes [25–31]. Jet modes, shown in the bottom row, include the cone-jet, oscillating-jet, precession, and multi-jet modes [32].

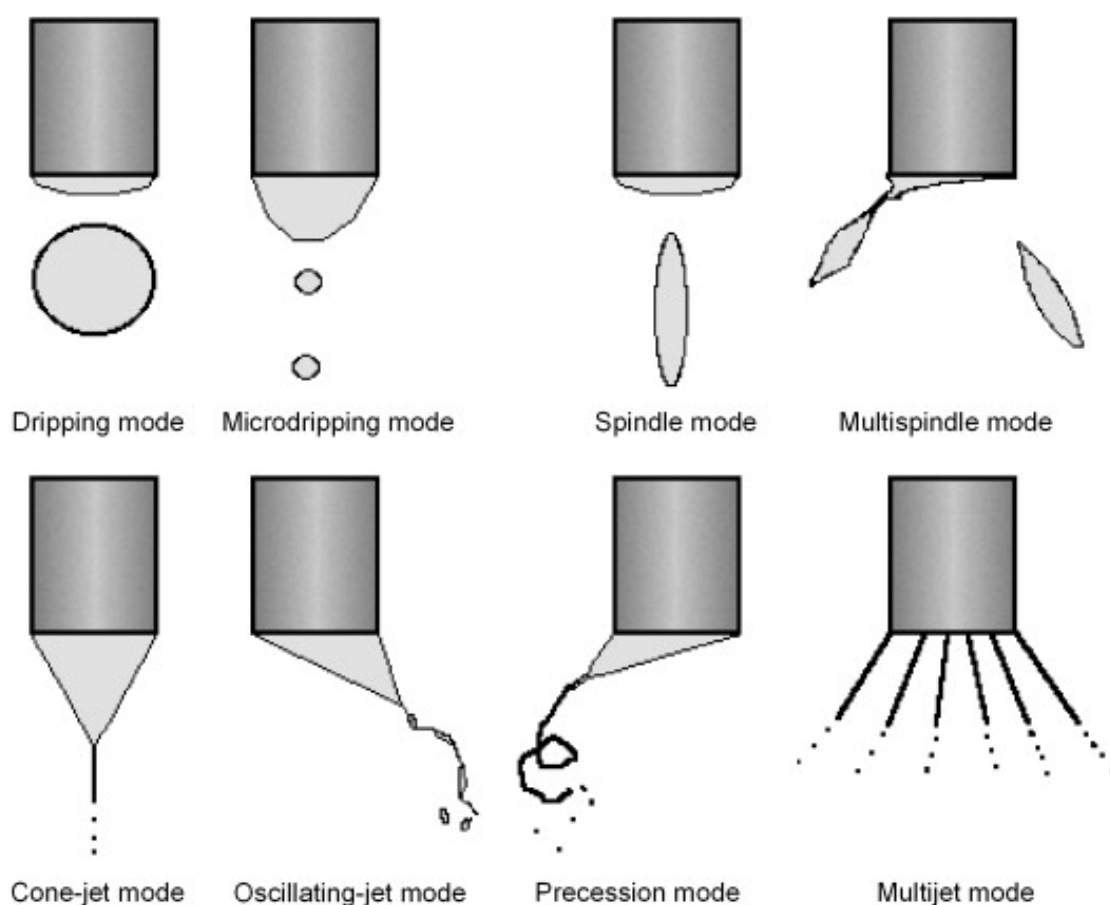


Figure 3 Pulsating electrospray modes are depicted at the top, while jet modes are illustrated at the bottom. Reprinted with permission from reference [32]. Copyright © 2008, Elsevier.

All these spray modes are not well understood. Nevertheless, the cone-jet mode is the most useful one as it is able to form a stable jet region on the apex of the Taylor cone [24]. In the jet region, breakup can occur, leading to the formation of a charged aerosol known as the spray plume, where ionization occurs. The cone-jet mode requires a specific onset potential, which depends on the surface tension, the permittivity of the

surrounding gas, and the capillary's radius. Liquids with high surface tension, such as water, require a significantly higher onset potential compared to most organic solvents. Consequently, the ion source design must be capable of preventing electrical discharge when high voltages are applied. [6–8].

### 1.1.3 The Onset Potential

If a planar counter electrode is utilized, the electric field at the capillary tip can be calculated using the equation 1.1 [19]:

$$E_c = \frac{2V_c}{[r_c \ln\left(\frac{4d}{r_c}\right)]} \quad \text{Equation 1.1}$$

$V_c$ : applied potential

$r_c$ : capillary outer radius

$d$ : distance from the capillary to the counter electrode

The voltage required to induce the formation of an emitting Taylor cone can be approximated by the equation 1.2 [19]:

$$E_{on} \approx \left( \frac{2\gamma \cos \theta}{\epsilon_0 r_c} \right)^{\frac{1}{2}} \quad \text{Equation 1.2}$$

$\theta$ : half angle of the Taylor cone (49.3°)

$\gamma$ : surface tension of the solvent

Upon combining Equation 1.1 with Equation 1.2, an approximation of the required onset potential can be expressed as follows [19]:

$$V_{on} \approx \left( \frac{r_c \gamma \cos \theta}{2\epsilon_0} \right)^{\frac{1}{2}} \times \ln\left(\frac{4d}{r_c}\right) \quad \text{Equation 1.3}$$

Equation 1.3 was used to calculate the approximate onset potential on two setups using various solvents:

Setup 1:  $r_c = 3.5$  mm,  $d = 7$  mm

Setup 2:  $r_c = 0.01$  mm,  $d = 1$  mm

Table 1 Calculated onset potentials of various solvents using two setups.

solvent	$\gamma$ (25 °C)/mN·m <sup>-1</sup> [33]	$V_{on}$ setup 1 (kV)	$V_{on}$ setup 2 (kV)
methanol	22.17	3.29	0.506
acetonitrile	28.66	3.74	0.577
dimethyl formamide	42.92	4.16	0.704
water	72.06	5.92	0.912

#### 1.1.4 Electrospray Ionization Mechanisms

Currently, three different ionization mechanisms are proposed for the transfer of dissolved molecules into the gas phase. They include the charge residue model (CRM), the ion evaporation model (IEM), and the chain ejection model (CEM). None of these models is able to represent the real ionization process, which depends on numerous factors. Nevertheless, ionization models are widely used to describe the ionization process for certain analytes [8,34–43]. The three ionization models are briefly described:

##### **Ion Evaporation Model:**

The direct expulsion of an ion with a small solvation shell necessitates adequate field strength at the droplet surface and a low solute concentration (Figure 4 (a)). In addition, ion evaporation demands a small droplet size of approximately 10–20 nm and the evaporation rate is significantly influenced by the chemical properties of the ions. This model, proposed by Iribarne and Thomson in 1976, describes the evaporation of small ions [7,8,44,45]. Although, Fenn and coworkers took the IEM in consideration for the formation of larger ions as well [8,46].

##### **Charge Residue Model:**

The CRM assumes that the cascade of coulomb fission and solvent evaporation continues until an individual charged analyte ion is left in a solvent droplet and finally will be released into the gas phase by complete solvent evaporation (Figure 4 (b)). In the final step, residual charge from the solvent surface of the droplet can be transferred to the analyte ion. Experimental data focusing on the ionization mechanisms of globular proteins indicated that the CRM is much more likely for globular proteins than the IEM in the mass range of at least several thousand Daltons [6–8,22,45,47].

##### **Chain Ejection Model:**

The CEM, a relatively new model derived from molecular dynamics (MD) simulations, elucidates the ionization mechanisms of non-globular proteins. Acidic liquid chromatography (LC) conditions may trigger the unfolding of proteins, rendering an amino acid chain terminus accessible to the droplet surface. The ejection of a single chain terminus can lead to the sequential release of a protein into the gas phase (Figure 4 (c)). The prerequisites for this model include a disordered protein conformation, partial hydrophobicity, and the ability to bind an excess of charge carriers [45,48,49].

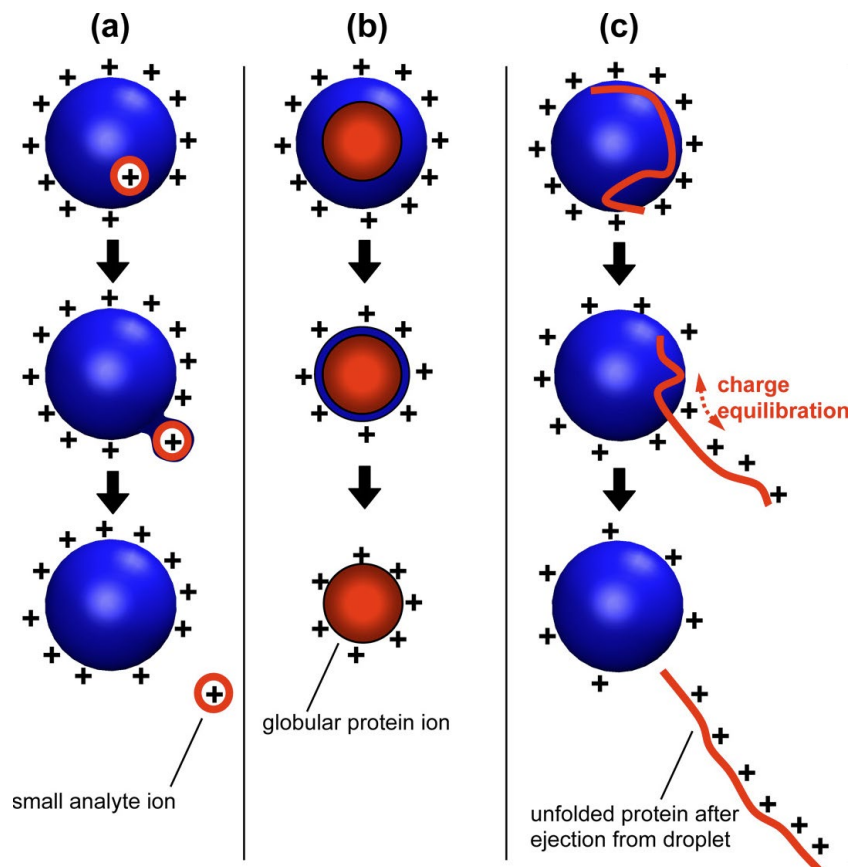


Figure 4 Illustration of the three ionization models: (a) Ion evaporation model, (b) Charge residue model, (c) Chain ejection model. Reprinted with permission from reference [45]. Copyright © 2013, American Chemical Society.

### 1.1.5 The Electrospray Ionization Efficiency

The signal response in electrospray ionization is influenced by a variety of factors, such as ion source design, ion source parameters, the spray solvent and its pH value, as well as the molecular properties of the analyte. Generally, an increase in the molecular volume, hydrophobicity, and basicity of the analyte correlates with an enhanced signal response for ions generated through protonation in the positive ionization mode [50–52]. In addition, the effect of the solvent pH is compound-related [53]. For analytes with low basicity, using the negative ionization mode is often advantageous [54,55]. Higher contents of organic solvents in mixtures with water can increase the signal response [56]. However, contrasting preferences emerge from different studies: one advocates for methanol over acetonitrile to achieve a higher signal response, while another promotes acetonitrile over methanol to enhance signal response [56,57]. Increasing the temperature and pressure of the ion source heater gas can promote ionization, but labile compounds may be susceptible to in-source decomposition [58–61].

The flow rates in electrospray ionization are highly variable depending on the ion source. They can range from a few nL/min to a few tens of nL/min in nanoelectrospray ionization, depending on the needle diameter and the application of back pressure [62]. However, at higher flow rates of up to 0.2–0.4 mL/min, found in LC-MS methods, the application of heater gas becomes mandatory to maintain ionization efficiency.

#### 1.1.6 Collisionally Activated Dissociation (CAD)

The generation of intact gas-phase ions lacks structural information. For structural elucidation, dissociation of gas-phase molecules in tandem mass spectrometry is applied as a powerful and widely applied tool. Gas-phase dissociation using collisionally activated dissociation (CAD) is applied in many research fields to obtain structural information. CAD is applied to various types of analytes, ranging from small molecules, such as metabolites [63–65], modified amino acids [66,67], mycotoxins [68–71], and pesticides [72–76], to oligonucleotides [77,78], peptides [79–83] and even proteins [84–87]. However, the study of fragmentation patterns and their correlated dissociation mechanisms is highly demanding. For compound identification, the use of large spectral libraries has become an important tool [88–90].

To achieve fragmentation of ions, the internal energy must be increased. For molecular ions, the internal energy is distributed among the internal degrees of freedom. To increase the internal energy of ions in CAD mass spectrometry experiments, the analyte ions are accelerated and become projectile ions to collide with neutral collision partners (targets). Usually in mass spectrometry, nitrogen, argon, or helium gas is admitted to provide neutral collision partners inside the collision cell. Upon collision, energy is transferred to the projectile ion turning it into an activated ion, whereas its internal energy is increased through the translational energy. The excited ion has several options for relaxation: intravibrational relaxation (IVR), photon emission, collisional relaxation, and—the most useful in mass spectrometry for structural elucidation—molecular dissociation. The obtained fragment ion spectrum is the result of the competitive energetically accessible dissociation pathways [91,92].

In addition to the excitation of the projectile ion, a variety of energy transfer reactions can result from the collision event, as summarized in Table 2. These include the excitation of the collision partner (target), as well as the simultaneous excitation of both, the projectile and the neutral collision partner. Moreover, ionization events, along with concurrent excitation and ionization reactions involving the projectile ion

and/or collision partner, are feasible. Charge transfer reactions and charge stripping are also potential outcomes [91].

*Table 2 Energy transfer mechanisms in collisions between a projectile ion and a neutral collision partner are summarized [91].*

equation	description
$A^+ + X \rightarrow A^+ + X^*$	excitation of the target
$A^+ + X \rightarrow (A^+)^* + X$	excitation of the ion
$A^+ + X \rightarrow (A^+)^* + X^*$	excitation of both ion and target
$A^+ + X \rightarrow A^+ + X^+ + e$	ionization of the target
$A^+ + X \rightarrow (A^+)^* + X^+ + e$	excitation of the ion and ionization of the target
$A^+ + X \rightarrow (A^+)^* + (X^+)^* + e$	excitation of both ion and target and ionization of the target
$A^+ + X \rightarrow A + X^+$	charge transfer to form ground state species
$A^+ + X \rightarrow A^* + X^+$	charge transfer into an ion excited state
$A^+ + X \rightarrow A + (X^+)^*$	charge transfer into a target excited state
$A^+ + X \rightarrow A^* + (X^+)^*$	charge transfer into both target and projectile excited states
$A^+ + X \rightarrow A^{2+} + X + e$	charge stripping of the ion

Numerous parameters, such as the interaction potential (attractive and repulsive potential), and the impact parameter (angle between projectile and collision partner) play important roles in the collision process leading to electronic and vibrational/rotational excitation. The generated product ions and their intensity ratios depend on the collision gas, the collision energy, and the collision gas pressure [91].

To perform CAD, an on-resonance radio frequency (RF) can be applied for precursor ion activation in the ion trap. The kinetic energy of the precursor ions slowly increases and successive collisions with helium atoms gradually increase the internal energy until fragmentation of the precursor ions occurs. This fragmentation technique commonly favors the lowest energy fragmentation pathways [93]. Furthermore, the application of normalized collision energy allows for the adjustment of collision energy from 0 to 100%. The necessary collision energy for optimal fragmentation efficiency exhibits a linear correlation with the  $m/z$  ratio, whereas ions with a higher  $m/z$  require more energy. Consequently, a specific collision energy setting does not impart identical collision energies to precursor ions of varying  $m/z$  values [94].

### 1.1.7 Orbitrap Mass Analyzer

In 1923, Kenneth Hay Kingdon proposed a tube consisting of an inner and outer electrode, later termed as the Kingdon trap, that allowed trapping of oscillating gas-phase ions [95]. During the 1980's, Randall D. Knight continued developing ion trapping devices using ions from laser-produced plasma yielding a novel electrostatic trap with a harmonic axial potential [96]. Yet, none of these developments resulted in an accurate mass analyzer [97]. It was Yuri Konstantinovich Golikov who's invention received a patent for the concept of an Orbitrap mass analyzer in the year 1986 [98]. Alexander Makarov continued to make significant contributions for Orbitrap-based mass analyzers, including the development of the C-trap ion injector. The first commercially available Orbitrap-based mass spectrometer was released by the Thermo Electron corporation in 2005 [97–100]. The modern Orbitrap analyzer has a spindle-like central electrode which is under high-voltage when ions are trapped (Figure 5). The outer electrode, which is made up of two parts, is kept at ground potential. Both electrodes generate an electric field that is inhomogeneous in the radial and axial direction. The rotational and radial frequency of injected ions depend on initial energy, position or angle. On the other hand, the frequency of axial oscillation (or  $\omega$  = angular velocity) is only depending on the mass-to-charge ratio [99]:

$$\omega = \sqrt{\frac{k}{m/z}} \quad \text{Equation 1.4}$$

$k$  = a constant representing potential differences between both electrodes.

$m/z$  = mass-to-charge ratio

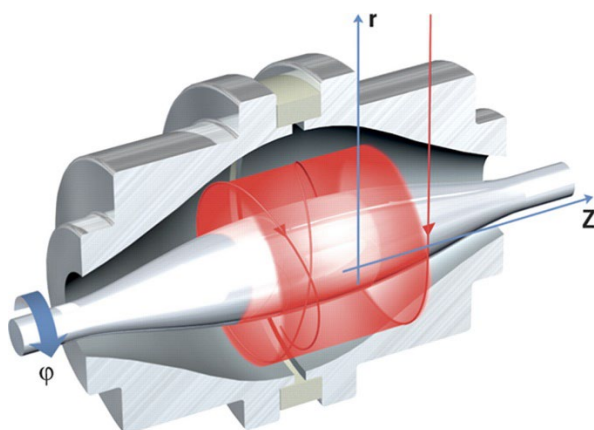


Figure 5 Schematic representation of an Orbitrap mass analyzer. Reprinted under CC BY license from reference [99].



## 1.2 Overview of Ambient Ionization Methods

Ambient ionization can be described as the generation of ions from unprepared to little prepared samples under ambient conditions and it includes condensed phase samples in air [101–103]. The following section explains the principles of different ambient ionization methods. A summarizing table of the presented ambient ionization techniques including method name, abbreviation, short description, and year of introduction can be found in Table 3.

*Table 3 Overview of well-known ambient ionization techniques, including method name, abbreviation, short description, and year of introduction.*

method name	abbreviation	short description	year
<b>desorption electrospray ionization</b>	DESI	sample desorption by charged droplets generated by electrospray.	2004
<b>direct analysis in real time</b>	DART	plasma based penning ionization, including hyphenated techniques for sample desorption.	2005
<b>electrospray-assisted laser desorption/ionization</b>	ELDI	laser ablation combined with electrospray ionization.	2005
<b>extractive electrospray ionization</b>	EESI	dual spray setup: solvent spray and sample spray.	2006
<b>easy ambient sonic-spray ionization</b>	EASI (DESSI)	sample desorption by charged droplets generated by sonic spraying.	2006
<b>probe electrospray</b>	PESI	a stainless-steel needle operated as electrospray emitter.	2007
<b>dielectric barrier discharge ionization</b>	DBDI	dielectric barrier discharge is used to generate an ionizing cold plasma.	2007
<b>paper spray</b>	PSI and PS	liquid analyte extraction combined with electrospray ionization.	2010
<b>swab spray, also termed as swab touch spray</b>	N/A	direct ion generation from swabs by application of solvent flow and electric potential.	2015

In 2004, a technique known as desorption electrospray ionization (DESI) was introduced, enabling the analysis of surfaces under ambient conditions for the first time. DESI is an electrospray-based method as the charged droplets are created by solvent flow and electric potential. A stream of charged droplets is produced and directed toward an electrically insulated sample surface with the aid of a high-velocity nebulizer gas, as depicted in Figure 6. The desorbed analyte molecules are then drawn into the mass spectrometer's inlet. DESI has been used to analyze a broad range of

molecules, from small molecules such as explosives, and terpenoids, to larger ones such as peptides and proteins [103]. In DESI, flow rates of several  $\mu\text{L}/\text{min}$  are applied [103,104].

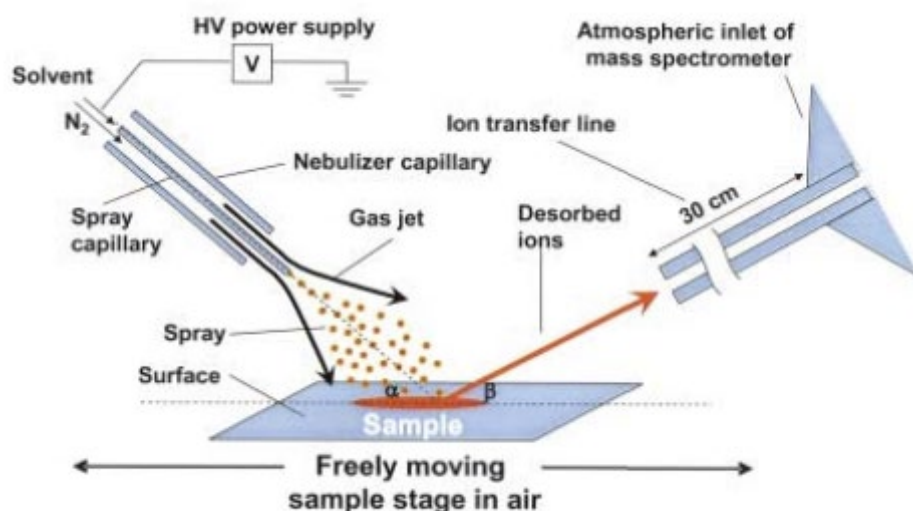


Figure 6 Illustration of a DESI ion source. A spray of charged aerosol is generated and directed onto the sample plate to desorb ions. Reprinted with permission from reference [103]. Copyright © 2004, the american society for the advancement of science.

DESI marked the advent of rapid advancements in ambient ionization techniques. Following DESI, Direct Analysis in Real Time (DART) was introduced in 2005. This compact and portable ion source functions by exciting gas species, such as nitrogen or helium, into a metastable state within a discharge chamber equipped with an anode and a cathode. This process categorizes DART as a plasma-based ionization method. Samples can be placed directly between the mass spectrometer inlet and the DART ion source. DART, recognized as a potent analytical technique, enables the examination of a wide spectrum of analytes including polar and non-polar small molecules, pharmaceuticals, drugs, chemical warfare agents, and explosives across diverse samples such as fruit, body fluids, business cards, human skin, and volatile organic compounds (VOCs). Moreover, quantitative analysis is facilitated by using an internal standard to offset variations in sample positioning, which can influence the ion source gas stream. [105]. A significant advantage of both DESI and DART is the elimination of sample preparation, which not only dramatically reduces analysis time but also has the potential for in-situ analysis.

In 2005, enhancements in sample desorption through laser ablation were introduced, known as electrospray-assisted laser desorption/ionization (ELDI). The laser source simultaneously facilitates the desorption and ionization of the analyte. However, due

to the absence of a matrix in ambient laser ionization, it is necessary to couple this technique with electrospray ionization to augment ionization efficiency [106]. Extractive electrospray ionization (EESI), unveiled in 2006, merges a sample spray with an ionizing solvent spray in a dual-probe configuration. This proved particularly advantageous in the analysis of raw body fluids [107]. Desorption sonic-spray ionization (DESSI) was renamed to easy ambient sonic-spray ionization (EASI) [108], it is built similar to DESI, but the spray of charged droplets is generated by solvent nebulization through a supersonic gas stream instead of high voltage [109]. A year later, probe electrospray ionization was presented which uses a stainless needle instead of a capillary for electrospray ionization. This innovation significantly reduced the risk of emitter clogging. However, the precise positioning of the needle in front of the inlet of the mass spectrometer is imperative, as it is a critical parameter that influences the ionization process [110].

In 2007, the dielectric barrier discharge ion source (DBDI) was introduced, expanding the repertoire of ionization methods. A DBDI ion source employs an alternating voltage across a dielectric glass slide, thereby producing an ionizing cold plasma [111]. A few years later, in 2010, paper spray ionization (PSI) was presented. It is another electrospray-based ambient ionization method, which was demonstrated for the qualitative and semi-quantitative analysis of dried blood spots. The method involves a sharply pointed paper affixed to a metal clip with an applied electric potential. When moistened with a specified volume of solvent, it facilitates ion generation similar to conventional ESI needle emitters, as illustrated in Figure 7. Quantitative results were achieved by volumetric blood deposition and comparison to a calibration curve [112].

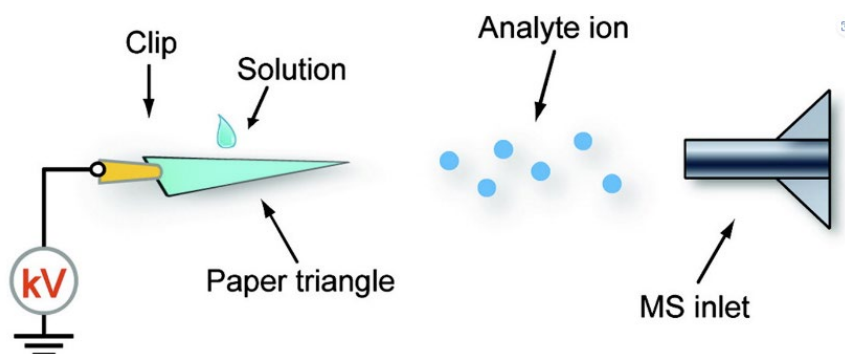


Figure 7 Illustration of paper spray ionization. Reprinted under CC BY-NC-ND license from reference [113].

The myriad of electrospray-based ambient ionization techniques highlights its high versatility for employment in ambient ionization techniques. In 2015, swab spray was presented as an innovative electrospray-based ambient ionization technique that

merges sample collection with swabs and subsequent ion generation through the application of solvent flow and electric potential directly to the swab head. Swab spray mass spectrometry originated from the Aston research laboratory of Prof. Graham Cooks at Purdue University in West Lafayette, Indiana. Numerous applications have been reported and will be discussed in detail in a subsequent section [114].

### 1.3 The Benefits of Ambient Ionization Techniques

Conventional mass spectrometry-based analysis requires arduous, time-consuming, and expensive sample preparation. These preparatory steps often include homogenization, dilution, digestion, derivatization, and chromatography [115]. In ambient ionization, sample preparation is minimal, significantly enhancing sample throughput and enabling in-situ analysis with portable mass spectrometers. Figure 8 illustrates ambient ionization techniques compared to conventional methods. Ionization primarily employs plasma and solvent-based techniques, while desorption is achieved utilizing laser, thermal, acoustic, and vibrational methods, as depicted in Figure 9 [101].

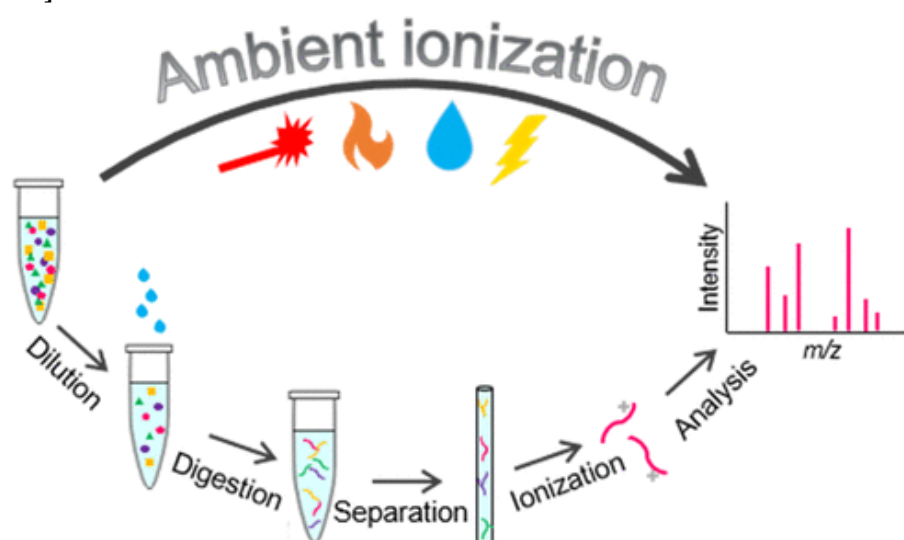


Figure 8 Illustration of ambient ionization versus conventional analysis. Reprinted with permission from reference [101]. Copyright © 2019, American Chemical Society.

Recent data suggest that DESI has become the preeminent ambient ionization technique, as reflected by the volume of publications in the year 2022. PSI and DART followed closely, securing the second and third positions, respectively. In terms of application fields, “Food and Agriculture” along with “Biological Materials” shared the top spot in the number of contributions. They were succeeded by “Technological Advancements”, “Forensics and Security”, “Disease Diagnostics”, and “Pharmaceuticals” [116].

While the rankings provide an interesting statistical summary, the true importance lies in the outcomes of analytical advancements achieved through ambient ionization techniques. For instance, applications that concentrate on diagnosing cancer tissues via ambient ionization hold a considerable potential for enhancing healthcare in the near future [117–123]. Furthermore, rapid and in-situ authentication of various food products including milk analysis by lipidomic profiling [124–126], differentiation of

Chinese oolong teas varieties [127], characterization of vanilla [128], and classification of coffee [129], among many more, improves consumer safety and product integrity.

In the area of forensic science, a variety of techniques have been reported to not only expedite sampling times but also to allow in-situ analysis at crime scenes utilizing portable mass spectrometers [116]. Consequently, the timeline of criminal investigations can be significantly shortened through the accelerated detection of drugs [101,116,130–133] and explosives [101,116,134–138]. Moreover, the application of document analysis for the investigation of forgery has been exemplified [139–141].

Environmental applications of ambient ionization techniques include the analysis of water for contaminants [142,143], pesticides [144–146], and neurotoxins produced by cyanobacteria [147]. Further fields of application include “elemental and isotope analysis” (i.e. uranium determination [148]), “reaction monitoring and catalysis” (i.e. monitoring of enzymatic reactions [149]), “in vivo analysis” (i.e. cancer tissue analysis by the surgical intelligent knife [150]), and “bioanalysis” (i.e. protein complex formation [151]). Figure 9 provides a concise overview of the most employed ionization techniques at the upper half of the center wheel and most frequent applied sample desorption techniques at the lower half of the center wheel [101].

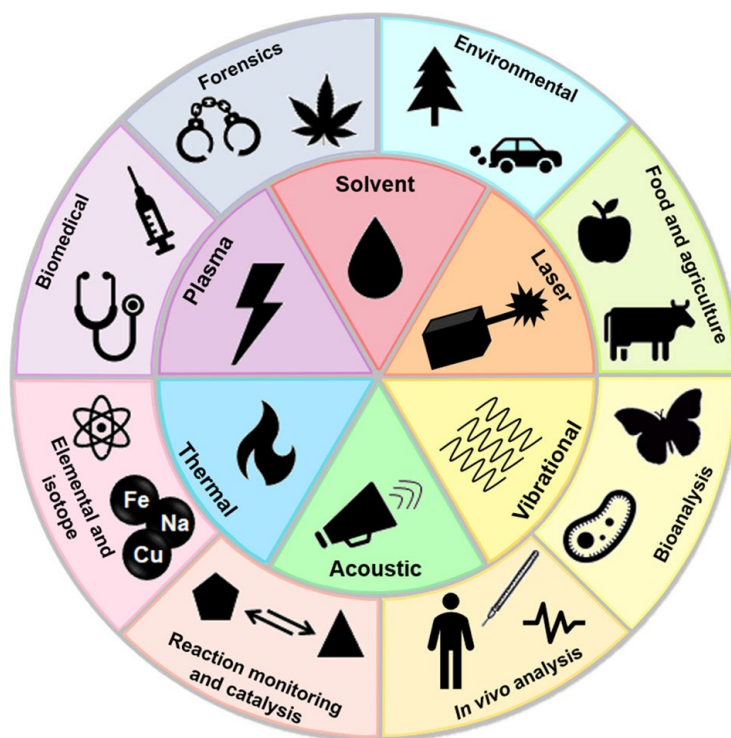


Figure 9 Illustration of sample ionization methods (top of inner wheel), sample desorption methods (bottom of inner wheel), and fields of application in ambient ionization (outer wheel). Reprinted with permission from reference [101]. Copyright © 2019, American Chemical Society.

## 1.4 Pesticides

### 1.4.1 Definition and Differentiation

The United States Environmental Protection Agency (EPA) defines a “pesticide” (with certain minor exception) as [152]:

- Any substance or mixture of substances intended for preventing, destroying, repelling, or mitigating any pest.
- Any substance or mixture of substances intended for use as a plant regulator, defoliant, or desiccant.
- Any nitrogen stabilizer.

Pests include fungi, bacteria, viruses, weeds, insects, mites, rodents, birds, and fish [152,153]. A pesticide is designed to kill, control, repel, attract or manage these pests [153]. Pesticides can be grouped by various approaches: contact and systemic pesticides, target pests, chemical structure, and mode of action.

An important distinction exists between contact and systemic pesticides. Contact pesticides effectively combat pests through direct contact. This can involve spraying pesticides directly onto insects or applying fungicides directly on fruit to prevent mold growth. Conversely, systemic pesticides are administered in a way that allows them to be absorbed by the plant or animal. Insects that feed on plant juice or animal diseased by internal parasites can be controlled this way [153]. Another pesticide differentiation can be made by the target pests as shown in Table 4 [153]:

*Table 4 A list of different pesticide types and target pests.*

pesticide type	target pest
acaricide	spiders, mites, and ticks
algicide	algae
avicide	birds
bactericide	bacteria
fungicide	fungi
growth regulator	plants and insects
herbicide	plants (mostly weeds)
insecticide	insects
miticide	mites
molluscicides	snails and slugs
nematicide	nematodes
piscicide	fish
rodenticides	rodents

In addition, pesticides can also be grouped by their chemical structure. For example, organophosphates, carbamates, neonicotinoids, organochlorines, and pyrethrins [154]. Furthermore, pesticides can be distinguished by their mode of action as well.

#### 1.4.2 Pesticide Development

The first application of pesticides is often credited to the Sumerians, who utilized sulfur compounds to control pest insects and mites already around 2500 B.C. [155–157]. Another illustration of early pest control practices is the use of plant derivatives as pesticides in ancient China, Egypt, Greece, and India more than two thousand years ago [158]. The sprinkling of alum was documented as an effective method against flies in the sixth or seventh century. Later, alum was used as an additive in seed treatments to prevent smut diseases. Other compounds utilized in medieval pest management include antimony, arsenic compounds, copper sulfate, iron salts, mercury, and nitric acid, among others [159]. The use of highly toxic inorganic products continued through the 19<sup>th</sup> century [155,157,160].

In 1939, the group of Paul Hermann Müller at Geigy chemical corporation synthesized 4,4'-dichlorodiphenyltrichloroethane (DDT), shown in Figure 10, and discovered its extraordinary insecticidal property. Although DDT was synthesized previously in 1873 by an Austrian graduate student, its insecticidal potential remained undisclosed. After securing patents and permissions, the Geigy chemical corporation launched



DDT under the product name gerasol in February 1942. This moment marked the inception of modern pesticide production and distribution. Germany placed an urgent order for 10'000 tons of the organochlorine gerasol, equivalent to 500 tons of pure DDT, to fight the potato beetle. Gerasol further found successful application against malaria in many countries. Paul Hermann Müller was awarded the Nobel prize in medicine "for his discovery of the high efficiency of DDT as a contact poison against several arthropods" in 1948. However, problems including resistance by insects, increased bird, and other wildlife mortality were discovered in the late 1940s [161]. The accumulation of DDT in fatty tissue and milk was investigated in 1944 by the University of Cincinnati on behalf of the Geigy chemical corporation. Nevertheless, DDT was not banned in Germany and the United States until 1972 [162,163]. The mode of action of DDT, which is based on disruption of ion channel functionality in the peripheric nervous system, remained unknown for decades [164].

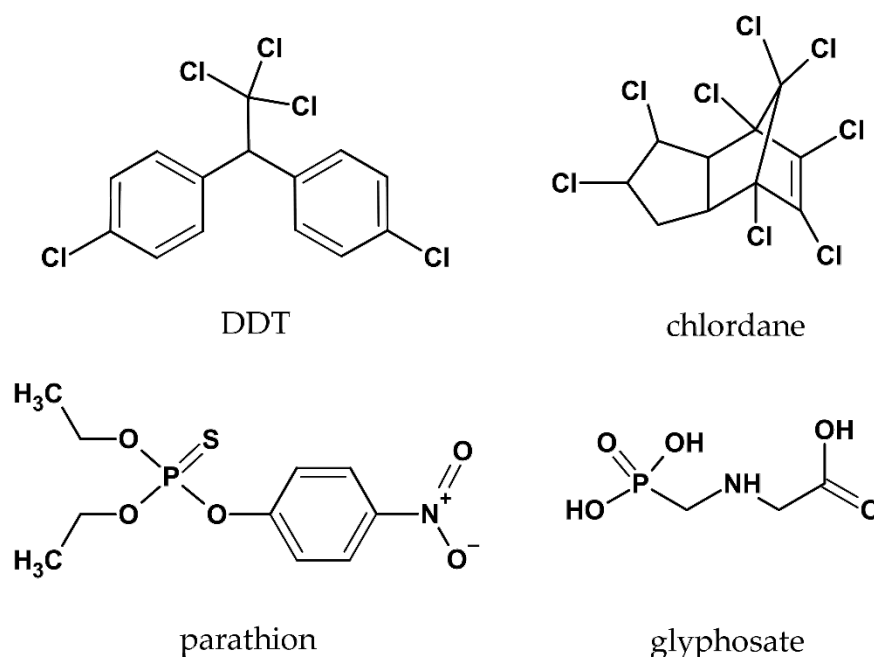


Figure 10 Structures of four early developed synthetic pesticides.

Chlordane, another pioneering synthetic insecticide depicted in Figure 10, is a chlorinated cyclodiene, first registered in the United States in 1948. Much like DDT, chlordane was eventually banned in numerous countries few decades later due to its detrimental environmental and human health effects. As a neurotoxin, chlordane functions as a non-competitive antagonist of the GABA receptor [165].

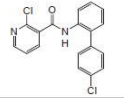
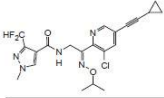
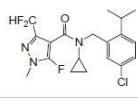
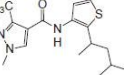
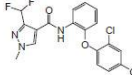
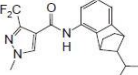
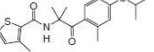
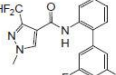
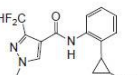
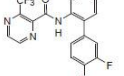
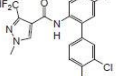
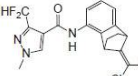
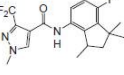
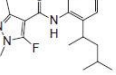
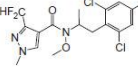
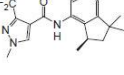
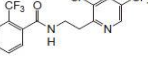
In 1944, the German chemist Gerhard Schrader developed a highly potent organophosphate pesticide parathion (illustrated in Figure 10), which demonstrated

tremendous toxicity against insects in all development states. In the post-war period, western companies took interest in German organophosphate pesticides, which led to the introduction of parathion in the United States in 1948. Parathion is a highly toxic compound that acts as an irreversible acetylcholinesterase inhibitor (AChEI) [166]. Even though aerial crop dusting with parathion improved crop yields, it faced banning in numerous western countries in the early 21st century due to its significant toxicity [167].

Glyphosate, illustrated in Figure 10, was initially synthesized by the Swiss chemist Henri Martin in 1950. It was patented as a non-selective herbicide by Monsanto in 1971 [168,169]. By 2010, it was used in over 130 countries with a global volume of approximately 600 kilotons [169]. Glyphosate acts by inhibiting the 5-enolpyruvylshikimate-3-phosphate synthase (EPSPS) which is exclusive to plants, fungi, and bacteria. However, applying glyphosate in such high volumes poses potential risks for the environment and human health, as concerns about its toxicity continue to grow [170].

The first period of the application of synthetic pesticides firmly neglected the impact of toxicity for the environment and humans. Nowadays, novel pesticide developments must meet advanced criteria: Pesticides need to be effective at a very low dosage, need to be degradable and less residual, and further they are desired to be highly selective [155]. Most novel fungicides are inhibiting the succinate dehydrogenase (SDHI), which belongs to the tricarboxylic acid cycle (Krebs cycle) and complex II of the mitochondrial respiratory chain [155,171]. Boscalid was the first SDHI fungicide launched by BASF (Badische Anilin- & Sodafabrik) in 2003 [172]. Table 5 shows approved SDHIs fungicides and a few which are still under development.

Table 5 List of SDHIs - approved or under development. Reprinted under CC BY-NC-ND license from reference [155].

Chemical structures	Common name Company name Registration year	Chemical structures	Common name Company name Registration year	Chemical structures	Common name Company name Registration year
	Boscalid BASF 2003		Pyrapropoyne Nissan Chemical Under development		Isoflucypram <sup>b)</sup> Bayer Under development
	Penthiopyrad Mitsui Chemicals Agro 2009		Flubeneteram <sup>b)</sup> Dongguan Hec Tech Under development		Isopyrazam Syngenta 2010
	Isofetamid Ishihara Sangyo Kaisha 2015		Fluxapyroxad (Xemium®) BASF 2011		Sedaxane Syngenta 2011
	Pyraziflumid Nihon Nohyaku 2018		Bixafen Bayer 2011		Benzovindiflupyr Syngenta 2012
	Fluindapyr <sup>b)</sup> Isagro/FMC Under development		Penflufen Bayer 2011		Pydiflumetofen Syngenta 2016
	Inpyrfluxam Sumitomo Chemical 2019 (Sept.)		Fluopyram Bayer 2012		

<sup>a)</sup> Partially modified and added new molecule to the Fig. 3 of Ref. 15.<sup>b)</sup> Compounds considered to be SDHI based on chemical structure.

Though SDHIs are modern fungicides generally exhibiting less toxicity to humans, there are still ongoing discussions about toxicity [173–176]. However, the future application of SDHIs is questionable due to arising resistance of fungi to this class of fungicides [177]. Besides SDHIs, demethylation inhibitors (DMI) and inhibitors of the mitochondrial electron transport chain complex III, including quinone outside inhibitors QoI and Quinone inside inhibitors (QiI) represent further groups of modern fungicides [155,178,179].

The first synthetic insecticides were primarily based on organophosphates, carbamates and synthetic pyrethroids, but nowadays the development of novel insecticides has changed to nicotinic and diamide compounds [155,180]. Nicotinic insecticides are derived from nicotine, a naturally occurring alkaloid present in many plants and act on the nicotinic acetylcholine receptors (nAChRs). Some of the nicotinic insecticides were prohibited due to high toxicity for honeybees [155,181]. Diamides, another group of insecticides, act on the ryanodine receptors, responsible for the release of calcium ions and are mostly used against lepidopteran pests [155,182]. Flubendiamide, the first diamide insecticide, was approved in the US in 2008 but withdrawn in 2016 due to concerns related to its toxicity [182].

While modern pesticide development prioritizes minimal environment harm, toxicity remains a significant challenge. Therefore, the development of innovative research fronts focusing on pesticide-free strategies is essential to significantly reduce pesticide consumption. These strategies encompass the introduction and promotion of ecological processes that facilitate the natural regulation of pests. The goal to curtail the usage of pesticides by increasing plant diversity, such as introduction of semi-natural habitats next to agriculture land, has become an important field of agricultural research [183].

## 1.5 Ambient Ionization Techniques for the Analysis of Pesticides in Food Products

In recent years, the application of numerous ambient ionization techniques has been demonstrated for the analysis of pesticide residues on natural products. Unlike conventional LC-MS analysis, which adheres to established sample preparation protocols, analyzing food samples, especially intact surfaces of fruit and vegetables, imposes new challenges.

The development of ambient ionization methods for the detection of pesticides on various samples requires extensive evaluation and optimization. A brief summary of multiple applications employing electrospray-based ambient ionization techniques is given below. The examination of sampling techniques, effects of spray/extraction solvents, reproducibility, sensitivity, and quantitative aspects will be discussed. However, specific details of instrumentation, such as geometrical parameters of DESI methods will not be addressed.

### 1.5.1 Desorption Electrospray-based Pesticide Detection

In 2009, a study compared the capability of DESI for quantitative pesticide analysis of fruit and vegetable extracts to a conventional LC-MS method encompassing 16 agricultural chemicals. The solvent combination for DESI was optimized to obtain a sensitive multiresidue method, whereas the combination of acetonitrile/water (80/20, *v/v*), including 1% formic acid to promote protonation of analytes, delivered the highest sensitivity overall. The usage of deuterated internal standards enhanced the accuracy. Despite a decreased sensitivity due to matrix effects, the analysis of food extracts by DESI delivered comparable results to LC-MS analysis, for example, the detection of imazalil in various fruit extracts yielded relative standard deviation (RSD) values below 15%. To compensate for analyte suppression, sample dilution was applied. The analysis of unprepared food samples was only briefly mentioned [184].

In another study, DESI was used for the analysis of pesticide residues on food samples without extractive sample preparation. The spray solvent consisted of acetonitrile/water (80/20, *v/v*) with 0.1% formic acid. Three different sampling methods were elaborated. The direct wiping of the glass plate on the food surfaces was described as the approach that delivered the best sensitivity. Direct surface analysis of a small, approximately 1 cm<sup>2</sup> peel section yielded slightly lower sensitivity but was challenging for fruit with a soft peel. The third method which yielded the lowest sensitivity, about one order of magnitude lower, involved using a cotton swab moistened with acetonitrile to wipe the food surface, followed by transferring the

sample onto a glass plate through rubbing. The analysis of intact food samples revealed the presence of 24 out of 32 pesticides. Notably, four systematically applied neonicotinoids remained undetectable. Additionally, effects on the limit of detection (LOD) and calibration slope of three different sample types were examined and briefly summarized. Pesticide reference materials dissolved in pure solvent and in strawberry extracts were both deposited on glass surfaces for analysis. Furthermore, the direct analysis from apple peel was performed. Regarding the calibration slope, the steepest slope was achieved by employing reference standards in a pure solvent, in the absence of matrix effects. The apple peel revealed the second steepest slope. The strawberry extract delivered the flattest calibration slope overall, indicating that matrix effects are higher in extracts than on the surface. For semi-quantitative experiments, deuterated compounds were used as internal standard. Pure pesticide solutions achieved a LOD of 1 pg/mm<sup>2</sup>, while the apple peel exhibited the lowest LOD of 33 pg/mm<sup>2</sup>. Furthermore, results indicated that the LOD is strongly influenced by the surface texture as well. Furthermore, converting surface concentration to mass concentration poses new challenges for natural products of various shape. However, the presented method was regarded suitable to be utilized as a preliminary selection tool to determine whether further comprehensive analysis using conventional methods is necessary [185].

Another demonstration of pesticide analysis via DESI involved the qualitative and semi-quantitative evaluation of chlorpropham on unwashed potato skin (illustrated in Figure 11), comprising compound identification by a MS<sup>4</sup> cascade.

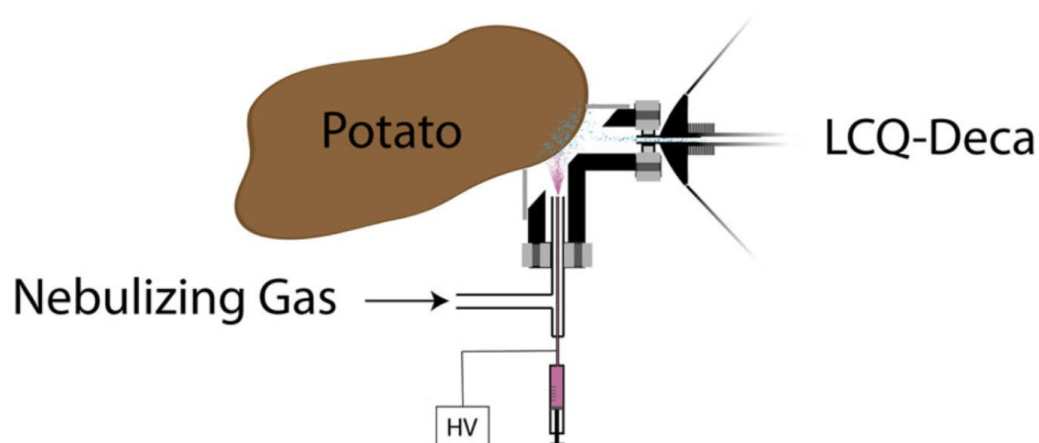


Figure 11 Illustration of a DESI ion source to examine an intact potato skin for chlorpropham. Reprinted with permission from reference [186]. Copyright © 2013, John Wiley and Sons.

The spraying solvent consisted of a mixture of methanol/water (50/50, *v/v*) with 1% acetic acid modifier. For calibration, three different potatoes were pneumatically spiked with different surface area concentration, corresponding to bulk concentrations of 3.7, 7.5 or 11.2 mg/kg. For semi-quantitative analysis, potatoes were pneumatically spiked with 6.0  $\mu\text{g}/\text{cm}^2$  chlorpropham, three spots of approximately 0.8  $\text{cm}^2$  were sampled on the potato by DESI for 30 seconds and the area under the curve was integrated. For repetitive 30 seconds sampling of the same spot a signal deviation of  $\pm 12\%$  was found. The signal deviation for three different spots on one potato was 12% compared to the signal deviation of 47% for three spots on three different potatoes. The recovery rates, which were calculated from the average signal from all three spots, were between 5% and 53%. Furthermore, the effect on storage was investigated, with the result that chlorpropham degradation products were found after several days of storage. The transformation of surface concentration to mass concentration, along with different surface properties, were described as a main challenge to establish a semi-quantitative method of unprocessed food samples [186].

The direct analysis of dimethoate, tebuconazole, and trifloxystrobin on olive and vine leaves via DESI was extensively studied in 2017. To maintain consistency in sampling leaves, a puncher, as visualized in Figure 12, was employed. The obtained specimens were mounted on the DESI PTFE platform using double-sided adhesive tape. Hereby the prominent sodium adduct formation of unprepared samples had to be taken into consideration. Dimethoate, a pesticide with an amide bond in its structure, exhibited a pronounced sodium adduct peak. This peak overshadowed the proton adduct. The low abundant proton adduct resulted in an information-rich  $\text{MS}^2$  spectrum, whereas the abundant sodium adduct failed to produce adequate fragment ions in  $\text{MS}^2$  analysis. The addition of ammonium acetate to the spray solvent facilitated the generation of the dimethoate proton adduct, but it did not work for tebuconazole and trifloxystrobin. Overall, the addition of 10 mM formic acid to the spray solvent was the best strategy to prevent sodium adduct formation in favor of the proton adduct. The signal intensity of dimethoate was amplified by methanol, whereas the intensity of tebuconazole was enhanced due to a higher water content of the spray solution. To obtain a suitable spray solvent for the simultaneous detection of all three pesticides a solvent mixture of methanol/water (80/20, *v/v*) was finally chosen.

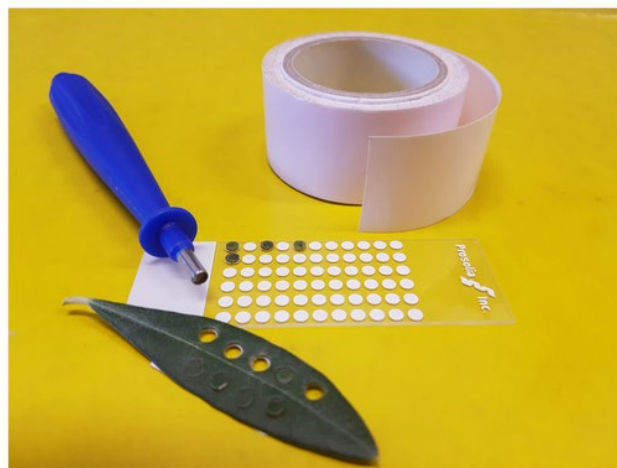


Figure 12 A punching tool was used to obtain reproducible leaf specimens, which were then fixed on the DESI PTFE plates using adhesive tape. Reprinted with permission from reference [187]. Copyright © 2017, John Wiley and Sons.

The use of an internal standard either by direct deposition on the leaves prior to analysis or by addition into the spray solvent was not considered an option [187]. Both methods were reported to not significantly improve quantitation for natural surfaces [188]. The LOD was elaborated by spiking leaf samples and was found to be 15 ng for dimethoate, 20 ng for trifloxystrobin, and 50 ng for tebuconazole. Calibration curves were based on five pesticide concentrations using two different preparations. First, the pure reference material was deposited on the PTFE DESI plate, next, the commercially available pesticide product was applied to both, the PTFE plate and the leaves. The first mentioned combination delivered a 5-fold increased sensitivity for the pesticide dimethoate over the last combination. For the pesticide detection on leaves, the LOD was determined to be 15 ng for dimethoate, 50 ng for tebuconazole, and 20 ng for trifloxystrobin. Whereas the LOQ was found to be 50 ng, 150 ng, and 60 ng, respectively. Results indicated that matrix effects from leaves and additional ingredients found in commercially available pesticides contributed to a decrease in sensitivity. Overall, the square of the correlation coefficient ranged from a moderate ( $R^2 = 0.8157$ ) to a high ( $R^2 = 0.9967$ ), depending on both pesticide and sample type. Furthermore, the intraday precision, expressed as relative standard deviation (RSD), was found to range between 13% and 27%, which was considered challenging [187].

Atrazine, a herbicide which is used in China can induce phytotoxicity in numerous plants, including Chinese cabbage. Distinguishing visually between necrotic spots caused by atrazine-induced phytotoxicity or by different other factors is challenging. Therefore, the development of a quick and accurate technique is desired to investigate herbicide induced phytotoxicity on plants. The DESI-based technique involved a spray solvent consisting of a water/acetonitrile (50/50, *v/v*) mixture containing 0.1% formic acid modifier. For establishing a calibration curve, atrazine reference material was



dissolved in water and externally applied on the leaves at different surface concentrations. This resulted in LOQs from 63 to 2525 pg/mm<sup>2</sup>. Each spot was analyzed by MS<sup>2</sup> for a duration of four minutes and a continuous decrease of the atrazine signal was observed. The atrazine concentration required to induce phytotoxicity in Chinese cabbage was found to be higher than the obtained LOQ. Thus, the method, which does not require any sample preparation at all, was considered adequate to rapidly obtain semi-quantitative results of necrotic spots on plants. Consequently, this method can be employed to safeguard food quality and prevent atrazine-induced toxic effects [189].

### 1.5.2 Paper Spray-based Pesticide Detection

Numerous studies demonstrated the detection of pesticides in food extracts using PSI techniques [190–192]. The following is a summary of applications, including direct sampling on food surfaces.

Liu et al. demonstrated the paper spray analysis of a lemon peel surface [193]. Sampling was performed by direct wiping with methanol-wetted chromatographic paper (3x3 cm) on a lemon peel surface of 10 cm<sup>2</sup>. The dried paper was cut to a triangular shape and wetted with 10 µL of a methanol/water mixture and subsequently analyzed by PSI. A dominant peak of the protonated fungicide thiabendazole ( $5.2 \times 10^6$  counts) and the corresponding sodium adduct peak were observed.

Similarly, filter paper, commercially available medical and lens wipes, wetted with isopropyl alcohol, were employed for direct sampling on orange peel surfaces. Subsequent analysis on a portable mass spectrometer resulted in the detection of thiabendazole. The application of the filter paper produced the highest signal intensity, while the medical wipes yielded half the intensity. The use of lens wipes led to further decreased intensity. Ion signal was detected for 93, 60, and 38 seconds, respectively [194]. These experiments were performed in-situ in a local grocery store and can be viewed online (<https://www.youtube.com/watch?v=o88FMvVdMU>).

In another series of experiments, Whatman Grade I filter paper in combination with water and acetonitrile (80/20, *v/v*), including 0.1% formic acid modifier, was applied to screen for pesticides [195]. The results of the analysis of extracts deposited on filter paper were compared with the data obtained by direct surface sampling. A solvent volume of 20 µL on the paper triangle in combination with a voltage of +3.2 kV generated a stable spray for a duration of approximately one minute. A stainless steel holder (shown in Figure 13) for the paper triangle was made to fit into the nanoelectrospray ion source housing, which allowed adjustments in all three dimensions. A distance of 5 mm between the tip of the paper triangle and the mass spectrometer inlet was chosen. For analyte identification, MS<sup>2</sup> was employed.

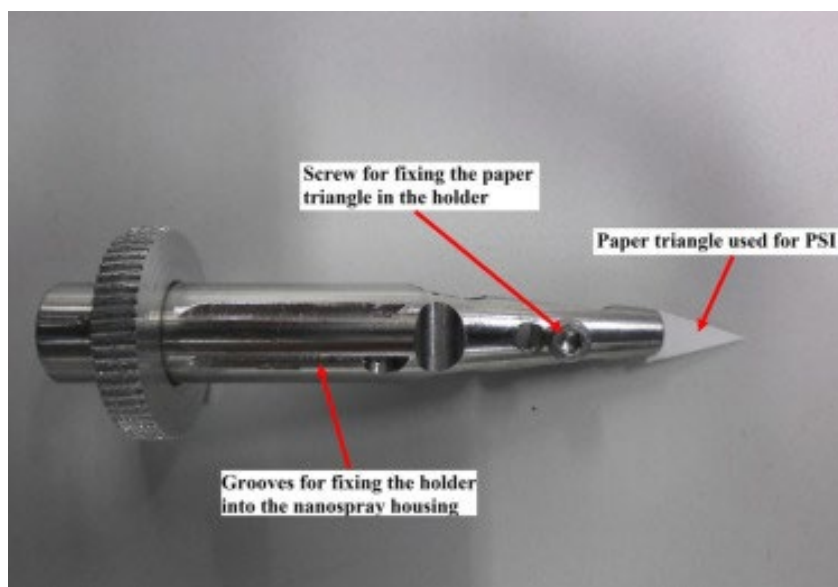


Figure 13 The stainless-steel holder allows to conduct PSI experiments. Reprinted with permission from reference [195]. Copyright © 2015, Elsevier.

For surface sampling, a 2 cm × 2 cm square piece of filter paper was cut and wetted with 50  $\mu$ L of the spray solvent. The entire surface area of the fruit was wiped for a duration of 20 seconds by applying gentle pressure on the filter paper. Afterwards, the filter paper was air-dried and cut to a triangular shape for the PSI analysis. For the analysis of food extracts, including homogenization, a knife mill was employed, and acetonitrile was added to yield a food extract, of which 5  $\mu$ L was directly applied on a filter paper triangle. The analysis of the food extract was reported to be more challenging due to strong matrix effects. The application of electrospray mode in PSI did not result in pesticide detection, however, the occurrence of atmospheric pressure chemical ionization (APCI) after the spraying solvent had dried out did allow for the detection of various pesticides in spiked extracts of tomato, orange, and grape. The analysis of imazalil and thiabendazole on oranges was compared using both extracts and surface sampling. Surface wiping produced a significantly higher S/N ratio for pesticide detection compared to the analysis of the food extract. In addition, imazalil and thiabendazole were detected on lime and grapefruit using the surface sampling method. The article concluded with a successful demonstration of rapid pesticide screening using PSI/MS<sup>2</sup>, but noted that matrix effects require further investigation [195].

Further literature describes the investigation of pesticide analysis of milk using PSI/MS<sup>2</sup> with a silica-coated paper substrate [196] and the analysis of fungicides in wine by paper capillary spray ionization [197]. Leaf spray is another ambient ionization technique applied in the qualitative and semi-quantitative pesticide analysis of food products. This method includes the preparation of plant material, such as pulp

or peel, to a triangular shape, and the direct application of solvent (1–15  $\mu\text{L}$ ) and an electric potential (2–5 kV) to generate ions by electrospray directly from plant tissue [198,199].

### 1.5.3 Summary of Pesticide Detection by Ambient Ionization

Several key findings regarding the application of ambient ionization techniques in pesticide analysis are concisely summarized:

- Numerous ambient ionization techniques including DESI, PSI, and leaf spray, have been successfully demonstrated for qualitative and semi-quantitative pesticide analysis.
- Surface sampling is rapid and facilitates detection of pesticides by reducing matrix effects.
- The analysis of food extracts is more challenging due to higher matrix effects.
- The analyte extraction of many ambient ionization methods is not well-studied.
- The choice of spray solvent and the addition of modifiers have an impact on adduct formation and signal intensity.
- Acquisition of quantitative data has been described as highly challenging.

## 1.6 Swab Spray Mass Spectrometry

A total of nine publications on swab spray mass spectrometry, eight of them focusing on applications of the method, have been presented over a period of four years from 2015 to 2019. Furthermore, two contributions from our group have been added to the table, resulting in a total of eleven articles focusing on swab spray mass spectrometry (summarized in Table 6).

Table 6 Summary of published work involving swab spray mass spectrometry as of February 2024.

publication title	year	analytes
direct drug analysis from oral fluid using medical swab touch spray mass spectrometry [114]	2015	various drugs
detection of strep throat causing bacterium directly from medical swabs by touch spray-mass spectrometry [200]	2015	bacterial phospholipids
medical swab touch spray-mass spectrometry for newborn screening of nicotine and cotinine in meconium [201]	2016	nicotine and cotinine
swab touch spray mass spectrometry for rapid analysis of organic gunshot residue from human hand and various surfaces using commercial and fieldable mass spectrometry systems [202]	2017	organic gunshot residues
analysis of human gliomas by swab touch spray-mass spectrometry: applications to intraoperative assessment of surgical margins and presence of oncometabolites [203]	2018	oncometabolites
analysis of residual explosives by swab touch spray ionization mass spectrometry [204]	2018	explosives
direct ion generation from swabs [205]	2018	fundamentals
quantitative swab touch spray mass spectrometry for oral fluid drug testing [206]	2019	various drugs
ambient ionization mass spectrometry: advances in monitoring clandestine activities,... (PhD thesis) [207]	2019	various
exploring a route to a selective and sensitive portable system for explosive detection– swab spray ionisation coupled to of high-field assisted waveform ion mobility spectrometry (faims) [208]	2019	explosives
analysis of pesticide residues on fruit using swab spray ionization mass spectrometry [88]	2023	pesticides
influence of solvent relative permittivity in swab spray mass spectrometry [209]	2024	fundamentals

As no commercial swab spray ion source is available, custom manufacture is required. It is necessary to optimize swab materials, solvents, and the electric potential to achieve consistent operational conditions. The following summary focuses on the material, methods, and ion source setups of previously demonstrated work, presented in chronological order.

A swab spray-based method was first demonstrated in February 2015 for analyzing drugs in oral fluids [114]. The detection of 14 drugs was accomplished through MS<sup>2</sup> and MS<sup>3</sup> experiments, with results obtained within a matter of minutes. Given that this application marks the beginning of swab spray mass spectrometry, the experimental setup is described in detail. The direct application of solvent flow to the swab head (Copan 160C) was achieved by using a fused silica capillary and a syringe pump. An electric potential of +6 kV was applied to the aluminum applicator to generate an electrospray emitting a Taylor cone at the tip of the swab head. The experimental setup is shown in Figure 14. Swab orientation, distance to the MS inlet and swab manufacturing deviations were described as the most important factors regarding signal intensity and reproducibility. To maintain reproducibility, the vertical swab position, in combination with a distance of 5–8 mm to the MS inlet, resulted in an average relative standard deviation of 33% (range 10–68%) for absolute ion intensity. This behavior was further described as independent of the analyte and its concentration. Different solvent combinations involving methanol, water, and acetonitrile were evaluated. Acetonitrile, in combination with 0.1% formic applied at a flow rate of 19  $\mu$ L/min to the swab head, delivered the best signal intensity [114].

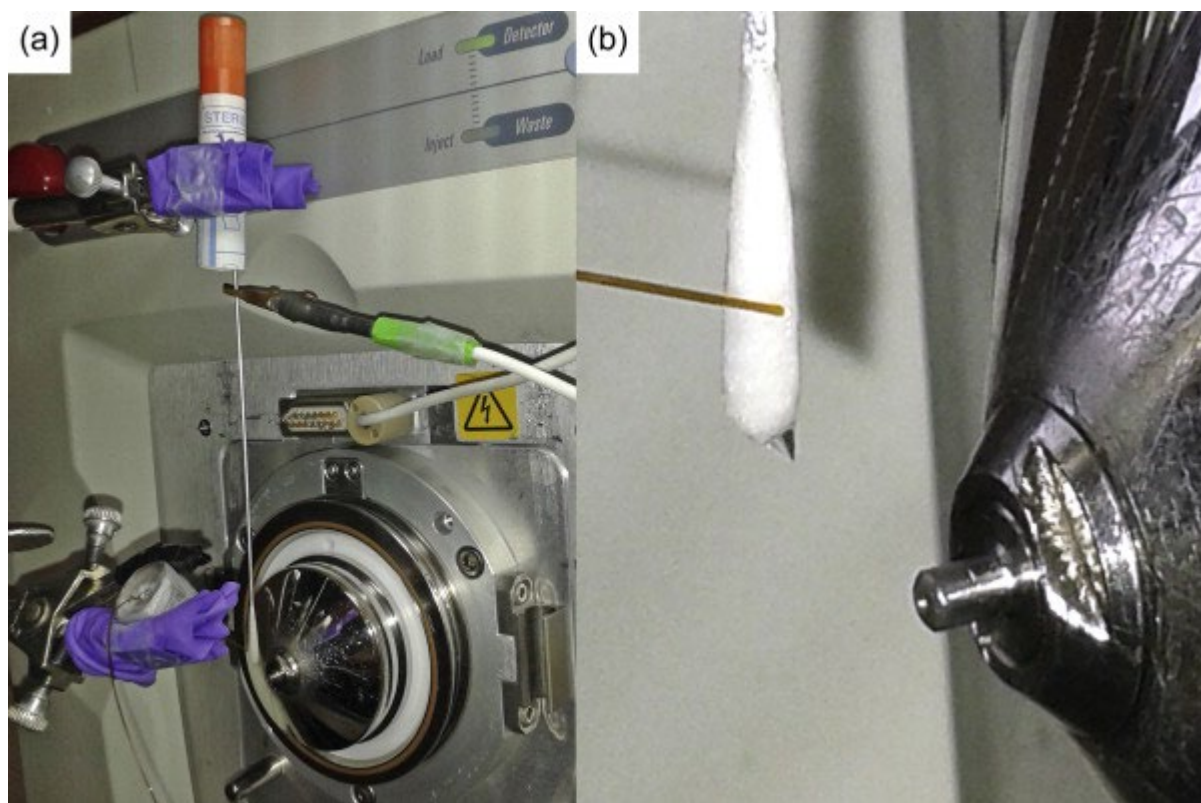


Figure 14 (a) Overview of the experimental setup at the front of the mass spectrometer inlet. (b) Emerging Taylor cone at the tip of the swab head during operation. Reprinted with permission from reference [114]. Copyright © 2015, Elsevier.

The development of a point-of-care application for diagnosing step-throat causing bacteria using swab touch spray mass spectrometry was published in October 2015. The setup involved methanol as the spray solvent, combined with an electric potential of -5 kV. Several swabs were evaluated for signal stability and background signals. Among these, the Copan 160C swabs, including an aluminum applicator, delivered the best results, surpassing polyester and cotton swabs. The swabs were used as received, without any pretreatment. Sampling was conducted *in vitro* on bacteria cultures and through simulated throat sampling, which included the addition of oral fluids to the swab. By directly adding solvent to the swab head using a pipette, a spray duration of 5-10 seconds was achieved. The full-scan data enabled the identification of bacteria based on their membrane lipids in both *in vitro* and simulated throat samples [200].

For newborn screening of nicotine and cotinine in meconium, a swab spray mass spectrometry-based method was developed [201]. The method involved the use of cotton swabs with a bamboo handle, which were positioned 8 mm away and 5 mm above the MS inlet. A potential of +4 kV was applied in combination with methanol and a 0.1% formic acid modifier. The bamboo handle was described as becoming conductive after the application of solvent to the swab head. 50  $\mu$ L methanol were

directly applied to the cotton head without a continuous solvent supply. The qualitative acquisition method allowed for the detection of nicotine and cotinine in quantities of few ng/g in meconium. This method was based on MS<sup>2</sup> experiments and the authors concluded that further research is required to improve the method to a quantitative level [201].

In a further publication, the qualitative analysis of organic gunshot residues by swab spray mass spectrometry, using Copan 160C swabs in combination with a varying methanol flow rate between 10–30 µL/min and an electric potential of +5.5 kV, was demonstrated as a rapid alternative to LC-MS based analysis [202]. Dry swabbing by approximately 20 circular motions was performed on different surfaces, including human skin, vinyl gloves, nitril gloves, and latex gloves. The limit of detection for methyl centralite and ethyl centralite, two organic gunshot residues, were described to be lower than 50 ng using a Thermo Fisher Scientific LTQ Orbitrap XL mass spectrometer. Furthermore, the method was deemed compatible for in-situ mass spectrometry using a homebuilt Mini 12 ion trap mass spectrometer [202].

Another application involves the detection of human oncometabolites in human tissues using swab touch spray mass spectrometry [203]. Sample collection was performed by gentle swabbing (using Copan 160C) on human tissue samples. Subsequent ion generation occurred by applying a solvent mixture of acetonitrile/DMF/ethanol (45/5/50, *v/v*) along with an electric potential of -6.5 kV. Additionally, octyl β-d-glucopyranoside at a concentration of 250 ng/mL was added to the spray solvent to facilitate the solvent flow on the sample. Furthermore, N-acetylaspartate-d<sub>3</sub> (a deuterated oncometabolite) at a concentration of 10 µg/mL was added to the spray solvent as an internal standard. This addition aimed at compensation of swab irregularities and minor variations in positioning, but it did not correct for signal suppression caused by matrix effects. During analysis, a solvent flow rate of 25 µL/min was applied to achieve a consistent electrospray. The ion source featured an upward bent extended inlet capillary (as shown in Figure 15), which improved spray stability at the cost of ion transmission [203].



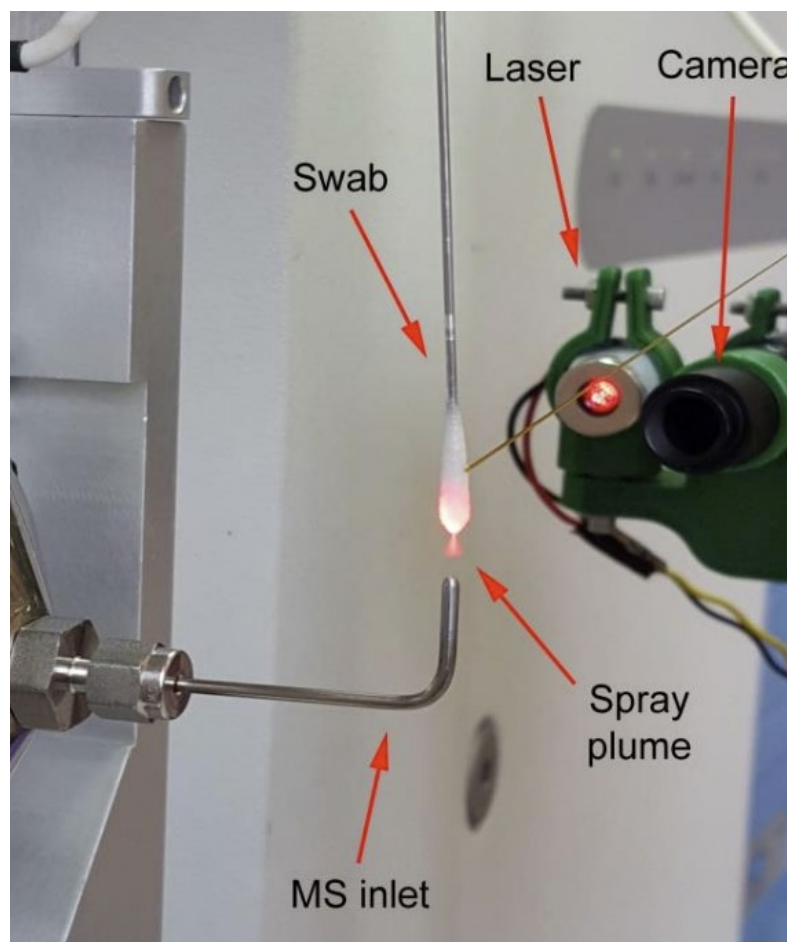


Figure 15 Custom-built swab spray ion source. Reprinted with permission from reference [205]. Copyright © 2018, Elsevier.

In 2018, the analysis of residual explosives by swab spray mass spectrometry highlighted another forensic application [204]. Sampling was performed by prewetting Copan 160C swabs with 20  $\mu\text{L}$  of acetonitrile, in combination with circular movements on the sample surface. Tested surfaces included glass, PTFE, stainless steel, polyethylene, vinyl glove, nitrile glove, latex glove, and human skin. For analysis, the swab was positioned 5–10 mm above the mass spectrometer inlet. For spray generation, a varying acetonitrile flow of 10–30  $\mu\text{L}/\text{min}$  was combined with a potential of  $\pm 5.5$  kV. Analyte identification was based on  $\text{MS}^2$  experiments, with approximate LODs ranging from 1 pg to 100 ng, depending on type of explosive and sample surface material [204].

In a more detailed study, the focusing was on the solvent effects during spray generation [205]. The experimental setup, as depicted in Figure 15, involved positioning the swab head 5–8 mm above the modified inlet. The data presented in this section were obtained using Copan 160C swabs. The study explored a wide range of solvents, spanning from hexane to DMF (as shown in Table 7). Deviations in swab manufacturing did not allow to report exact onset values for each solvent. Therefore,

the onset potential was given in a range of  $\pm 0.5$  kV. For example, the onset potential of acetonitrile ( $6.0 \pm 0.5$  kV) was reported to be higher than the onset value of methanol ( $5.5 \pm 0.5$  kV). This difference was explained by the higher surface tension of acetonitrile. The addition of solvents with low surface tension to reduce the onset potential was described as an effective way to lower the onset potential. However, it was recognized that this effect is nonlinear and difficult to predict. The addition of more than 5% of deionized water to the spray solvent resulted in discharging events (Figure 16 E), which can be attributed to the increased surface tension. The use of pure DMF was also responsible for discharging events. Contrary to expectations, the addition of octyl  $\beta$ -D-glucopyranoside surfactant to the spray solvent did not significantly reduce the onset potential [205]. Higher potentials necessitated an increase in the flow rate. However, for solvents with lower surface tension and viscosity, the solvent flow rate had to be reduced accordingly. When using hexane or chloroform, a stable spray generation was not achievable, which was attributed to rapid solvent evaporation on the swab head.

Table 7 The solvent effects on onset potential, spray mode, and flow rate using both the positive and negative ionization mode. Reprinted with permission from reference [205]. Copyright © 2018, Elsevier.

Solvent	Positive Ionization Mode				Negative Ionization Mode			
	Onset Voltage (kV)	Spray Mode	Surfactant*	Solvent Flow Rate ( $\mu\text{L}/\text{min}$ )	Onset Voltage (kV)	Spray Mode	Surfactant	Solvent Flow Rate ( $\mu\text{L}/\text{min}$ )
Acetone	$5.5 \pm 0.5$	Cone jet	n/a**	$35 \pm 3$	$5.75 \pm 0.5$	Cone jet	n/a	$35 \pm 3$
ACN	$6.0 \pm 0.5$	Cone jet	Insoluble	$15 \pm 3$	$> 5.75$	Pulsating	Insoluble	$> 18$
Chloroform	$5.5 \pm 0.5$	Cone jet; pulsating	n/a	$8 \pm 3$	$> 6.0$	Pulsating alternated with ramified Jet	n/a	$> 5$
Dichloromethane	$> 5.0$	Pulsating	n/a	$> 5$	$> 5.5$	Pulsating	n/a	$> 5$
DMF	$6.25 \pm 0.5$	Cone jet	nsd***	$5 \pm 3$	$> 5.75$	Pulsating; discharging	nsd	–
Ethanol	$5.5 \pm 0.5$	Cone jet	nsd	$20 \pm 3$	$6.0 \pm 0.5$	Cone Jet	nsd	$25 \pm 3$
Ethyl acetate	$5.5 \pm 0.5$	Cone jet	n/a	$25 \pm 3$	$> 5.75$	Pulsating; discharging	nsd	–
Isopropyl alcohol	$5.5 \pm 0.5$	Cone jet	n/a	$15 \pm 3$	$6.0 \pm 0.5$	Cone jet	nsd	$20 \pm 3$
Hexanes	$> 5.0$	Pulsating	nsd	$> 35$	$> 5.0$	Pulsating	nsd	$> 35$
Methanol	$5.5 \pm 0.5$	Cone jet	nsd	$15 \pm 3$	$6.5 \pm 0.5$	Ramified jet alternated with cone jet	nsd	$18 \pm 3$

\* Octyl  $\beta$ -D-glucopyranoside (Conc  $\leq 250$  ppm).

\*\* n/a = not tested.

\*\*\* nsd = not significantly different.

In addition to Copan 160C swabs, several Puritan medical swabs with an aluminum applicator and different head materials were tested. The onset potentials were similar to those found for the Copan 160C swabs, however, different flow rates were required to maintain continuous operation with a stable spray. Furthermore, electrostatic dissipative (ESD) plastic handle swabs with a polyurethane head were examined. These swabs yielded inferior results in terms of spray stability and signal intensity [205].

Microscopic videography was employed to describe the electrospray formation on the swab head. It was differentiated between pulsating mode, stable cone-jet, and ramified cone-jet. While conductivity (which was not tested in this study), surface tension, and flow rate of the solvents play crucial roles, the electric field strength was found to also contribute to observable changes in electrospray formation. However, correlations between different spray modes, ion yields, and solvent properties were not established. The use of isopropanol exhibited the longest jet among all tested solvents (as shown in Figure 16 C). Additionally, the swab background signal was also considered to be solvent-dependent [205].

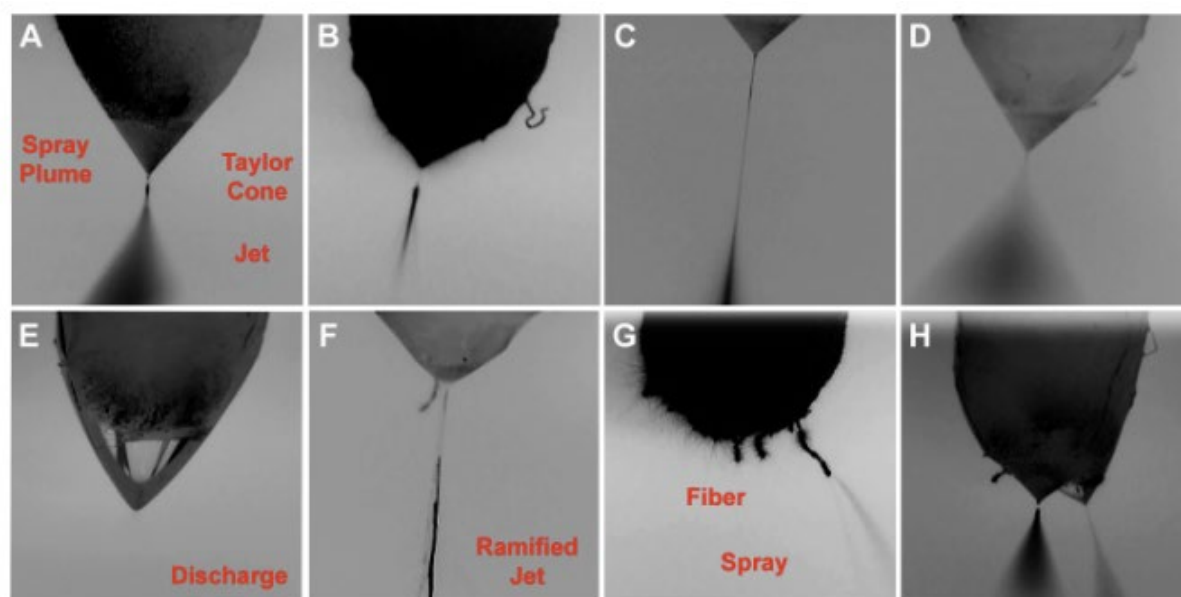


Figure 16 Photographs of electrospray generated from Copan rayon swabs, a red laser pointer was used to illuminate the electrospray plume. (A) Ethanol doped with 0.25 mg/mL of octyl  $\beta$ -D-glucopyranoside, voltage +5.5 kV. (B) Ethanol, voltage +5.5 kV. (C) Isopropyl alcohol, voltage +6.0 kV. (D) Ethanol doped with 0.25 mg/mL of octyl  $\beta$ -D-glucopyranoside, voltage -6.25kV. (E) DMF, voltage -6.5kV. (F) Acetone-acetonitrile 50:50,v/v, voltage -6.5kV. (G) Acetone, voltage +5.5kV. (H) Acetone, voltage +5.5kV. Reprinted with permission from reference [205]. Copyright © 2018, Elsevier

Protruding fibers can lead to a spray mode termed as fiber spray (as shown in Figure 16 G). Unfortunately, this mode was reported to yield negligible signal intensity only. Occasionally, the formation of multiple jets (as visualized in Figure 16 H) was observed. The addition of surfactants did enlarge the spray plume angle, but it did not improve the signal intensity. However, the swab positioning was facilitated alongside with an improved reproducibility (Figure 16 A/D versus Figure 16 B). The mixing of DMF, which exhibits a high surface tension, with ethanol or acetone to decrease the overall surface tension, was described as an effective strategy to obtain a stable Taylor cone. Additionally, for methanol, acetonitrile, and chloroform, the observation of ramified and pulsed modes was mentioned (Figure 16 F). In connection with this

phenomenon observed in particular solvents, minor deviations in the dimension of the Taylor cone resulted in transitions between cone, pulsating, and ramified jet modes. The presence of the cone-jet mode is critical for signal stability, as pulsating or ramified modes do not yield significant signal intensity. Beside swab deviations, the results in this study were described to be of high reproducibility. The development of swab spray-based techniques necessitates thorough solvent evaluation. Therefore, the visual observation of the spray formation becomes an important tool to optimize the solvent conditions to achieve a stable cone jet electrospray [205].

In 2019, a quantitative swab touch spray method for oral fluid drug testing was presented. This method utilized volumetric Mitra devices in conjunction with an adapted mass spectrometer inlet as depicted in Figure 17. The spray solvent, applied at a flow rate of 5  $\mu\text{L}/\text{min}$ , consisted of a combination of acetonitrile/isopropanol (50/50, *v/v*), including both 0.1% formic acid and 500 ng/mL of octyl  $\beta$ -D-glucopyranoside as surfactant. The surfactant was added to reduce the surface tension and to further improve the spray stability. For electrospray formation, an electric potential of +7 kV, was directly applied to the Mitra device from an external power supply through a metallic curved teasing needle. Five-points calibration curves were established in the range of 25 ng/mL to 1000 ng/mL. Deuterated compounds were used to compensate for matrix effects originating from oral fluids. The volumetric Mitra device allowed exact sampling of 10  $\mu\text{L}$  of fluid, which further facilitated quantitation over swab sampling. The method, which allowed screening for 30 drugs in under two minutes, was described to produce acceptable values in precision, accuracy, reproducibility, and carryover effects [206].

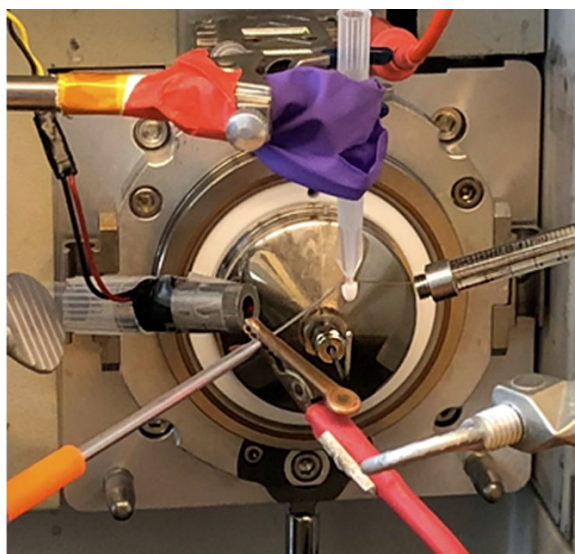


Figure 17 Electro spray generation using volumetric mitra devices. Reprinted with permission from reference [206]. Copyright © 2018, Elsevier

Another study investigated swab spray-based detection of explosives and found that using swab spray resulted in slightly better performance compared to PSI. This improvement was attributed to enhanced sample collection capabilities and cleaner backgrounds. In the study, sodium chloride and ammonium nitrate were added to the methanol spray solvent to facilitate the formation of adducts. The swab heads consisted of Nomex material, but the design of the swab spray ion source was not further explicated. [208].

Crucial insights from the discussed swab spray methods are summarized below:

- The design of a swab spray ion source must incorporate proper swab fixation at an optimal distance from the mass spectrometer inlet. Additionally, it should facilitate the application of solvent and electric potential to the swab head.
- Several studies originating from the Aston research laboratory have employed a custom-made extension for the mass spectrometer inlet to enhance swab spray stability, albeit at the expense of signal intensity.
- For a limited duration, swab spray can be performed by direct solvent deposition on the swab head using a pipette. However, to achieve continuous operation, the application of solvent flow via a capillary and syringe pump is required.
- To generate a stable spray, the solvent flow rate and electric potential—which depend on the swab material and solvent—must be elaborated upon. Additionally, the swab background is also solvent-dependent

- Swab materials that include a conductive applicator are advantageous. In particular, Copan 160C swabs have been described as a highly valuable swab material.
- The surface tension of solvents was reported to play a crucial role in spray stability and reproducibility. Therefore, the addition of surfactants was regularly performed based on analyses conducted at the Aston research laboratory.
- The use of an internal analyte directly added to the spray solvent can only be considered to compensate either for matrix effects or swab irregularities.

Further research into the investigation of solvent properties and their impact on spray mode, stability, and jet length is essential. A deeper understanding will enhance the ability to predict solvent behavior in swab spray mass spectrometry, thereby facilitating method development and optimization. The potential use of swab spray mass spectrometry in pesticide detection, which has not yet been reported, may offer a promising avenue for food analysis.

## 2 Results and Discussion

### 2.1 Swab Spray Ion Source Construction

As ion sources designed for swab spray mass spectrometry are not commercially available, the construction of a custom swab spray ion source had to be realized. The high-resolution Thermo Fisher Scientific LTQ Orbitrap Velos served as the mass spectrometer. The new ion source was built on the basis of a Thermo Fisher Scientific nanospray source housing. As the original nanospray ion source did not allow the application of voltages higher than +3 kV without the occurrence of audible discharge events inside the source voltage plugs, the electrical connections had to be rebuilt and relocated. Plugs were eliminated as far as possible, and the wiring of the ion source voltage was directly fed to the swab by a Teflon-insulated wire.

The modified ion source allowed for potentials up to +6.5 kV. Still, manipulation during operation had to be made carefully, as the ion source housing was not completely enclosed. The swab holder was constructed from two small grooved square metal plates held together by screws (Figure 18). To switch swabs, the pressure between the metal plates was released by turning both screws 90 degrees. The swab holder allowed robust swab fixation and swab mounting/demounting in less than half a minute. Swab positioning was achieved by the 3-axis translational stage, which was part of the Thermo Fisher Scientific nanospray ion source. On top of the ion source housing a camera was placed, which served for spray observation. Illumination for the camera was achieved by a red LED on the bottom of the ion source housing.

Swab spray mass spectrometry is preferably used in combination with a continuous solvent supply directly applied to the swab head. Thus, a 3-axis translational stage was mounted on the left of the ion source housing to hold the solvent capillary in place. The solvent capillary was adjusted for direct solvent delivery onto the swab head, as illustrated in Figure 18. To ensure safety for the operator, the capillary system was upstream grounded on the injection valve of the mass spectrometer. A PEEK capillary was utilized with an outer diameter of 1/16" and an inner diameter of 0.13 mm. This configuration resulted in low upstream currents (less than 1  $\mu$ A, when using methanol) and no clogging issues. The solvent was delivered using a Harvard Apparatus syringe pump, which was placed on top of the mass spectrometer.



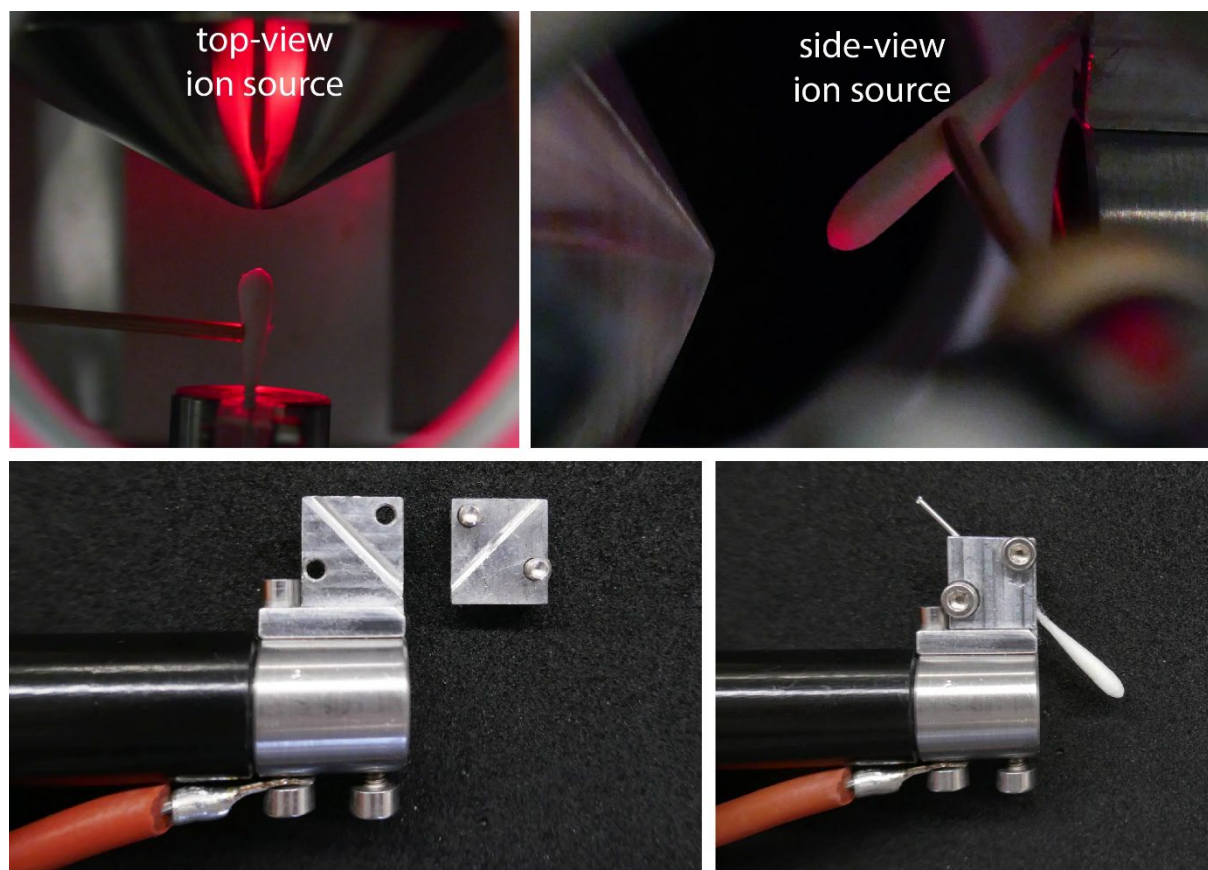


Figure 18 Top row: View inside the swab ion source from the top and from side. Bottom row: Demounted swab holder on the left and mounted swab holder on the right.

The entire swab spray system mounted on a Thermo Fisher Scientific LTQ Velos mass spectrometer is depicted in Figure 19. For illustration of swab spray performance, the top-mounted camera was replaced by a green flashlight, and pictures were taken from the ion source opening on the right side.



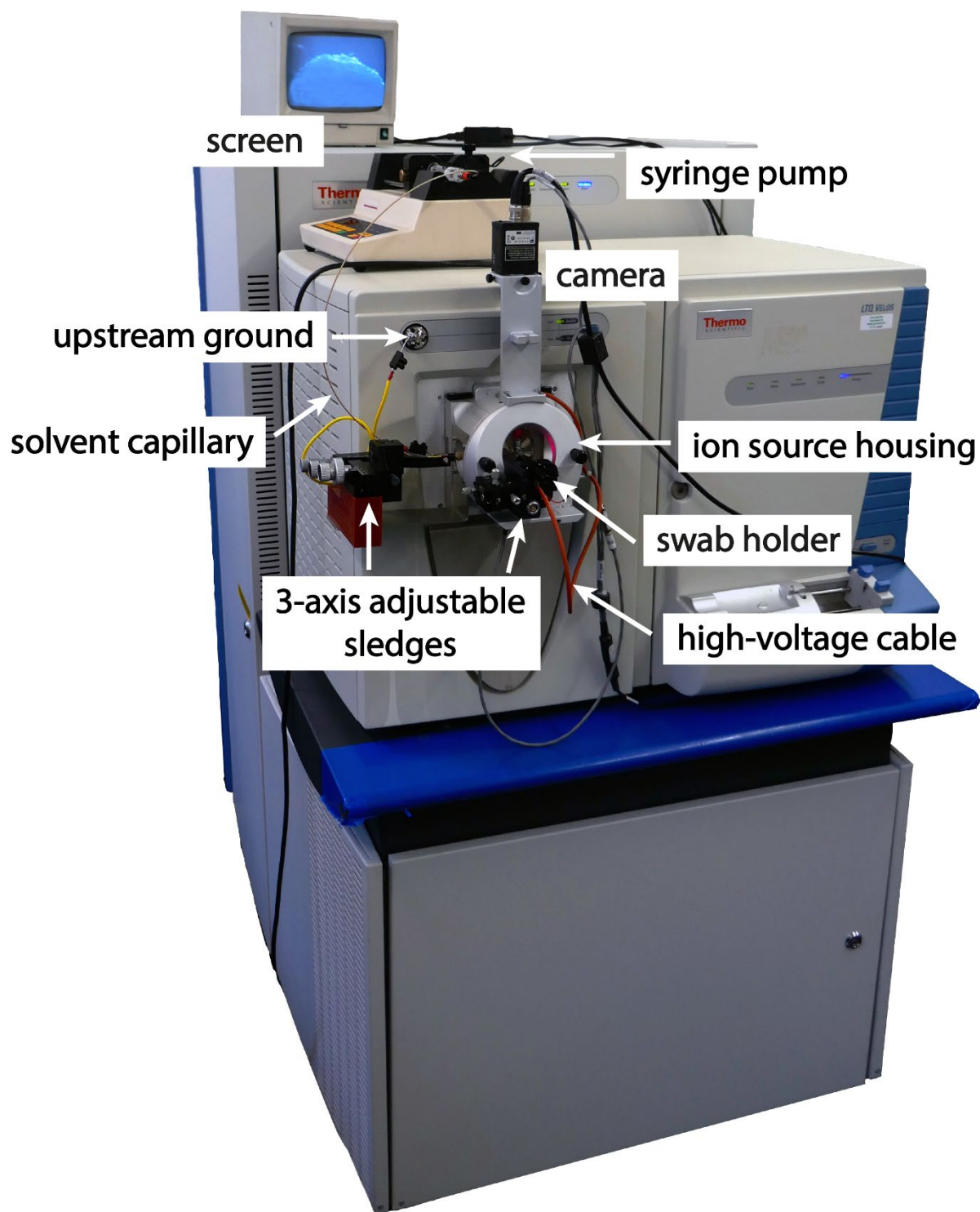


Figure 19 Overview of the system: the swab spray ion source, along with its solvent supply, is attached to the Thermo Fisher Scientific LTQ Orbitrap Velos mass spectrometer.

## 2.2 Initiation of Swab Electrospray

In conventional electrospray ionization, the Taylor cone emerges from the tip of the needle. In swab spray ionization, the Taylor cone evolves at the swab tip as depicted in Figure 20. At the apex of the Taylor cone, the jet region expands and subsequently breaks up into the spray plume, where the ionization process occurs.

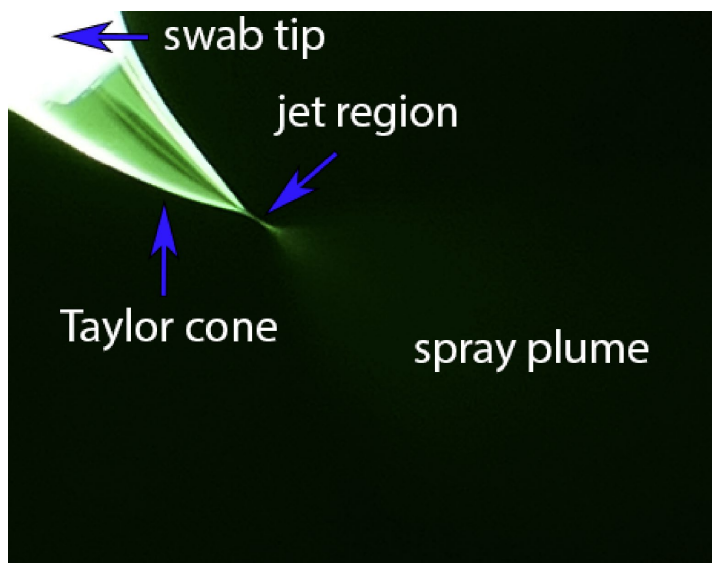


Figure 20 Photograph of an electrospray generated on a swab tip, including Taylor cone, jet region, and spray plume.

For the initiation of electrospray, it is essential to accumulate a sufficient amount of solvent at the swab tip. If the electric potential (+5 kV) and solvent flow (methanol at 45  $\mu\text{L}/\text{min}$ ) were activated simultaneously, spraying often occurred through small fibers or the solvent capillary. Consequently, the solvent supply was initiated first, allowing for the accumulation of solvent on the swab head. Upon confirmation of adequate solvent accumulation via the top-mounted camera, the electric potential was applied. The optimal scenario for electrospray initiation is depicted in Figure 21, illustrating the gradual formation of the Taylor cone. No pulsation events were observed and no solvent droplets were dispersed. The seamless transition of the solvent depot into a Taylor cone is imperative for reproducibility. The operator's proficiency in visual observation is essential for achieving consistent reproducibility.

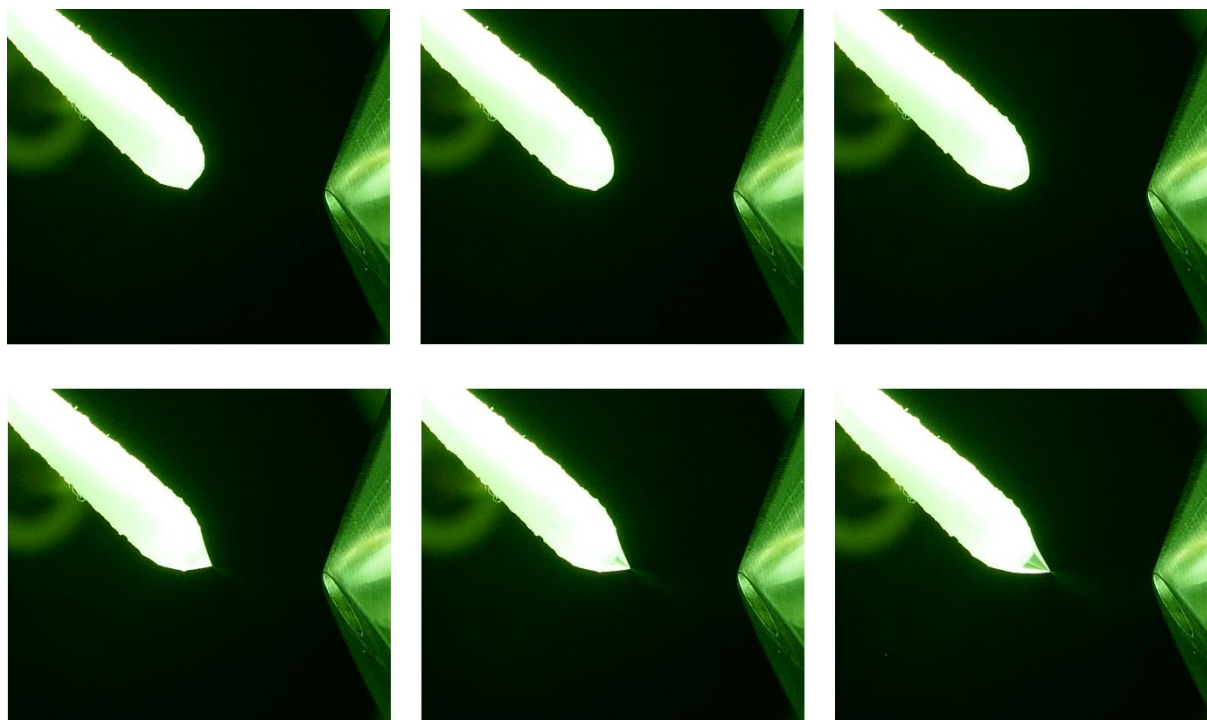
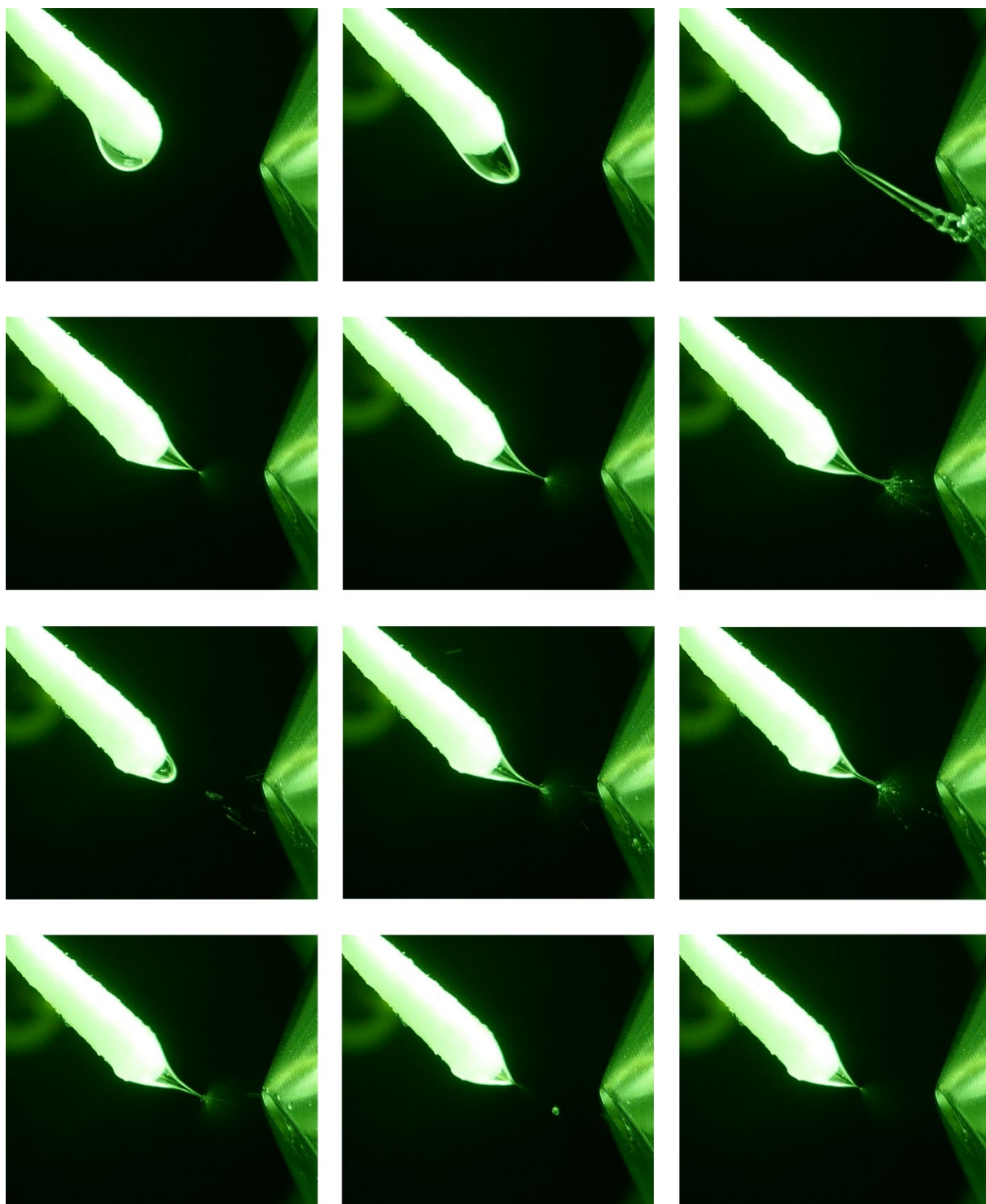


Figure 21 Initiation of swab spray in the optimum scenario. The series of picture was recorded at 30 fps. Each picture depicts a single frame and is following one after another.

If too much solvent accumulated before the electric potential is applied, instabilities can occur. This effect is visualized in Figure 22. The large solvent depot cannot effectively convert into a Taylor cone, and solvent is directly ejected and lost at the counter electrode. The loss of solvent includes dissolved analytes, which significantly decreases the reproducibility. Although a Taylor cone is subsequently formed, further instabilities occur. The jet region expands in width and length, adopting a spindle-like shape, before collapsing. This pulsation mode is termed as spindle mode [25–29]. The spindle mode is accompanied by solvent splashes and microdroplets, which are responsible for the loss of solvent that is associated with the loss of analyte molecules. Additionally, the spindle mode does not allow efficient ionization as the spray plume is irregular and diminished in size. The ionization efficiency is low if pulsation occurs. Therefore, pulsation events must be prevented to achieve decent reproducibility and sensitivity. Further details of the spindle mode observed in swab spray mass spectrometry are explicated in the publication discussing the relative permittivity of spray solvents [209].

Figure 21 depicts the optimum situation for swab spray formation, and Figure 22 illustrates the worst-case scenario. The initiation quality can lie within the range exemplified by these two extremes. Also, minor pulsation events or small solvent splashes can occur. These findings on spray initiation refer to the positive ionization

mode. The application of negative potentials could not be achieved due to technical difficulties with the mass spectrometer.



*Figure 22 A series of pictures illustrates the effects during swab spray initiation when too much solvent was accumulated before the electric potential was applied. The series of pictures was recorded at 30 fps. Each picture depicts a single frame and follows one after another.*

## 2.3 Counter Electrode Set-up

In the Aston laboratory at Purdue University, an extended and bent ion transfer capillary was employed, resulting in reduced signal intensity, as described in the introduction. Our swab holder design permits the fixation of swabs at a 45-degree angle, enabling solvent accumulation at the swab tip. This arrangement allows for the use of the genuine Thermo Fisher Scientific ion transfer capillary, thereby maintaining sensitivity.

The electric field is established between the swab and the counter electrode, which may be either the ion sweep cone or the ion transfer capillary if the cone is removed. It was examined whether the influence of the counter electrode on the electric field affects the Taylor cone formation in our setup. Figure 23 illustrates the Taylor cone using Copan 160C swabs, combined with an electric field of +5 kV and methanol + 0.1% formic acid as the spray solvent, at a flow rate of 45  $\mu\text{L}/\text{min}$ , employing both the ion sweep cone and the ion transfer capillary as the counter electrode.

The alteration in the electric field geometry did not result in significant differences in either the Taylor cone formation or the spray plume, both of which evolved similarly in the two setups. The fact that the Taylor cone on the right side of Figure 23 appears elongated is attributed to a slight variation in electric field strength. Minor discrepancies in electric field strength arise from subtle changes in the distance between the swab tip and the counter electrode. Nonetheless, the signal intensity was found to be comparable. More importantly, the ion sweep cone effectively prevents contamination and potential clogging of the ion transfer capillary. This is particularly crucial for samples with a dense matrix. In instances where contamination of the ion sweep cone occurred, a significant reduction in signal intensity was observed. Consequently, it was decided to consistently utilize the ion sweep cone. Nonetheless, regular cleaning of both the ion sweep cone and the ion transfer capillary through ultrasonication in methanol had to be performed.



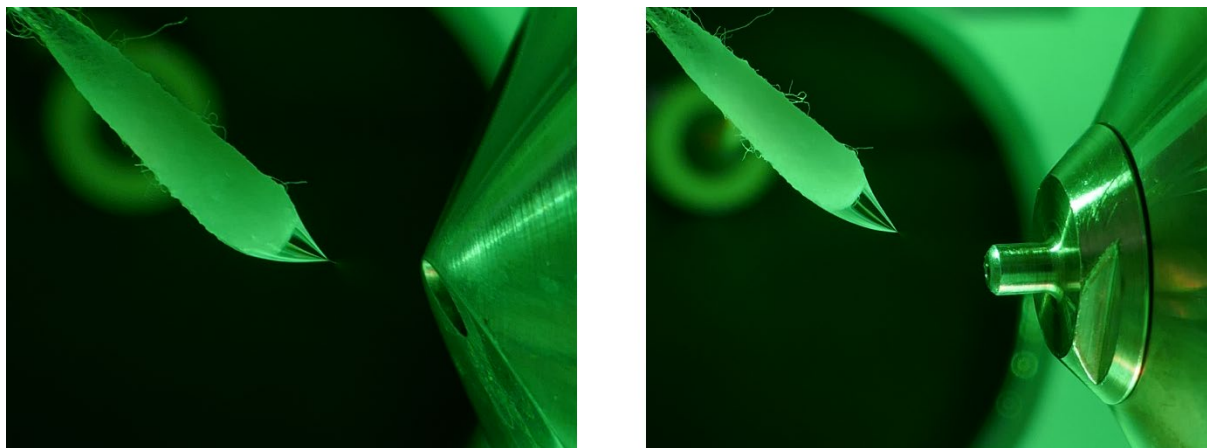


Figure 23 On the left, electrospray with mounted ion sweep cone. On the right, electrospray with bare ion transfer capillary.

## 2.4 Swab Positioning

The horizontal distance of the swab to the ion sweep cone, which serves as the counter electrode, is a crucial ion source parameter. It affects signal intensity and must be chosen responsibly to prevent electric discharges while maintaining signal intensity. Different horizontal distances from the swab to the counter electrode were probed using Copan 160C swabs and methanol with a 0.1% formic acid modifier as the spray solvent at a flow rate of 45  $\mu\text{L}/\text{min}$ . The resulting electrosprays are depicted in Figure 24. A longer distance from the swab to the counter electrode provides more room for the spray plume to develop. As the ionization process occurs within the spray plume, it is reasonable to assume that ample space is necessary for the cascades of solvent evaporation and Coulomb fission, which result in the generation of gas-phase ions. On the contrary, if the spray plume is excessively distant from the orifice, the formed ions may become too remote to be adequately drawn into the electrospray interface.

A distance of less than 6 mm significantly elevates the risk of electrical discharge. While reducing the electric potential may prevent discharges, it complicates the formation of the electrospray and constrains the space available for the ionization process. Indeed, markedly low signal intensities were recorded when the distance was set below 6 mm. The distance for optimal signal intensity was determined to be between 6 and 8 mm. This range represents a sweet spot that precludes electrical discharges while promoting electrospray formation, ensuring the spray plume has sufficient space for ionization without becoming overly distant from the inlet. In contrast, a distance of 11 mm was found to substantially reduce signal intensity. As depicted in Figure 24, the expansive spray plume extended significantly above and below the mass spectrometer's inlet, resulting in ion loss.

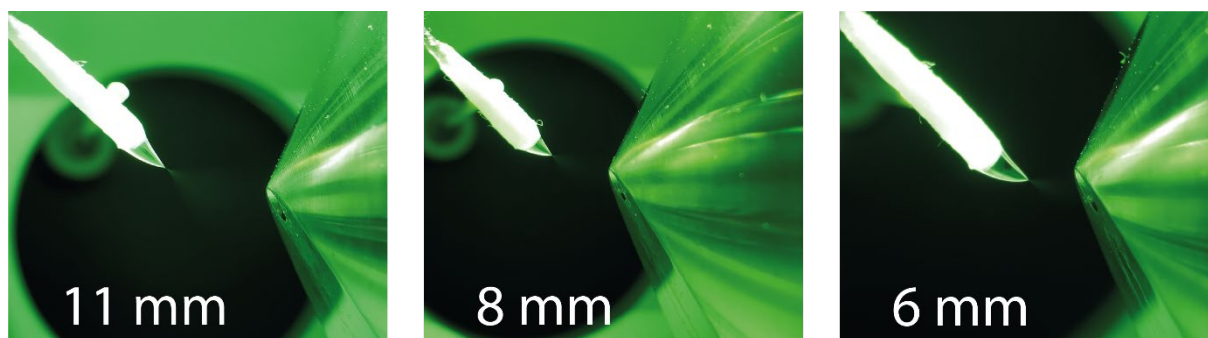


Figure 24 Illustration of different horizontal alignments.

Small variations in the vertical swab position did not result in different signal intensities. It was reported that in conventional capillary-based electrospray ionization, the distance from the spray capillary to the orifice had a greater impact on signal intensities than horizontal variations as well [210].

The addition of the non-ionic surfactant octyl  $\beta$ -D-glucopyranoside at a concentration of 250 ppm was described to produce wider spray plumes, which facilitated swab positioning and increased reproducibility [205]. However, in our experiments, the use of octyl  $\beta$ -D-glucopyranoside at the specified concentration did not manifest a visual influence on the spray plume. On the contrary, an intense peak corresponding to the sodium adduct of octyl  $\beta$ -D-glucopyranoside was detected at  $m/z$  315.18. A compound present at a concentration of 250 ppm may exert a suppressive effect on the ionization of other analytes. Consequently, the decision was made to proceed without surfactants, as the spray plume exhibited adequate properties without surfactants.

## 2.5 Evaluation of Swab Material

As there is no designated swab material available for applications involving swab-based ambient ionization methods, evaluating various swab materials was essential. The tested swabs encompass different head materials such as rayon, cotton, polyester, and polyurethane, as well as handles made of aluminum or polypropylene. Figure 25 depicts the tested swabs, and Table 8 lists their corresponding data, including number, manufacturer, item number, material, dimensions, and shape.

Evaluation of swabs encompassed key criteria crucial for swab spray mass spectrometry, including solvent resistance, electrospray stability, background signals, dimensions/shape, and ease of use. Several solvents were used during the evaluation, all of which contained 1 ppm of salicylanilide as a suppression marker (SM). The suppression marker aids in demonstrating the ionization performance. The background signals of swabs are of paramount importance. A pronounced swab background can hinder ionization and preclude the detection of analyte molecules. Moreover, minimizing background peaks is crucial to facilitate proper precursor isolation and prevent the co-isolation of background peaks, which can yield misleading CAD spectra. To compare the background ions of various swabs and solvents, three-dimensional plots depicting relative ion intensity over time are provided.



Table 8 List of all tested swab materials, including their specifications.

number	manufacturer	item number	material (head, handle)	dimension in mm (max width, length) *	shape
1	Copan, Italy	160C	rayon, aluminium	2.5, 16	round
2	Applimed SA, France	1901199	cotton, aluminium	2.8, 18	round
3	Ideal-tek, USA	IT38140	polyester, polypropylene	3.5, 11	elliptic
4	Ideal-tek, USA	IT38040	polyester, polypropylene	3.5, 12	elliptic
5	Ideal-tek, USA	IT38540	polyester, polypropylene	3.5, 11	flat
6	Ideal-tek, USA	IT48040	polyurethane, polypropylene	3.3, 10.5	round
7	Ideal-tek, USA	IT44070	polyurethane, polypropylene	3.0, 10.5	pointed
8	Chemtronics, USA	CF4050	polyurethane, polypropylene	4.0, 12.5	round

\*Small manufacturing deviations may occur.

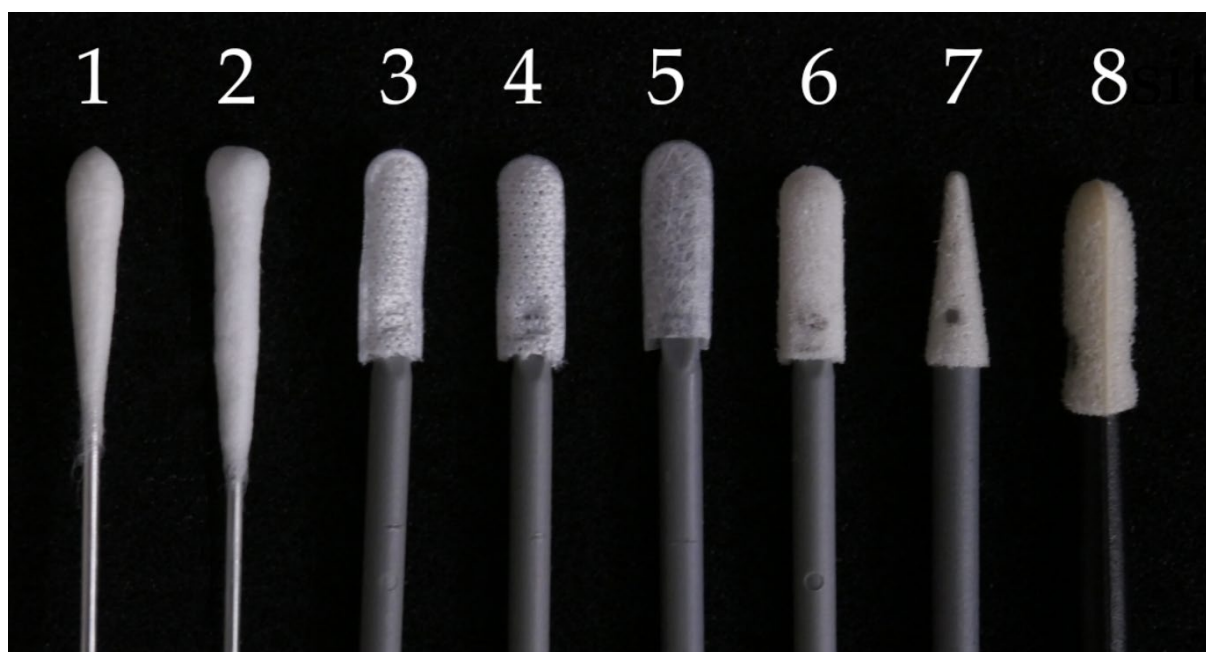


Figure 25 Overview of tested swab materials

The conductive aluminum handles, featured in swabs produced by Copan and Applimed, facilitate the direct connection of the electrical potential to the swab head. On the other hand, swabs with non-conductive polypropylene handles, found in products by Ideal-tek and Chemtronics, necessitate the attachment of a wire to connect the ion source's electric potential to the swab head, introducing an additional step in swab handling.

The Copan 160C swabs (#1 in Figure 25) were evaluated as the optimal choice for swab spray mass spectrometry. The integrated aluminum applicator ensures ease of handling, while the round and smooth rayon swab head enables electrospray formation with high reproducibility and stability. Electrospray formation on Copan 160C swabs is illustrated in Figure 30 (a) on page 61. The background signal of Copan 160C swabs is significantly influenced by the spray solvent. Notably, a mixture of ethyl acetate/methanol (70/30, *v/v*) with a 0.1% formic acid modifier yielded the fewest background ions. However, a significant drawback was the inconsistency in background levels across different swabs. For instance, a specific swab exhibited significant background ions at the onset of the spray, resulting in the suppression of the salicylanilide marker, as illustrated in Figure 26 (top). After one minute of spraying, the background ions diminished, allowing the suppression marker to become visible at  $m/z$  214.09. To prevent analyte suppression by swab background ions, a brief prewashing procedure using ethyl acetate and ultrasonication for two minutes was applied. The effect of swab prewashing is illustrated in Figure 26 (bottom). The suppression marker is now visible at the initiation of the spray. Two peaks, visible at  $m/z$  89.06 and  $m/z$  111.04, are related to the proton and sodium adduct of ethyl acetate, which did not cause relevant analyte suppression. In addition, no issues were observed regarding solvent resistance even with the head material apparently attached by adhesives. The effect of swab prewashing and solvent selection is further thematized in the publication titled "Analysis of Pesticide Residues on Fruit Using Swab Spray Ionization Mass Spectrometry" [88].

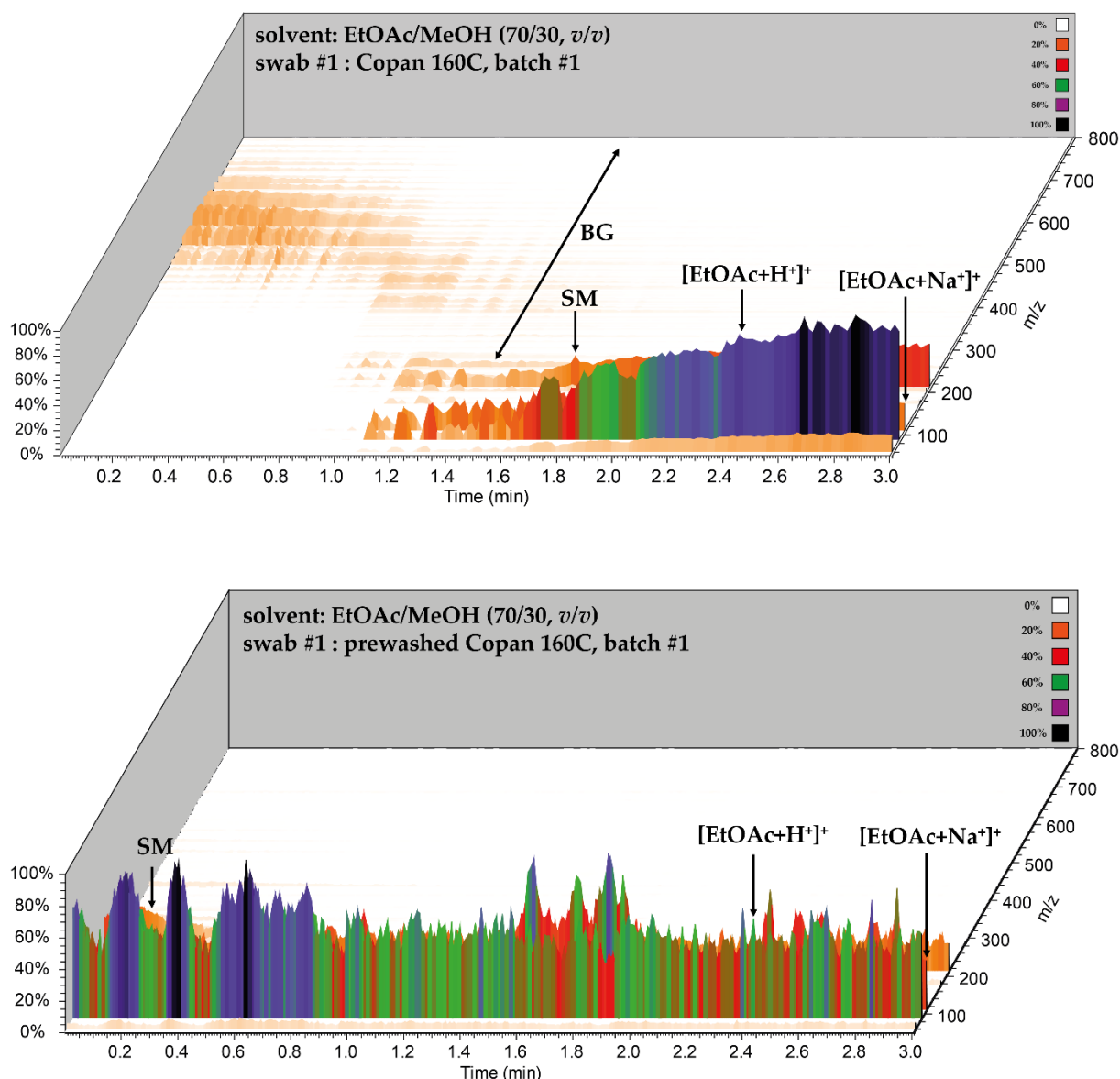


Figure 26 Visualization of swab backgrounds using Copan 160C swabs without prewashing (top) and after prewashing (bottom) using ethyl acetate/methanol (70/30, *v/v*) as the spray solvent.

The second batch of Copan 160C exhibited the same background behavior as the first batch. But the third batch demonstrated a divergent response regarding the correlation between spray solvent and signal background. Reducing the background by a prewashing procedure did not yield the previously achieved low background. The swabs displayed a consistent background across various spray solvents, as depicted in Figure 27, which illustrates the background for acetonitrile (top), trichloromethane/methanol (80/20, *v/v*) (center), and acetone/methanol (80/20, *v/v*) (bottom). Each solvent combination included 0.1% formic acid and salicylanilide as the suppression marker. All solvents produced several background peaks, potentially interfering with the identification and isolation of precursor ions. More importantly, the suppression marker at *m/z* 214.09 is present with adequate peak abundance,

indicating that the presence of background ions does not impede proper ionization of the analytes.

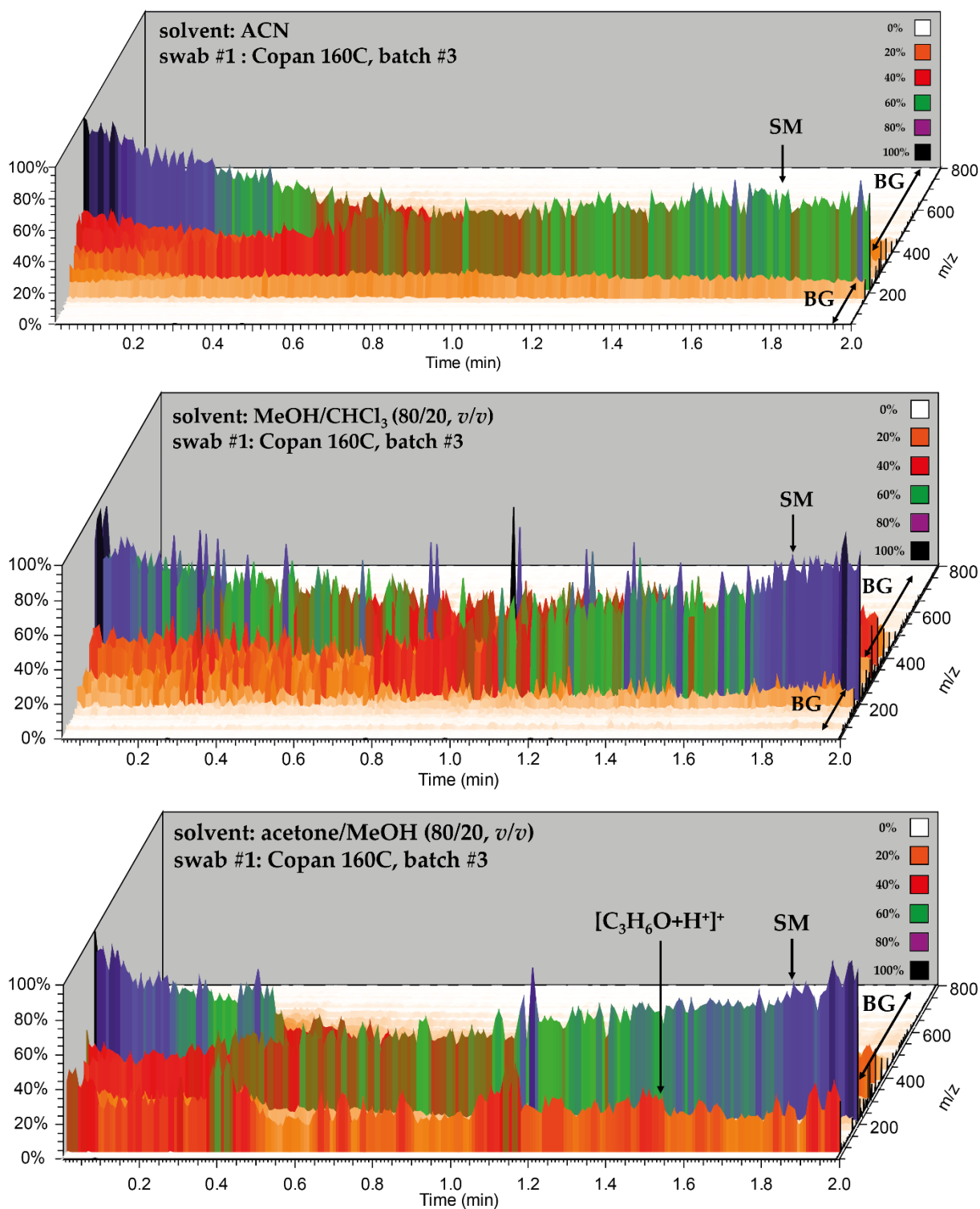
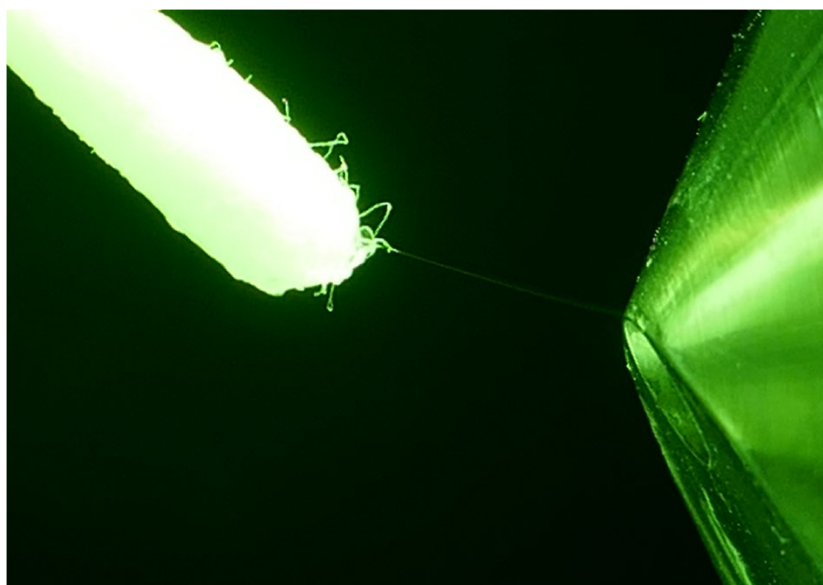


Figure 27 Background visualization obtained with Copan 160C swabs in combination with acetonitrile (70/30, v/v) (top), trichloromethane/methanol (80/20, v/v) (center), and acetone/methanol (80/20, v/v) (bottom) as the spray solvent. All solvents exhibited a comparable background level.

Examining batch-to-batch variability is mandatory in swab material evaluation, as similar swab types may exhibit different background ions.

Although the swab produced by Applimed (#2 in Figure 25) features an aluminum handle that facilitates easy electrospray generation, as depicted in Figure 30 (b), the stability of the electrospray over time was found to be inferior compared to Copan 160C swabs. Additionally, a large portion of Applimed cotton swabs exhibited heads with elongated fibers, impeding proper electrospray formation due to the initiation of fiber spray. Figure 28 depicts fiber spray, which precludes proper analyte extraction and ionization.



*Figure 28 Illustration of fiber spray using 2-propanol and an Applimed swab.*

During evaluation of the swab background with several solvents, an elevated noise level was observed at the onset of spraying, as depicted in Figure 29, which persisted throughout the electrospray operation. Even after two minutes of spraying, the background noise remained high. Most importantly, the suppression marker was barely detectable, indicating that strong analyte suppression occurred due to the presence of the background ions. Consequently, Applimed cotton swabs were excluded from further experimentation.

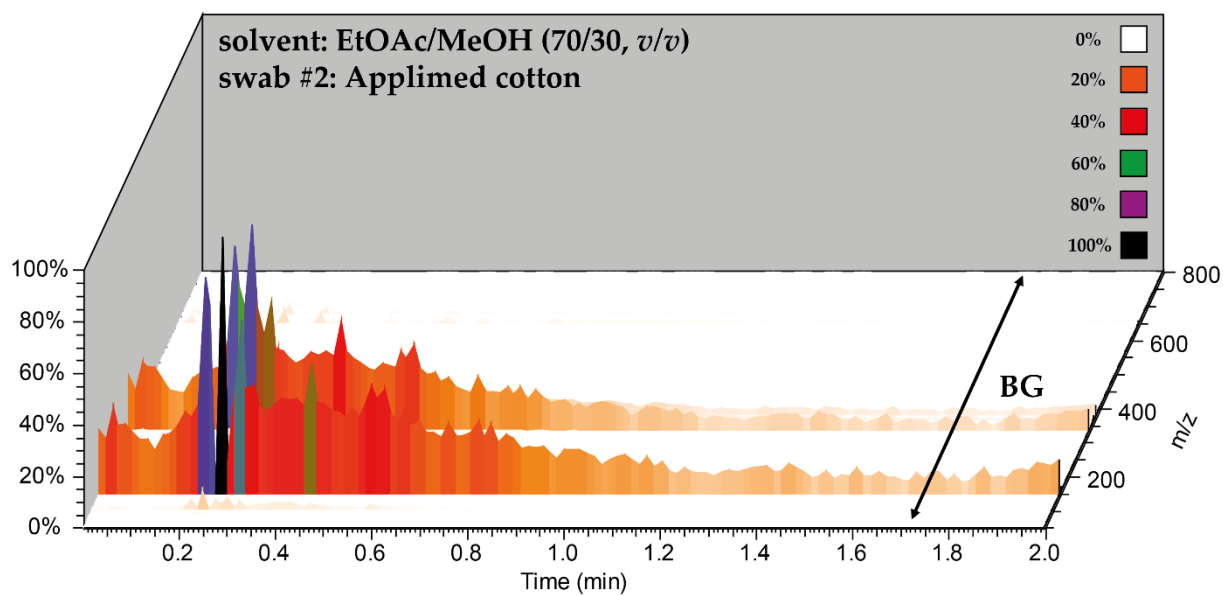


Figure 29 Visualization of the swab background using a Applimed cotton swab in combination with ethyl acetate/methanol (70/30, v/v) as spray solvent.



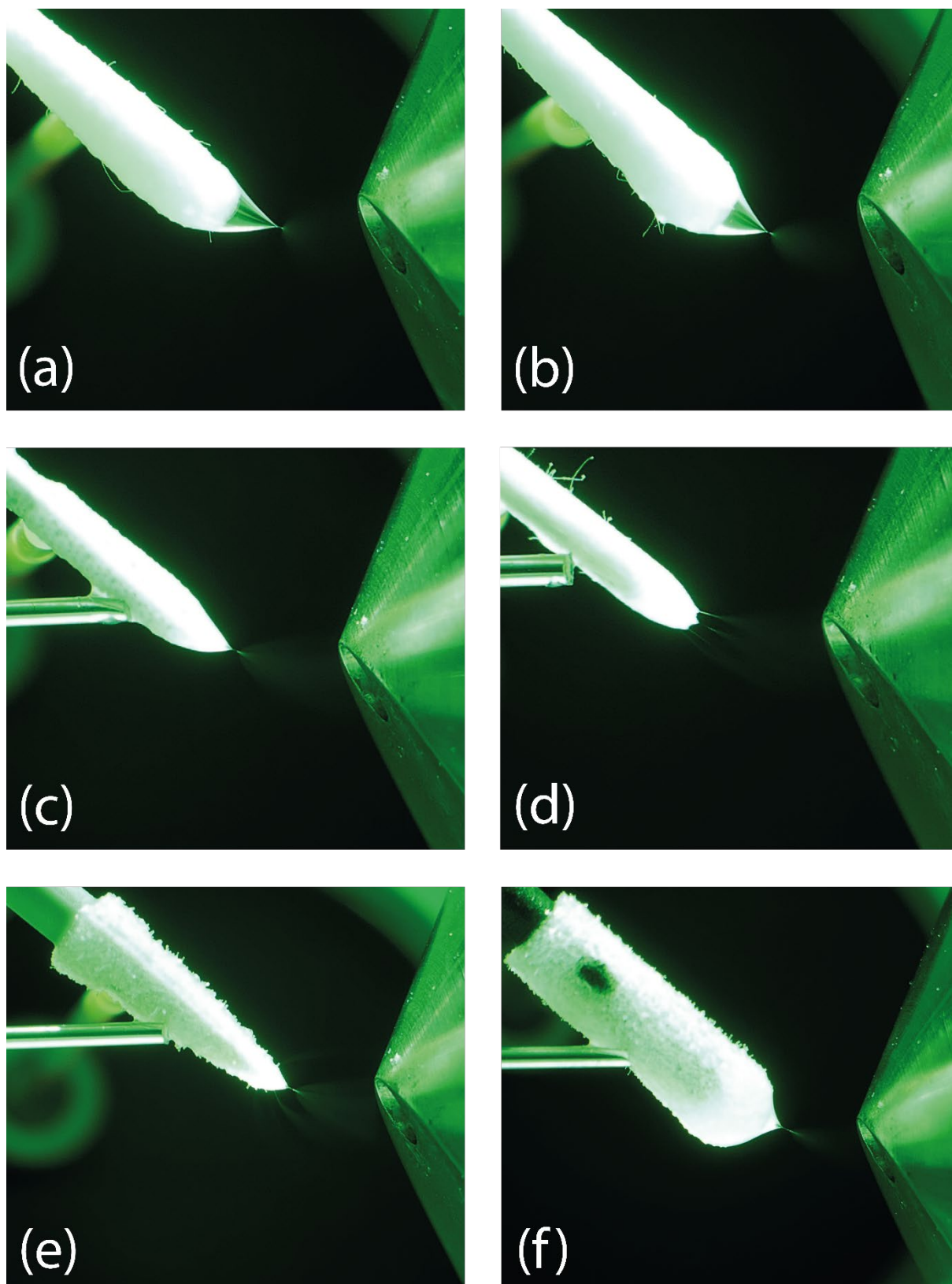


Figure 30 Illustration of electro spray formation using different swabs with methanol as the spray solvent in combination with an electric potential of +5 kV: (a) Copan 160C swab (#1); (b) Applimed cotton swab (#2); (c) Polyester swab (#3); (d) Polyester swab (#5); (e) Polyurethan swab (#7); (f) Polyurethan swab (#8).

The elliptic polyester swabs (#3 and #4) are considered equally applicable for swab spray mass spectrometry. The polyester head material exhibits minimal manufacturing deviations and no protruding fibers. Additionally, the swab heads demonstrated resistance to all tested solvents, a result of the mechanical attachment of the swab head to the handle, and electrospray formation was found to be stable and reproducible. The swab background remained consistently low during the two minutes of spraying, as illustrated in Figure 31. Elevated signal intensities at the onset of the spray may be attributed to a larger spray plume with enhanced ion emission, which persist until the equilibrium between solvent feed and spraying is achieved. The suppression marker, observed at  $m/z$  214.09, represented the dominant peak in the spectrum, indicating low analyte suppression by the swab background ions. Nevertheless, all swabs lacking electrically conductive handles require an additional handling step to direct the potential to the swab head, which is illustrated in Figure 30 (c) for the swab #3.

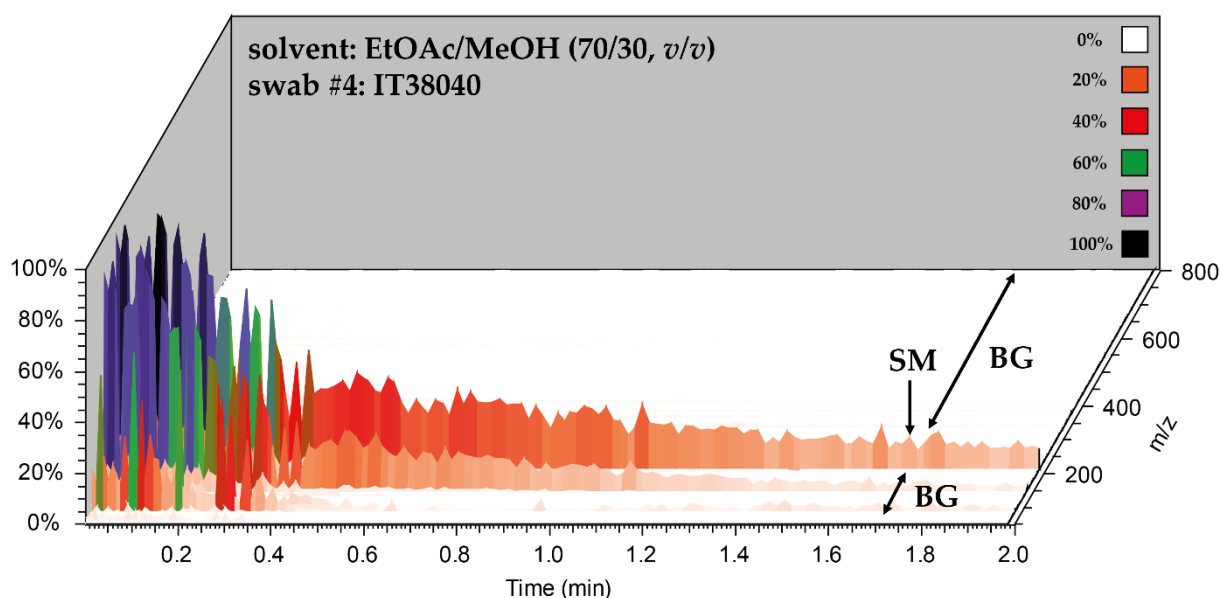


Figure 31 Background spectra obtained using an IT38040 swab using ethylacetate/methanol and 0.1% formic acid (70/30, v/v) at spray initiation (top) and after 120s of electrospraying (bottom).

The flat polyester swabs (#5) require precise positioning to prevent a skewed swab head, which can result in erratic electrospray formation, leading to irregular signal intensity and sporadic pulsation events. Furthermore, these swabs were found to be prone to multi-jet formation, as visible in Figure 30 (d). Consequentially, these swabs were not considered for further experimentation.

The three polyurethane swabs (#6–8) did not provide sufficient solvent stability. While these swabs were able to generate an electrospray, they were prone to multi-jet



formation. However, the most critical issue was the gradual decomposition of the swab head material, resulting in visible contamination on both, the ion sweep cone and the ion transfer capillary. Electrospray formation is illustrated in Figure 30 (e) and (f) using the swabs with #7 and #8. Due to low solvent compatibility, swab materials with polyurethane head material were found to be inappropriate for swab spray mass spectrometry. It was also observed that the huge swab head of swab #8 was impractical due to the excessive solvent volume required for electrospray generation.

Inducing electrospray by an electrostatic field using wooden tips and plant tissues has been described for the analysis of raw food materials [211]. In swabs without electrically conductive handle, electrospray can also be induced by an electrostatic field if a metal wire is mounted without contacting the swab head. In this ionization mode, no contact is made between the spray solvent and the electrically charged metal surface, preventing potential electrochemical reactions. However, since electrochemical reactions of analytes were not observed in our swab spray experiments, this setup did not offer any advantages.

## 2.6 Analyte Extraction

During electrospray, the analyte molecules are continuously extracted from the swab head by the solvent flow. The solvent capillary was positioned on the upper third of the swab head to maintain a low background signal, as with this configuration, the solvent does not flow through the entire swab head, yet still enabling analyte extraction. The sample extraction was visually investigated for both analyte deposition on the tip and on the flank of the swab head. Fluorescein was dissolved in methanol at a concentration of 1 mg/ml. A volume of 4  $\mu$ l was directly applied to either the flank or the tip of the swab head using a pipette.

The analyte extraction process is visualized in Figure 32 with the aid of a 365 nm UV light source. The photographs on top of Figure 32 demonstrate the situation for analyte deposition at the tip of the swab which enables proper analyte extraction over a period of five minutes. If the analytes were deposited laterally (bottom of Figure 32), analyte extraction was hindered and after one minute of extraction, the analytes diffused upwards into a dead spot. Even after five minutes of extraction, the analytes remained trapped in the upper part of the swabs. To ensure efficient analyte extraction and enable quantitation, sampling must always occur at the swab tip.

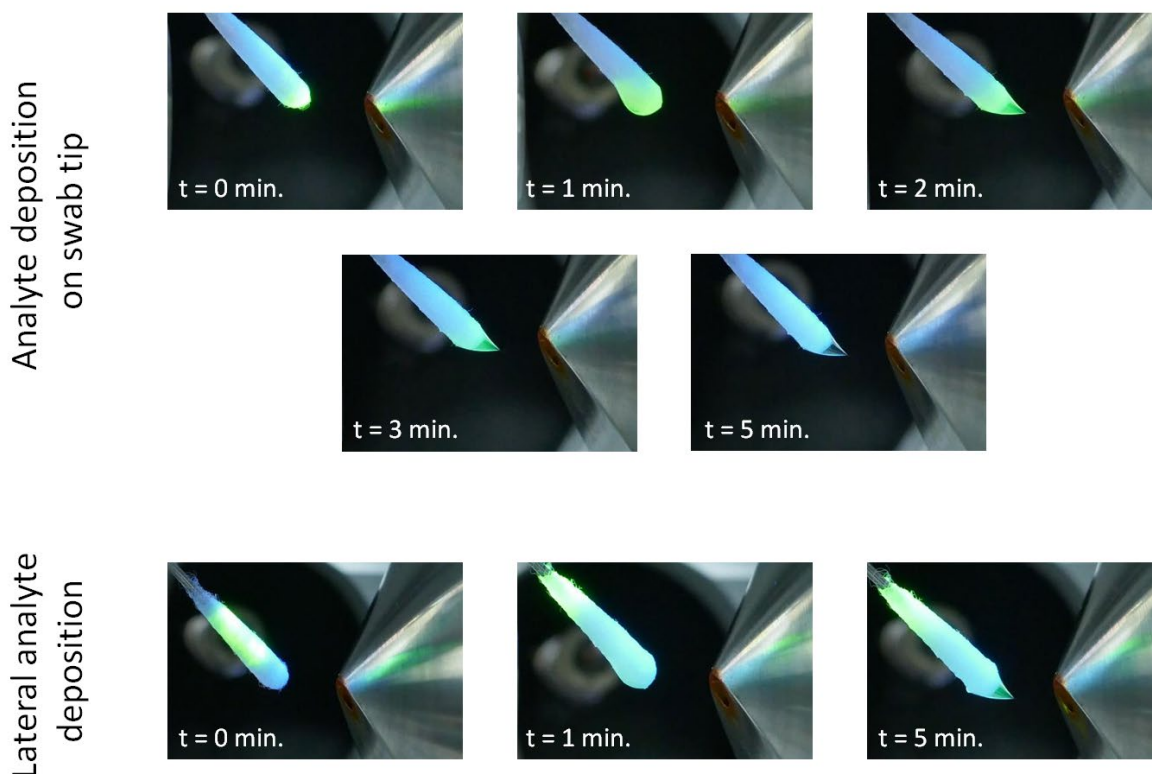


Figure 32 Visualization of the solvent extraction process using fluorescein illuminated with 365 nm UV light. At the top, the analyte was deposited on the tip. At the bottom, the analyte was deposited laterally.

The possibility of interactions between analyte molecules and swab material was assumed in previous work [205]. However, such hypothesis has never been investigated further. In our experiments, analyte-swab interactions were investigated using three different analytes, including octylamine, quinine, and thiabendazole, in combination with three solvents. These analytes offer varying polarity and opportunities for intermolecular interactions with the rayon swab head. The molecular structure of the analytes and rayon fibers is presented in Figure 33. The extracted ion current of the analytes served for monitoring the depletion process. The depletion curves of the three analytes using methanol/water (90/10, *v/v*), ethyl acetate/methanol (70/30, *v/v*), and acetonitrile as solvents are presented in Figure 34. In case of analyte-swab interactions, retention of analytes might occur and the extraction process would be influenced by the eluting strength of the solvent. However, in our experiment, all compounds eluted simultaneously using different solvents. Therefore, analyte swab interactions were not further considered. Nonetheless, the depletion curves may display slight variations among swabs, attributable to minor variations in the swab head composition, and are not the result of analyte or solvent effects. This behavior was further examined in the publication focusing on rapid pesticide detection [88].

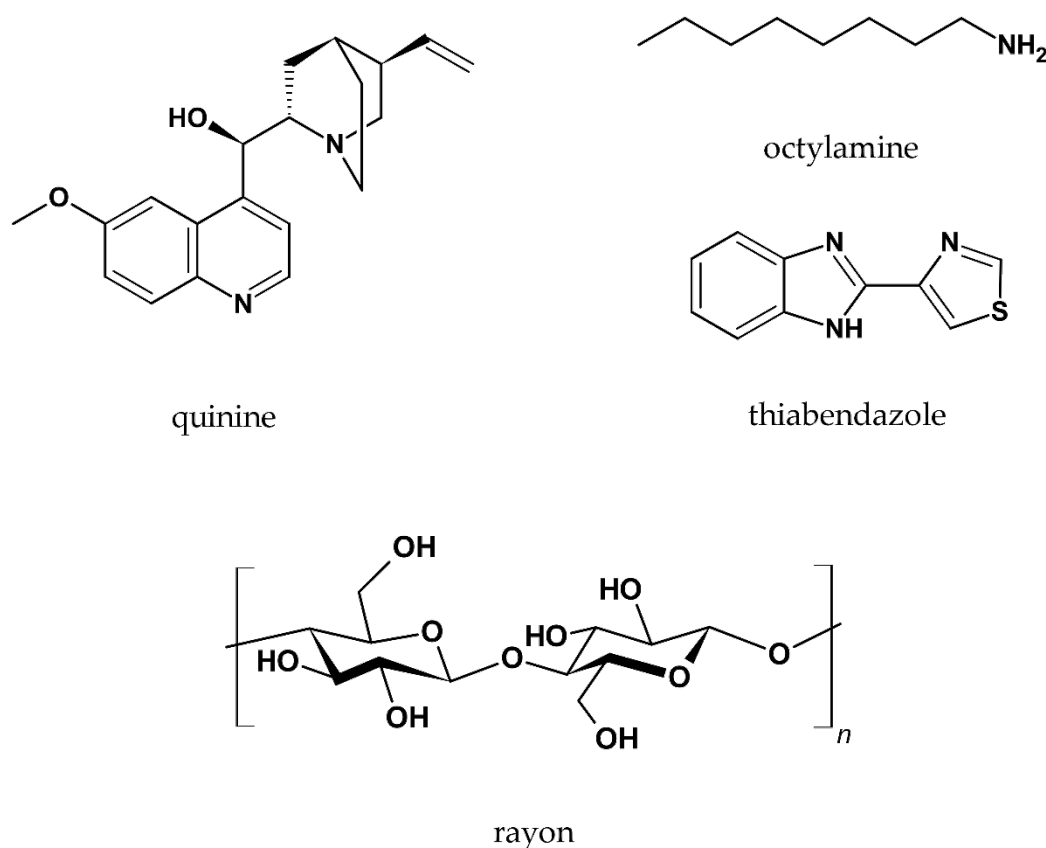


Figure 33 Depiction of the molecular structure of quinine, octylamine, thiabdenazole, and rayon.

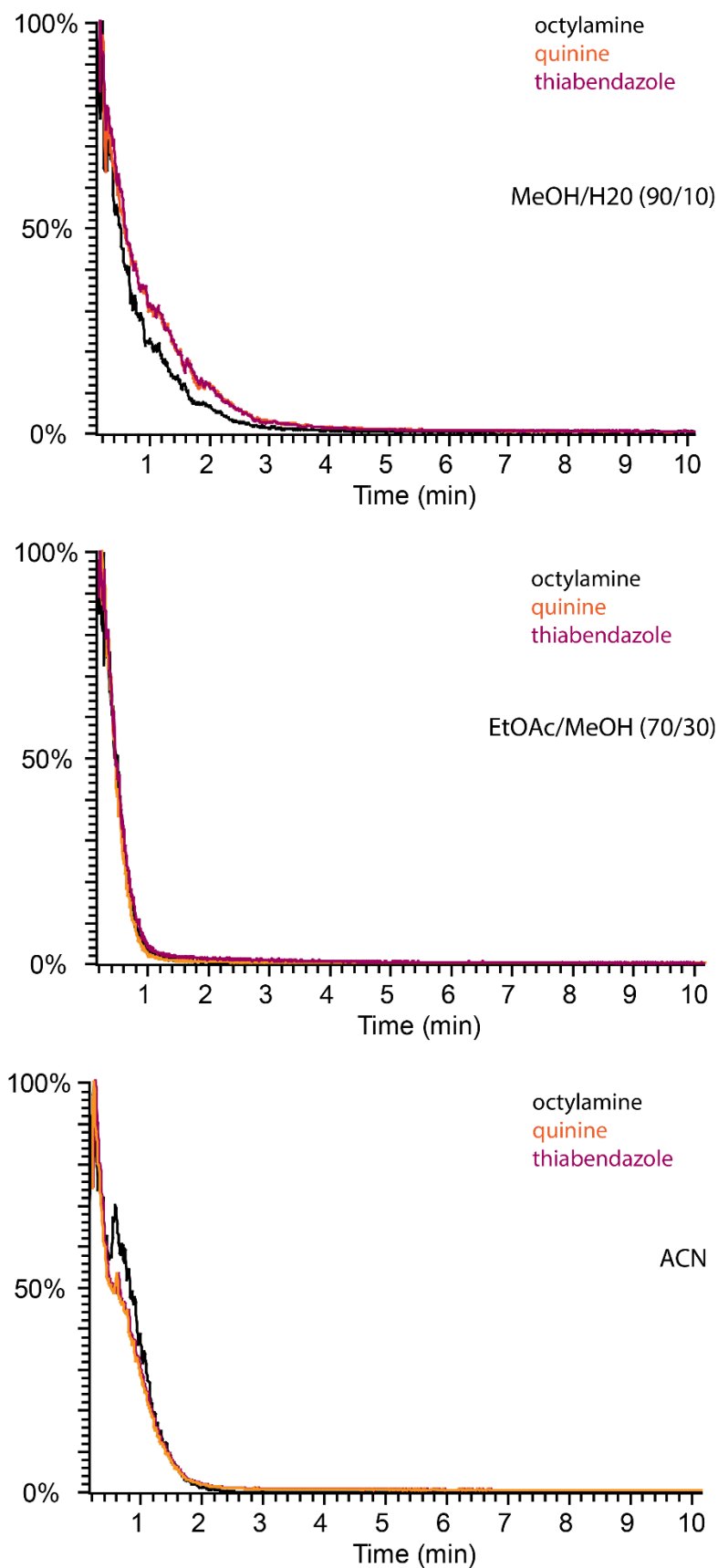


Figure 34 Depletion curves of octylamine, quinine, and thiabendazole, obtained using their extracted ion current and three different spray solvents, show that the compounds were extracted almost simultaneously, independent of their structural features. The flow rate in all experiments was set to 45  $\mu\text{L}/\text{min}$ .

In contrast to the extracted ion currents of eluting analytes, which yield depletion curves, the extracted ion current of the salicylanilide suppression marker remains almost constant, as depicted in Figure 35. The suppression marker was directly added to the spray solvent at a concentration of 1 ppm. The signal intensity at the beginning of the analysis is lower due to suppression by the swab background. The marker is highly important for evaluating swab backgrounds, solvents, analyzing matrix suppression of samples, and checking ion source functionality.

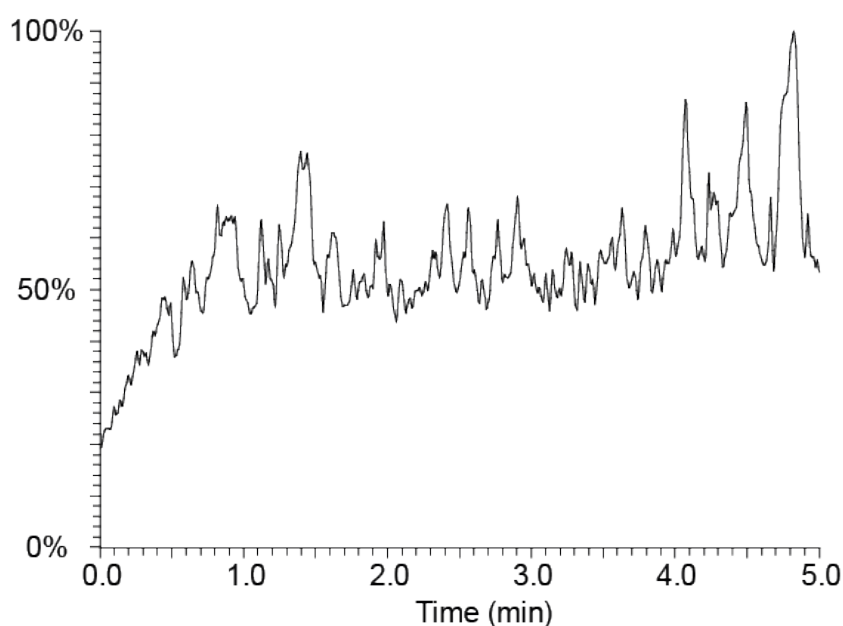


Figure 35 The extracted ion current of the suppression marker is characterized by an intensity level that remains almost constant. However, a slight suppression effect can be observed at the beginning of the analysis, attributable to swab background ions. The flow rate was set to 45  $\mu\text{L}/\text{min}$ .

## 2.7 Solvent Effects in Swab Spray

The influence of the solvent relative permittivity on electrospray formation in swab spray mass spectrometry is extensively discussed in the publication “Influence of solvent relative permittivity on electrospray formation in swab spray mass spectrometry” [209], presented in the next section. Particularly, the impact on jet length, dependent on the relative permittivity of the spray solvent, was studied in detail and the different pulsation modes, such as the dripping and spindle modes, are demonstrated. Moreover, this section focuses on ionization efficiency and presents additional pictures of electrospray formation, including another pulsation mode. Additional supplementary data is available on:

“[www.mdpi.com/article/10.3390/molecules29174274/s1](http://www.mdpi.com/article/10.3390/molecules29174274/s1)”

### 2.7.1 Ionization Efficiency and Reproducibility

The third batch of Copan 160C exhibited similar background ions when using various spray solvents, as demonstrated in the section 2.5 “Evaluation of Swab Materials”. This enabled a comparison of the ionization efficiency of the salicylanilide suppression marker using different solvents.

The suppression marker was added at a concentration of 1 ppm in the spray solvents. Prewashed swabs were used and for each solvent combination three full-scan spectra were recorded for a duration of five minutes. The signal intensity was obtained by integration over five minutes using a gaussian smooth of five points in combination with an extracted ion current (XIC) of  $m/z$  214.05–214.12. The obtained signal areas are presented in Figure 36. Methanol and ethyl acetate/methanol (70/30, *v/v*) delivered comparable signal intensities, whereas acetone/methanol (80/20, *v/v*) exhibited a slightly higher signal yield. In contrast, chloroform/methanol (80/20, *v/v*) resulted in almost twice the intensity of the former two. Acetonitrile as the spray solvent displayed the highest ionization efficiency in this experiment. The relative standard deviation (RSD) of the areas under the XIC depletion curves, as a mean for reproducibility, was found to be between 5% and 18%, is affected by swab fiber texture and variations in swab positioning.

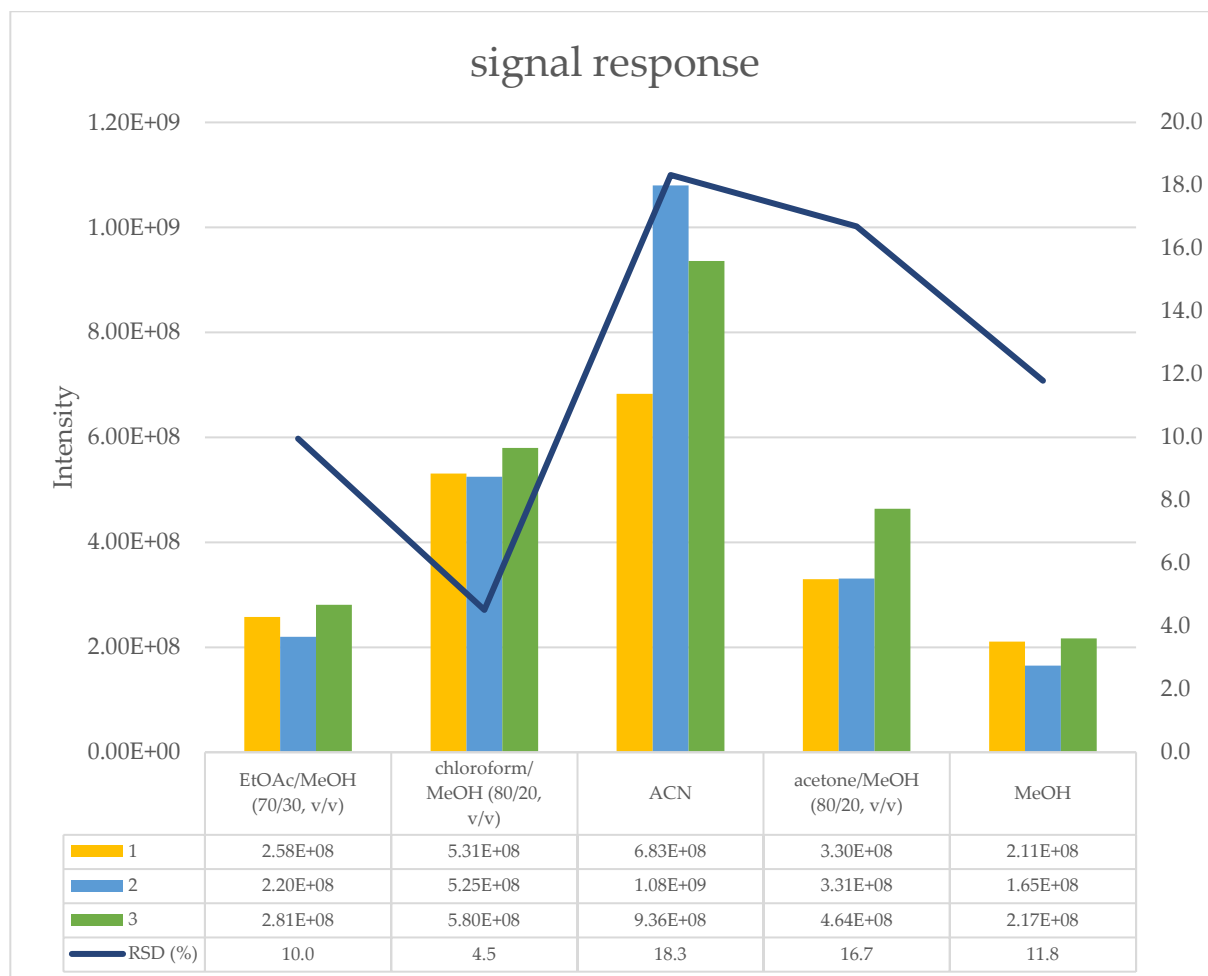


Figure 36 Absolute intensities and relative standard deviation (RSD) of the salicylanilide suppression marker using various spray solvents in combination with an integration window of five minutes. Numbers indicate repetitions.

A connection between solvent properties, such as vapor pressure, enthalpy of vaporization, surface tension, and boiling point (shown in Figure 37) and ionization efficiency could not be established. For example, methanol exhibits a higher vapor pressure in combination with a lower boiling point and a lower surface tension than acetonitrile. Nevertheless, methanol displayed a lower ionization efficiency. During the ionization process, cluster formation and charge transfer play an important role. It was shown that protic solvents like methanol can remove a proton from an analyte and affect ionization [212]. In many studies, it was demonstrated that the ionization efficiency is further affected by analyte properties (basicity, surface area, polarity), flow rate, solvent composition, ionization mode, pH value, additive concentration, ion source settings (applied potentials, gas temperature and pressure) and geometry. For small analytes ionized through ion evaporation, surface activity, influenced by solvent composition, becomes a critical factor. Analytes with nonpolar surface areas commonly exhibit higher ionization efficiency compared to polar compounds when the positive ionization mode is applied. Furthermore, an increased organic content in

the spray solvent was found to correlate with higher ionization efficiency in non-heated electrospray ion sources [55,210,213–219].

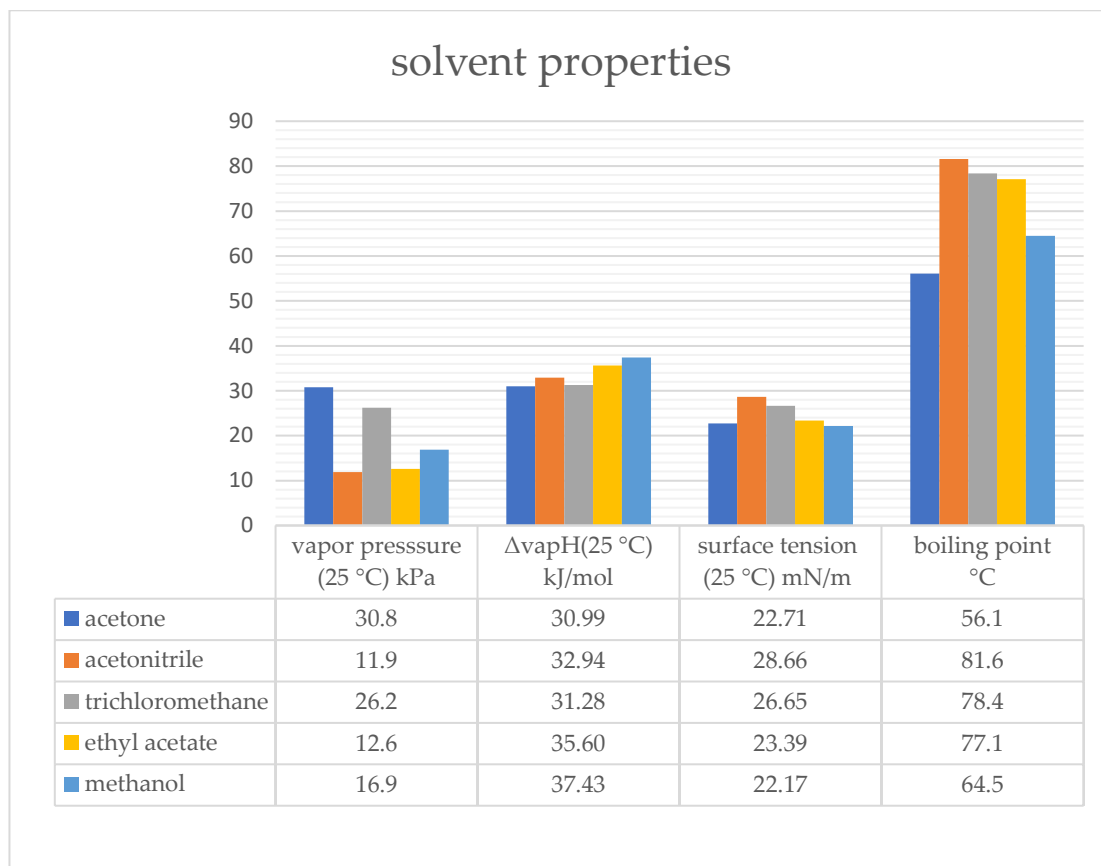


Figure 37 Solvent properties of investigated solvents. Solvent data was taken from reference [33].



### 2.7.2 Effect of Flow Rate on Ionization Efficiency

In a further experiment, the effect of the flow rate on the ionization efficiency of the suppression marker was probed. Acetonitrile was used as the spray solvent in combination with a flowrate of either 45  $\mu\text{L}/\text{min}$  or 200  $\mu\text{L}/\text{min}$ . A full-scan spectrum was recorded for a duration of one minute and the signal of the salicylanilide suppression marker was integrated. The XIC ( $m/z$  214.05–214.12) of salicylanilide is depicted in Figure 38 for both flow rates. The integration over a spray duration of one minute yielded an area of  $1.21\text{E}+08$  counts for a flow rate of 45  $\mu\text{L}/\text{min}$  and an area of  $9.73\text{E}+07$  counts for a flow rate of 200  $\mu\text{L}/\text{min}$ . Although the flow rate is more than fourfold higher, thereby increasing the amount of suppression marker within the same dimension, the resultant signal area does not show a corresponding increase. This implies that the ionization efficiency is higher when lower flow rates are applied. The result can be explained by the broadening of the jet occurring at higher flow rates, which leads to the formation of larger primary droplets [8,220,221]. The spray plume, at a flow rate of 200  $\mu\text{L}/\text{min}$ , is depicted in Figure 39 (a), illustrating visible primary droplets. Larger primary droplets adversely affect the ionization efficiency due to a lower surface-to-volume ratio, requiring additional cascades of Coulomb fission and solvent evaporation for ionization. The effect of the flow rate on the ionization efficiency is particularly important in non-heated electrospray sources such as the swab spray ion source.

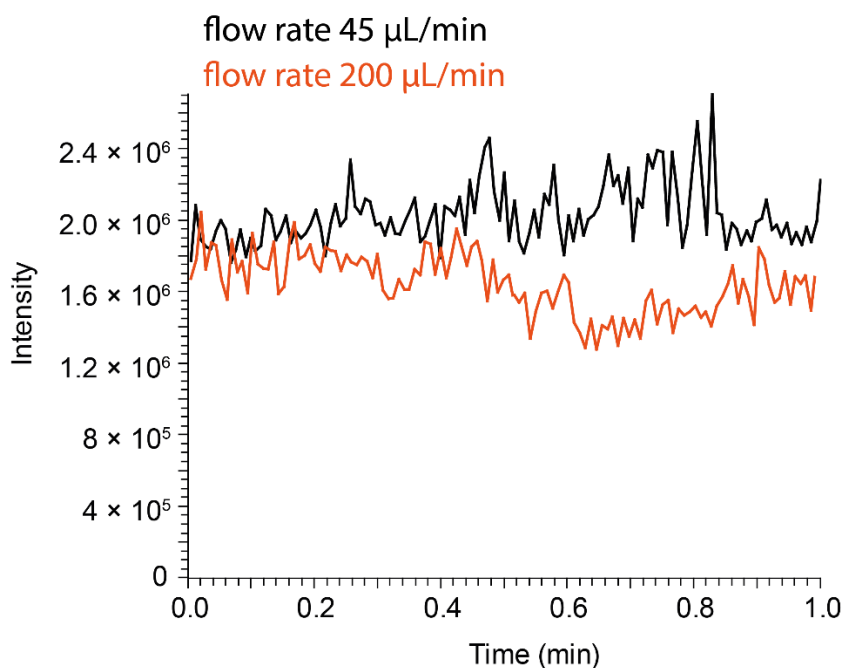


Figure 38 Unsmoothed extracted ion current (XIC) of salicylanilide as suppression marker.

### 2.7.3 Further Spray Observations

Further visual outcomes of electrospray formation using various spray solvents are presented. The application of electric potentials higher than 6 kV at a distance of 7 mm to the counter electrode led to electric discharge through the spray plume, which is depicted in Figure 39 (b). The use of methanol/water (80/20, *v/v*) produced strong turbulences as visible in Figure 39 (c). The result of combining toluene/ethyl acetate (70/30, *v/v*) as the spray solvent is depicted in Figure 39 (d). It points at a phase separation induced in the Taylor cone due to the presence of the strong electric field. Toluene is forming a droplet shape and ethyl acetate is flowing on top of it to eject a long jet.

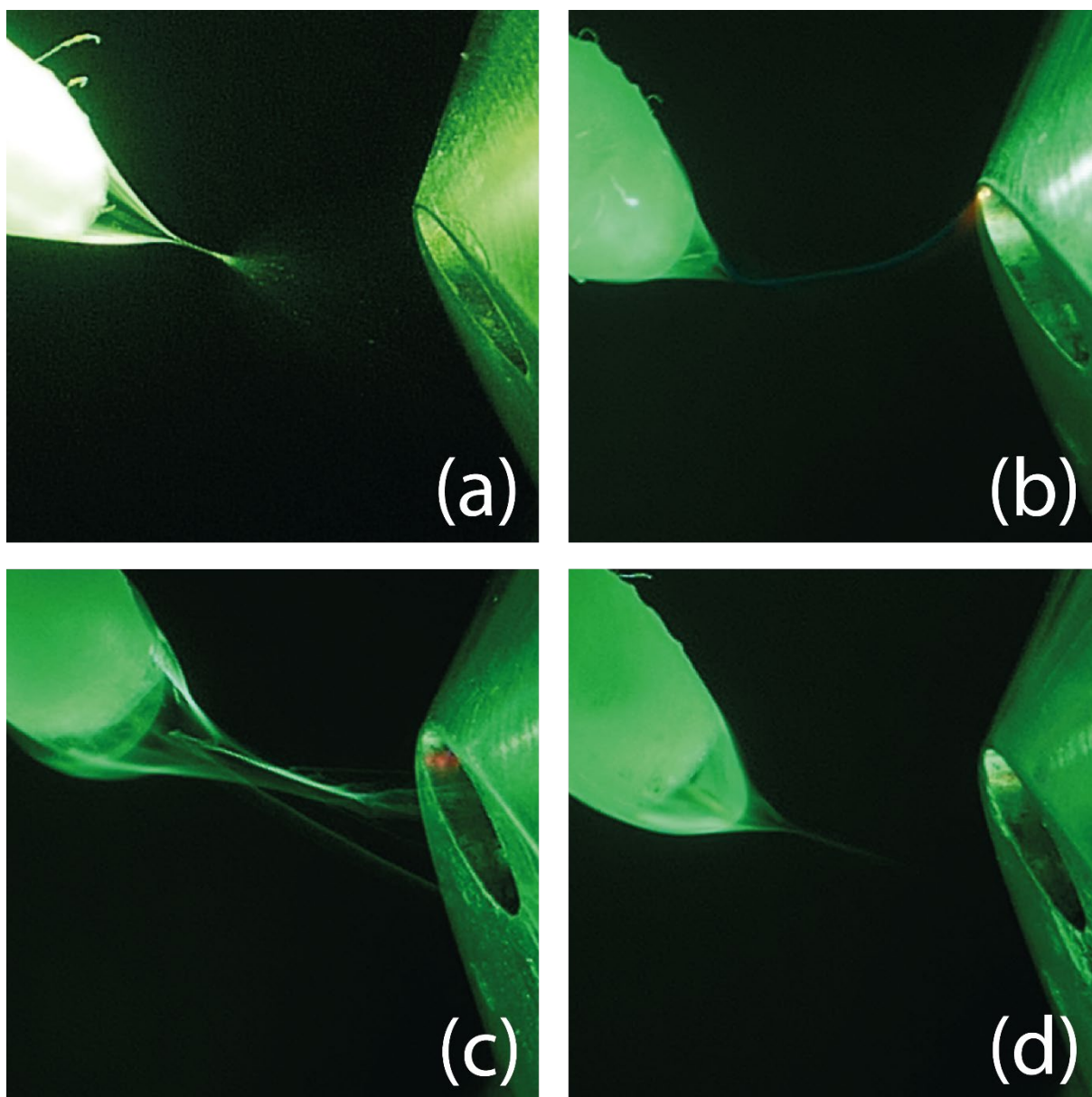


Figure 39 (a) Acetonitrile in combination with a flow rate 200  $\mu\text{L}/\text{min}$ . (b) Electric discharge using methanol at +6.5 kV. (c) Turbulences using methanol/water (80/20, *v/v*) at +5 kV. (d) Taylor cone formation using toluene/ethyl acetate (70/30, *v/v*).

Another example of layer formation within the Taylor cone was observed when a mixture of toluene/methanol (50/50, *v/v*) was used as the spray solvent. The solvent combination exhibited complete miscibility without any phase separation when prepared. A potential of +5.0 kV and a flow rate of 45  $\mu\text{L}/\text{min}$  was applied for spray generation. During operation spontaneous layer formation was observed, as shown in Figure 40 on the left. Methanol appears more transparent than toluene. However, the layer formation persisted only for a brief moment and then transformed into a more homogeneous state, as shown in Figure 40 on the right. The layer formation is assumed to be the result of the electric field, but the complex fluid dynamics within the Taylor cone works against it.

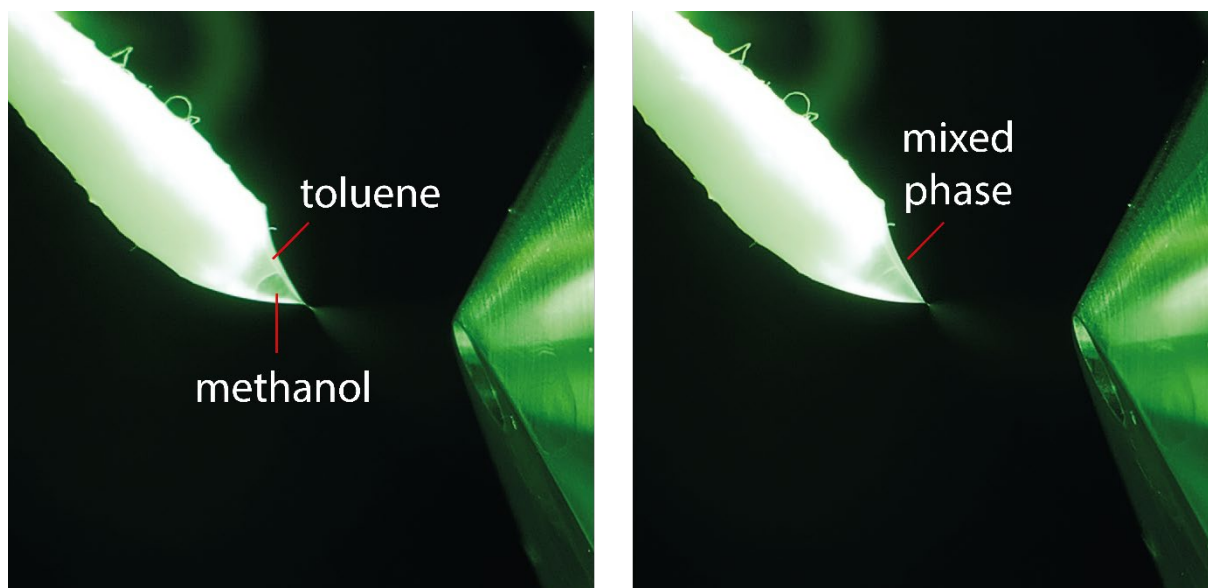


Figure 40 Layer formation in the Taylor cone using toluene/methanol (50/50, *v/v*) as spray solvent.

### 2.7.4 Additional Pulsation Spray Mode

An additional pulsation spray mode is presented in Figure 41. The combination of toluene/ethyl acetate (80/20, *v/v*) led to the formation of a pulsation spray mode, which could not be linked to literature. A pulsation cycle of approximately half a second duration was observed at a potential of +5 kV in combination with a flowrate of 45  $\mu\text{L}/\text{min}$  and a distance of 7 mm to the counter electrode. At the beginning of the cycle, the solvent at the swab tip transitions from a droplet into a conical shape, followed by the emission of a long jet observable for roughly one-tenth of a second before the jet collapses and the solvent reverts to a droplet form at the swab tip. This pulsation mode can be viewed as a transition between the dripping pulsation of pure toluene and the emitting of a long jet by pure ethyl acetate. However, this spray mode did not yield any signal.

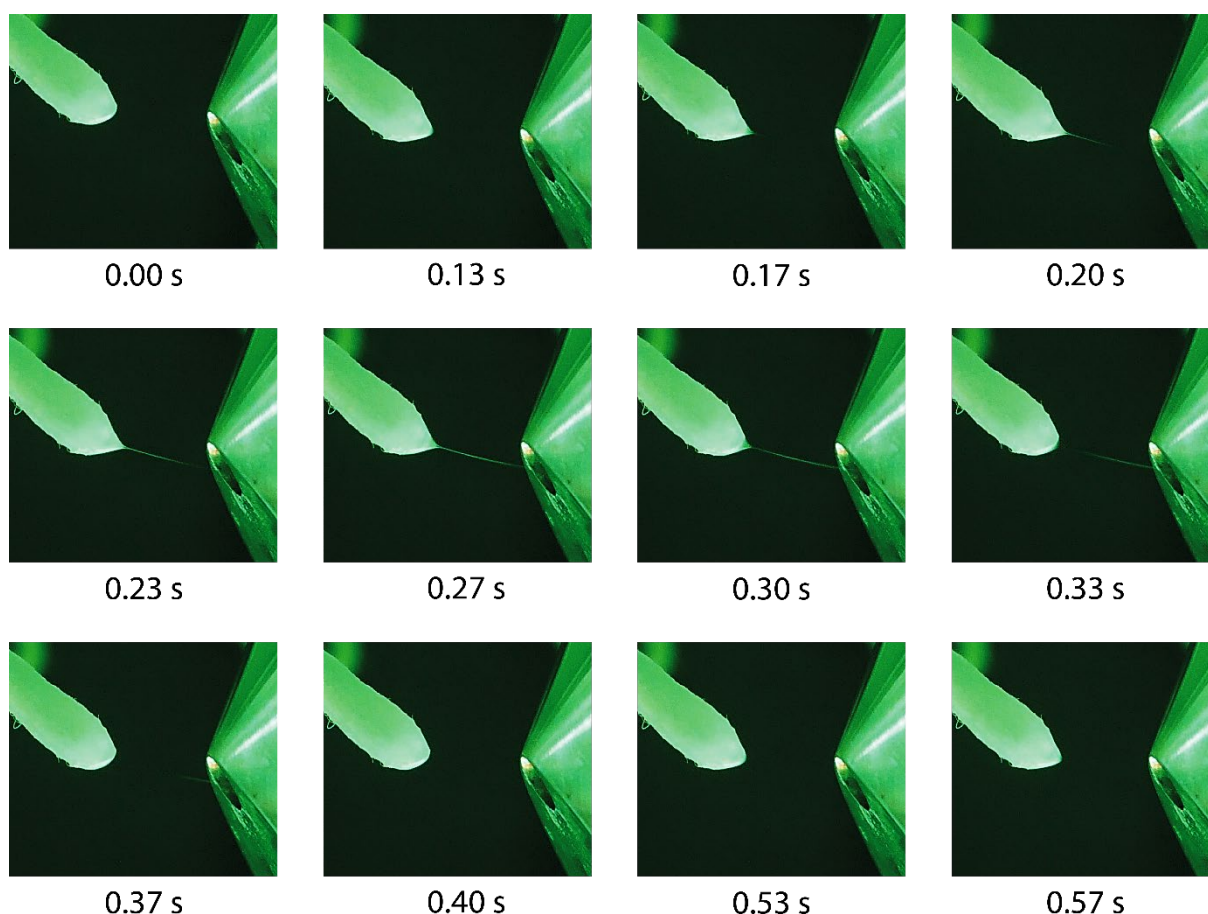


Figure 41 A pulsating spray mode obtained using toluene/ethyl acetate (80/20, *v/v*) shows the ejection of a long jet.

### 2.7.5 Onset Potentials

The onset potentials for various solvents are discussed in detail in the publication “Influence of Solvent Relative Permittivity in Swab Spray Mass Spectrometry” [209]. In summary, the surface tension is the decisive factor that determines the onset potential. A relative permittivity above 4 is required for charge separation, which is mandatory for Taylor cone formation. The calculated onset potentials discussed in section 1.1.2 are put into relation with the observed values. The onset potential ( $V_{\text{on}}$ ) for setup 1, with an emitter diameter of 3.5 mm and 7 mm distance to the counter electrode, corresponding to the swab head diameter and the distance to the ion sweep cone, is 3.29 kV, 3.74 kV, 4.16 kV, 5.92 kV for methanol, acetonitrile, DMF, and water, respectively. Comparable onset potentials were observed for the former two solvents, methanol and acetonitrile, ranging between +3.5 and +3.9 kV. DMF exhibited a slightly higher onset potential of approximately +4.7 kV, while water did not permit Taylor cone formation due to the occurrence of electrical discharge. Differences can be explained by the swab, which accumulates solvent on tip, with the conductive metal handle located inside the swab head. This is in contrast to conductive needles applied in conventional electrospray setups.

For calibration of the mass spectrometer, a PicoTip nanoelectrospray emitter was used in combination with a calibration solution in acetonitrile. The calculated onset potential for a nanoelectrospray needle in combination with acetonitrile as the spray solvent corresponds to 0.58 kV ( $V_{\text{on}}$  setup 2). A slightly higher value of +0.6–0.7 kV was required as onset potential.



## Article

# Influence of Solvent Relative Permittivity in Swab Spray Mass Spectrometry

Thomas Michael Muggli  and Stefan Schürch \*

Department of Chemistry, Biochemistry and Pharmaceutical Sciences, University of Bern, 3012 Bern, Switzerland; thomas.muggli@unibe.ch

\* Correspondence: stefan.schuerch@unibe.ch

**Abstract:** The influence of solvent properties on ion generation by swab spray ionization was investigated. The ability of a variety of solvents of different relative permittivity, surface tension, and viscosity to form a stable and reproducible electrospray was examined. It is demonstrated that in swab spray ionization, a crucial balance between solvent composition, applied potential, and the solvent flow fed to the swab head must be maintained. The solvent composition was found to significantly affect the shape of the Taylor cone and the emerging cone jet, which eventually have an impact on the resulting ion yield. The results indicate that the relative permittivity of solvents measured under standard conditions is the main factor governing jet shaping, and consequently, the ionization efficacy. Short jets, which are required for maximum ion yield, were observed for solvents with relative permittivity  $\epsilon_r$  higher than 25. Solvents exhibiting lower relative permittivity required the addition of 20% to 60% methanol to limit the jet length and to avoid the ineffective dripping pulsation. The observed effects were compared to conventional electrospray ionization and paper spray ionization.

**Keywords:** swab spray mass spectrometry; electrospray ionization; Taylor cone formation; ambient ionization; relative permittivity; paper spray



**Citation:** Muggli, T.M.; Schürch, S. Influence of Solvent Relative Permittivity in Swab Spray Mass Spectrometry. *Molecules* **2024**, *29*, 4274. <https://doi.org/10.3390/molecules29174274>

Academic Editor: Marcello Locatelli

Received: 30 July 2024

Revised: 29 August 2024

Accepted: 6 September 2024

Published: 9 September 2024



**Copyright:** © 2024 by the authors. Licensee MDPI, Basel, Switzerland. This article is an open access article distributed under the terms and conditions of the Creative Commons Attribution (CC BY) license (<https://creativecommons.org/licenses/by/4.0/>).

## 1. Introduction

### 1.1. Discovery of Electrospray

Due to its soft ionization characteristics, electrospray has emerged as a widely used technique for the ionization of small organic compounds up to large biomolecules. The evolution of electrospray has taken place over the last century. Fundamentals were already discovered in 1913 by John Zeleny in his essential work about electric discharge from liquid points [1]. Sir Geoffrey Ingram Taylor continued to make significant contributions describing processes of liquids in a strong electric field, including the Taylor–Melcher model [2,3]. As of then, the liquid cone emerging from a spray capillary under the influence of a strong electric field became known as the Taylor cone. At the apex of the Taylor cone, the formation of a jet can be observed. The structure of the jet differs in length and diameter [4,5]. Malcolm Dole was the first to demonstrate the use of electrospray for the generation of macroions and their detection by a Faraday cage [6]. Further progress was reported by John Bennet Fenn, who demonstrated the potential of electrospray ionization to access large, labile, and nonvolatile compounds, which was not realizable by other methods [7]. This work eventually peaked in the ionization of large biomolecules by electrospray ionization coupled to mass spectrometry [8]. For his pioneering work, John B. Fenn was awarded the Nobel prize in chemistry in 2002. A comparable advancement that enabled “electrostatic atomization of liquid analytes at ambient gas pressure”, termed ERIAD, was developed by the research group of Lidija Gall. ERIAD was first used to demonstrate the ionization of progesterone and amino acids at the onset of the 1980s [9].



### 1.2. Principles of Electrospray

Despite thousands of publications per year involving electrospray ionization, only few focus on the fundamental mechanisms of ion generation by electrospray. Principles involve complex fluid dynamics and electrostatic processes, and many aspects are still the subject of discussion as emphasized by the literature [5,10,11]. A Taylor cone results from a liquid drop deformation into a conical shape in the presence of a strong electric field, typically at the tip of a thin electrically conductive capillary. For an ideal conducting liquid, a Taylor cone half angle of  $49.3^\circ$  was calculated, although various factors including pressure and space charge were not considered [2,5]. Numerous solvent properties, such as the relative permittivity, viscosity, surface tension, conductivity, density, and the composition of the surrounding gas impact Taylor cone formation. Moreover, the system is influenced by the applied electric potential, solvent pressure, capillary diameter, and the distance of the capillary tip to the counter electrode [5]. Recent studies even give evidence for altered solvent properties in high electric fields, such as the viscosity of water in an electric field between 0 and 0.9 V/nm, which was communicated to become unisotropic [12], and the surface tension of various liquids, which was reported to be influenced by high electric fields as well [13].

Viscosity, electrical resistivity, and solvent flow rate are described in the literature as decisive factors governing the length of the jet [4,14]. In addition, the Taylor cone angle is directly related to the applied electric potential with increasing potential resulting in a larger cone angle [15]. Taylor cones of different shapes and modes have been defined, such as tilted jets, multi jets, ramified jets, rotated jets, and pulsation modes, such as the microdripping and spindle modes [4,16–22]. However, the cone-jet mode is the most desired in electrospray ionization mass spectrometry, as it is mandatory for the proper ionization of analytes [18]. The jet formed at the apex of the Taylor cone breaks up and turns into a spray plume consisting of charged droplets [5,23]. In the spray plume, the ionization of analyte molecules takes place. Models of the ionization process are categorized into the ion evaporation model (IEM), charge residue model (CRM), or the chain ejection model (CEM) [10,24]. In addition, the solvent also plays a crucial role, as it directs the charge states of the analytes [25,26]. Nevertheless, further investigation of the physical effects associated with Taylor cone formation is required for gaining deeper insight into electrospray-based ionization techniques.

### 1.3. Electrospray Ionization in Ambient Mass Spectrometry

More recent developments in mass spectrometry involve ambient ionization methods, which enable direct in situ ionization without the requirement for sample preparation steps. Among them are electrospray-based methods, such as desorption electrospray ionization (DESI) [27], established in 2004, and paper spray, which was first described in 2010 [28]. Swab spray is a further electrospray-based ambient ionization method that has been introduced in 2015 by the group of Graham Cooks [29]. Meanwhile, swab spray mass spectrometry has demonstrated its potential as a hassle-free sampling and sensitive analytical method, especially for medical diagnostics, forensic investigations, and environmental analyses [30–39].

Current–voltage curves were previously applied to differentiate between the electrospray mode and the occurrence of corona discharge when spherical sampler probes were used as spray emitters [40]. The present work focuses on fundamental aspects of ion generation by swab spray with an emphasis on the influence of different solvent properties on the formation of the Taylor cone and the associated jet. Photographic observations provided evidence to differentiate between various electrospray modes and to determine the jet length, even in the absence of a signal. In the performed experiments, it was observed that the emission of a short jet is pivotal for optimizing signal yield in swab spray mass spectrometry. To evaluate ionization efficacy, a suppression marker, either salicylanilide or tetrabutylammonium iodide, was directly added to the spray solvent, and full-scan data



were acquired. To our knowledge, the impact of the solvents relative permittivity on jet shaping was not demonstrated previously in ambient ionization techniques.

## 2. Results and Discussion

### 2.1. Impact of the Electric Potential on Taylor Cone Formation

The formation of a Taylor cone at the tip of a swab head can immediately be observed after the application of solvent and sufficient electric potential. Application of a potential below the onset value leads to a dripping pulsation mode, whereas the pulsation frequency increases with increasing potential. When the onset voltage is reached, the formation of a stable Taylor cone can be observed. The required onset potential depends on the type of solvent and the distance between the swab head and the counter electrode, which was held constant at 7 mm for all experiments. Manufacturing variations of swab heads can cause deviations of the onset voltage of about  $\pm 0.2$  kV. Nevertheless, for methanol, ethanol, and acetone, onset voltages in the range between 3.5 and 3.9 kV were determined. The surface tensions of methanol, ethanol, and acetone correspond to 22.17 mN/m, 21.91 mN/m, and 22.71 mN/m, while the relative permittivities are 33.02, 25.32, and 21.01, respectively.

The surface tension of the liquid must be overcome by the force of the electric potential to transform the solvent droplet into a Taylor cone. Hereby, the relative permittivity (dielectric constant) acts as an insulating factor. However, a sufficient relative permittivity is necessary for charge separation, which promotes Taylor cone formation.

The high surface tension of water (72.06 mN/m) prevents the formation of a Taylor cone. Instead, the water droplet undergoes elongation until a sudden electric discharge to the ion sweep cone takes place, as visualized in Figure 1.

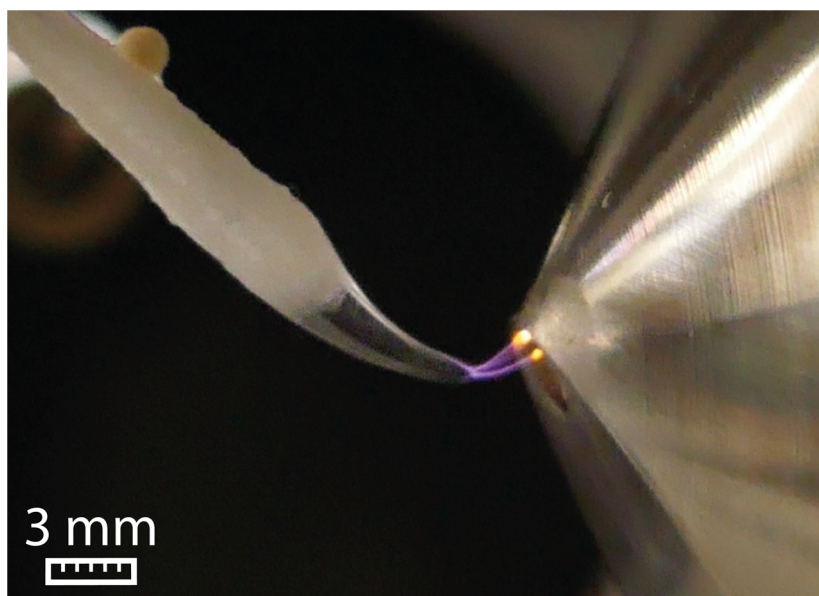


**Figure 1.** Electric discharge between the swab and the ion sweep cone serving as counter electrode for water at 5 kV and a flow rate of 45  $\mu$ L/min.

Significantly higher onset potentials than found for methanol, ethanol, and acetone were observed for nitromethane (4.8 kV), dimethyl sulfoxide (DMSO) (5.3 kV), and N,N-dimethylformamide (DMF) (4.7 kV), which is explained by the higher surface tensions of these solvents. The relative permittivities of nitromethane, DMSO, and DMF are 37.27, 47.242, and 38.25, while their surface tensions are 36.53 mN/m, 42.92 mN/m, and 35.52, respectively. Toluene, which exhibits a relative permittivity of 2.38 and a surface tension of 27.91 mN/m, did not promote Taylor cone formation. The very low relative permittivity does not provide sufficient charge separation, and an addition of 50% methanol was required for Taylor cone formation at an onset potential of 4.2 kV.

The impact of the applied voltage on the Taylor cone angle is visualized in the series of pictures in Figure 2 using methanol as a spray solvent. The Taylor cone angle increased at elevated potentials, which was observed for all solvents that generated a short jet. Additional photographs of Taylor cones at different voltages using DMF and a mixture of toluene/methanol (50/50, *v/v*) is available in Supplementary Data S1. A similar relation between Taylor cone angles and applied voltages was demonstrated using spherical sampler probes [40].

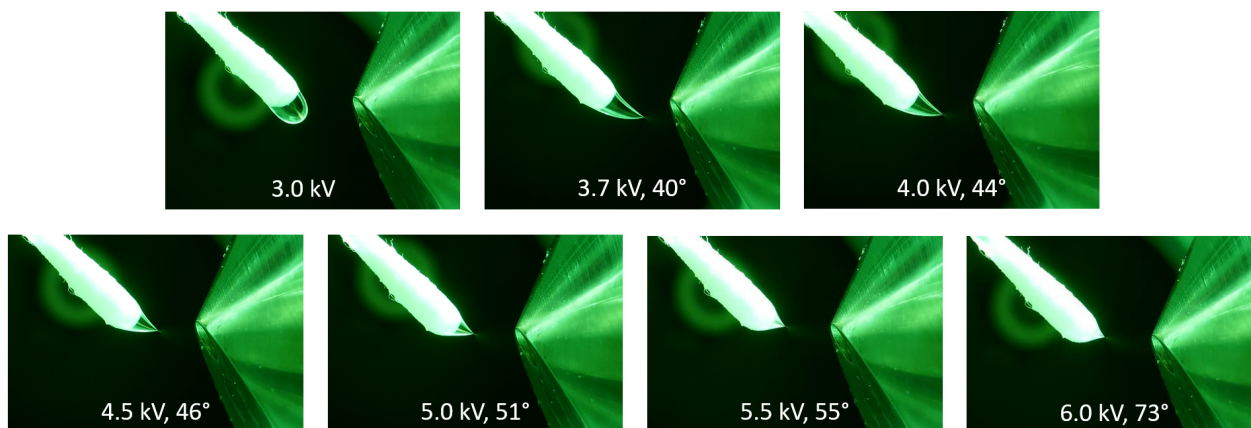


**Figure 2.** The influence of the electric potential on the Taylor cone angle at different voltages using methanol as the solvent at a flow rate of 45  $\mu\text{L}/\text{min}$ . At 3.0 kV, the droplet is dripping and slightly drawn toward the counter electrode. At the onset potential of 3.7 kV, the formation of a Taylor cone becomes visible. At higher potentials, the Taylor cone angle starts to increase, which leads to a shorter cone with decreased volume.

## 2.2. The Different Taylor Cone Modes

The shape and stability of the Taylor cone and the emerging jet are crucial for the electrospray ionization process [5], and dripping pulsation [17,20,21,41,42] and spindle pulsation [17,18,20,21] of the Taylor cone must be avoided as well. Therefore, the applied electric potential, the solvent composition, and the flow rate of the solvent fed to the swab head must be chosen carefully. In our experiments, high ion yields were only obtained with short jets, as the ionization process takes place in the spray plume after the jet breaks up. A short jet was found to generate a voluminous spray plume which promotes efficient ionization and simultaneously facilitates the alignment of the swab in front of the electrospray interface. On the other hand, a voluminous spray plume is detrimental to accurate quantitative analysis by swab spray ionization, as part of the sprayed sample is lost at the ion sweep cone. Solvents that generate Taylor cones with long jets prevent proper ionization because the formation of a spray plume, in which the ionization process takes place, is impeded.

## 2.3. Taylor Cones with Short Jets

The suitability of different solvents for efficient swab spray ionization was evaluated in a series of experiments in which a variety of solvents was tested with the aim to generate a stable Taylor cone with a short jet. Results indicated that a sufficiently high relative permittivity ( $\epsilon_r$ ) is crucial for producing a short jet. Amongst the most suitable solvents for swab spray ionization were solvents with relative permittivity larger than 25, such as DMSO, nitromethane, acetonitrile, methanol, DMF, and ethanol (Table 1). Acetone, with a relative permittivity of 21.01, has to be considered as a borderline case, as it produced jets from short to long in multiple experiments. Ethanol, with its slightly higher relative permittivity of 25.32, always created a short jet in repeated experiments. The sprays generated by selected solvents and at different solvent flow rates are visualized in Figure 3.

**Table 1.** Relative permittivity, viscosity, and surface tension of various pure solvents [43,44]. The green-colored solvents allow the formation of a Taylor cone with a short jet. The yellow-colored solvents lead to the formation of long jets, whereas the red-colored solvents result in a dripping pulsation mode. The required portion of methanol to produce a short jet is given in volume percentage. Water is in yellow color, as it represents a special case, where strong surface tension was preventing Taylor cone formation. Glycerol is in brown color, because its high viscosity produced a long jet. Full-scan data of various solvent mixtures with methanol are provided in Supplementary Data S2.

Spray Mode	Solvent	MeOH Content <i>v/v</i> in % for Short Jet	Relative Permittivity $\epsilon_r$ (20 °C)	Viscosity $\eta$ (25 °C) mPa·s	Surface Tension $\gamma$ (25 °C) mN/m
dripping pulsation	hexane	immiscible	1.887	0.300	17.88
	1,4-dioxane	≥60	2.219	1.177	32.75
	toluene	≥50	2.379 (23 °C)	0.560	27.91
	dibutyl ether	≥60	3.083	0.637	N/A
Taylor cone with long jet	diethyl ether	≥30	4.267	0.224	16.50
	anisole	≥50	4.302 (21 °C)	1.056	35.10
	trichloromethane	≥20	4.807	0.537	26.65
	propyl acetate	≥30	5.622	0.544	23.80
	ethyl acetate	≥30	6.081	0.423	23.39
	methyl acetate	≥30	7.072 (15 °C)	0.364	24.73
	1-chlorobutane	≥40	7.276	0.422	23.18
	tetrahydrofuran	≥30	7.522 (22 °C)	0.456	26.40 (20 °C)
	dichloromethane	≥20	8.936 (25 °C)	0.413	27.20
	3-pentanone	≥30	17.002	0.444	24.74
	2-propanol	≥30	20.182	2.040	20.92
	acetone	≥20	21.012	0.306	22.71
	1-nitropropane	≥30	24.702 (15 °C)	0.798	N/A
Taylor cone with short jet	ethanol		25.320	1.074	21.91
	methanol		33.020	0.544	22.17
	acetonitrile		36.642	0.369	28.66
	nitromethane		37.272	0.630	36.53
	<i>N,N</i> -dimethylformamide		38.250	0.794	35.52
	dimethyl sulfoxide		47.242	1.987	42.92
	water	≥90	80.120	0.890	72.06
	glycerol		46.532	934	62.50

Nevertheless, short jets do not ensure high ionization efficacy. Methanol (Figure 3a), ethanol (Figure 3c), and acetonitrile (Figure 4, top) sprayed at 45  $\mu\text{L}/\text{min}$  all resulted in the protonation of salicylanilide, which was added to the solvent at a concentration of 1 ppm for monitoring the ionization efficacy. Despite the short jet formed by DMF, DMSO, and nitromethane, no signal of the protonated salicylanilide was observed as shown for DMSO in Figure 4 (center). This is likely attributed to the low ionization efficacy of salicylanilide in these solvents. Additional full-scan spectra for several other solvents, including nitromethane, ethanol, and DMF, are available in the Supplementary Data S2.

When tetrabutylammonium iodide, a pre-charged analyte, was used as the suppression marker, comparable signal intensities were found in DMSO and DMF (spectra available in the Supplementary Data S3). This indicates that salicylanilide exhibits a lower proton affinity in these solvents.



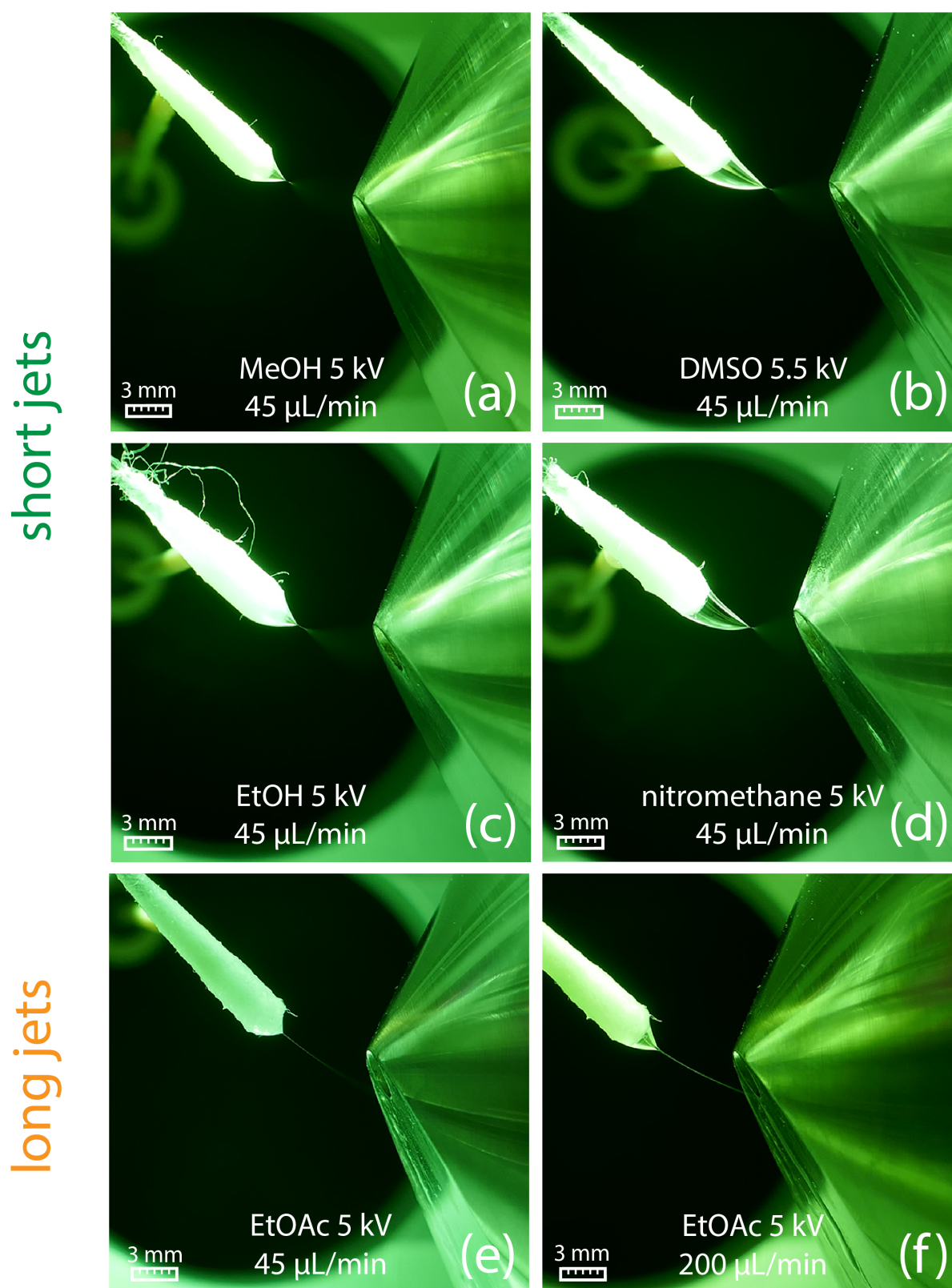


**Figure 3.** (a–d) Generation of a short jet at a flow rate of 45  $\mu\text{L}/\text{min}$  for different solvents. (e) Ethyl acetate generates a long jet already at a solvent flow rate of 45  $\mu\text{L}/\text{min}$ , which starts to break up into a spray plume in front of the counter electrode. (f) At a flow rate of 200  $\mu\text{L}/\text{min}$ , a broader and longer jet is created, which directly hits the counter electrode.

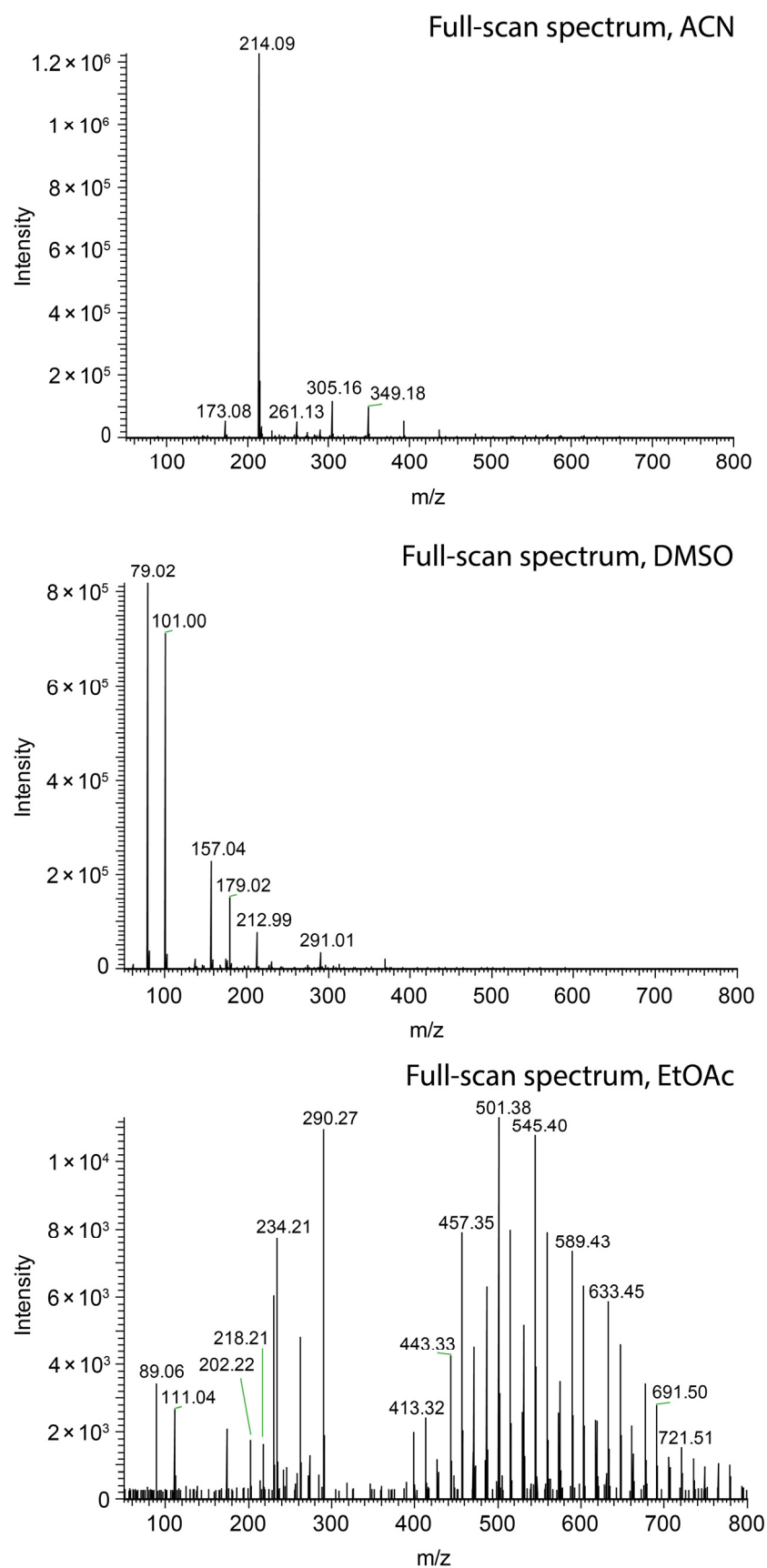


**Figure 4.** Comparison of swab spray mass spectra of salicylanilide ( $[M + H]^+$  at  $m/z$  214.09) obtained with acetonitrile (**top**), DMSO (**center**), and ethyl acetate (**bottom**) as the solvents.

#### 2.4. Taylor Cones with Long Jets

All tested solvents with relative permittivity lower than 21 produced a long jet (see Table 1), which, in most cases, reached the ion sweep cone serving as the counter electrode in our experiments. The formation of long jets adversely affects the signal intensity, as illustrated in Figure 4 (bottom) for ethyl acetate. In addition to the solvents' relative permittivity, the jet length is also influenced by the solvent flow rate, with higher flow rates resulting in elongated stabilized jets, as shown for ethyl acetate at 45  $\mu\text{L}/\text{min}$  and 200  $\mu\text{L}/\text{min}$  in Figure 3e,f, respectively. No electric discharge occurred, which was presumably due to the low electric conductivity of the ethyl acetate.

Upon spray formation, a small expansion of the swab head due to solvent saturation was observed. Therefore, the jets of solvents exhibiting a low relative permittivity, e.g., tetrahydrofuran and 2-pentanone, were not yet stabilized, and jets only appeared to be short during spray initiation but quickly expanded into longer jets after 10–30 s.

Raising the relative permittivity of the solution by the addition of methanol [45] was found to be a very effective method for jet shortening and improving the signal intensity. Table 1 shows the required portion of methanol in binary mixtures with different solvents for establishing a short jet. The methanol content was gradually increased by steps of 10% until a short jet was observed. For example, an ethyl acetate/methanol mixture in a 70/30 (*v/v*) ratio was required for the best results. Despite the existence of several equations to predict the relative permittivity of a mixture [46], calculations could not predict the necessary methanol percentage required to generate a short jet in solvent mixtures. We assume that the complex fluid dynamics within the Taylor cone [5] under the influence of the electric field contribute decisively to the jet formation in solvent mixtures.

In addition to methanol, a similar effect was observed by the addition of other solvents exhibiting high relative permittivity. A minimum percentage of 20% DMF or 30% nitromethane had to be mixed with ethyl acetate to obtain short jets. However, in these experiments, the resulting ion current obtained for salicylanilide was very low again.

Setting the correct solvent flow is crucial for establishing a continuous electrospray with high ionization efficacy. In favor of the ionization efficacy, the formation of small primary droplets is mandatory. Excess solvent flow results in a broader jet and larger primary droplets and eventually decreases the ionization efficacy [47]. As jet broadening comes along with jet elongation, spray plume formation comes in close proximity to the counter electrode, which is detrimental for high ion yields (Figure 3f). On the other hand, too low flow rates promote fiber spray instead of establishing a cone jet [37]. In fiber spray, the ions are emitted from a single fiber rather than from the entire swab head. Although fiber spray experiments generated a strong analyte signal with low background, we experienced low reproducibility and inefficient analyte extraction from the swab, which impedes quantitative work [39]. Consequently, the aim is to set the flow rate as low as possible without disrupting the electrospray and simultaneously tolerating the positional and geometrical variations of the swab heads.

#### 2.5. Dripping Pulsation Mode

Solvents with the lowest relative permittivities examined in this work include hexane, 1,4-dioxane, toluene, and dibutyl ether. In all cases, the formation of a pulsating Taylor cone was observed. The pulsation mode of toluene is exemplarily shown in the series of photographs in Figure 5. The solvent droplet emerging from the swab head undergoes a slow elongation process and approaches the counter electrode until the droplet is suddenly ejected after 17.47 s. During the elongation process, the formation of a tiny jet is shortly visible, which can be observed at 8.87, 12.80, and 17.00 s in Figure 5; however, no ions were generated. The pulsation frequency was found to depend on the applied voltage and flow rate; increasing the voltage and flow rate led to a higher pulsation frequency. This kind of pulsation is referred to as the “dripping pulsation mode”, as reported previously for capillary-based electrospray [17,20,21,41,42]. The solvent must allow electric field-induced charge separation to generate a Taylor cone emitting a spray of charged



primary droplets [48]. Strongly polar solvents that exhibit a high relative permittivity support charge separation in the Taylor cone. The lack of charge separation in solvents with very low relative permittivity inhibits Taylor cone formation and is likely to be responsible for the dripping pulsation mode.

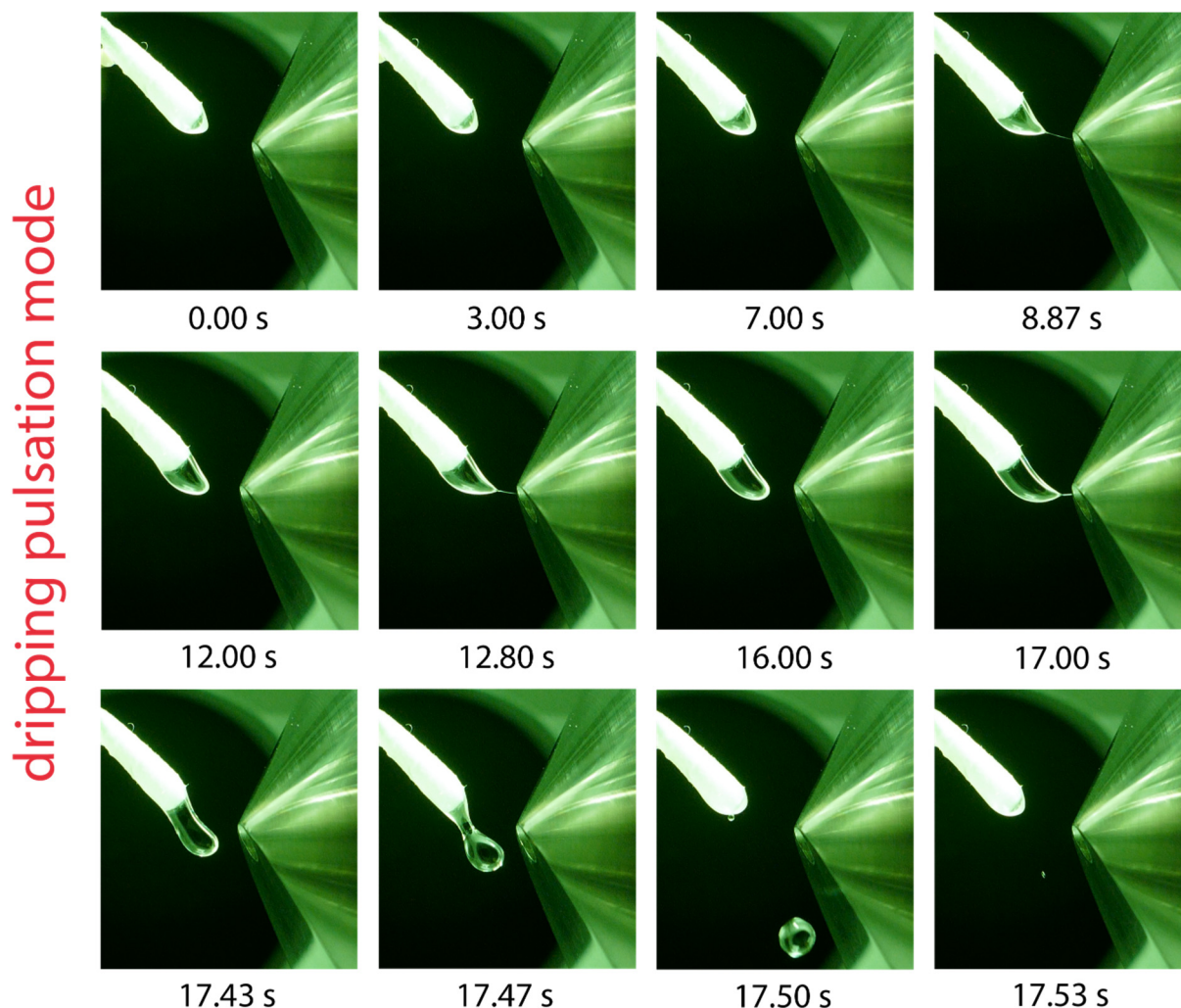


**Figure 5.** Visualization of one dripping pulsation cycle using toluene as the solvent, a flow rate of 45  $\mu\text{L}/\text{min}$  and a potential of 5.5 kV applied to the swab. Droplet elongation and sporadically occurring jet formation is visible before the elongated droplet is ejected after 17.5 s and another cycle starts.

To cure the dripping pulsation mode problem, the addition of methanol proved to be successful. For example, toluene mixed with 50% methanol generated a stable spray with a short jet (visualization is provided in Supplementary Data S1). Furthermore, the mixture of toluene/methanol (50/50,  $v/v$ ) provided abundant ionization efficacy for both salicylanilide and tetrabutylammonium iodide as suppression markers (full-scan spectra are presented in Supplementary Data S2 and S3).

## 2.6. Spindle Pulsation Mode

The pulsation mode observed for solvents with a very low relative permittivity differs from the pulsation modes observed for polar solvents. Although methanol mostly produced a stable Taylor cone with a short jet, pulsation was observed in certain cases, especially at elevated flow rates or when the swab position or applied potential were changed during operation. In rare cases, pulsation shortly occurred at initiation of the spray or randomly during operation.

The pulsation mode of methanol, which was easily provoked by increasing the distance to the counter electrode during operation (from 7 mm to approximately 9 mm), is shown in Figure 6. This pulsation mode is referred to as the “spindle mode” [17,18,20,21], which generates fluctuating ion currents. The broadening and elongation of the jet eventually leads to the ejection of a spindle-shaped droplet. Due to ejection of the droplet, the spray plume collapses and ion generation ceases. Figure 6 shows the total ion current chromatogram recorded under spindle mode conditions. The size of the ejected droplets varies, and breakdown of the ion current occurs within irregular cycles of several seconds under the given conditions (45  $\mu\text{L}/\text{min}$  solvent flow and 5.5 kV potential).

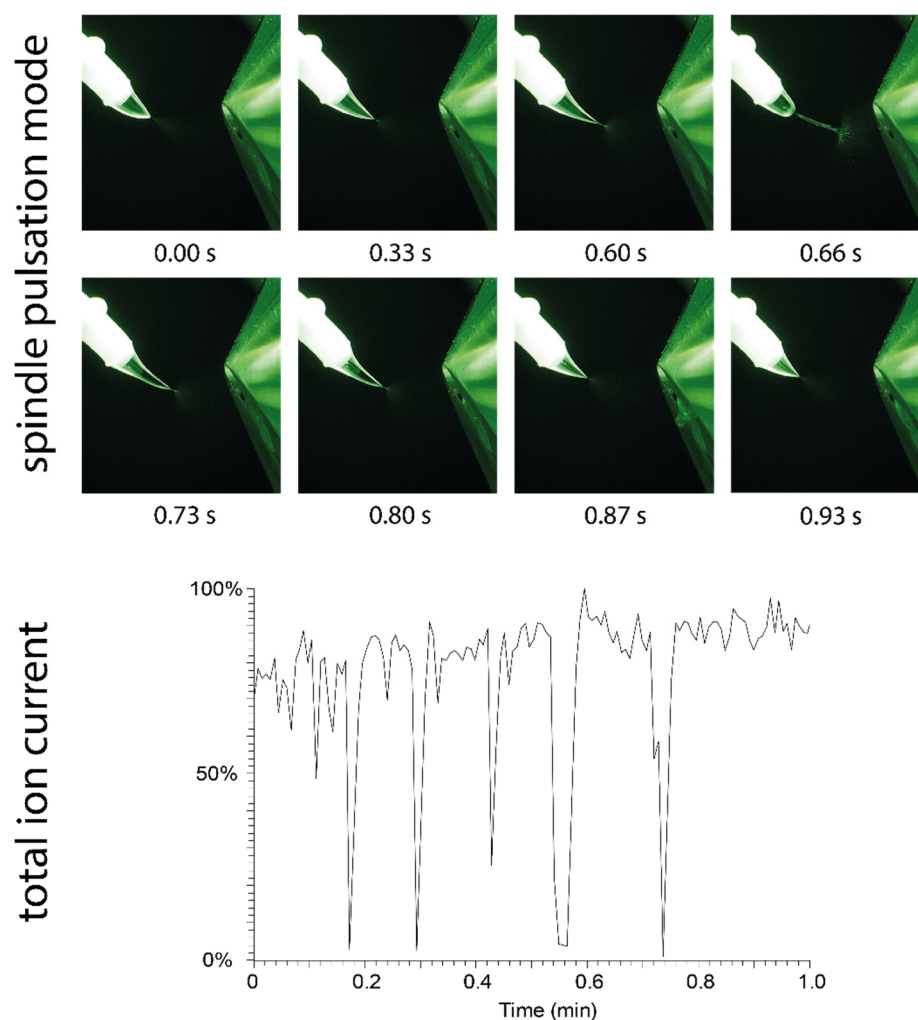


**Figure 6.** (Top): Visualization of the spindle mode: The Taylor cone formed by methanol undergoes an elongation process, which creates a spindle-shaped droplet that is quickly ejected after 0.66 s. (Bottom): The impact of repeated spindle mode pulsation events on the total ion current is shown. During ejection of the spindle, the spray plume collapses, and no ions are generated.

### 2.7. Taylor Cones with Long Jets by Non-Viscous Solvents

The deposition of pure highly viscous glycerol ( $\eta = 934 \text{ mPa}\cdot\text{s}$ ) to a Copan 160C swab resulted in a drastic increase in the jet length, which is in agreement with the common understanding that the jet length is directly related to the viscosity of the solvent due to better stabilization [4,14]. However, our experiments revealed that the jet lengths of organic solvents suitable for electrospray ionization do not follow the order of viscosities. Investigated solvents span over a viscosity range of approximately 0.2 to 2.0  $\text{mPa}\cdot\text{s}$ . The viscosities of solvents are given in Table 1, and the observed jet characteristics are indicated by the font color. Notably, diethyl ether, which has the lowest viscosity, produced a long jet.



This stands in contrast to DMSO, which exhibits the second highest viscosity among the listed solvents and produced a short jet. The higher relative permittivity of DMSO promotes charge separation within the jet under the influence of the electric field. The resulting higher charge density helps to overcome the surface tension, facilitating jet break-up into the plume of charged droplets, which eventually leads to ionization. The opposite process applies to the production of a long jet by diethyl ether. Therefore, the long jets formed by organic solvents with low viscosity cannot be the result of spray stabilization by viscosity but are related to their low relative permittivity. Overcoming the surface tension by the electric force is required for spray plume formation and subsequent ionization [49–51]. Low relative permittivity dampens charge separation within the jet and consequently prevents spray plume formation and ionization.

Concerns that solvents of lower polarity may extract adhesives and other swab-related contaminants, which could potentially influence solvent properties such as the viscosity, were refuted by an experiment, where the swab was replaced by a metal screw. The metal screw imitates the swab by offering solvent accumulation on the screw head similar to a swab head but without the risk of adhesive extraction. The sprays generated by 2-propanol and a mixture of 2-propanol (70/30, *v/v*) with methanol from a metal screw are shown in Figure 7, demonstrating that the flow-related characteristic of the Taylor cone is comparable to the experiments with Copan 160C swabs shown in Figure 3e,f. Consequently, a contribution from the swab material can be excluded.

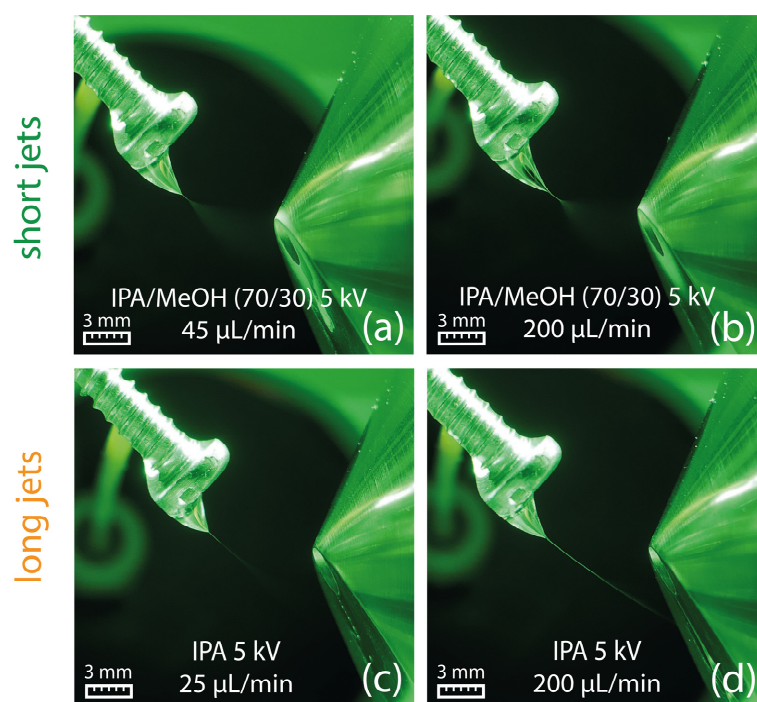


**Figure 7.** Formation of a Taylor cone with a short jet using 2-propanol/methanol (70/30, *v/v*) at 45 µL/min (a) and 200 µL/min (b). Formation of a Taylor cone with a long jet on a metal screw using 2-propanol at a flow rate of 25 µL/min (c) and 200 µL/min (d).

Although recent studies revealed that properties of liquids are altered in strong electric fields, the influence on electrospray ionization has not been investigated yet. Available data indicate only minor changes in very high electric fields [12,13]. Therefore, the use of standard solvent constants is considered appropriate to explain the phenomenon of increasing jet length. Conclusively, for the investigated solvents, the relative permittivity of solvents measured under standard condition is the decisive factor when it comes to jet shaping.

### 2.8. Jet Formation in Capillary-Based Electrospray Ion Sources

To further investigate the described effects, a similar experiment was performed in a conventional electrospray ion source. Hereby, the solvent was pumped through a thin conductive electrospray emitter. The nebulizer and heater gas were turned off to prevent disintegration of the jet by gas flow. The solvent, including 0.1% formic acid and 1 ppm suppression marker, was delivered at a flow rate of 45  $\mu\text{L}/\text{min}$  in all experiments. The use of ethyl acetate as the spray solvent delivered hardly any signal over a period of five minutes, as illustrated in Figure 8 (top), which must be related to the formation of a long jet. When methanol was used as the spray solvent, an abundant signal over the course of five minutes could be observed (Figure 8 center). A significant improvement of the ionization was achieved by the addition of methanol to ethyl acetate, resulting in ion currents comparable to the ones obtained with pure methanol (shown in Figure 8 (bottom) for 60% MeOH). Compared to the swab spray experiments, the higher percentage of MeOH is most likely due to the different electrospray emitter geometry.

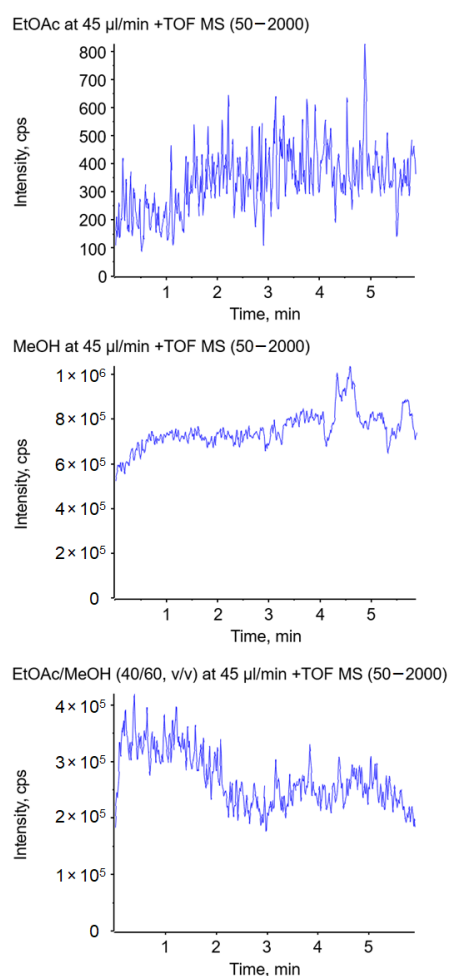


**Figure 8.** Impact of the solvent on the total ion current using ethyl acetate (**top**), methanol (**center**), and a mixture of ethyl acetate/methanol (40/60, v/v) (**bottom**) in a conventional electrospray ion source without the assistance of nebulizer and heater gas.

These experiments demonstrate that the observed effect of the relative permittivity on jet formation is transferable to other electrospray ion sources that do not provide ion source gases and are operated at comparably low solvent flow rates. For ambient ionization that does not provide gas to assist ionization, the relative permittivity of the spray solvent is a crucial factor, as the formation of a short jet is mandatory for ionization.

### 2.9. Jet Formation in Paper Spray

The formation of a short jet is crucial for efficient ion generation in any electrospray-based ionization technique. In swab spray ionization, the Taylor cone and the subsequent jet emit from a rather large and geometrically less defined surface area, which is opposed to the conventional well-defined capillary emitters. In paper spray, the sample is deposited on a triangular piece of paper, and the spray is formed at the vertex pointing toward the counter electrode. Compared to swab spray, the Taylor cone originates from a smaller surface area, and spray emission is supported by paper fibers. Indeed, paper spray requires lower ionization potential and a reduced solvent flow rate [52–54]. In our experiments, a potential of +3.5 kV and a flow rate of 30  $\mu\text{L}/\text{min}$  only were sufficient to generate a stable electrospray in our experiments using different solvents.

Similar to swab spray, DMSO and methanol resulted in short jets (Figure 9a,b), whereas longer jets were observed for 2-propanol and ethyl acetate (Figure 9c,d). Under the given conditions, paper spray was found to be not susceptible to the adverse spindle pulsation mode observed in swab spray, which can be attributed to paper fibers that support spray emission.

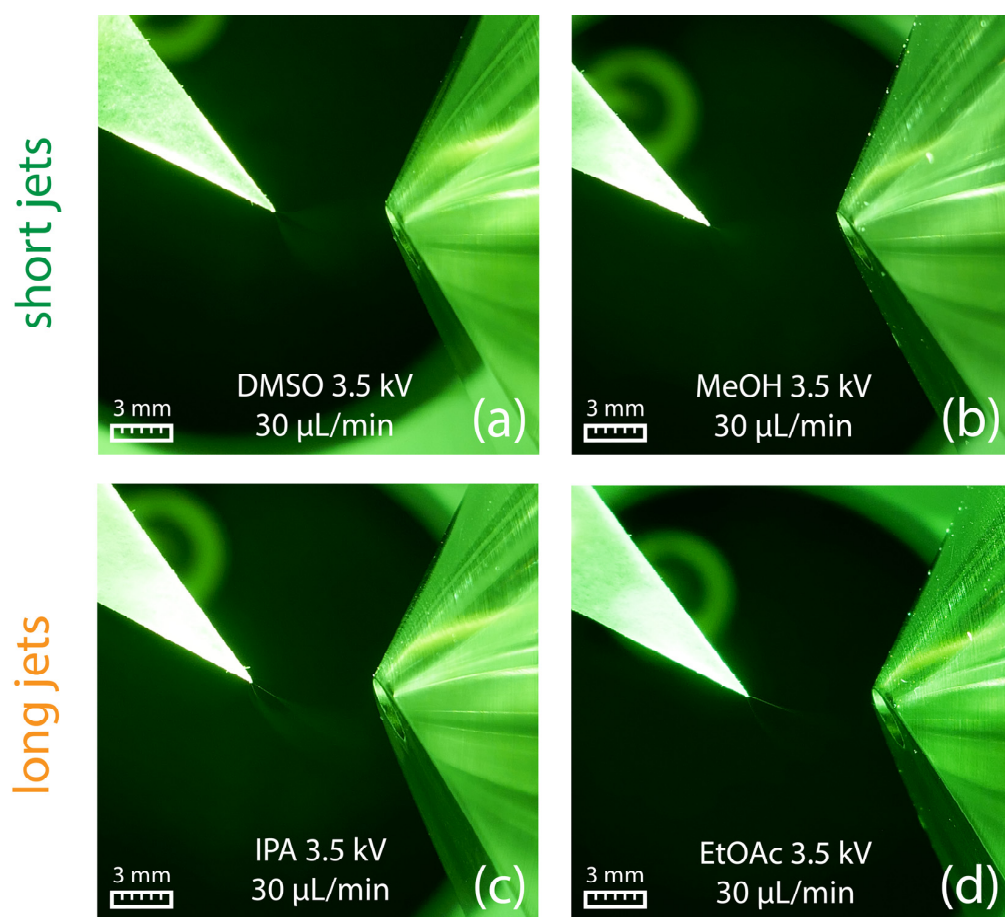


**Figure 9.** Paper spray in combination with DMSO (a) and methanol (b) produced short jets. In contrast, 2-propanol (c) and ethyl acetate (d) led to the formation of long jets. All pictures were obtained using a flow rate of 30  $\mu\text{L}/\text{min}$  in combination with an electric potential of +3.5 kV.

The ionization efficacy of paper spray was probed by monitoring the ion current of salicylanilide, which was added to the spray solvent at a concentration of 1 ppm. As in the case of swab spray, jet-shaping effects governed by the solvent relative permittivity were observed. However, the detrimental effect on ion generation was not encountered. Ethyl acetate as the solvent yielded an ion current of protonated salicylanilide comparable to the

one detected with methanol, as indicated by the peaks at  $m/z$  214.09 in Figure 10. The loss of solvent by evaporation and the occurrence of multiple jets, as evidenced by Figure 9a,c,d, further reduced the effective flow rate in individual jets. These effects counteract the formation of very long jets and enable ionization even in the case of 2-propanol and ethyl acetate as the solvents. Hence, paper spray is less sensitive to solvent selection and does not require the same level of solvent optimization as swab spray.

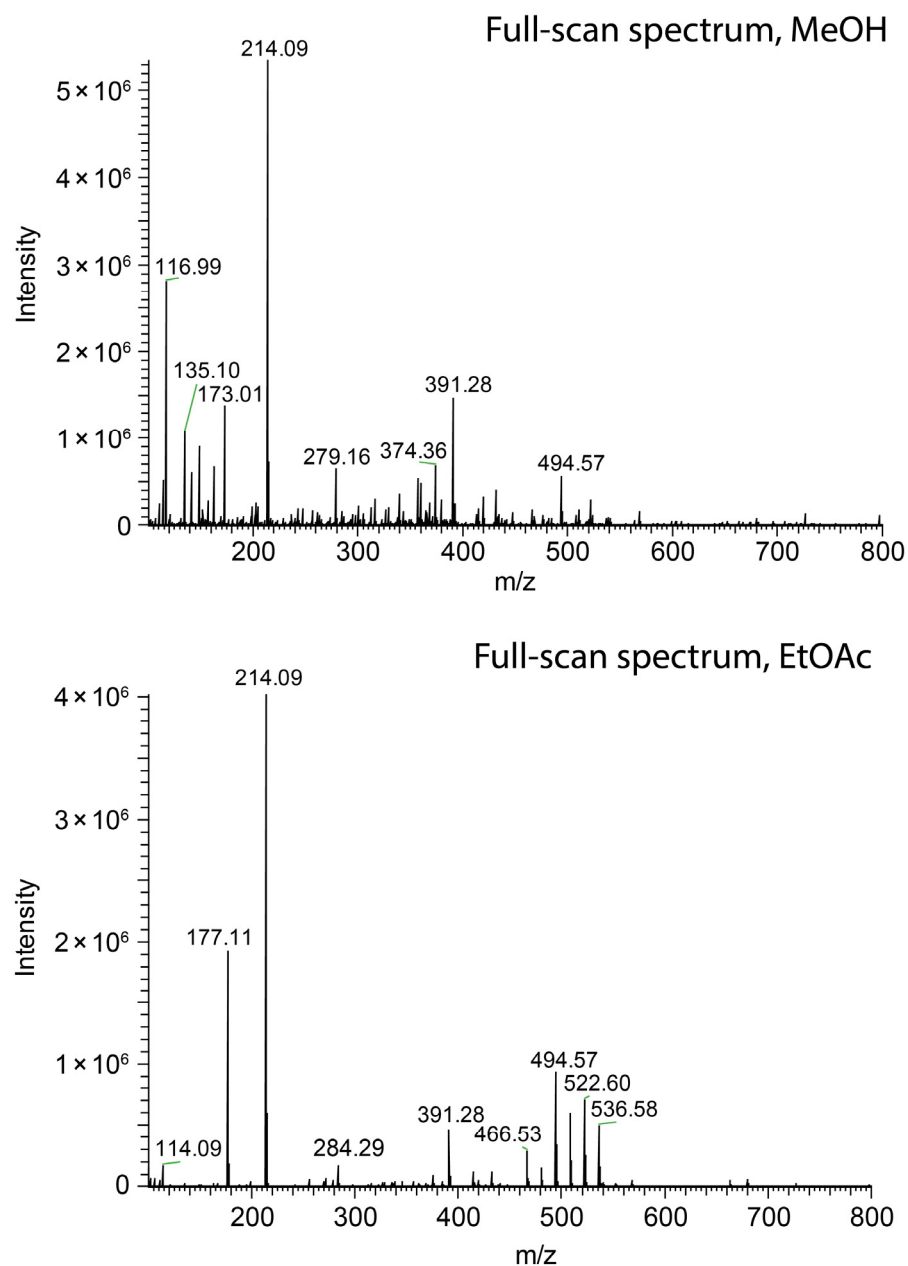


**Figure 10.** Comparison of paper spray mass spectra of salicylanilide ( $[M + H]^+$  at  $m/z$  214.09) obtained with methanol (**top**) and ethyl acetate (**bottom**) as the solvents.

### 3. Material and Methods

#### 3.1. Instrumentation

The instrumentation consisted of a custom-made swab spray ion source connected to a Thermo Fisher Scientific (Reinach, Switzerland) LTQ Orbitrap Velos mass spectrometer. The ion source allowed swab fixation in a 45-degree angle, direct application of the electric potential, and continuous solvent supply by a syringe pump. The method has previously

been described in detail [39]. All experiments were performed in positive ionization mode. For Taylor cone formation, the solvent flow rate was set to 45  $\mu\text{L}/\text{min}$  (with the exception of acetone, dichloromethane, and diethyl ether, where the flow rate was set to 60  $\mu\text{L}/\text{min}$  due to high solvent evaporation rates). The solvent flow was started about 1–2 min prior to the application of the electric potential to ensure solvent saturation of the swab head. A distance of 7 mm from the swab head to the counter electrode was chosen for all experiments, as such a setup was beneficial for signal intensity and for the prevention of electrical discharges. For photographic observation, a green flashlight was placed on top of the ion source housing (replacing the top-mounted camera), whereas the pictures were taken from the side. To monitor the ionization efficacy and background signal, salicylanilide was added to all solvents as a suppression marker at a concentration of 1 ppm. To facilitate ionization, 0.1% formic acid was added to all solvent combinations.

A Turbo V ion source was used for conventional electrospray on a Sciex X500B (AB Sciex, Baden, Switzerland) quadrupole time-of-flight mass spectrometer operated in the positive ionization mode at +5.5 kV. The curtain gas was set to 35 psi, and the solvent was supplied at a flow rate of 45  $\mu\text{L}/\text{min}$ . The nebulizer and heater gas were turned off in these experiments.

### 3.2. Chemicals and Materials

The following chemicals were purchased from Merck/Sigma-Aldrich (Buchs, Switzerland): methanol, ethyl acetate, acetonitrile, 2-propanol (all Supelco Lichrosolv<sup>®</sup> hypergrade for LC-MS, Merck/Sigma-Aldrich (Buchs, Switzerland)), trichloromethane (Chromasolv<sup>TM</sup> plus for HPLC, 99.8%, Honeywell Specialty Chemicals (Seelze, Germany)), formic acid (for LC-MS, 98–100%), water (LC-MS grade), toluene (HPLC grade, 99.9%), methyl acetate (99.5%, anhydrous), 3-pentanone ( $\geq 99.0\%$ ), propyl acetate (99%), dibutyl ether ( $\geq 99.0\%$ ), 1-nitropropane ( $\geq 98.5\%$ ), DMSO ( $\geq 99.0\%$ ), n-hexane ( $\geq 99\%$ ), 1,4-dioxane ( $\geq 99\%$ ), N,N-dimethylformamide ( $\geq 99.8\%$ ), anisole (99%), tetrabutylammonium iodide (98%), and salicylanilide (99%). Nitromethane ( $\geq 98\%$ ) and dichloromethane (99.7%, HPLC grade, stabilized with amylene) were purchased from Thermo Fisher Scientific (Reinach, Switzerland). THF and acetone (both HPLC grade, HiPerSolv Chromanorm<sup>®</sup>, VWR International (Dietikon, Switzerland)) were both purchased from VWR International (Dietikon, Switzerland). Ethanol absolute (HPLC grade) was purchased from Honeywell Specialty Chemicals (Seelze, Germany) and 1-chlorobutane (biopure solvent) was purchased from Romil (Waterbeach, UK).

The Copan 160C minitip rayon swabs with aluminum applicator contained in a sealed plastic tube were purchased from VWR International (Dietikon, Switzerland). A swab prewashing procedure was applied by ultrasonication in ethyl acetate according to the literature [39]. The metal screw which was used as an electrospray emitter was cleaned by ultrasonication in 2-propanol for 15 min at 40 °C. For paper spray, filter paper type 589/1 (Schleicher & Schuell, Göttingen, Germany) was cut into a triangle and mounted in the swab holder at a distance of approximately 7 mm from the counter electrode. The solvent supply capillary was directly positioned on the upper part of the filter paper.

## 4. Conclusions

The formation of a Taylor cone with a short spray jet is mandatory for successful electrospray-based swab spray mass spectrometry. The present investigation shows that the relative permittivity of spray solvents is the key parameter in swab spray that determines the electrospray mode and therefore the ionization efficacy. Solvents are subdivided into three groups that exhibit different electrospray modes. Solvents with a relative permittivity larger than 25 were found to generate a Taylor cone with a short jet that enables high ionization efficacy, whereas spray solvents with intermediate relative permittivity in the range between 4 and 25 formed Taylor cones with long jets resulting in decreased ionization efficacy. A dripping pulsation mode was observed for solvents with low relative permittivity below 4. The addition of varying portions of methanol is recommended or



even required to raise the relative permittivity of spray solvents that exhibit long jets or a dripping pulsation mode. On the other hand, ionization efficacy in paper spray remained unaffected by elongated jets due to different spray emission and lower flow rates.

**Supplementary Materials:** The following supporting information can be downloaded at: <https://www.mdpi.com/article/10.3390/molecules29174274/s1>, Figure S1: Taylor cone angles at different voltages using toluene/methanol (50/50, v/v) and dimethyl formamide; Figure S2: Full-scan spectra of nitromethane and ethanol; Figure S3: Full-scan spectra of trichloromethane/methanol (80/20, v/v), ethyl acetate/methanol (70/30, v/v), and methanol; Figure S4: Full-scan spectra of dibutyl ether/methanol (40/60, v/v), acetone/methanol (80/20, v/v), and dimethyl formamide; Figure S5: Full-scan spectra of anisole/methanol (50/50, v/v), toluene/methanol (50/50, v/v), and diethyl ether; Figure S6: Full-scan spectra of dimethyl formamide, dimethyl sulfoxide, and toluene/methanol (50/50, v/v)

**Author Contributions:** T.M.M. performed the experiments, visualized the data and wrote the original draft. S.S. and T.M.M. were both responsible for the methodology and conceptualization. S.S. supervised the experiments, provided funding/resources, reviewed and edited the manuscript. All authors have read and agreed to the published version of the manuscript.

**Funding:** This research received no external funding.

**Institutional Review Board Statement:** Not applicable.

**Informed Consent Statement:** Not applicable.

**Data Availability Statement:** Additional data is provided in the Supplementary Materials. Further data is available upon request.

**Conflicts of Interest:** There are no conflicts to declare.

## References

1. Zeleny, J. The Electrical Discharge from Liquid Points, and a Hydrostatic Method of Measuring the Electric Intensity at Their Surfaces. *Phys. Rev.* **1914**, *3*, 69–91. [\[CrossRef\]](#)
2. Taylor, G.I. Disintegration of Water Drops in an Electric Field. *Proc. R. Soc. Lond. A Math. Phys. Sci.* **1964**, *280*, 383–397. [\[CrossRef\]](#)
3. Melcher, J.R.; Taylor, G.I. Electrohydrodynamics: A Review of the Role of Interfacial Shear Stresses. *Annu. Rev. Fluid. Mech.* **1969**, *1*, 111–146. [\[CrossRef\]](#)
4. Cloupeau, M.; Prunet-Foch, B. Electrohydrodynamic Spraying Functioning Modes: A Critical Review. *J. Aerosol Sci.* **1994**, *25*, 1021–1036. [\[CrossRef\]](#)
5. de la Mora, J.F. The Fluid Dynamics of Taylor Cones. *Annu. Rev. Fluid. Mech.* **2006**, *39*, 217–243. [\[CrossRef\]](#)
6. Dole, M.; Mack, L.L.; Hines, R.L.; Mobley, R.C.; Ferguson, L.D.; Alice, M.B. Molecular Beams of Macroions. *J. Chem. Phys.* **1968**, *49*, 2240–2249. [\[CrossRef\]](#)
7. Yamashita, M.; Fenn, J.B. Electrospray Ion Source. Another Variation on the Free-Jet Theme. *J. Phys. Chem.* **1984**, *88*, 4451–4459. [\[CrossRef\]](#)
8. Fenn, J.B.; Mann, M.; Meng, C.K.; Wong, S.F.; Whitehouse, C.M. Electrospray Ionization for Mass Spectrometry of Large Biomolecules. *Science* **1989**, *246*, 64–71. [\[CrossRef\]](#)
9. Verenchikov, A.N.; Krasnov, N.V.; Shkurov, V.A. Electrospray Ionization Developed by Lidija Gall's Group. *Int. J. Mass Spectrom.* **2023**, *490*, 117067. [\[CrossRef\]](#)
10. Wilm, M. Principles of Electrospray Ionization. *Mol. Cell. Proteom.* **2011**, *10*, M111.009407. [\[CrossRef\]](#)
11. Subbotin, A.V.; Semenov, A.N. Electrohydrodynamics of Stationary Cone-Jet Streaming. *Proc. R. Soc. A Math. Phys. Eng. Sci.* **2015**, *471*, 20150290. [\[CrossRef\]](#)
12. Zong, D.; Hu, H.; Duan, Y.; Sun, Y. Viscosity of Water under Electric Field: Anisotropy Induced by Redistribution of Hydrogen Bonds. *J. Phys. Chem. B* **2016**, *120*, 4818–4827. [\[CrossRef\]](#) [\[PubMed\]](#)
13. Bateni, A.; Amirfazli, A.; Neumann, A.W. Effects of an Electric Field on the Surface Tension of Conducting Drops. *Colloids Surf. A Physicochem. Eng. Asp.* **2006**, *289*, 25–38. [\[CrossRef\]](#)
14. Ismail, A.S.; Yao, J.; Xia, H.H.; Stark, J.P.W. Breakup Length of Electrified Liquid Jets: Scaling Laws and Applications. *Phys. Rev. Appl.* **2018**, *10*, 064010. [\[CrossRef\]](#)
15. Zhou, H.; Shi, Z.; Wan, X.; Fang, H.; Yu, D.-G.; Chen, X.; Liu, P. The Relationships between Process Parameters and Polymeric Nanofibers Fabricated Using a Modified Coaxial Electrospinning. *Nanomaterials* **2019**, *9*, 843. [\[CrossRef\]](#)
16. Wang, Q.; Wang, Z.; Jiang, Y.; Yang, S. Experimental Study of Electro-Spraying Modes of Deionized Water in Atmospheric Environment. *Exp. Comput. Multiph. Flow* **2021**, *3*, 38–46. [\[CrossRef\]](#)

17. Kim, H.-H.; Kim, J.-H.; Ogata, A. Time-Resolved High-Speed Camera Observation of Electrospray. *J. Aerosol Sci.* **2011**, *42*, 249–263. [\[CrossRef\]](#)
18. Nemes, P.; Marginean, I.; Vertes, A. Spraying Mode Effect on Droplet Formation and Ion Chemistry in Electrosprays. *Anal. Chem.* **2007**, *79*, 3105–3116. [\[CrossRef\]](#)
19. Jaworek, A.; Krupa, A. Generation and Characteristics of the Precession Mode of Ehd Spraying. *J. Aerosol Sci.* **1996**, *27*, 75–82. [\[CrossRef\]](#)
20. Pongráč, B.; Kim, H.-H.; Negishi, N.; Machala, Z. Influence of Water Conductivity on Particular Electrospray Modes with Dc Corona Discharge—Optical Visualization Approach. *Eur. Phys. J. D* **2014**, *68*, 224. [\[CrossRef\]](#)
21. Castillo-Orozco, E.; Kar, A.; Kumar, R. Electrospray Mode Transition of Microdroplets with Semiconductor Nanoparticle Suspension. *Sci. Rep.* **2017**, *7*, 5144. [\[CrossRef\]](#) [\[PubMed\]](#)
22. Kim, J.Y.; Lee, S.J.; Hong, J.G. Spray Mode and Monodisperse Droplet Properties of an Electrospray. *ACS Omega* **2022**, *7*, 28667–28674. [\[CrossRef\]](#) [\[PubMed\]](#)
23. Gomez, A. The Electrospray: Fundamentals and Applications. In *Experimental Heat Transfer, Fluid. Mechanics and Thermodynamics 1993*; Kelleher, M.D., Sreenivasan, K.R., Shah, R.K., Joshi, Y., Eds.; Elsevier: Amsterdam, The Netherlands, 1993; pp. 270–282. ISBN 978-0-444-81619-1.
24. Konermann, L.; Ahadi, E.; Rodriguez, A.D.; Vahidi, S. Unraveling the Mechanism of Electrospray Ionization. *Anal. Chem.* **2013**, *85*, 2–9. [\[CrossRef\]](#)
25. Thinius, M.; Polaczek, C.; Langner, M.; Bräkling, S.; Haack, A.; Kersten, H.; Benter, T. Charge Retention/Charge Depletion in ESI-MS: Experimental Evidence. *J. Am. Soc. Mass Spectrom.* **2020**, *31*, 773–784. [\[CrossRef\]](#)
26. Valeja, S.G.; Tipton, J.D.; Emmett, M.R.; Marshall, A.G. New Reagents for Enhanced Liquid Chromatographic Separation and Charging of Intact Protein Ions for Electrospray Ionization Mass Spectrometry. *Anal. Chem.* **2010**, *82*, 7515–7519. [\[CrossRef\]](#)
27. Takáts, Z.; Wiseman, J.M.; Gologan, B.; Cooks, R.G. Mass Spectrometry Sampling under Ambient Conditions with Desorption Electrospray Ionization. *Science* **2004**, *306*, 471–473. [\[CrossRef\]](#)
28. Liu, J.; Wang, H.; Manicke, N.E.; Lin, J.-M.; Cooks, R.G.; Ouyang, Z. Development, Characterization, and Application of Paper Spray Ionization. *Anal. Chem.* **2010**, *82*, 2463–2471. [\[CrossRef\]](#) [\[PubMed\]](#)
29. Pirro, V.; Jarmusch, A.K.; Vincenti, M.; Cooks, R.G. Direct Drug Analysis from Oral Fluid Using Medical Swab Touch Spray Mass Spectrometry. *Anal. Chim. Acta* **2015**, *861*, 47–54. [\[CrossRef\]](#)
30. Yang, B.; Wang, F.; Yang, X.; Zou, W.; Wang, J.; Zou, Y.; Liu, F.; Liu, H.; Huang, O. Medical Swab Touch Spray-Mass Spectrometry for Newborn Screening of Nicotine and Cotinine in Meconium. *J. Mass Spectrom.* **2016**, *51*, 1237–1242. [\[CrossRef\]](#)
31. Pirro, V.; Llor, R.S.; Jarmusch, A.K.; Alfaro, C.M.; Cohen-Gadol, A.A.; Hattab, E.M.; Cooks, R.G. Analysis of Human Gliomas by Swab Touch Spray-Mass Spectrometry: Applications to Intraoperative Assessment of Surgical Margins and Presence of Oncometabolites. *Analyst* **2017**, *142*, 4058–4066. [\[CrossRef\]](#)
32. Costa, C.; van Es, E.M.; Sears, P.; Bunch, J.; Palitsin, V.; Cooper, H.; Bailey, M.J. Exploring a Route to a Selective and Sensitive Portable System for Explosive Detection—Swab Spray Ionisation Coupled to of High-Field Assisted Waveform Ion Mobility Spectrometry (FAIMS). *Forensic Sci. Int.* **2019**, *1*, 214–220. [\[CrossRef\]](#)
33. Bain, R.M.; Fedick, P.W.; Dilger, J.M.; Cooks, R.G. Analysis of Residual Explosives by Swab Touch Spray Ionization Mass Spectrometry. *Propellants Explos. Pyrotech.* **2018**, *43*, 1139–1144. [\[CrossRef\]](#)
34. Jarmusch, A.K.; Pirro, V.; Kerian, K.S.; Cooks, R.G. Detection of Strep Throat Causing Bacterium Directly from Medical Swabs by Touch Spray-Mass Spectrometry. *Analyst* **2014**, *139*, 4785–4789. [\[CrossRef\]](#) [\[PubMed\]](#)
35. Fedick, P.W.; Bain, R.M. Swab Touch Spray Mass Spectrometry for Rapid Analysis of Organic Gunshot Residue from Human Hand and Various Surfaces Using Commercial and Fieldable Mass Spectrometry Systems. *Forensic Chem.* **2017**, *5*, 53–57. [\[CrossRef\]](#)
36. Morato, N.M.; Pirro, V.; Fedick, P.W.; Cooks, R.G. Quantitative Swab Touch Spray Mass Spectrometry for Oral Fluid Drug Testing. *Anal. Chem.* **2019**, *91*, 7450–7457. [\[CrossRef\]](#) [\[PubMed\]](#)
37. Jarmusch, A.K.; Pirro, V.; Logsdon, D.L.; Cooks, R.G. Direct Ion Generation from Swabs. *Talanta* **2018**, *184*, 356–363. [\[CrossRef\]](#)
38. Beneito-Cambra, M.; Gilbert-López, B.; Moreno-González, D.; Bouza, M.; Franzke, J.; García-Reyes, J.F.; Molina-Díaz, A. Ambient (Desorption/Ionization) Mass Spectrometry Methods for Pesticide Testing in Food: A Review. *Anal. Methods* **2020**, *12*, 4831–4852. [\[CrossRef\]](#)
39. Muggli, T.M.; Schürch, S. Analysis of Pesticide Residues on Fruit Using Swab Spray Ionization Mass Spectrometry. *Molecules* **2023**, *28*, 6611. [\[CrossRef\]](#)
40. Shamraeva, M.A.; Bormotov, D.S.; Shamarina, E.V.; Bocharov, K.V.; Peregudova, O.V.; Pekov, S.I.; Nikolaev, E.N.; Popov, I.A. Spherical Sampler Probes Enhance the Robustness of Ambient Ionization Mass Spectrometry for Rapid Drugs Screening. *Molecules* **2022**, *27*, 945. [\[CrossRef\]](#)
41. Budhwani, K.I.; Pekmezi, G.M.; Selim, M.M. Measuring Surface and Interfacial Tension In Situ in Microdripping Mode for Electrohydrodynamic Applications. *Micromachines* **2020**, *11*, 687. [\[CrossRef\]](#)
42. Maheshwari, S.; Chetwani, N.; Chang, H.-C. Alternating Current Electrospraying. *Ind. Eng. Chem. Res.* **2009**, *48*, 9358–9368. [\[CrossRef\]](#)
43. Rumble, J. (Ed.) *CRC Handbook of Chemistry and Physics*, 104th ed.; CRC Press: Boca Raton, FL, USA, 2023.
44. Haynes, W.M. (Ed.) *CRC Handbook of Chemistry and Physics*, 95th ed.; CRC Press: Boca Raton, FL, USA, 2014; ISBN 9780429170195.

45. Neumaier, L.; Schilling, J.; Bardow, A.; Gross, J. Dielectric Constant of Mixed Solvents Based on Perturbation Theory. *Fluid Phase Equilibria* **2022**, *555*, 113346. [[CrossRef](#)]
46. Chen, W.-S.; Hsieh, M.-Y. Dielectric Constant Calculation Based on Mixture Equations of Binary Composites at Microwave Frequency. *Ceram. Int.* **2017**, *43*, S343–S350. [[CrossRef](#)]
47. Tang, K.; Smith, R.D. Physical/Chemical Separations in the Break-up of Highly Charged Droplets from Electrosprays. *J. Am. Soc. Mass Spectrom.* **2001**, *12*, 343–347. [[CrossRef](#)]
48. Gao, J.; Austin, D.E. Mechanistic Investigation of Charge Separation in Electrospray Ionization Using Microparticles to Record Droplet Charge State. *J. Am. Soc. Mass Spectrom.* **2020**, *31*, 2044–2052. [[CrossRef](#)] [[PubMed](#)]
49. Hartman, R.P.A.; Brunner, D.J.; Camelot, D.M.A.; Marijnissen, J.C.M.; Scarlett, B. Jet break-up in electrohydrodynamic atomization in the cone-jet mode. *J. Aerosol Sci.* **2000**, *31*, 65–95. [[CrossRef](#)]
50. Morad, M.R.; Rajabi, A.; Razavi, M.; Sereshkeh, S.R.P. A Very Stable High Throughput Taylor Cone-Jet in Electrohydrodynamics. *Sci. Rep.* **2016**, *6*, 38509. [[CrossRef](#)]
51. Collins, R.T.; Harris, M.T.; Basaran, O.A. Breakup of Electrified Jets. *J. Fluid Mech.* **2007**, *588*, 75–129. [[CrossRef](#)]
52. Kim, D.; Lee, J.; Kim, B.; Kim, S. Optimization and Application of Paper-Based Spray Ionization Mass Spectrometry for Analysis of Natural Organic Matter. *Anal. Chem.* **2018**, *90*, 12027–12034. [[CrossRef](#)]
53. McBride, E.M.; Mach, P.M.; Dhumakupt, E.S.; Dowling, S.; Carmany, D.O.; Demond, P.S.; Rizzo, G.; Manicke, N.E.; Glaros, T. Paper Spray Ionization: Applications and Perspectives. *TrAC Trends Anal. Chem.* **2019**, *118*, 722–730. [[CrossRef](#)]
54. Nguyen, T.M.H.; Song, W.-Y.; Kim, T.-Y. Characterization of Spray Modes and Factors Affecting the Ionization Efficiency of Paper Spray Ionization. *Front. Chem.* **2022**, *10*, 864184. [[CrossRef](#)] [[PubMed](#)]

**Disclaimer/Publisher’s Note:** The statements, opinions and data contained in all publications are solely those of the individual author(s) and contributor(s) and not of MDPI and/or the editor(s). MDPI and/or the editor(s) disclaim responsibility for any injury to people or property resulting from any ideas, methods, instructions or products referred to in the content.



## 2.9 Pesticide Analysis

For the analysis of pesticides on food products, a multiresidue method was developed. The method was evaluated using Copan 160C and ITS polyester swabs with a triazine and an organophosphorus mixture.

### 2.9.1 Triazine Mixture

To evaluate the performance of both Copan 160C and ITS polyester swabs for qualitative pesticide detection, a pesticide reference mixture consisting of several triazines was chosen. Full-scan spectra recorded for the initial ten seconds were accumulated, and the masses of the triazine compounds were searched. All seven triazine compounds, as listed in Table 9, were simultaneously detected as proton adducts with abundant signal intensity. The full-scan spectrum obtained using the ITS polyester swab is depicted in Figure 42 (top). The most abundant peak at  $m/z$  242.12 yielding  $1.6 \times 10^6$  signal counts, corresponds to the isobaric compounds prometryn and terbutryn. The Copan 160C swabs exhibited a comparable full-scan spectrum, enabling the detection of all triazine compounds in the mixture. Both swabs demonstrated similar capabilities for qualitative triazine detection. Nevertheless, the ITS polyester swab requires an additional handling step as the non-conductive polymer handle requires the addition of a metal wire to guide the electric potential to the swab head.

Table 9 Components of the triazine pesticide reference mixture, including their chemical compositions and the mass of their theoretical proton adducts.

compound	composition	[M+H] <sup>+</sup> (m/z)
ametryn	C <sub>9</sub> H <sub>17</sub> N <sub>5</sub> S	228.1278
atrazine	C <sub>8</sub> H <sub>14</sub> ClN <sub>5</sub>	216.1011
prometon	C <sub>10</sub> H <sub>19</sub> N <sub>5</sub> O	226.1662
prometryn	C <sub>10</sub> H <sub>19</sub> N <sub>5</sub> S	242.1434
propazine	C <sub>9</sub> H <sub>16</sub> ClN <sub>5</sub>	230.1167
simazine	C <sub>7</sub> H <sub>12</sub> ClN <sub>5</sub>	202.0854
terbutryn	C <sub>10</sub> H <sub>19</sub> N <sub>5</sub> S	242.1434

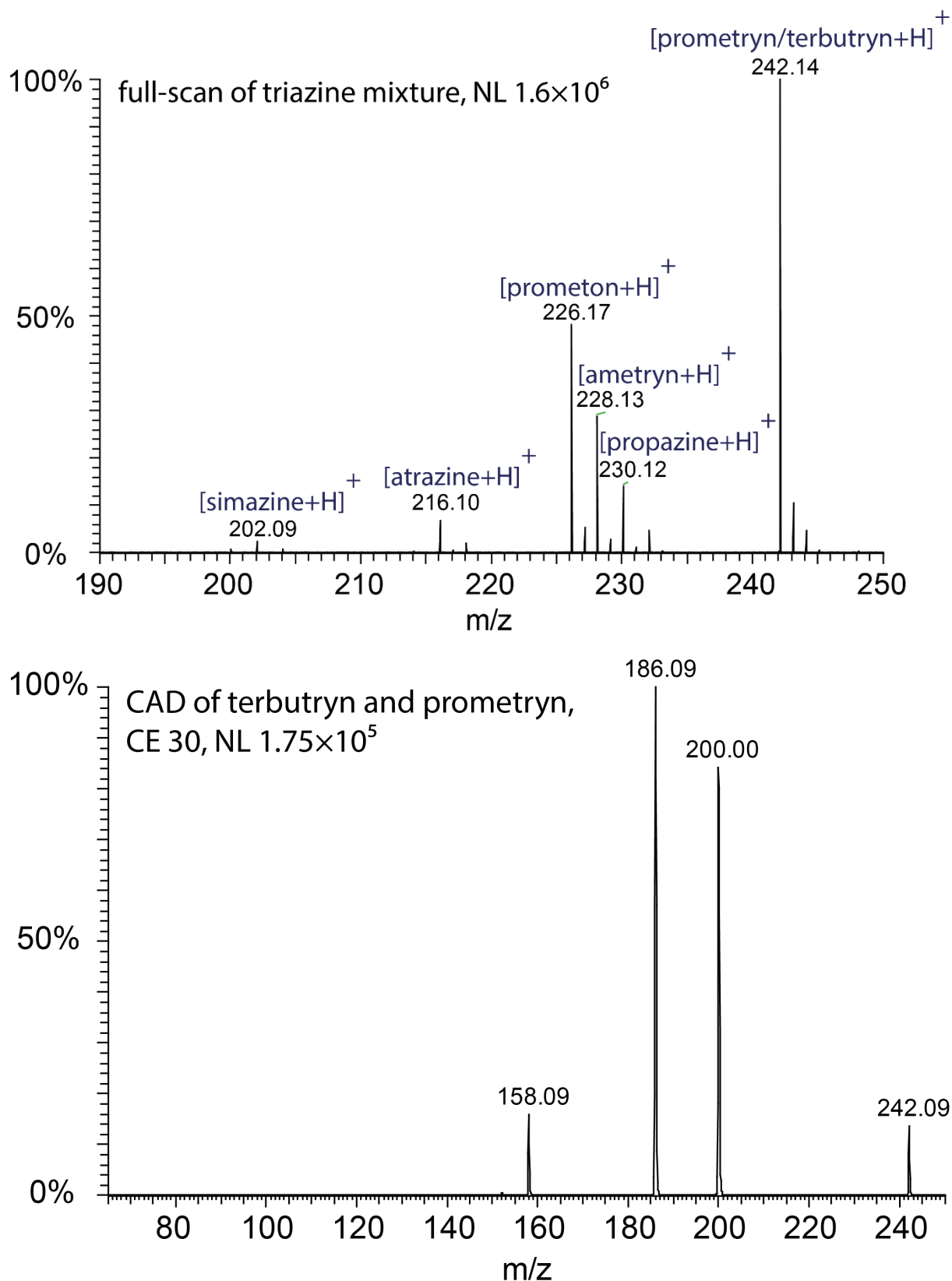


Figure 42 At the top, full-scan spectrum of the triazine mixture, showing the proton adducts of all compounds. At the bottom, CAD spectrum of the  $m/z$  242 precursor, which corresponds to terbutryn and prometryn.

To identify the isobaric prometryn and terbutryn precursor ions, CAD experiments were performed. The obtained CAD spectrum is presented in Figure 42 (bottom), and the proposed fragment ions are depicted in Figure 43. The applied collision energy is indicated at the top of the spectrum, in combination with the normalized level (NL). The proposed fragmentation pattern of prometryn includes the loss of either one or both isopropyl side chains [222]. The cleavage of an isopropyl side chain from prometryn yields a fragment with a theoretical  $m/z$  200.10, observed at an experimental  $m/z$  of 200.00. On the other hand, the cleavage of the tert-butyl sidechain from terbutryn forms a fragment with a theoretical  $m/z$  186.08, observed at  $m/z$  186.09. The fragment ion at  $m/z$  186.09 most likely results from either the loss of both isopropyl side chain of prometryn or from the loss of both the tert-butyl and ethyl side chain of terbutryn. However, the loss of the ethyl side chain of terbutryn which would yield a fragment ion at  $m/z$  214.11 was not observed. The absence of this fragment ion implies that the loss of both sidechains of prometryn is more likely responsible for the peak at  $m/z$  158.09.

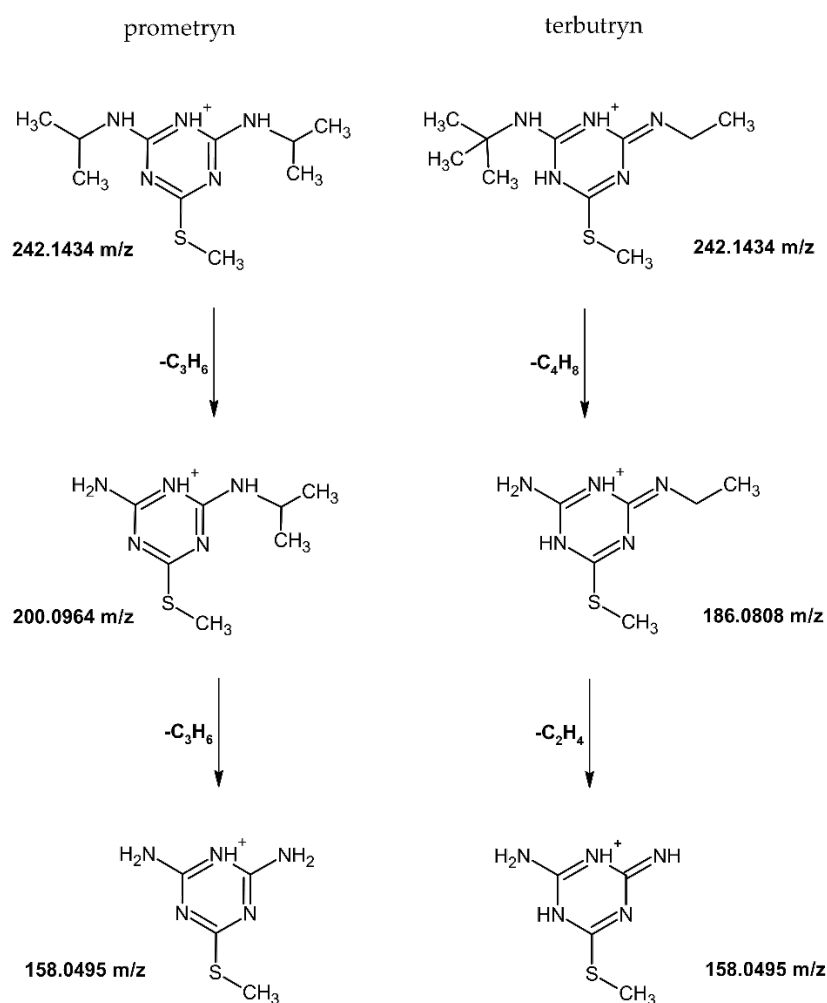


Figure 43 Proposed fragmentation patterns of prometryn and terbutryn.

### 2.9.2 Organophosphorus Mixture

In order to further evaluate the swab spray-based multiresidue pesticide detection method, a more challenging pesticide mixture, comprising ten organophosphorus compounds, was analyzed. The specific compounds, including their proton and sodium adducts are listed in Table 10. Both Copan 160C and ITS polyester swabs were evaluated, utilizing different solvents. The Copan swabs were tested with both ethyl acetate/methanol (70/30, *v/v*) and chloroform/methanol (80/20, *v/v*), which provide low background ions. The ITS polyester swabs were tested with ethyl acetate/methanol (70/30, *v/v*), acetone, acetonitrile, and methanol, all of which yielded low background ions. Each solvent included 0.1% formic acid to support protonation.

Table 10 Compounds of the organophosphorus pesticide reference mixture.

compound	composition	[M+H] <sup>+</sup> (m/z)	[M+Na] <sup>+</sup> (m/z)
dimethoate	C <sub>5</sub> H <sub>12</sub> NO <sub>3</sub> PS <sub>2</sub>	230.0069	251.98884
disulfoton-sulfone	C <sub>8</sub> H <sub>19</sub> O <sub>4</sub> PS <sub>3</sub>	307.02559	329.00753
disulfoton-sulfoxide	C <sub>8</sub> H <sub>19</sub> O <sub>3</sub> PS <sub>3</sub>	291.03067	313.01261
famphur	C <sub>10</sub> H <sub>16</sub> NO <sub>5</sub> PS <sub>2</sub>	326.02803	348.00997
parathion	C <sub>10</sub> H <sub>14</sub> NO <sub>5</sub> PS	292.04031	314.02225
parathion-methyl	C <sub>8</sub> H <sub>10</sub> NO <sub>5</sub> PS	264.00901	285.99095
phorate	C <sub>7</sub> H <sub>17</sub> O <sub>2</sub> PS <sub>3</sub>	261.02011	283.00205
sulfotep	C <sub>8</sub> H <sub>20</sub> O <sub>5</sub> P <sub>2</sub> S <sub>2</sub>	323.03002	345.01196
thionazin	C <sub>8</sub> H <sub>13</sub> N <sub>2</sub> O <sub>3</sub> PS	249.04573	271.02767
O,O,S-triethyl thiophosphate	C <sub>6</sub> H <sub>15</sub> O <sub>3</sub> PS	199.05528	221.03722

In the first step, the precursors were identified in the full-scan spectrum, followed by performing CAD experiments for structural confirmation. Table 11 shows the identified pesticide adducts, in combination with the tested swabs and spray solvents.

Table 11 Overview of detected organophosphorus compounds in combination with two different swabs and various spray solvents.

compound	Copan 160C swab, chloroform/MeOH (80/20, v/v)		Copan 160C swab, EtOAc/MeOH (70/30, v/v)		IT38040 swab, acetone		IT38040 swab, ACN		IT38040 swab, MeOH		IT38040 swab, EtOAc/MeOH (70/30, v/v)	
	H+	Na+	H+	Na+	H+	Na+	H+	Na+	H+	Na+	H+	Na+
dimethoate	✓	✓	✓	✓	✓	✓	✓	✓	✓	✓	✓	✓
disulfoton-sulfon												
disulfoton-sulfoxide	(✓)	(✓)	✓	✓								
famphur	✓	✓	✓	✓	✓	✓	(✓)	(✓)	✓	✓	✓	✓
parathion	(✓)											
parathion-methyl	(✓)											
phorate	✓	✓		✓								
sulfotep	✓	✓	✓	✓	✓	✓		(✓)	✓	✓	✓	✓
thionazin	✓	✓	✓	✓	(✓)		✓	✓	✓	(✓)	✓	✓
O,O,S-triethyl thiophosphate	(✓)	(✓)		(✓)								

A strong signal intensity is denoted by a dark check mark, while a light-green check mark corresponds to a weak signal intensity. The ITS polyester swabs primarily detected the four pesticides dimethoate, famphur, sulfotep, and thionazin. On the other hand, the Copan 160C swabs in combination with chloroform/methanol (80/20, v/v) additionally detected disulfoton-sulfoxide, parathion, parathion-methyl, and O,O,S-triethyl thiophosphate. The Copan 160C swabs in combination with ethyl acetate/methanol (70/30, v/v) detected dimethoate, disulfoton-sulfoxide, famphur, phorate, sulfotep, thionazin, and O,O,S-triethyl thiophosphate. Although the ITS polyester swabs permitted a broad selection of diverse spray solvents, the Copan 160C swabs were more powerful in the detection of organophosphorus pesticides. However, the use of chloroform/methanol (80/20, v/v) as spray solvent performed slightly better than ethyl acetate/methanol (70/30, v/v). Furthermore, ethyl acetate/methanol (70/30, v/v) was used with both swabs, but the Copan 160C swab performed better, indicating that the swab head material influences the analyte detection. This could be attributed to the suppression of analytes by swab background ions or the suppression by

compounds that are not visible in the spectrum. Although ITS polyester swabs exhibited a low background and an abundant signal of the salicylanilide suppression marker as discussed in section 2.5 “Evaluation of swab material”, the background ions may more strongly suppress organophosphorus compounds. Furthermore, the spray plume emission, as shown in Figure 30 (page 61), differed between Copan 160C swabs (a) and ITS polyester swabs (c). The Taylor cone in Copan 160C swab is more voluminous, and the resulting spray plume is broader. In contrast, ITS polyester swabs exhibit a smaller Taylor cone and a denser spray plume. Despite identical voltages being applied, the attachment of a wire in ITS polyester swabs might result in a different electric field at the swab tip. These alterations in the spray plume can impact the ionization efficiency. A higher spray plume density may decrease the ion desolvation rate, thereby reducing ionization efficiency. Space-charge effects may contribute to the ionization efficiency as well [223–226]. In addition, salt contaminations in the swab head material can affect the solvent's conductivity and influence both spray plume generation and the ionization process.

In the next step, structural confirmation via CAD of the detected organophosphorus compounds was performed. The applied collision energy is shown at the top of each spectrum. If the protonation site of the precursor ion is difficult to predict, the proton is illustrated in a delocalized state in the following figures.

The fragmentation pattern of dimethoate is depicted in Figure 44 (top). The nitrogen of the amid bond is reported to be the site of protonation [227,228]. The cleavage of the methylamine group leads to the formation of an acylium ion, which was observed as a single dominant fragment ion at  $m/z$  198.92 [72].

The CAD spectrum of famphur is presented in Figure 44 (bottom). The cleavage of the dimethylamine group yields a fragment ion observed at  $m/z$  281.00. The fragment ion occurring at  $m/z$  217.00 corresponds to the release of the sulfonamide group. However, the extrusion of the SO<sub>2</sub> moiety, typically observed in certain sulfonamide groups, was not detected. Such fragmentation has been reported to be dependent on both, the ability of the C-S and S-N to polarize and the degree of stabilization of the positive charge at the ipso position on the aromatic ring. Moreover, the migrating nitrogen group must also possess adequate stability and nucleophilicity [229].

The proposed fragmentation mechanism of thionazin is depicted in Figure 45 (top). The dominant fragment ion of thionazin corresponds to the loss of an ethyl group by ethylene loss and proton transfer to form the ion observed at  $m/z$  220.92. The subsequent loss of another ethyl group formed a fragment ion visible at  $m/z$  192.92. A

protonated oxygen of an ethyl ester moiety is observed to cleave an ethanol moiety to yield an ion observed at  $m/z$  202.92 [230]. Subsequent loss of an ethyl group corresponds to the ion of low intensity found at  $m/z$  174.92.

O,O,S-Triethyl thiophosphate was only accessible for CAD by isolating the sodiated precursor ion. The spectrum is presented in Figure 45 (bottom). The prominent fragment ion at  $m/z$  192.92 correlates to the loss an ethyl group by ethylene loss.

The suggested fragmentation pathway of sulfotep is illustrated in Figure 46. The loss of one of the four ethyl groups by ethylene loss generates the prominent fragment ion at  $m/z$  295.00. The subsequent loss of a second ethyl moiety yields an ion visible at  $m/z$  266.92. The cleavage of an ethanol group generates an ion observed at  $m/z$  277.00.

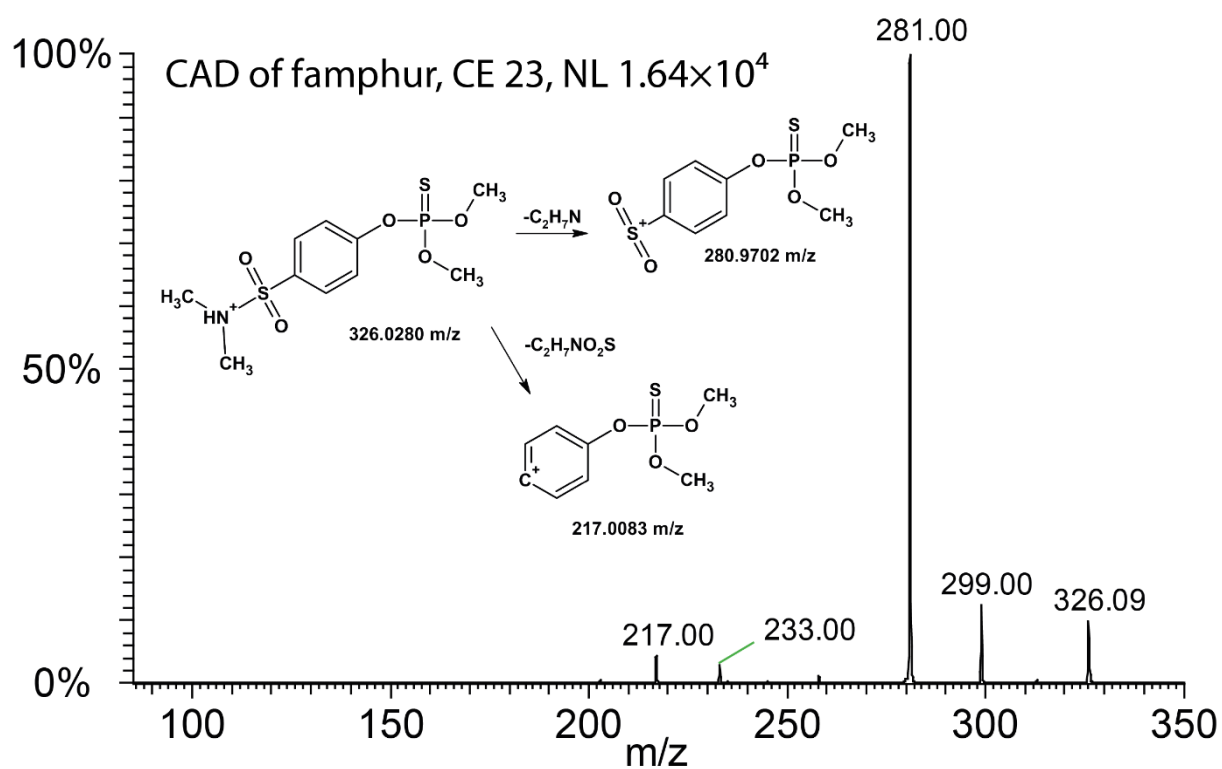
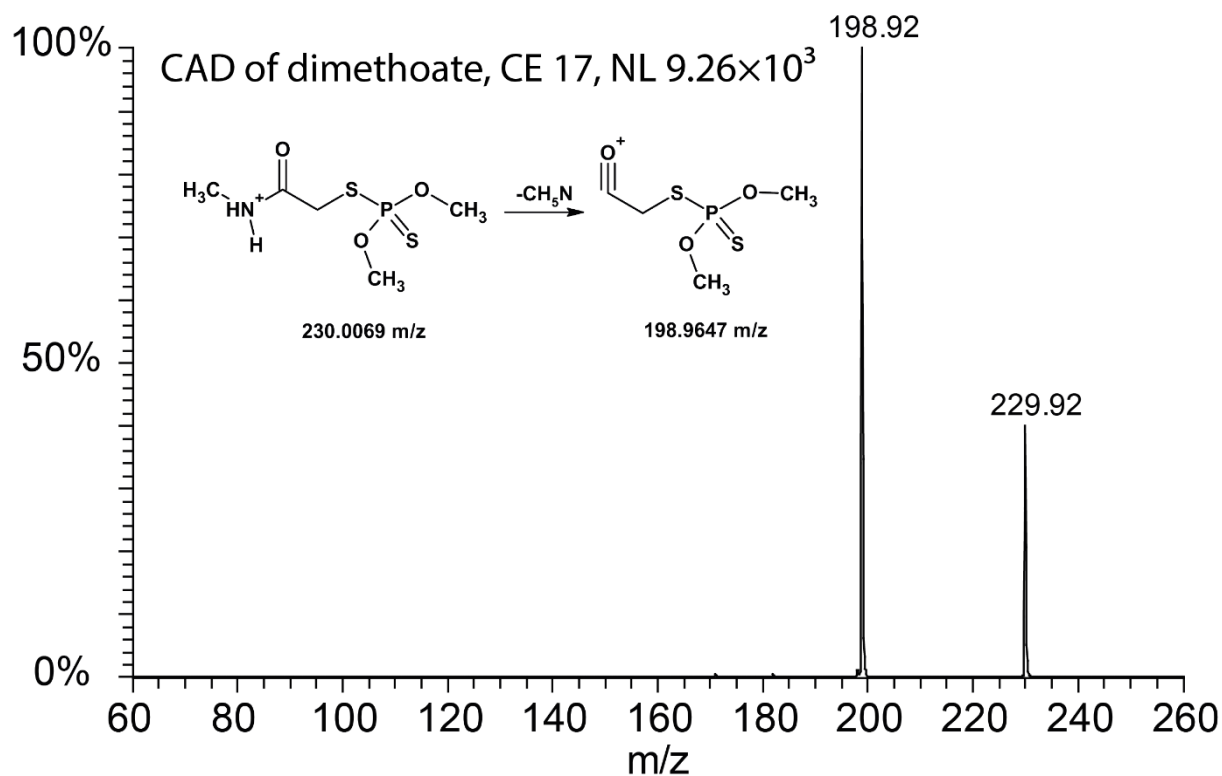


Figure 44 Fragment ion spectra of dimethoate (top) and famphur (bottom).



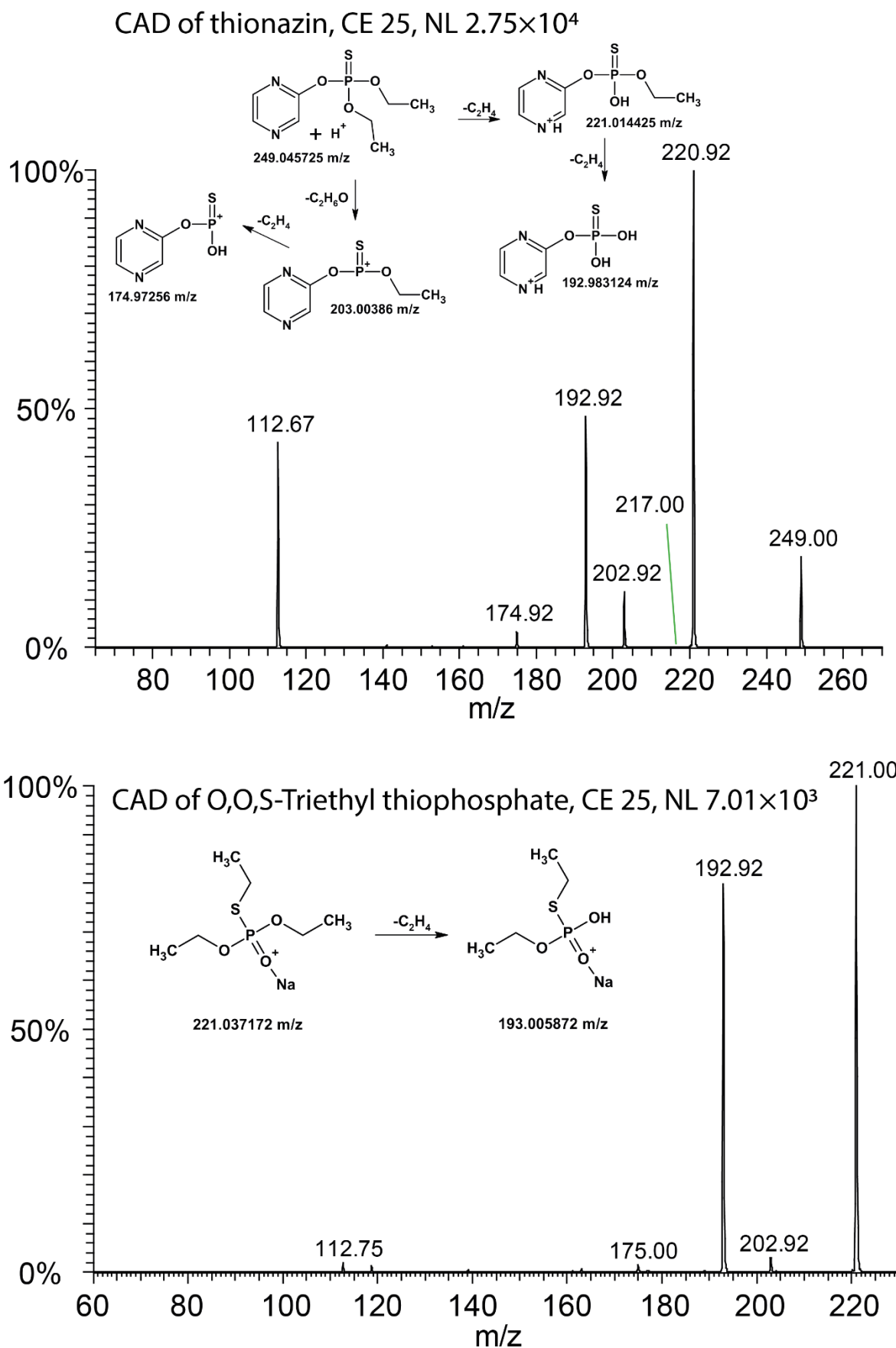


Figure 45 Fragment ion spectra of thionazin (top) and O,O,S-triethyl thiophosphate (bottom).

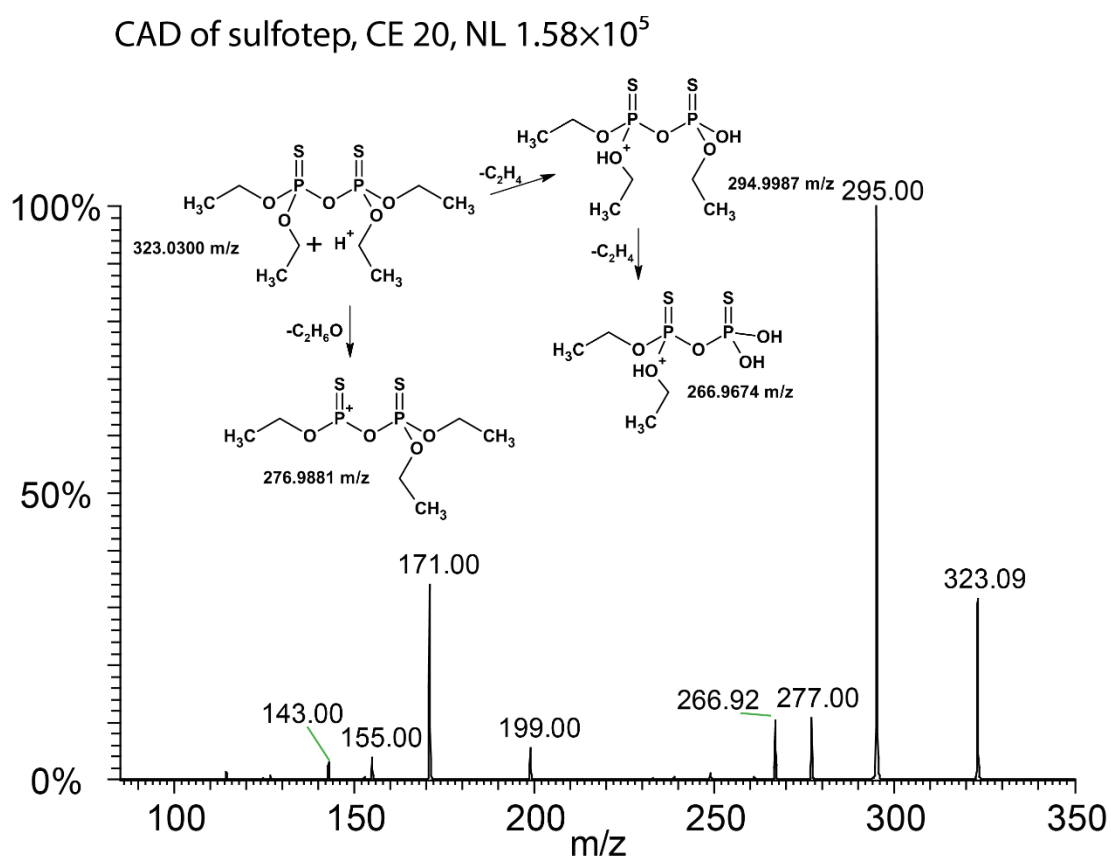


Figure 46 Fragment ion spectrum of sulfotep.

## 2.10 Pesticide Analysis on Food Products

For pesticide analysis on food products a FS-MS/DDA-MS<sup>2</sup> method was applied. It combines acquisition of a survey scan (full-scan spectrum) and data-dependent acquisition (DDA) (also known as information-dependent acquisition (IDA)) using CAD. In DDA, the selection of precursor ions for fragmentation is determined by the information gathered in the survey scan.

In the initial step, a full-scan spectrum, referred to as a survey scan, was acquired for approximately ten seconds. The survey scan was examined for ions of known pesticides, based on a pesticide library from SCIEX [231]. Because ambient ionization methods are more susceptible to adduct formation, an Excel list was created, which included the exact masses of the proton, sodium, and ammonium adducts for 556 pesticides. For data analysis, the survey scan was accumulated over an acquisition duration of 10 seconds, and the top 1000 ions were exported into the Excel sheet to be matched with pesticide precursors. The resulting table was filtered for both, the parts-per-million (ppm) deviation and ion intensity. A low ppm deviation coupled with high intensity strongly indicated a hit, whereas a low ppm deviation paired with low signal intensity was most likely associated with matrix ions. In the next step, the experimental isotopic pattern was compared to the theoretical pattern. Notably, the presence of chlorine in numerous pesticides facilitated the precursor identification. Furthermore, it was observed that pesticides which exhibited similarly the proton and sodium adduct at high intensity often feature a doubly bound oxygen in their structure.

The uppermost portion of the top 1000 ion list obtained from the full-scan of the bell pepper surface, discussed in the publication on rapid pesticide analysis, is presented in Figure 47 [88]. The top 1000 precursor ions were entered into the Excel sheet, the resulting table for potential proton adducts is depicted in Figure 48 (top). The ion with an experimental  $m/z$  of 343.0394 was identified as protonated boscalid (theoretical  $m/z$  343.0399), exhibiting the top intensity and a low deviation of -1.6 ppm only. Many presumed proton adducts, such as methacrifos, azinphos-ethyl, ethofumesate, and others, exhibited relatively high ppm deviations and could not be verified as pesticides and were considered false positives. Furthermore, the <sup>13</sup>C isotope of boscalid resulted a false-positive hit for prothioconazole.

The results table of potential sodium adducts ranks the sodium adduct of boscalid at  $m/z$  365.0219 as the fifth highest in intensity, combined with a ppm deviation of -1.6 ppm (visible at the bottom of Figure 48). The experimental isotopic pattern of boscalid corresponded to the theoretical isotopic pattern. The presence of the amide bond in boscalid likely facilitated the formation of sodium adducts. Identifying boscalid in its

protonated and sodiated forms, along with a matching isotopic pattern, met the criteria for structural verification by CAD. The fragmentation pattern of boscalid is discussed in detail in the enclosed publication focusing on pesticide analysis by swab spray mass spectrometry [88].

When encountering manifold matrix ions, whether they originate from the swab or from the food surface, identifying precursors using accurate mass spectrometry and isotopic pattern matching is essential to detect potential pesticide compounds before conducting the more time-consuming MS<sup>2</sup> analysis.

	m/z	Intensity	Relative
suppression marker (protonated salicylanilide)	177.1121	835822.7	100.00
	343.0394	753019.2	90.09
protonated boscalid	144.1019	735395.2	87.98
	214.0862	593314.0	70.99
	345.0363	506044.4	60.54
	144.0991	329952.3	39.48
	245.0867	305957.2	36.61
	259.1025	276533.6	33.09
	239.0337	230940.2	27.63
	112.0450	204055.2	24.41
	533.2786	171992.9	20.58
	344.0430	148841.4	17.81
	199.0940	147065.3	17.60
	487.3599	126315.2	15.11
	241.0318	111105.7	13.29
	112.0427	107674.2	12.88
	460.4498	106008.7	12.68
	346.0401	102268.0	12.24
	531.3855	98731.0	11.81
	443.3332	98459.5	11.78
	853.4657	97709.9	11.69
	809.4397	92225.2	11.03
	765.4124	88649.3	10.61
	160.0967	86013.7	10.29
	307.0629	85893.3	10.28
	782.5651	83960.4	10.05
	166.0839	82047.3	9.82
	897.4912	81872.3	9.80
	941.5195	75390.3	9.02
	559.4167	73933.8	8.85

Figure 47 Partial ion list from the full-scan spectrum of a bell pepper surface, including their absolute and relative intensity. Boscalid exhibited the monoisotopic peak at m/z 343.0394 and the <sup>37</sup>Cl isotope containing peak at 345.0363.

	A	B	C	D	E
1					
2					
3	<b>Results H<sup>+</sup> adducts</b>				
4	<b>Number</b>	<b>Name</b>	<b>Theoretical H<sup>+</sup></b>	<b>Deviation ppm</b>	<b>Intensity</b>
171	60	Boscalid	343.03994	-1.6	753019.2
173	445	Prothioconazole	344.03857	12.9	148841.4
185	346	Methacrifos	241.02941	9.9	111105.7
190	41	Azinphos-ethyl	346.04435	-12.3	102268.0
195	451	Pyraclostrobin	388.10586	1.1	65741.7
220	207	Ethofumesate	287.09477	-9.6	21687.8
230	519	Thiodicarb	355.0563	18.3	10204.9
233	211	Etofenprox	377.21112	-11.7	7414.3
257	274	Forchlorfenuron	248.05852	-9.4	6369.6
282	293	Imazamethabenz-methyl	289.15467	-1.3	6155.4
284	129	Cyprodinil	226.13387	-0.3	5940.9
287	416	Piperophos	354.1321	-19.2	3324.8
296	75	Cadusafos	271.09499	-25.4	2885.3
298	267	Flusilazole	316.10761	4.7	2761.7
319	360	Metrafenone	409.06451	-21.5	2761.1
327	498	Tebuthiuron	229.11176	-28.6	2604.5
352	152	Diclotophos	238.08389	-11.3	2597.7
4000					

	A	B	C	D	E
1					
2					
3	<b>Results Na<sup>+</sup> adducts</b>				
4	<b>Number</b>	<b>Name</b>	<b>Theoretical Na<sup>+</sup></b>	<b>Deviation ppm</b>	<b>Intensity</b>
148	109.0	Clomeprop	346.0372	8.4	102268.0
149	118.0	Cyazofamid	347.0340	-0.8	69314.0
151	451.0	Pyraclostrobin	410.0878	-1.7	45478.0
185	435.0	Propazine-d14	272.2551	14.9	24414.8
202	60.0	Boscalid	365.0219	-1.6	11012.7
208	417.0	Pirimicarb	261.1322	-3.4	3944.2
209	429.0	Propamocarb	211.1417	6.2	3016.4
221	417.0	Pirimicarb	261.1322	-20.3	2998.1
224	192.0	EPIC	212.1080	23.3	2850.8
287	256.0	Fluometuron	255.0716	-6.5	2793.2
288	138.0	Desmethyl-formamido-pirimicarb	275.1115	7.4	2693.4
307	133.0	DEET	214.1202	12.5	2620.8
354	29.0	Atrazine	238.0830	-7.5	2597.7
4000					

Figure 48 Excel result files showing possible hits of proton adducts (top) and sodium adducts (bottom).

Pesticides were reliably identified based on the three criteria deviation of precursor ion mass in ppm, isotopic pattern, and fragment ion pattern. The advantage of the presented FS-MS/DDA-MS<sup>2</sup> method is the compatibility of data acquired on a Thermo Fisher Scientific LTQ Orbitrap Velos mass spectrometer, which could be transferred into an Excel sheet for searching pesticide precursors using data from the pesticide library provided by SCIEX. Therefore, the FS-MS/DDA-MS<sup>2</sup> approach delivered rapid pesticide identification through the survey scan and verification by MS<sup>2</sup> experiments.

In data independent acquisition (DIA), data acquisition is unaffected by the acquired data, enhancing sample coverage in particular applications [232]. For pesticide analysis, DIA like Sequential Window Acquisition of all Theoretical Mass Spectra (SWATH) provides the benefit of generating a comprehensive data archive of the entire sample within predefined mass windows [233]. Particularly, the risk of missing an analyte due to failed identification in the survey scan is no longer present. On the other hand, DIA, often applied for pesticides or drug residues, demands more sophisticated software for data analysis [234–239]. Applying DIA with instrumentation and compound library from two different vendors would have posed significant software challenges. Furthermore, the risk of missing an analyte by a failed survey scan was considered acceptable, and the need for a full data archive was not necessary for the demonstration of swab spray mass spectrometry in rapid pesticide screening.

## 2.11 Effect of the Spray Solvent on Adduct Formation

The degree of adduct formation for the three pesticides thiabendazole, imazalil, and boscalid was investigated at increased sodium acetate and ammonium acetate concentration. The impact of the presence of salt on adduct formation using pure methanol and ethyl acetate/methanol (70/30, *v/v*), both containing 0.1% formic acid as modifiers, is discussed. In the experiments, 100 ng of each pesticide compound was directly applied to the swab head. For the addition of sodium acetate and ammonium acetate, either 10  $\mu$ L of a 0.1 M sodium acetate solution or a 0.1 M ammonium acetate solution, both prepared in methanol, were directly applied to the swab head.

### 2.11.1 Adduct Formation with Methanol as Spray Solvent

The spectra obtained with methanol and 0.1% formic acid as the spray solvent in the absence of salt are presented in Figure 50 at the top. The proton adduct of thiabendazole was visible at high intensity at  $m/z$  202.04, and the sodium adduct appeared at  $m/z$  224.02 with low intensity. Imazalil exhibited an abundant proton adduct at  $m/z$  297.05 and a sodium adduct of low abundance at  $m/z$  319.03. Boscalid appeared primarily as the sodium adduct at  $m/z$  365.02, alongside with its proton adduct found at  $m/z$  343.02 with low intensity.

The effect of sodium acetate addition is depicted in the center of Figure 50. The proton and sodium adduct of thiabendazole appeared with equivalent intensity. On the other hand, imazalil still exhibited the proton adduct with the highest intensity. Notably, the absolute intensity of the imazalil proton adduct slightly decreased compared to the first experiment without sodium acetate addition. On the other hand, a relative increase in the intensity of the sodium adduct of boscalid was observed. Furthermore, the proton adduct of boscalid was absent. The addition of sodium acetate revealed the differing affinities of the analytes to form sodium adducts. Boscalid, which includes an amide group in the structure, exhibited the strongest affinity for sodium adduct formation. Thiabendazole, capable of chelating a sodium ion with two opposing nitrogens, displayed a moderate affinity for sodium adduct formation. Imazalil showed the lowest affinity to form sodium adducts, as explained by its chemical structure that does not support formation of sodium adducts through doubly bond oxygen or a chelation site. The structures and their proposed sodium adducts are illustrated in Figure 49.

Studies focusing on sodium adduct formation in ESI have concluded that structural features are responsible for sodium adduct formation. In general, doubly bound oxygen, as present in amides, esters, ketones, and aldehydes, demonstrate a high

affinity for sodium adduct formation. On the other hand, amines are less prone to form sodium adduct but exhibit a higher proton affinity [240].

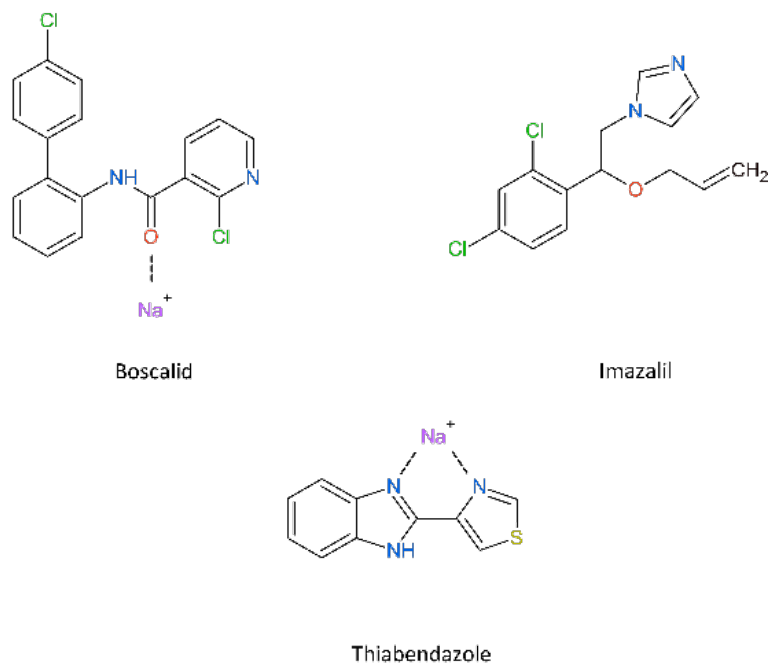


Figure 49 Proposed structures of the three pesticides illustrate the formation of sodium adducts: in boscalid, through its doubly bonded oxygen, and in thiabendazole, through nitrogen chelation.

The addition of ammonium acetate, presented at the bottom of Figure 50, did not lead to the formation of ammonium adducts. However, it suppressed the formation of sodium adducts for all three pesticides. Notably, the proton adduct of boscalid became more abundant than its sodium adduct. The likely explanation for the suppression of sodium adducts is increased proton availability. Overall, the signal intensities slightly increased compared to the first experiment without ammonium acetate additive.



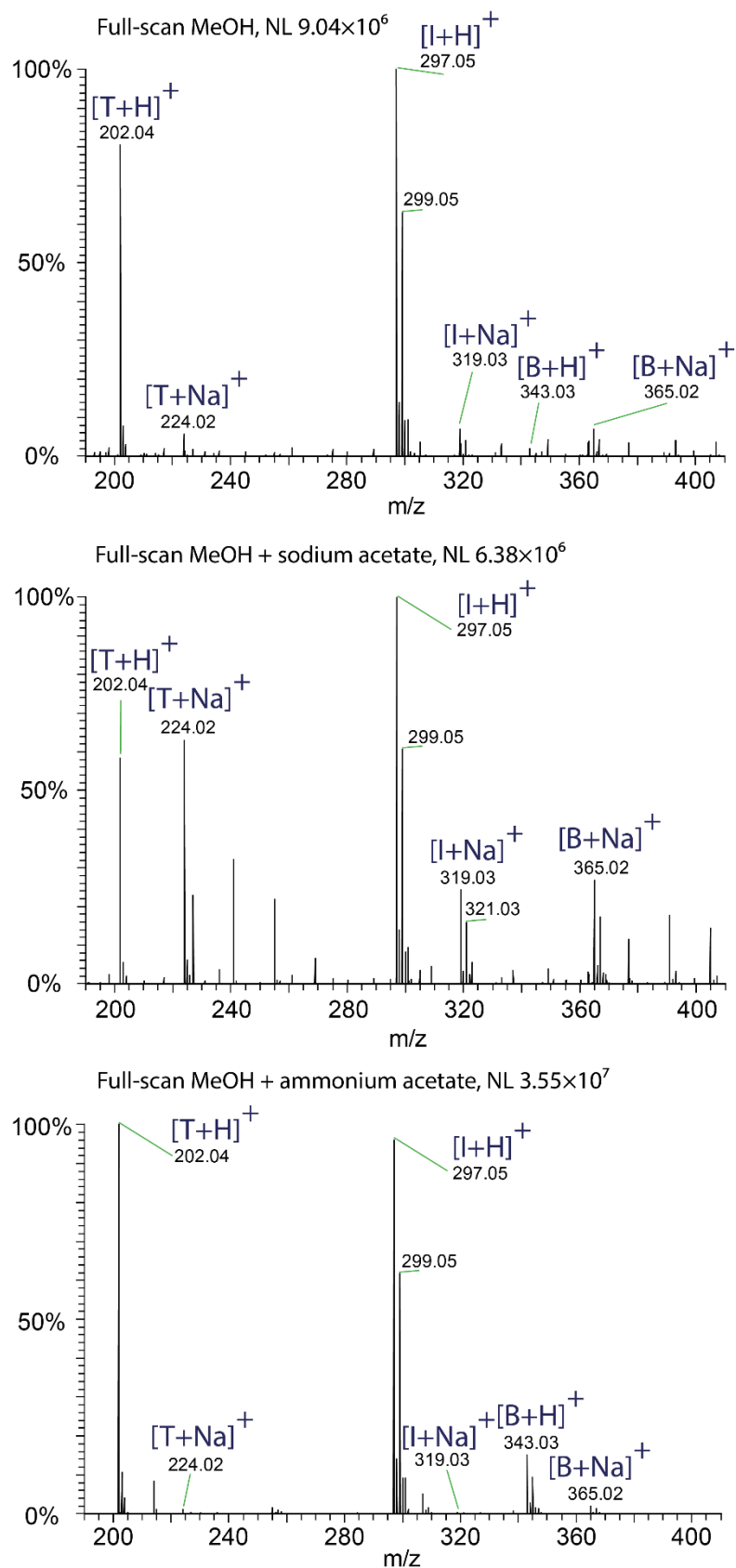


Figure 50 Full-scan spectra obtained with methanol including 0.1% formic acid as the spray solvent. At the top, without additive; in the center, sodium acetate was added; and at the bottom, ammonium acetate was added. Thiabendazole is denoted by T, imazalil by I, and boscalid by B.

### 2.11.2 Adduct Formation with Ethyl Acetate/Methanol (70/30, v/v) as Spray Solvent

The spectra obtained with ethyl acetate/methanol (70/30, *v/v*) and 0.1% formic acid as the spray solvent, without the addition of additives, are illustrated at the top of Figure 51. All pesticides were predominantly visible in their protonated forms. Overall, this experiment yielded the highest signal intensities.

The results of sodium acetate addition directly to the swab head are presented in the center of Figure 51. The sodium adducts of imazalil and thiabendazole remained low in intensity compared to their proton adducts. Boscalid showed a slight increase for the sodiated form attributed to a higher abundance of sodium ions. The diminished intensity of sodium adducts when using ethyl acetate/methanol (70/30, *v/v*) over methanol can be attributed to the excess of ethyl acetate, which binds sodium ions. Consequently, the formation of sodium adducts was significantly reduced compared to the analysis with methanol only. The absolute signal intensities slightly decreased compared to the first experiment without the addition of sodium acetate.

The addition of ammonium acetate, illustrated at the bottom of Figure 51, did not result in the formation of ammonium adducts. Instead, the analytes predominantly appeared as proton adducts. Ammonium adduct formation was shown to be depending on the basicity of the analyte, whereas a higher basicity decreased the intensity of ammonium adducts. Furthermore, it was suggested that ammonium adducts may decompose into protonated analytes and ammonia in the gas phase when atmospheric pressure chemical ionization (APCI) is used at higher gas temperatures [241]. Although, this effect was not further investigated for ESI. Molecular dynamic simulations of  $\text{NH}_4\text{Ac}$  containing electrospray droplets suggested proton transfer from  $\text{NH}_4^+$  to  $\text{Ac}^-$  forming ammonia and acetic acid. Ammonia has a higher volatility than acetic acid and evaporates faster, thus acetic acid is accumulating inside the droplet forming an acetic acid buffer  $\text{AcH}/\text{Ac}^-$  [242].

In summary, the incorporation of ethyl acetate into the spray solvent notably reduced sodium adduct formation. This reduction can be advantageous for  $\text{MS}^2$  analysis, as the proton adduct is commonly preferred for elucidating fragmentation mechanisms. Comparable observations of diminished sodium adduct formation with the use of ethyl acetate have been reported in the analysis of fruit samples, as detailed in our publication on rapid pesticide detection in fruits presented in the next section [88]. Additional supplementary data can be found on:

“[www.mdpi.com/article/10.3390/molecules28186611/s1](http://www.mdpi.com/article/10.3390/molecules28186611/s1)”

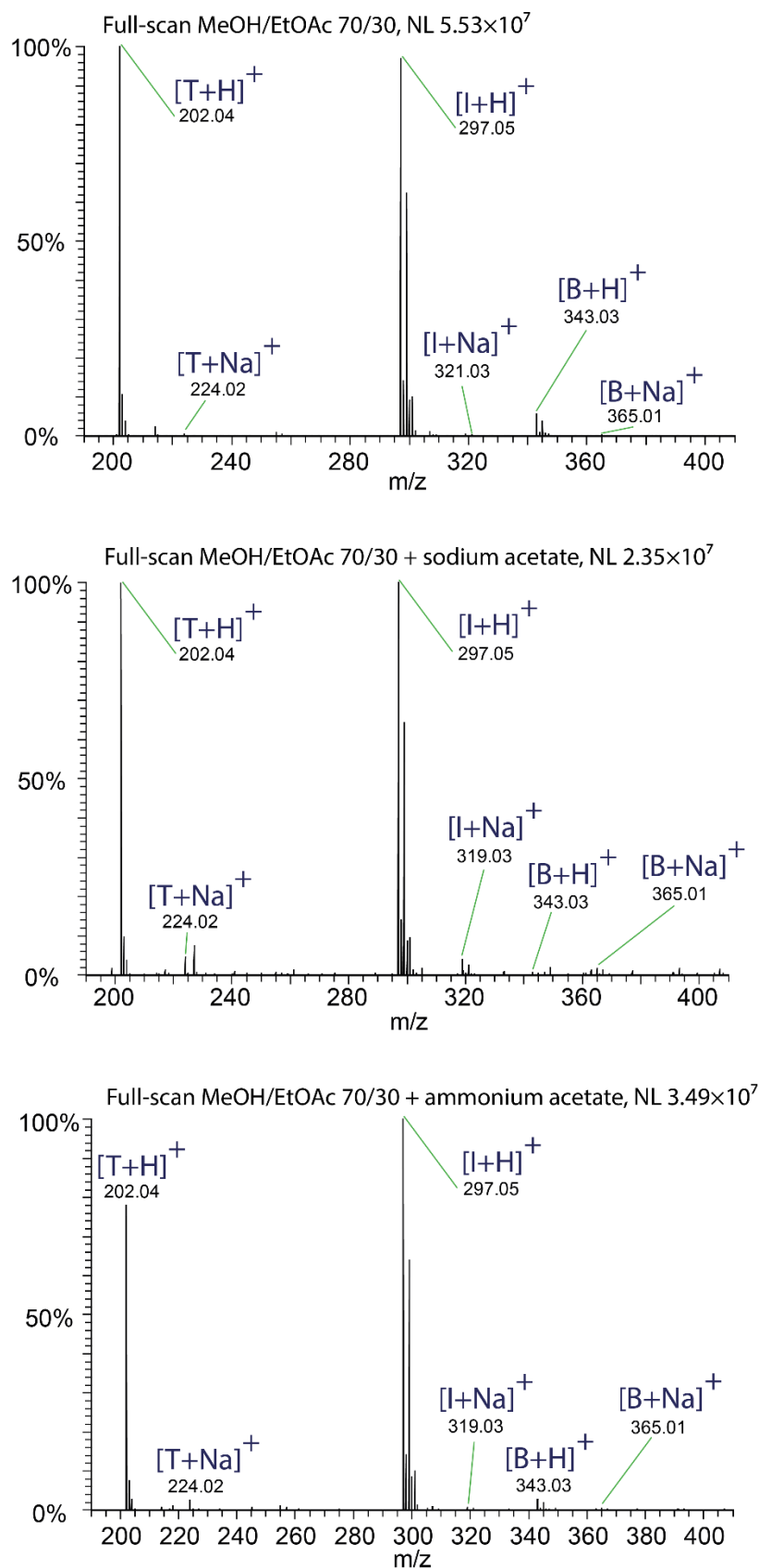


Figure 51 Full-scan spectra obtained with methanol/ethyl acetate (70/30, v/v) including 0.1% formic acid as the spray solvent. At the top, no additive was used; in the middle, sodium acetate was added; and at the bottom, ammonium acetate was added. Thiabendazole is denoted by T, imazalil by I, and boscalid by B.



## Article

# Analysis of Pesticide Residues on Fruit Using Swab Spray Ionization Mass Spectrometry

Thomas Michael Muggli  and Stefan Schürch \* 

Department of Chemistry, Biochemistry and Pharmaceutical Sciences, University of Bern, 3012 Bern, Switzerland; thomas.muggli@unibe.ch

\* Correspondence: stefan.schuerch@unibe.ch

**Abstract:** The vast quantity and high variety of pesticides globally used in agriculture entails considerable risks for the environment and requires ensuring the safety of food products. Therefore, powerful analytical tools are needed to acquire qualitative and quantitative data for monitoring pesticide residues. The development of ambient ionization mass spectrometry methods in the past two decades has demonstrated numerous ways to generate ions under atmospheric conditions and simultaneously to reduce the need for extended sample preparation and circumvent chromatographic separation prior to mass analysis. Swab spray ionization enables the generation of ions directly from swabs via the application of high voltage and solvent flow. In this study, swab sampling of fruit surfaces and subsequent ionization directly from the swab in a modified electrospray ion source was employed for the screening and quantitation of pesticide residues. Aspects regarding sample collection, sampling efficacy on different surfaces, and swab background are discussed. The effect of solvent composition on pesticide-sodium adduct formation and the suppression of ionization by the background matrix have been investigated. Furthermore, a novel approach for the quantitation of pesticide residues based on depletion curve areas is presented. It is demonstrated that swab spray ionization is an effective and quick method for spectral library-based identification and the quantitative analysis of polar contact pesticide residues on food.

**Keywords:** pesticide analysis; quantitation; ambient ionization; swab spray ionization; mass spectrometry



**Citation:** Muggli, T.M.; Schürch, S. Analysis of Pesticide Residues on Fruit Using Swab Spray Ionization Mass Spectrometry. *Molecules* **2023**, *28*, 6611. <https://doi.org/10.3390/molecules28186611>

Academic Editor: Hiroyuki Kataoka

Received: 10 August 2023

Revised: 6 September 2023

Accepted: 13 September 2023

Published: 14 September 2023



**Copyright:** © 2023 by the authors. Licensee MDPI, Basel, Switzerland. This article is an open access article distributed under the terms and conditions of the Creative Commons Attribution (CC BY) license (<https://creativecommons.org/licenses/by/4.0/>).

## 1. Introduction

### 1.1. Ambient Ionization

The generation of ions represents the indispensable initial step of any mass spectrometric experiment, and numerous techniques have been developed for the ionization of a wide variety of compounds of different polarity and mass. While established techniques enable automated analysis protocols and ensure the efficient formation of ions, they usually require some sort of sample preparation. On the other hand, ambient ionization methods circumvent the need for sample preparation as ionization occurs directly on or above the surface of a specimen under ambient atmospheric conditions [1–3]. Since the advent of desorption electrospray ionization (DESI) in 2004 [3] and direct analysis in real time (DART) in 2005 [4], a multitude of ambient ionization techniques have been presented [5,6], which have turned mass spectrometry into a versatile and powerful analytical tool for the rapid and hassle-free detection of environmental pollutants, food contaminants, forensic traces, and drug and clinical markers on surfaces [7–10]. Due to the feasibility of in situ analysis, mass spectrometry has entered novel fields of application, such as homeland security [11] and point-of-care diagnostics [12].

### 1.2. Swab Spray Ionization

Sample collection using swabs and the direct generation of ions from the swabs by applying a high voltage and solvent flow is an attractive approach for pesticide screening,

which circumvents laborious sample preparation and cuts down analysis time. Swab spray ionization mass spectrometry was demonstrated for the first time by the Cooks group [13]. This technique, also referred to as swab touch spray mass spectrometry [14], is based on the electrospray ionization (ESI) mechanism and involves the formation of a Taylor cone, a jet region, and a spray plume [15]. Several applications of swab spray ionization have been presented in the past few years, including in the analysis of drugs [13,16], organic gunshot residues [17], and explosives [18,19], as well as in the analysis of biological material such as human gliomas [14], bacteria [20], and newborn screening for nicotine and cotinine [21]. The swab allows easy and effective sample collection on any surface and serves as a depleting analyte reservoir. The applied solvent flow is responsible for continuous analyte extraction during analysis [15]. Due to the rather inhomogeneous texture of swab heads, appropriate choices of solvent, solvent flow rate, applied voltage, and swab positioning are crucial for the formation of a stable electrospray which provides high signal intensity [15]. Swab irregularities and matrix effects can be compensated for by the use of an internal standard, either included in the extraction solvent or otherwise directly deposited onto the swab head [13,14,16,19,21]. Regarding the type of swab head material, rayon swabs featuring an aluminum applicator that conducts the high voltage to the swab head have been demonstrated to be beneficial for many applications [13–15,17,18,20,22]. As most ambient ionization techniques are implemented on an experimental level, the modification of commercial electrospray ion sources to meet the specific requirements of swab spray ionization is required.

### 1.3. Pesticide Analysis on Food

According to the Food and Agriculture Organization (FAO) of the United Nations [23], global pesticide usage in agriculture reached 2.7 million tons of active ingredients in 2020. Analytical methods for the detection of pesticide residues on food are indispensable for ensuring food safety at all steps, from the producers to the consumers, therefore avoiding exposure and toxic effects to humans [24–26]. Furthermore, the global pesticide usage causes environmental impacts, including the transformation of known pesticides into hitherto unknown agents [27].

Most established procedures for quantitative pesticide analysis in food extracts employ GC-MS [28–32] or LC-MS/MS [33–38] combined with extensive sample preparation and method optimization to achieve adequate compound separation and to avoid matrix effects. Within the past decade, various ambient ionization mass spectrometric techniques have also been applied to the detection of pesticides in fruit and vegetables. A recent review gives an overview of these applications and discusses the analytical challenges imposed by direct sampling from surfaces, inhomogeneous pesticide distribution, and matrix effects [6].

In the current study, swab spray ionization mass spectrometry is evaluated for the qualitative and quantitative analysis of polar contact pesticides on fruit and vegetables. While most ambient ionization methods generate ions directly from a surface or from the atmosphere above a surface, sampling with a swab results in a deposition of compounds, which is continuously depleted during the electrospray ionization process. This intrinsic feature of swab spray ionization requires a novel approach for the quantitation of pesticides based on the extracted ion currents of the depleting analyte ions. Furthermore, sampling efficacy, swab background, analyte extraction from swabs, analyte suppression by the matrix, and sodium adduct formation are discussed.

## 2. Results and Discussion

### 2.1. Swab Background Evaluation

The head material of commercially available swabs creates a strong background signal, which causes peak overlaps and analyte suppression during analysis. The washing of the swabs prior to sampling and analysis is required. To demonstrate the effect of the washing step on the remaining chemical noise, Copan rayon swabs, as obtained from the manufacturer, were mounted in the ion source. Salicylanilide at a concentration of 1 ppm

was fed to the swab head through the capillary. The mass spectra of salicylanilide dissolved in solvent A (Figure 1a) and solvent B (Figure 1b) recorded immediately after application of the spray voltage give evidence for the inherently strong background originating from the swab head material, with ions recorded up to several hundred mass units. The continuous extraction of contaminants from the swab results in a rapid decrease in the background load in the case of solvent A (ethyl acetate/methanol + 0.1% HFO), with only a handful of ions observed after two minutes (Figure 1d). Removing the chemical background also dampens ion suppression, as demonstrated by the extracted ion chromatogram ( $m/z$  214.07–214.10) of protonated salicylanilide in Figure 1g. Initially, the high background strongly suppressed the formation of this ion, but after spraying for about two minutes the ion current reached a stable plateau at a three-fold-higher abundance level. In comparison, solvent B (methanol + 0.1% HFO) was found to be less effective in eliminating chemical background from the rayon swabs (Figure 1e) and preconditioning for several minutes was required to reduce ion suppression to an acceptable level (Figure 1h).

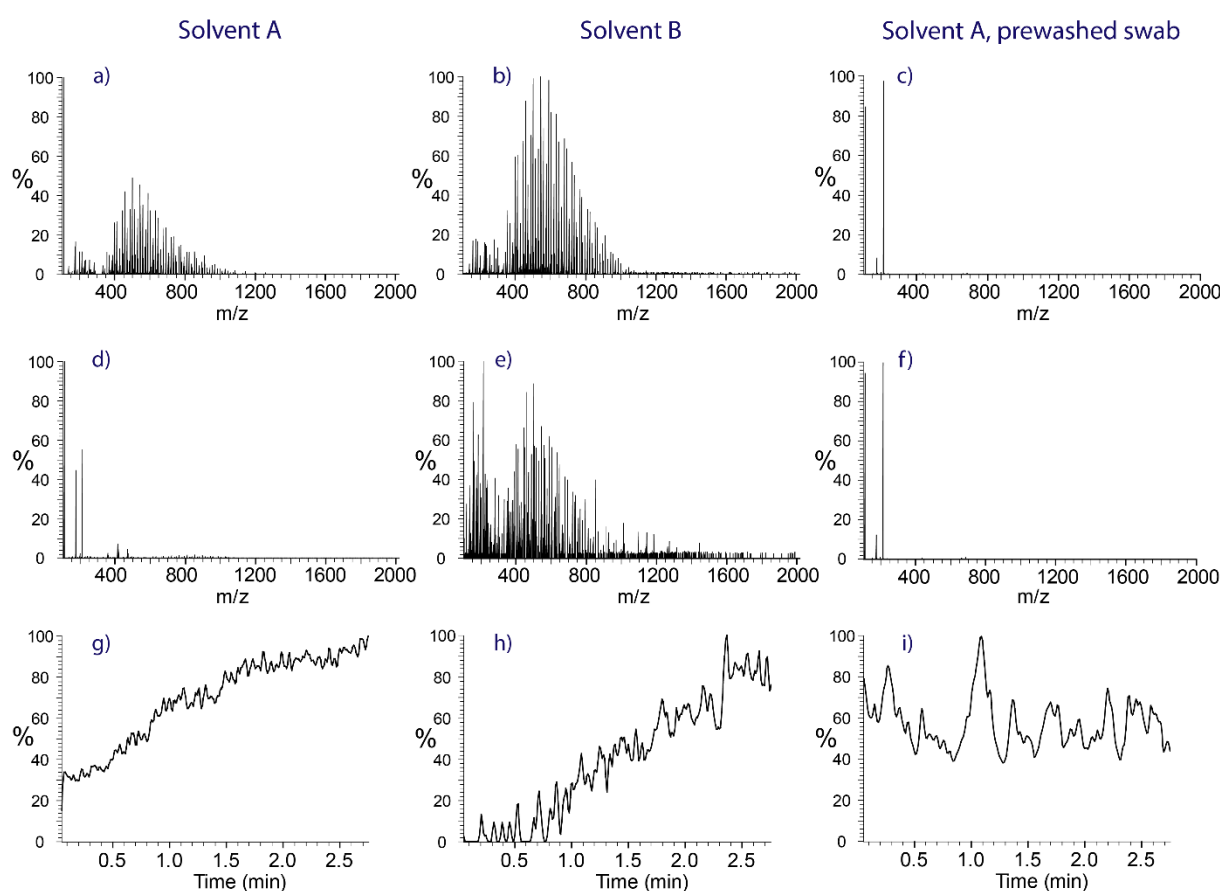


**Figure 1.** Mass spectra obtained from rayon swabs spiked with salicylanilide, demonstrating the effect of removing contaminations from swabs. **Left row:** Rayon swab as obtained from the manufacturer sprayed with solvent A. **Middle row:** Rayon swab as obtained from the manufacturer sprayed with solvent B. **Right row:** Prewashed rayon swabs sprayed with solvent A. (a–c) represent the background at the beginning of the measurement, while (d–f) demonstrate the background at the end of the experiment. (g–i): extracted ion current traces (gaussian smooth of 7 points) of protonated salicylanilide, indicating the decrease in analyte ion suppression over time.

These experiments demonstrate the importance of removing background contaminants from the swab heads prior to sampling to avoid overlapping peaks and to decrease analyte suppression. The same cleaning effect as accomplished by the continuous extraction of contaminants from the swab head using electrospray (Figure 1d) was also achieved with a washing step using ethyl acetate and sonication. The efficacy of the washing step is

illustrated by the spectra in the right row of Figure 1. Three minutes of washing reduced the swab background to a level comparable to two minutes of electrospray with the ethyl acetate/methanol solvent, as indicated by the full-scan spectra in Figure 1c,f and the extracted ion current trace of protonated salicylanilide in Figure 1i.

To illustrate the advantages in terms of sensitivity and quantitative capabilities, the area of the extracted ion current of salicylanilide was integrated for all three experiments, which yielded 26.1 million counts for solvent B, 181.7 million counts for solvent A, and 467.5 million counts for the prewashed swab in combination with solvent A. Therefore, prewashed swabs in combination with solvent A will deliver the highest sensitivity for quantitative experiments.

## 2.2. Qualitative Workflow

The sampling of the surfaces of an apple and a bell pepper, both purchased at a local supermarket, was performed with prewashed rayon swabs wetted with solvent A. The swabs were wiped over the sample surface for a few seconds and mounted in the holder for direct analysis immediately after sampling. Following the application of the solvent flow and the electrospray voltage, full-scan spectra were recorded for ten seconds and the individual spectra were summed. The identification of compounds was based on the exact masses and the isotopic patterns of the top 1000 ions found in the full-scan mass spectra, and on matching with the high-resolution pesticide precursor ion library. In contrast to LC-MS analysis on reversed-phase stationary phases, ambient ionization is inherently prone to adduct formation, which must be accounted for. The lack of a preceding separation step increases the tendency for adduct formation, and therefore the exact masses of pesticides in protonated form and as sodium and ammonium adducts were considered as well.

The full-scan mass spectrum shown in Figure 2a gives evidence for the presence of the imidazole fungicide imazalil ( $[M+H]^+$ ,  $m/z$  297.06) and the benzimidazole thiabendazole ( $[M+H]^+$ ,  $m/z$  202.04) on apple skin. The same pesticides were also detected on clementine peel and orange peel, both harvested in South Africa (Supplementary Data S1). The carboxamide fungicide boscalid ( $[M+H]^+$ ,  $m/z$  343.03) was found to be highly abundant on the surface of the bell pepper (Figure 2b). Sampling from strawberry leaves gave evidence for fluopyram (Figure 2c), which was detected in protonated form ( $[M+H]^+$ ,  $m/z$  397.05) and as the sodium adduct ( $[M+H]^+$ ,  $m/z$  419.04). Swab contaminants were reduced to a minimum due to the washing step performed prior to sampling.

Further confirmation of the pesticide's identity was gathered using tandem mass spectrometric experiments. Product ion spectra obtained through ion trap collision-induced dissociation (CID) were matched against the HRMS pesticide library. Though the lack of upfront chromatographic separation increases the risk of co-isolation of the precursor ions and may lead to contaminant fragment ion peaks in the product ion spectra, the peaks of the most indicative fragment ions dominated the spectra, as demonstrated by the insets in Figure 2. Protonated imazalil ( $(C_{14}H_{15}Cl_2N_2O)^+$ ,  $m/z$  297.06) primarily underwent a loss of the neutral propene moiety ( $C_3H_6$ , 42.05 Da), resulting in the abundant  $C_{11}H_9Cl_2N_2O^+$  fragment ion with  $m/z$  255.01. Secondary fragmentation via the opening of the imidazole ring and release of a neutral  $C_3H_4N$  fragment (54.03 Da) led to the fragment ion detected at  $m/z$  200.92. If propene is lost in conjunction with the ejection of N-methyl-imidazole ( $C_4H_6N_2$ , 82.05 Da), the fragment with  $m/z$  172.96 will be formed. The release of the dichlorinated tropylium ion ( $C_7H_5Cl_2^+$ ) was responsible for the peak at  $m/z$  158.98 [39]. Under the applied CID conditions, the fragmentation of protonated boscalid was dominated by the loss of hydrochloric acid from the pyridine ring, resulting in the peak corresponding to  $C_{18}H_{12}N_2OCl^+$  observed at  $m/z$  307.09. Cleavage of the amide bond released the chlorinated carboxy-pyridine ion  $C_6H_3NOCl^+$  indicated by the peak at  $m/z$  140.00. The weak fragment ion detected at  $m/z$  111.58 was generated by release of the chloro-pyridine ion [40]. The product ion spectrum of fluopyram was dominated by the peak at  $m/z$  208.01, which corresponded to the fragment ion  $(C_8H_6NCIF_3)^+$  obtained by cleavage next to the



amide bond. Cleavage of the amide bond yielded the acylium ion  $C_8H_4OF_3^+$  observed at  $m/z$  173.02.

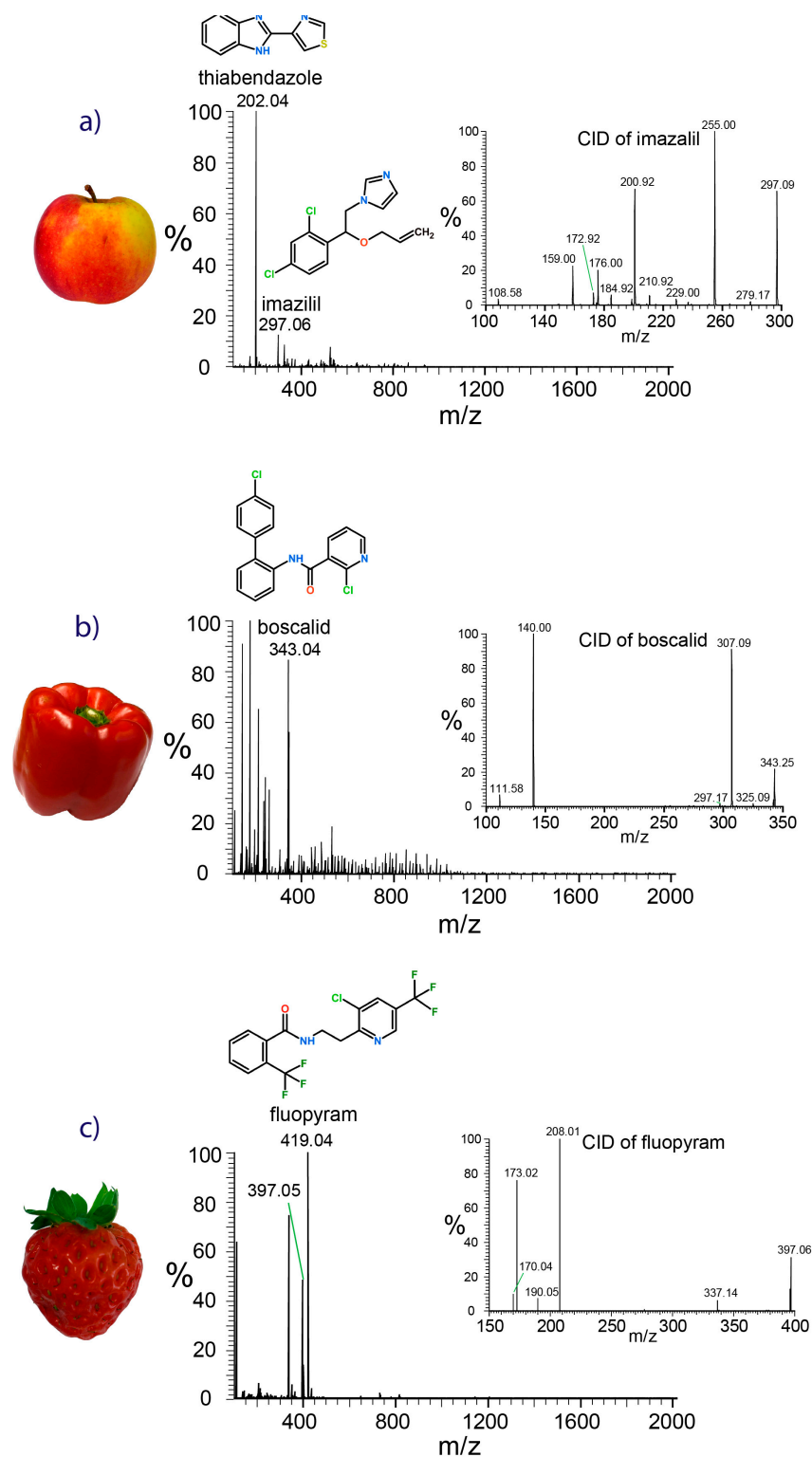


**Figure 2.** Full-scan swab spray mass spectra of samples taken from the skin of an apple harvested in Switzerland (a), a bell pepper from Spain (b), and strawberry leaves from Switzerland (c), showing the peaks of fungicides. Evidence for compound identities is given by the exact masses, the isotopic patterns, and the product ion spectra (insets).

### 2.3. Structure and Solvent Effects on the Formation of Sodium Adducts

Structural features of analyte molecules play a crucial role in sodium adduct formation. Sodium ions show a high propensity to bind to the partially negatively charged oxygen atoms of carbonyl groups, e.g., in amides and esters [41]. This is reflected by the experiments performed on apricots harvested in Italy. The spectrum shown in Figure 3a indicates the presence of protonated tebuconazole ( $m/z$  308.15) and fluopyram ( $m/z$  397.05), as well as the sodium adduct of fluopyram ( $m/z$  419.04). Tebuconazole does not contain any carbonyl groups, which explains the very low abundance of the corresponding sodium adduct peak in the spectrum.

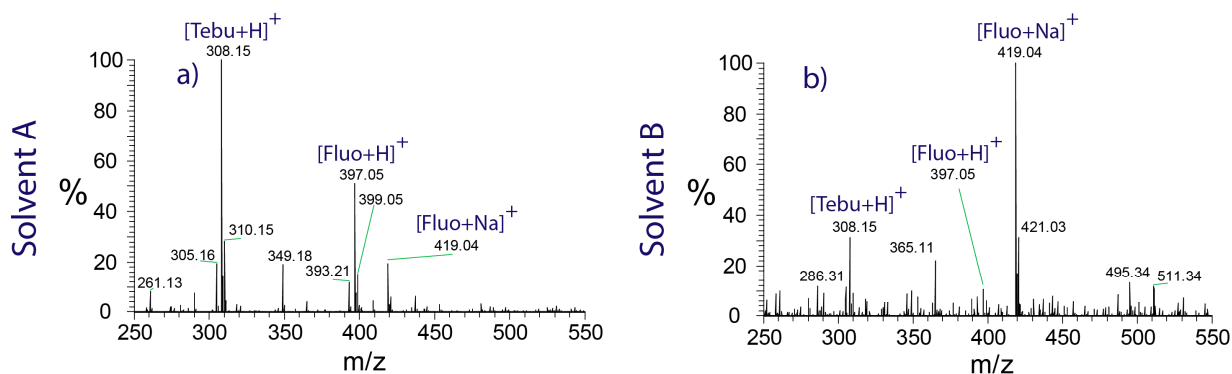


**Figure 3.** Swab spray ionization mass spectra of an apricot skin sample, demonstrating the influence of the solvent on the formation of sodium adducts. (a) Solvent A promoting the formation of protonated analyte, and (b) solvent B, shifting the equilibrium to the side of sodium adducts.

However, the extent of sodium adduct formation was found to be affected by the choice of the solvent, as well. The spectrum in Figure 3a was recorded using solvent A, which contains 70% ethyl acetate. Analyte molecules compete with excess ethyl acetate molecules for the available sodium ions, which limits the degree of analyte-sodium adduct formation. In contrast, the spectrum shown in Figure 3b was recorded using methanol as the solvent. Methanol exhibits a lower affinity towards sodium ions and causes fluopyram to be detected almost exclusively in sodiated form.

### 2.4. Quantitative Analysis

**Depletion curves:** In contrast to flow injection analysis, where the sample concentration remains constant throughout the duration of the analysis, swab spray shows a continuous depletion of sample compounds due to permanent solvent delivery. This requires the analysis time to be taken into account for quantitative work. Quantitative information is obtained from the area under the 7-point Gaussian-smoothed extracted ion current traces (referred to as depletion curves in the following) of the protonated pesticides. The depletion curve of the boscalid  $[M+H]^+$  ion sampled from bell pepper using a rayon swab and recorded with a continuous solvent feed is depicted in Figure 4a. The signal of boscalid is continuously decreasing due to the extraction of analyte from the swab. Within the first minute of spraying, 40% of the boscalid deposition had already been extracted and the deposition had been reduced to less than five percent after six minutes. The integration of the ion signal over the full analysis time of ten minutes was performed for quantitation.

**Reproducibility:** The erratic structures of the fibrous swab head material, positional variations of the mounted swabs, and time required for the stabilization of the Taylor cone at the moment of voltage application limited the reproducibility and accuracy of quantitative analysis. Repeated experiments ( $n = 5$ ) performed by loading 100 ng imazalil dissolved in 4  $\mu$ L methanol on rayon swabs revealed considerable variations in the shapes of the depletion curves, although recorded under identical experimental conditions (Figure 4b). Complete depletion had already occurred after less than four minutes of electrospraying

and the areas under the depletion curves showed deviations within +21% and −14% from the mean area (Supplementary Data S2).

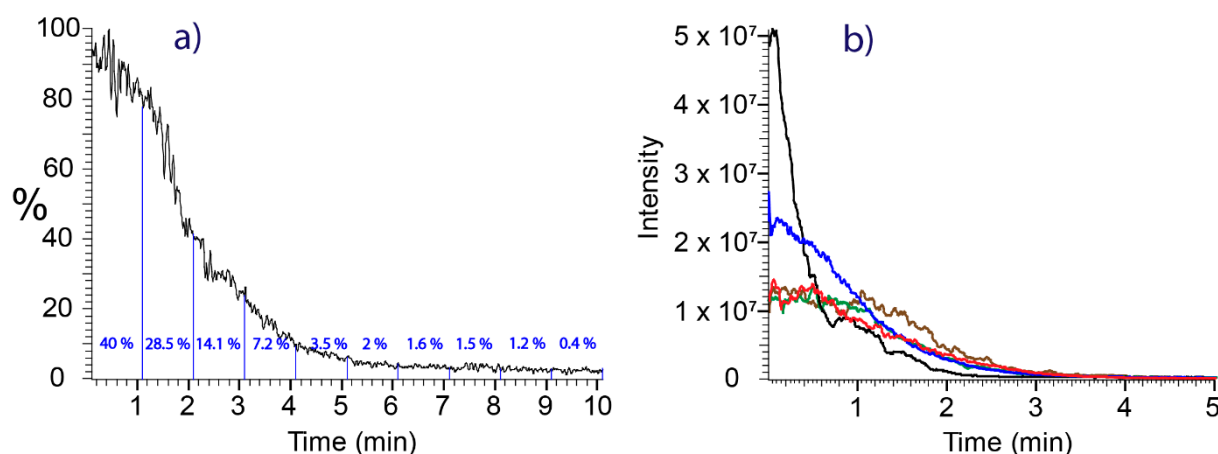


**Figure 4.** (a) Depletion curve (XIC  $m/z$  342.9–343.2) of the boscalid  $[M+H]^+$  ion sampled from the skin of a bell pepper. The sections show fractions of material depleted within time slots of 60 s. (b) Depletion curves of imazalil reference material (XIC  $m/z$  297.01–297.10) recorded after spiking 100 ng imazalil dissolved in 4  $\mu$ L solvent A on swabs. The overlay of five differently colored curves demonstrates the variations in curve shape.

**Calibration curves:** For establishing a calibration curve, prewashed swabs were spiked with 2  $\mu$ L boscalid reference material at concentrations of 5, 25, 50, 250, 500, 2500, and 5000 ng/ $\mu$ L, resulting in depots of 10, 50, 100, 500, 1000, 5000, and 10,000 ng, respectively. Analyses were performed with solvent A continuously fed to the swab heads at a flow rate of 45  $\mu$ L/min. The areas under the extracted ion current traces ( $m/z$  342.90–343.20) of the boscalid proton adduct were considered for establishing the calibration curve (Figure 5, Supplementary Data S3). As the integration time intervals were dependent on the depletion kinetics, a 5 min range was chosen for depots up to 1000 ng and a 10 min range for the two larger depots. The LOD was determined using visual evaluation and the Thermo Fisher Scientific Xcalibur genesis algorithm was applied to calculate the RMS signal-to-noise ratio. The limit of detection (LOD) of boscalid was found to be 5 ng (S/N RMS: 82) and the limit of quantitation was 10 ng. The LODs of imazalil and thiabendazole corresponded to 1 ng (S/N RMS: 196) and 2 ng (S/N RMS: 145), respectively (Supplementary Data S4).

The calibration curve gave a coefficient of determination of  $R^2 = 0.9922$  in the range from 10 ng to 10  $\mu$ g. While the calibration curve is based on defined amounts of reference material depleted from the swabs, the actual amount of sampled analyte depends on its surface concentration, the sampled surface area, and the sampling efficacy. The mass spectrum of the bell pepper sample revealed the presence of boscalid, which was responsible for the peak of high intensity in the spectrum shown in Figure 2b. For fruit skin sampling, an area of 15 cm<sup>2</sup> (15 cm  $\times$  1 cm) was wiped once with a prewetted rayon swab. Data were acquired for 10 min., and the extracted ion current of the protonated fungicide was Gaussian-smoothed and integrated. A comparison of the obtained depletion curve area of  $3.47 \times 10^8$  counts with the calibration curve resulted in a total of 1386 ng boscalid. The bell pepper weighed 232 g and had a circumference of 24 cm, giving a total surface area of approximately 200 cm<sup>2</sup>. Consequently, the total amount of boscalid fungicide on the bell pepper could be estimated to 82  $\mu$ g per kg fruit (Supplementary Data S5). The European Commission for Health and Food Safety defines the maximum residue level of boscalid on bell peppers as 3 mg/kg [42].

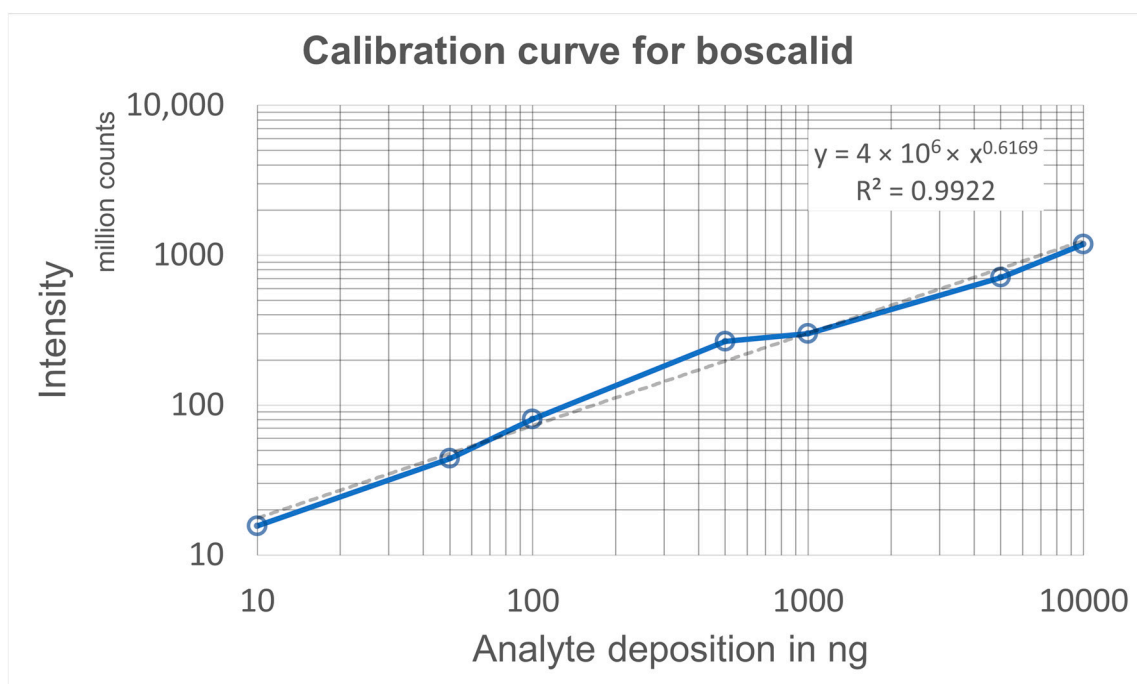


**Figure 5.** Calibration curve for boscalid.

Quantitative results obtained using swab spray analysis may be compromised by incomplete analyte collection from a given surface area and by competitive ionization events leading to analyte suppression. The analyte collection efficacy was found to greatly depend on the surface texture and porosity of the investigated object. Sample recovery was investigated on a glass surface and on fruit skin. Then, 5  $\mu\text{L}$  of an imazalil pesticide standard solution, prepared in methanol, at concentrations of 10  $\mu\text{g/mL}$ , 100  $\mu\text{g/mL}$ , and 1000  $\mu\text{g/mL}$  was applied on 4  $\text{cm}^2$  glass surface areas, resulting in the deposition of 50 ng, 500 ng, and 5000 ng imazalil. Three repeated samplings (single smears) from the same 4  $\text{cm}^2$  surface area were analyzed. The resulting individual depletion curve areas were compared to the total signal intensity of all three analyses to represent the sample collection efficacy of a single smear. Recovery from the glass surface was generally high, though it depended on the amount of analyte deposited, with higher surface concentrations giving higher recovery (Table 1). Additionally, the sample collection efficacy on food products including azoxystrobin (sodium adduct, XIC  $m/z$  425.96–426.26) on tomato skin (Supplementary Data S1), harvested in Switzerland, and imazalil (proton adduct, XIC  $m/z$  297.04–297.07) on orange peel was examined. The first smear on tomato skin delivered 72% of the total signal intensity compared to the next two smears, consisting of only 16% and 12% of the total signal intensity of the three analyses. In contrast to the smooth tomato surface, the sampling of imazalil from the rough and porous orange peel gave a low sample collection efficacy with almost identical portions of 33%, 28%, and 38%.

**Table 1.** Sample recovery rate from different surfaces.

Compound/Surface	Smear (Relative Signal Intensity)		
	1	2	3
Azoxystrobin on tomato skin	72%	16%	12%
Imazalil on orange peel	33%	28%	38%
5000 ng imazalil on glass	76%	12%	11%
500 ng imazalil on glass	68%	20%	12%
50 ng imazalil on glass	41%	38%	21%

These results indicate the variations in sampling efficacy from different surfaces. Swab sampling on rough and porous surfaces is feasible; however, it has a limited ability for quantification only. Regarding the inhomogeneous pesticide distribution on food samples [6], sampling of a larger surface area will be advantageous for obtaining more accurate results.

**Suppression effects:** Due to the lack of upfront chromatographic separation, swab spray ionization is prone to analyte suppression caused by the unavoidable presence of matrix compounds originating from the swab heads or collected from sample surfaces. The extent of analyte suppression depends on the molecular structures, the total amounts, and the depletion characteristics of all compounds present on the swab. Two examples of analyte suppression encountered during swab spray ionization are shown in Figure 6. The XIC chromatograms in Figure 6a correspond to boscalid sampled from bell pepper skin and salicylanilide, which was added at a concentration of 1 ppm to the solvent continuously fed to the swab as a suppression marker for monitoring potentially hindered analyte ionization.

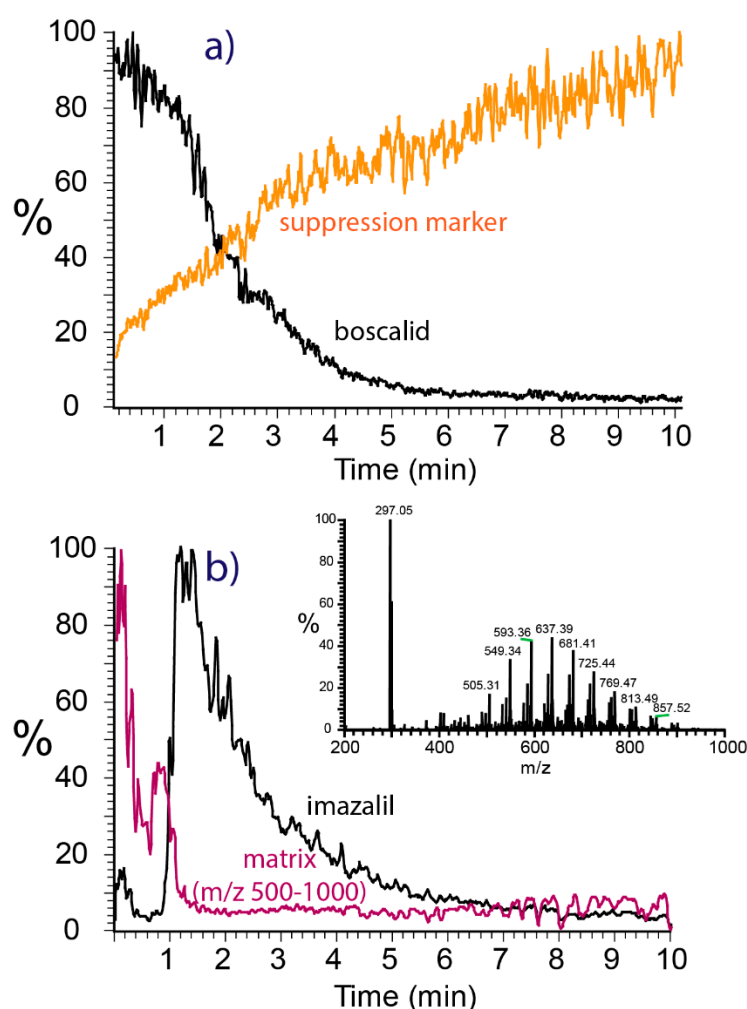


**Figure 6.** Suppression of ionization encountered during swab spray ionization. (a) XIC chromatograms of boscalid sampled from bell pepper and the salicylanilide suppression marker. (b) XIC chromatograms of imazalil and the PEG matrix ( $m/z$  500–1000) sampled from orange peel. The inset shows the full-scan spectrum with the peaks of imazalil at  $m/z$  297 and the PEG matrix.

The XIC of boscalid was high at the very beginning of the analysis and declined over the first five to six minutes due to the continuous depletion of material from the swab. No suppression of the boscalid signal was observed. However, the signal of the salicylanilide suppression marker, which was constantly present at a low concentration,

suffered from severe suppression and rose from zero to higher abundance over the whole acquisition period of ten minutes. The suppression of salicylanilide may be caused by both the predominant boscalid analyte and the matrix compounds. However, since the decrease in the boscalid signal occurs at a much faster rate than the increase in the suppression marker signal, the matrix is most likely the primary cause of suppression. Because the matrix is depleted as well, the suppression of salicylanilide decreases over time, explaining the curve shape observed.

The data for the fungicide imazalil were recorded from an orange peel sample, harvested in Spain, and demonstrate the suppression of the analyte by strong matrix constituents (Figure 6b). In addition to imazalil, polyethylene glycol (PEG) was found on orange peel, a compound added by the food industry as a coating agent for extending the post-harvest shelf-life of fruit [43,44]. The PEG signal detected in the range from  $m/z$  500 to 1000 led to a massive suppression of the ionization of imazalil. The depletion of PEG was found to be rapid and the suppression of the fungicide was significant during the first minute of analysis only. However, the non-simultaneous extraction of analyte and PEG require further investigation to understand the extraction kinetics of analytes of different polarities.

The presence of sample constituents of relatively high concentration also interferes with quantitative work. The extent of suppression was examined in a series of experiments performed with 10 ng, 50 ng, 100 ng, 500 ng, 1000 ng, 5000 ng, and 10,000 ng boscalid spiked onto swabs and electrosprayed with a continuous solvent flow containing 1000 ng/mL (1.264 ppm) salicylanilide as the suppression marker. This setup resulted in the injection of 45 ng salicylanilide per minute at a continuous flow rate of 45  $\mu$ L/min. No suppression of salicylanilide was observed for swabs loaded with up to 1000 ng boscalid. An analysis of the samples with higher boscalid load, however, revealed the suppression of salicylanilide within the first two minutes, until the boscalid level decreased to lower values (Supplementary Data S6). Nevertheless, these experiments demonstrate two potential causes of analyte suppression during swab spray analysis: the presence of a second abundant analyte and the unavoidable presence of the matrix.

### 3. Material and Methods

#### 3.1. Chemicals and Materials

Copan 160C minitip rayon swabs with an aluminum applicator contained in a plastic tube (Copan Italy, Brescia, Italy) were used for all experiments. Glass vials for the preparation of stock solutions and silanized inserts for the preparation of the dilution series were purchased from BGB Analytik AG (Böckten, Switzerland). Methanol and ethyl acetate (LiChrosolv hypergrade LC-MS quality), formic acid (Lichropur LC-MS grade), salicylanilide (99%), boscalid, imazalil, and thiabendazole standards (PESTANAL, analytical standards) were purchased from Merck/Sigma-Aldrich (Buchs, Switzerland). Experiments were performed with either a mixture of methanol/ethyl acetate (30/70,  $v/v$ ) (solvent A) or with methanol (solvent B), both containing 0.1% formic acid modifier.

#### 3.2. Instrumentation

The instrumentation was based on a modified nanoelectrospray ion source attached to a Thermo Scientific LTQ Orbitrap Velos (Thermo Fisher Scientific, Reinach, Switzerland) high resolution mass spectrometer, shown in Figure 7. The swabs were mounted to point down in a 45° angle and the position of the swab was adjustable in all three dimensions, which allowed the exact positioning of the swab head for the best signal intensity and stability. The solvent supply capillary was adjustable in three dimensions for exact positioning on the swab head. A syringe pump (Harvard apparatus, Holliston, MA, USA) was used for solvent delivery to the swab head through an electrically grounded PEEK capillary. The swab head was positioned at a horizontal distance of 7 mm from the ion sweep cone of the mass spectrometer. This setting also prevented electrical discharges and the pulsation of



the Taylor cone, which would lead to signal disruption. The ion source was equipped with a camera for monitoring the swab position and electrospray formation.

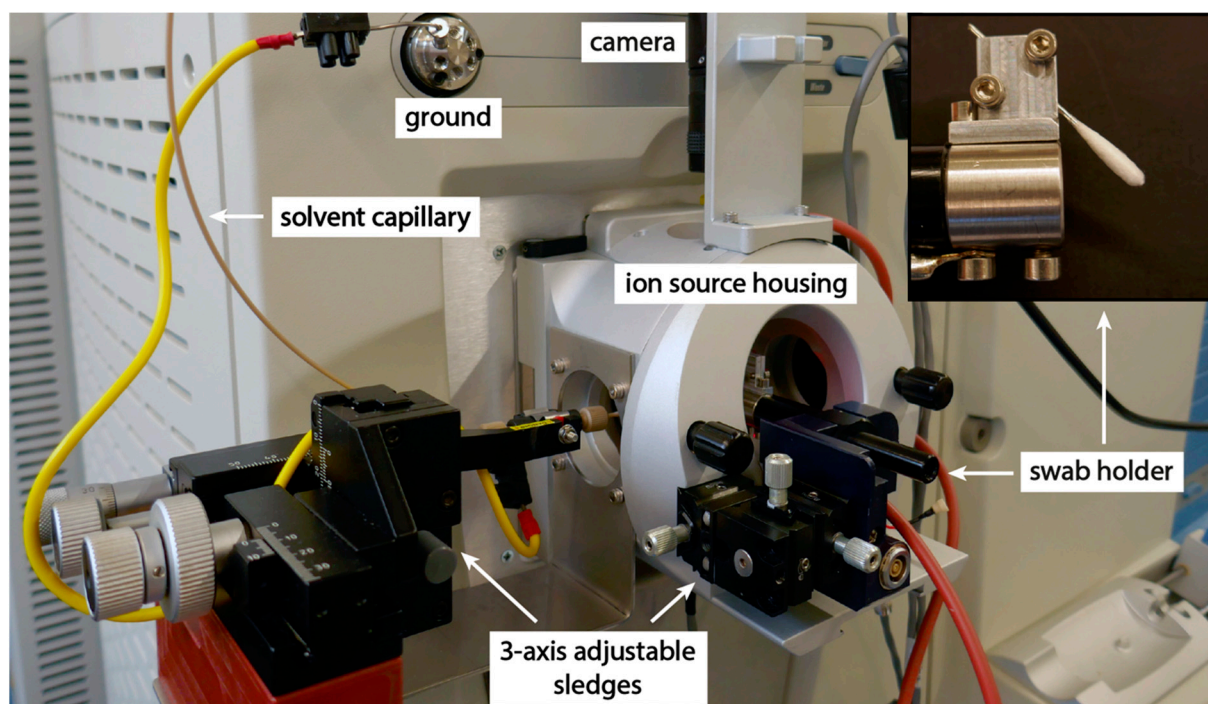


**Figure 7.** Modified nanoelectrospray ion source with the swab holder and the solvent capillary mounted on 3-axis translation stages for exact positioning. The inset shows the mounting position of the swab.

The mass spectrometer was operated in the positive ion mode with a spray voltage of +5.5 kV. Mass spectra were recorded in the range of  $m/z$  50–2000. The mass resolution was set to 30,000 ( $m/\Delta m$  @  $m/z$  400). The temperature of the transfer tube was set to 200 °C to prevent thermal degradation of labile analytes. Salicylanilide as a suppression marker was added directly to the solvent at a concentration of 1 ppm to monitor the swab background and to observe analyte suppression during sample acquisition. Tandem mass spectrometric experiments were performed in the LTQ ion trap with a precursor ion selection width of 1  $m/z$ , helium as the collision gas, a normalized collision energy of 25%, and an ion activation time of 10 ms. The Thermo Scientific Xcalibur 2.2 (Thermo Fisher Scientific, Reinach, Switzerland) software was used for instrument control and data acquisition, and compound identification was assisted by the Sciex high-resolution MS/MS pesticide library comprising 557 compounds (AB Sciex, Baden, Switzerland).

### 3.3. Swab Spray Handling Procedure

The handle of the swab was cut a distance of a few centimeters from the swab head and mounted on the swab holder. The solvent capillary was aligned with the higher end of the swab head. Solvents were applied to the swab head at a flow rate of 45  $\mu\text{L}/\text{min}$ . As soon as the accumulation of solvent appeared on the swab head, which was observed by the top-mounted camera on the ion source housing, the spray voltage was applied to the swab head via its aluminum handle.

To reduce the background signals, a prewashing procedure of the Copan 160C swabs was performed by adding 3.5 mL ethyl acetate to the swab plastic tube and sonicating the swab in the closed tube for three minutes at 40 °C. The swab was removed from the tube and air-dried before usage.

### 3.4. Evaluation of Quantitation

A stock solution of imazalil reference material was prepared in methanol at a concentration of 1 mg/mL. Then, 25  $\mu$ L of the stock solution was diluted by a factor of 40 to yield a concentration of 25  $\mu$ g/mL. Then, 4  $\mu$ L of the solution was directly deposited on the prewashed swab to examine the depletion of imazalil during an extraction period of 5 min with solvent A. The procedure was carried out five times in total.

Sampling of defined surface areas was performed with the aid of parafilm masks, which were positioned over the sampling areas. Analyte sampling was performed using horizontal and vertical movements of the prewetted swab head.

## 4. Conclusions

The monitoring of pesticide residues on food is of high importance to ensure consumer safety. Ambient ionization techniques, such as swab spray ionization, offer the advantages of rapid sample collection from any fruit surface and analysis with minimum sample preparation. Pesticides are separated by mass spectrometry without upfront chromatographic separation, even in the case of rather complex samples. The reliable identification of pesticide residues is achieved by assessing the exact masses of the ions, their isotopic patterns, and the product ion spectra.

Due to the lack of a chromatographic separation step, swab spray ionization is prone to analyte suppression caused by the presence of abundant sample constituents and the unavoidable matrix. Background ions originating from the swab manufacturing process are easily removed in a washing step prior to sampling. The extent of analyte suppression can be monitored by adding a suppression marker at a low concentration to the solvent flow. Though the formation of sodium adducts can be lessened by appropriate selection of the extraction solvent, this has to be taken into consideration for compound identification and quantitative analysis. Shifting the equilibrium from sodium to proton adducts increases the limits of quantitation and facilitates compound identification via MS/MS. Despite swab manufacturing variations, matrix effects, and the surface-dependent sampling efficacy, the method provides quantitative data through the integration of the area under the extracted ion current trace (depletion curve) of a pesticide ion. The reproducibility was found to be on the order of  $\pm 21\%$  and the limit of quantitation was in the low ng range, which seems adequate for a rapid, quite quantitative screening method.

**Supplementary Materials:** The following supporting information can be downloaded at: <https://www.mdpi.com/article/10.3390/molecules28186611/s1>, Figure S1: Detection of pesticides on clementine, orange, and tomato; Figure S2: Depletion curves of 10 ng and 50 ng boscalid; Figure: S3 Depletion curves of 100 ng and 500 ng boscalid; Figure S4: Depletion curves of 1000 ng and 5000 ng boscalid; Figure S5: Depletion curve of 10,000 ng boscalid; Figure S6: Detection of low pesticide amounts; Table S1: Reproducibility of swab spray ionization mass spectrometry; Table S2: Boscalid quantitation on bell pepper; Figure S7: Suppression of marker.

**Author Contributions:** Conceptualization, S.S.; methodology, T.M.M.; formal analysis, T.M.M.; investigation, T.M.M. and S.S.; resources, S.S.; writing—original draft preparation, T.M.M.; writing—review and editing, S.S. and T.M.M.; visualization, T.M.M.; supervision, S.S.; project administration, S.S.; funding acquisition, S.S. All authors have read and agreed to the published version of the manuscript.

**Funding:** This research received no external funding.

**Institutional Review Board Statement:** Not applicable.

**Informed Consent Statement:** Not applicable.

**Data Availability Statement:** Data related to this work are available from the corresponding author on request.

**Conflicts of Interest:** The authors declare no conflict of interest.

**Sample Availability:** Not applicable.



## References

- Feider, C.L.; Krieger, A.; DeHoog, R.J.; Eberlin, L.S. Ambient Ionization Mass Spectrometry: Recent Developments and Applications. *Anal. Chem.* **2019**, *91*, 4266–4290. [CrossRef]
- Huang, M.-Z.; Cheng, S.-C.; Cho, Y.-T.; Shiea, J. Ambient Ionization Mass Spectrometry: A Tutorial. *Anal. Chim. Acta* **2011**, *702*, 1–15. [CrossRef]
- Takáts, Z.; Wiseman, J.M.; Gologan, B.; Cooks, R.G. Mass Spectrometry Sampling under Ambient Conditions with Desorption Electrospray Ionization. *Science* **2004**, *306*, 471–473. [CrossRef]
- Cody, R.B.; Laramée, J.A.; Durst, H.D. Versatile New Ion Source for the Analysis of Materials in Open Air under Ambient Conditions. *Anal. Chem.* **2005**, *77*, 2297–2302. [CrossRef]
- Rankin-Turner, S.; Reynolds, J.C.; Turner, M.A.; Heaney, L.M. Applications of Ambient Ionization Mass Spectrometry in 2021: An Annual Review. *Anal. Sci. Adv.* **2022**, *3*, 67–89. [CrossRef]
- Beneito-Cambrá, M.; Gilbert-López, B.; Moreno-González, D.; Bouza, M.; Franzke, J.; García-Reyes, J.F.; Molina-Díaz, A. Ambient (Desorption/Ionization) Mass Spectrometry Methods for Pesticide Testing in Food: A Review. *Anal. Methods* **2020**, *12*, 4831–4852. [CrossRef]
- Chen, R.; Deng, J.; Fang, L.; Yao, Y.; Chen, B.; Wang, X.; Luan, T. Recent Applications of Ambient Ionization Mass Spectrometry in Environmental Analysis. *Trends Environ. Anal. Chem.* **2017**, *15*, 1–11. [CrossRef]
- Forbes, T.P.; Sisco, E. Recent Advances in Ambient Mass Spectrometry of Trace Explosives. *Analyst* **2018**, *143*, 1948–1969. [CrossRef]
- Boronat Ena, M.D.M.; Cowan, D.A.; Abbate, V. Ambient Ionization Mass Spectrometry Applied to New Psychoactive Substance Analysis. *Mass. Spectrom. Rev.* **2023**, *42*, 3–34. [CrossRef]
- Li, L.-H.; Hsieh, H.-Y.; Hsu, C.-C. Clinical Application of Ambient Ionization Mass Spectrometry. *Mass Spectrom.* **2017**, *6*, S0060. [CrossRef]
- Burns, D.; Mathias, S.; McCullough, B.J.; Hopley, C.J.; Douce, D.; Lumley, N.; Bajic, S.; Sears, P. Ambient Ionisation Mass Spectrometry for the Trace Detection of Explosives Using a Portable Mass Spectrometer. *Int. J. Mass Spectrom.* **2022**, *471*, 116735. [CrossRef]
- Ferreira, C.R.; Yannell, K.E.; Jarmusch, A.K.; Pirro, V.; Ouyang, Z.; Cooks, R.G. Ambient Ionization Mass Spectrometry for Point-of-Care Diagnostics and Other Clinical Measurements. *Clin. Chem.* **2016**, *62*, 99–110. [CrossRef]
- Pirro, V.; Jarmusch, A.K.; Vincenti, M.; Cooks, R.G. Direct Drug Analysis from Oral Fluid Using Medical Swab Touch Spray Mass Spectrometry. *Anal. Chim. Acta* **2015**, *861*, 47–54. [CrossRef]
- Pirro, V.; Llor, R.S.; Jarmusch, A.K.; Alfaro, C.M.; Cohen-Gadol, A.A.; Hattab, E.M.; Cooks, R.G. Analysis of Human Gliomas by Swab Touch Spray-Mass Spectrometry: Applications to Intraoperative Assessment of Surgical Margins and Presence of Oncometabolites. *Analyst* **2017**, *142*, 4058–4066. [CrossRef] [PubMed]
- Jarmusch, A.K.; Pirro, V.; Logsdon, D.L.; Cooks, R.G. Direct Ion Generation from Swabs. *Talanta* **2018**, *184*, 356–363. [CrossRef]
- Morato, N.M.; Pirro, V.; Fedick, P.W.; Cooks, R.G. Quantitative Swab Touch Spray Mass Spectrometry for Oral Fluid Drug Testing. *Anal. Chem.* **2019**, *91*, 7450–7457. [CrossRef]
- Fedick, P.W.; Bain, R.M. Swab Touch Spray Mass Spectrometry for Rapid Analysis of Organic Gunshot Residue from Human Hand and Various Surfaces Using Commercial and Fieldable Mass Spectrometry Systems. *Forensic Chem.* **2017**, *5*, 53–57. [CrossRef]
- Bain, R.M.; Fedick, P.W.; Dilger, J.M.; Cooks, R.G. Analysis of Residual Explosives by Swab Touch Spray Ionization Mass Spectrometry. *Propellants Explos. Pyrotech.* **2018**, *43*, 1139–1144. [CrossRef]
- Costa, C.; van Es, E.M.; Sears, P.; Bunch, J.; Palitsin, V.; Cooper, H.; Bailey, M.J. Exploring a Route to a Selective and Sensitive Portable System for Explosive Detection- Swab Spray Ionisation Coupled to of High-Field Assisted Waveform Ion Mobility Spectrometry (FAIMS). *Forensic Sci. Int.* **2019**, *1*, 214–220. [CrossRef]
- Jarmusch, A.K.; Pirro, V.; Kerian, K.S.; Cooks, R.G. Detection of Strep Throat Causing Bacterium Directly from Medical Swabs by Touch Spray-Mass Spectrometry. *Analyst* **2014**, *139*, 4785–4789. [CrossRef]
- Yang, B.; Wang, F.; Yang, X.; Zou, W.; Wang, J.; Zou, Y.; Liu, F.; Liu, H.; Huang, O. Medical Swab Touch Spray-Mass Spectrometry for Newborn Screening of Nicotine and Cotinine in Meconium. *J. Mass Spectrom.* **2016**, *51*, 1237–1242. [CrossRef] [PubMed]
- Snyder, D.T.; Szalwinski, L.J.; Schrader, R.L.; Pirro, V.; Hilger, R.; Cooks, R.G. Precursor and Neutral Loss Scans in an RF Scanning Linear Quadrupole Ion Trap. *J. Am. Soc. Mass Spectrom.* **2018**, *29*, 1345–1354. [CrossRef]
- Statistical Yearbook 2021 World Food and Agriculture. Available online: [www.Fao.Org/3/Cb4477en/Cb4477en.Pdf](http://www.Fao.Org/3/Cb4477en/Cb4477en.Pdf) (accessed on 13 March 2023).
- d’Hose, D.; Isenborghs, P.; Brusa, D.; Jordan, B.F.; Gallez, B. The Short-Term Exposure to SDHI Fungicides Boscalid and Bixafen Induces a Mitochondrial Dysfunction in Selective Human Cell Lines. *Molecules* **2021**, *26*, 5842. [CrossRef] [PubMed]
- Costa, L.G.; Giordano, G.; Guizzetti, M.; Vitalone, A. Neurotoxicity of Pesticides: A Brief Review. *Front. Biosci.* **2008**, *13*, 1240–1249. [CrossRef] [PubMed]
- El-Nahhal, Y.; El-Nahhal, I. Cardiotoxicity of Some Pesticides and Their Amelioration. *Environ. Sci. Pollut. Res.* **2021**, *28*, 44726–44754. [CrossRef]
- Tao, Y.; Liu, J.; Xu, Y.; Liu, H.; Yang, G.; He, Y.; Xu, J.; Lu, Z. Suspecting Screening “Known Unknown” Pesticides and Transformation Products in Soil at Pesticide Manufacturing Sites. *Sci. Total Environ.* **2022**, *808*, 152074. [CrossRef]

28. Khetagoudar, M.C.; Chetti, M.B.; Raghu, A.V.; Bilehal, D.C. Multiresidue Pesticide Analysis in Cabbage and Cauliflower Using Gas Chromatography Tandem Mass Spectrometry (GC-MS/MS). In *Pesticides in Crop Production*; Wiley: Hoboken, NJ, USA, 2020; pp. 221–231.
29. Wong, J.W.; Wang, J.; Chow, W.; Carlson, R.; Jia, Z.; Zhang, K.; Hayward, D.G.; Chang, J.S. Perspectives on Liquid Chromatography—High-Resolution Mass Spectrometry for Pesticide Screening in Foods. *J. Agric. Food Chem.* **2018**, *66*, 9573–9581. [\[CrossRef\]](#)
30. Hernández-Mesa, M.; Moreno-González, D. Current Role of Mass Spectrometry in the Determination of Pesticide Residues in Food. *Separations* **2022**, *9*, 148. [\[CrossRef\]](#)
31. Gormez, E.; Golge, O.; González-Curbelo, M.Á.; Kabak, B. Pesticide Residues in Mandarins: Three-Year Monitoring Results. *Molecules* **2023**, *28*, 5611. [\[CrossRef\]](#)
32. Kang, S.-M.; Won, J.-H.; Han, J.-E.; Kim, J.-H.; Kim, K.-H.; Jeong, H.-I.; Sung, S.-H. Chromatographic Method for Monitoring of Pesticide Residues and Risk Assessment for Herbal Decoctions Used in Traditional Korean Medicine Clinics. *Molecules* **2023**, *28*, 3343. [\[CrossRef\]](#)
33. Fan, X.; Tang, T.; Du, S.; Sang, N.; Huang, H.; Zhang, C.; Zhao, X. Simultaneous Determination of 108 Pesticide Residues in Three Traditional Chinese Medicines Using a Modified QuEChERS Mixed Sample Preparation Method and HPLC-MS/MS. *Molecules* **2022**, *27*, 7636. [\[CrossRef\]](#)
34. Constantinou, M.; Louca-Christodoulou, D.; Agapiou, A. Method Validation for the Determination of 314 Pesticide Residues Using Tandem MS Systems (GC-MS/MS and LC-MS/MS) in Raisins: Focus on Risk Exposure Assessment and Respective Processing Factors in Real Samples (a Pilot Survey). *Food Chem.* **2021**, *360*, 129964. [\[CrossRef\]](#) [\[PubMed\]](#)
35. Harischandra, N.R.; Pallavi, M.S.; Bheemanna, M.; PavanKumar, K.; Chandra Sekhara Reddy, V.; Udaykumar, N.R.; Paramasivam, M.; Yadav, S. Simultaneous Determination of 79 Pesticides in Pigeonpea Grains Using GC-MS/MS and LC-MS/MS. *Food Chem.* **2021**, *347*, 128986. [\[CrossRef\]](#) [\[PubMed\]](#)
36. Stachniuk, A.; Szmagara, A.; Czezko, R.; Fornal, E. LC-MS/MS Determination of Pesticide Residues in Fruits and Vegetables. *J. Environ. Sci. Health Part B* **2017**, *52*, 446–457. [\[CrossRef\]](#) [\[PubMed\]](#)
37. Guo, Z.; Zhu, Z.; Huang, S.; Wang, J. Non-Targeted Screening of Pesticides for Food Analysis Using Liquid Chromatography High-Resolution Mass Spectrometry—A Review. *Food Addit. Contam. Part A Chem. Anal. Control. Expo. Risk Assess* **2020**, *37*, 1180–1201. [\[CrossRef\]](#)
38. Yun, H.Y.; Won, E.-J.; Choi, J.; Cho, Y.; Lim, D.-J.; Kim, I.-S.; Shin, K.-H. Stable Isotope Analysis of Residual Pesticides via High Performance Liquid Chromatography and Elemental Analyzer–Isotope Ratio Mass Spectrometry. *Molecules* **2022**, *27*, 8587. [\[CrossRef\]](#)
39. Thurman, E.M.; Ferrer, I.; Zweigenbaum, J.A.; García-Reyes, J.F.; Woodman, M.; Fernández-Alba, A.R. Discovering Metabolites of Post-Harvest Fungicides in Citrus with Liquid Chromatography/Time-of-Flight Mass Spectrometry and Ion Trap Tandem Mass Spectrometry. *J. Chromatogr. A* **2005**, *1082*, 71–80. [\[CrossRef\]](#)
40. Jabot, C.; Daniele, G.; Giroud, B.; Tchamitchian, S.; Belzunces, L.P.; Casabianca, H.; Vulliet, E. Detection and Quantification of Boscalid and Its Metabolites in Honeybees. *Chemosphere* **2016**, *156*, 245–251. [\[CrossRef\]](#)
41. Krueve, A.; Kaupmees, K.; Liigand, J.; Oss, M.; Leito, I. Sodium Adduct Formation Efficiency in ESI Source. *J. Mass Spectrom.* **2013**, *48*, 695–702. [\[CrossRef\]](#)
42. Pesticide Residue(s) and Maximum Residue Levels (mg/kg). Available online: [https://ec.europa.eu/food/plant/pesticides/eu-pesticides-database/start/screen/mrls/details?lg\\_code=EN&pest\\_res\\_id\\_list=244](https://ec.europa.eu/food/plant/pesticides/eu-pesticides-database/start/screen/mrls/details?lg_code=EN&pest_res_id_list=244) (accessed on 13 September 2023).
43. CFR—Code of Federal Regulations Title 21. Available online: [www.Accessdata.Fda.Gov/Scripts/Cdrh/Cfdocs/Cfcfr/CFRSearch.Cfm?Fr=172.210](http://www.accessdata.fda.gov/scripts/cdrh/cfdocs/cfcfr/CFRSearch.Cfm?Fr=172.210) (accessed on 9 June 2023).
44. Jin, X.; Zhang, S.; Yang, J.; Li, Y. The Potential of Alkyl Polyglucosides and Polyethylene Glycol Glucosides Coatings for Improving the Storage and Shelf-Life of Pineapples. *Tenside Surfactants Deterg.* **2004**, *41*, 109–112. [\[CrossRef\]](#)

**Disclaimer/Publisher’s Note:** The statements, opinions and data contained in all publications are solely those of the individual author(s) and contributor(s) and not of MDPI and/or the editor(s). MDPI and/or the editor(s) disclaim responsibility for any injury to people or property resulting from any ideas, methods, instructions or products referred to in the content.

### 2.13 Comparison between Swab Spray and LC-MS

The strawberry presented in the publication underwent further analysis for contact pesticide residues using LC-MS<sup>2</sup>. For the LC-MS<sup>2</sup> analysis, the strawberry was homogenized, extracted, centrifuged, and filtered prior to vial transfer. The LC-MS<sup>2</sup> method utilized reverse phase liquid chromatography and information dependent acquisition (IDA). As for the analysis by swab spray, fluopyram, a SDHI fungicide, was detected. The corresponding extracted ion current chromatogram, showing fluopyram at a retention time of 7.5 minutes, and the obtained fragment ion spectrum are depicted in Figure 52. The entire process took approximately 95 minutes, in contrast to the swab spray analysis, which took about 13 minutes. A schematic representation of the procedural steps and their respective duration is illustrated in Figure 53. While both methods were successful in detecting fluopyram, swab spray offers a rapid alternative for the identification of contact pesticide residues. However, for the detection of systemic pesticides, homogenization and extraction remains a mandatory step in sample preparation.

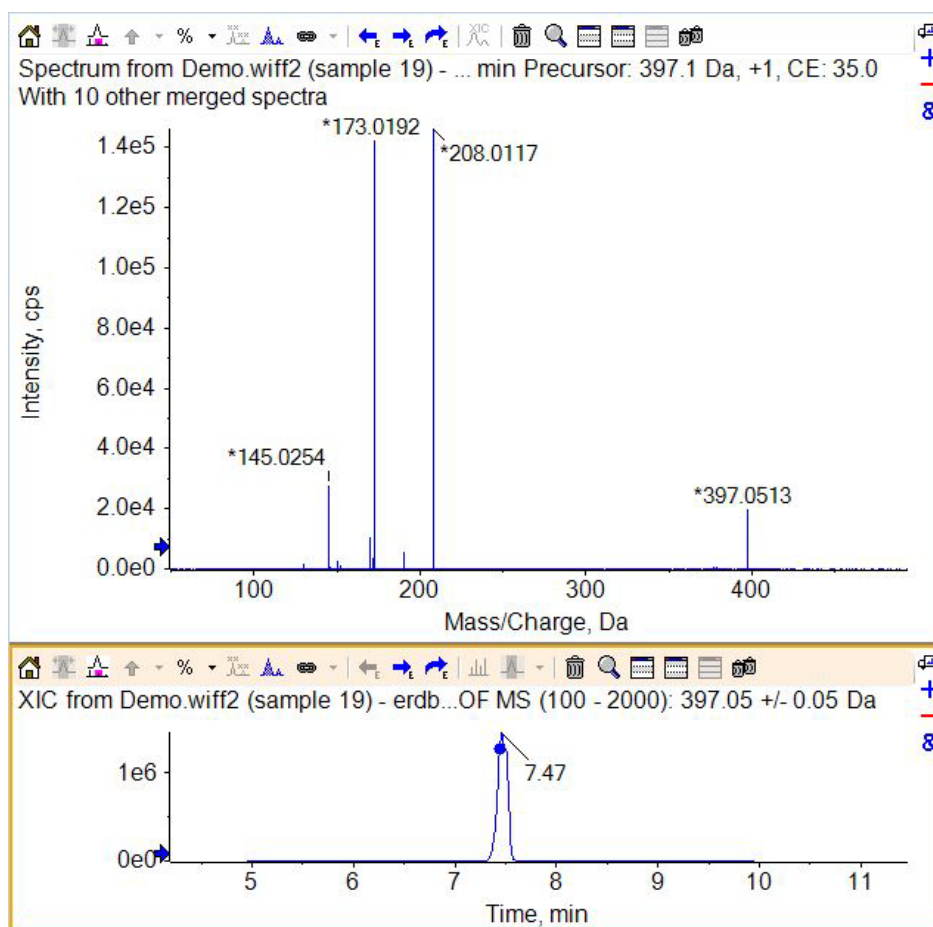


Figure 52 Fragment ion spectrum of fluopyram at the top and extracted ion current ( $m/z$  397.00-397.10) at the bottom.

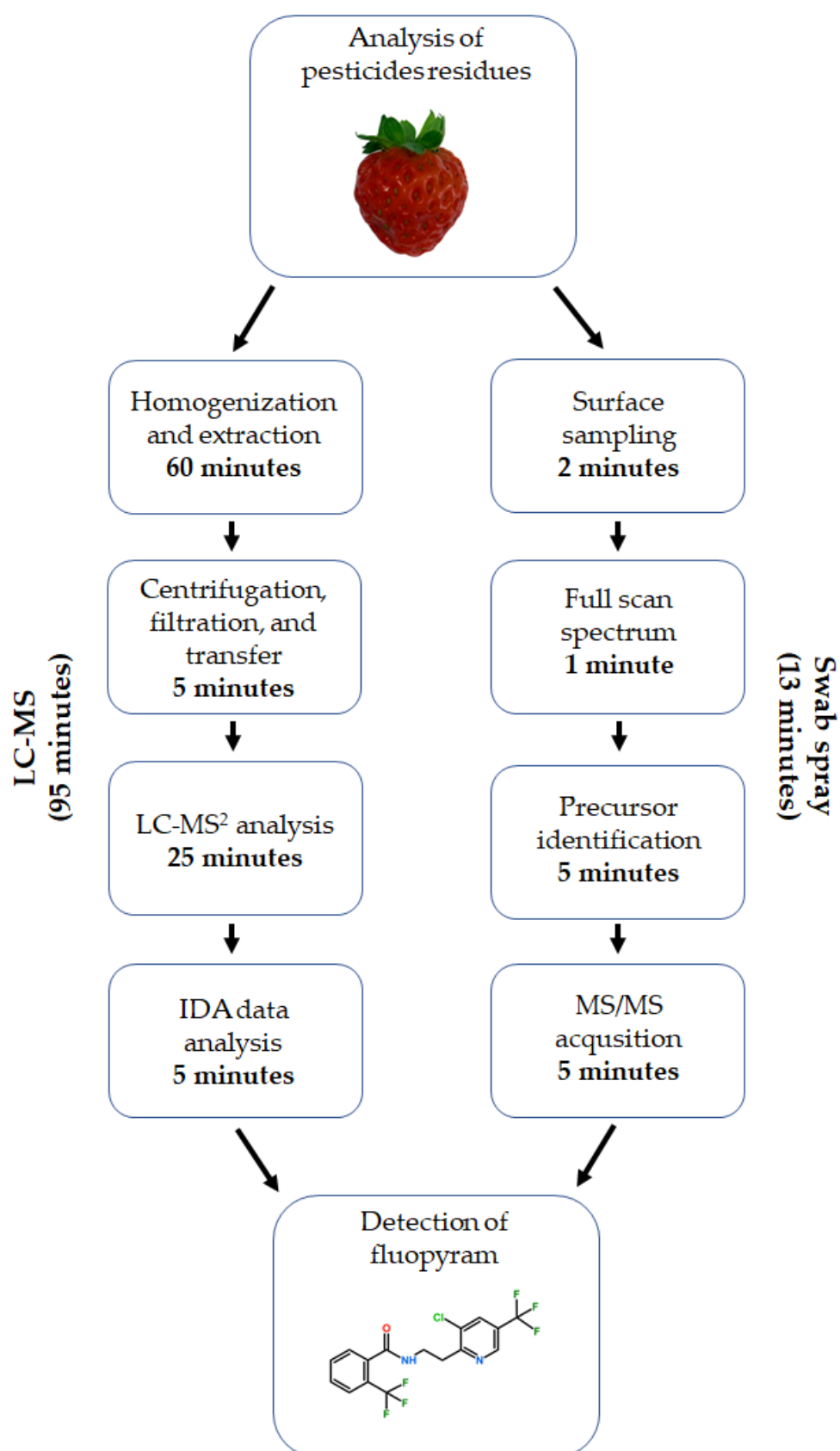


Figure 53 Comparison of analysis duration in LC-MS<sup>2</sup> and swab spray.

## 2.14 Simulated Forensic Applications

To evaluate the potential of swab spray mass spectrometry for forensic analysis, three simulated applications were conducted. These included the analysis of an unknown “white powder” and the testing of solid surfaces and human skin for organic compound residues.

### 2.14.1 Analysis of Unknown White Powder

A tablet containing pantoprazole was crushed to obtain a white powder, which was directly sampled with a prewetted swab. The visual estimation of sample uptake was in the range of several milligrams, corresponding to a very high sample load for mass spectrometry-based techniques. Nevertheless, the high sample amount did not lead to difficulties concerning spray generation and stability.

A full-scan spectrum of high intensity was obtained, revealing pantoprazole in its protonated form at  $m/z$  384.08 and in its sodiated form at  $m/z$  406.06. Another abundant peak was observed at  $m/z$  200.04. The protonated precursor was selected for MS<sup>2</sup> analysis. Both, the full-scan spectrum and CAD spectrum, are presented in Figure 54. The homolytic cleavage adjacent to the sulfoxide moiety yields the fragment ion at  $m/z$  153.00. Cleavage on the other side of the sulfoxid moiety in conjunction with [1,3]-H migration generates the fragment ion at  $m/z$  200.00. Both fragments include the pyridine heterocycle. Latter fragment ion was also visible in the full-scan spectrum as a result of in-source decomposition. However, no fragment ion containing the benzimidazole heterocycle was observed. The fragmentation patterns of several PPIs (proton pump inhibitors) were studied in 2023. Omeprazole, which, similar to pantoprazole, contains a sulfoxide group between two heterocycles, undergoes homolytic cleavage of the S(=O)-CH<sub>2</sub> bond. Furthermore, the [1,3]-H migration from the CH<sub>2</sub> moiety to the heterocyclic carbon atom adjacent to the SO group was observed for the sodiated omeprazole precursor [243].

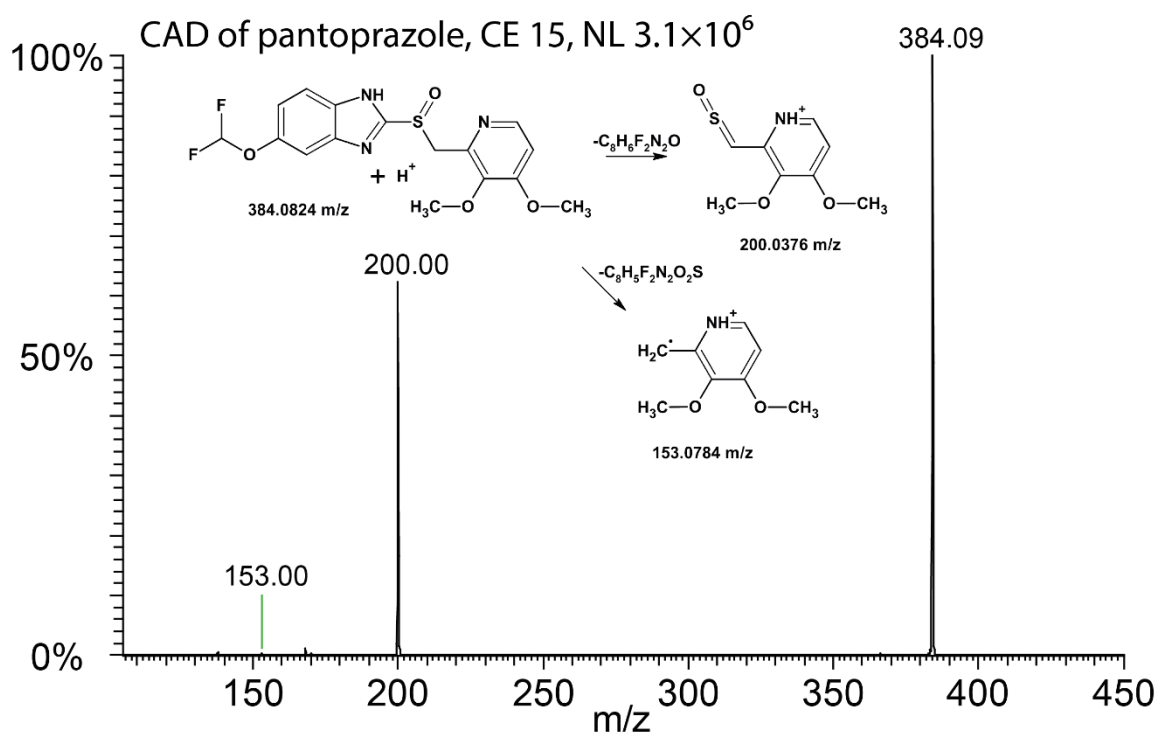
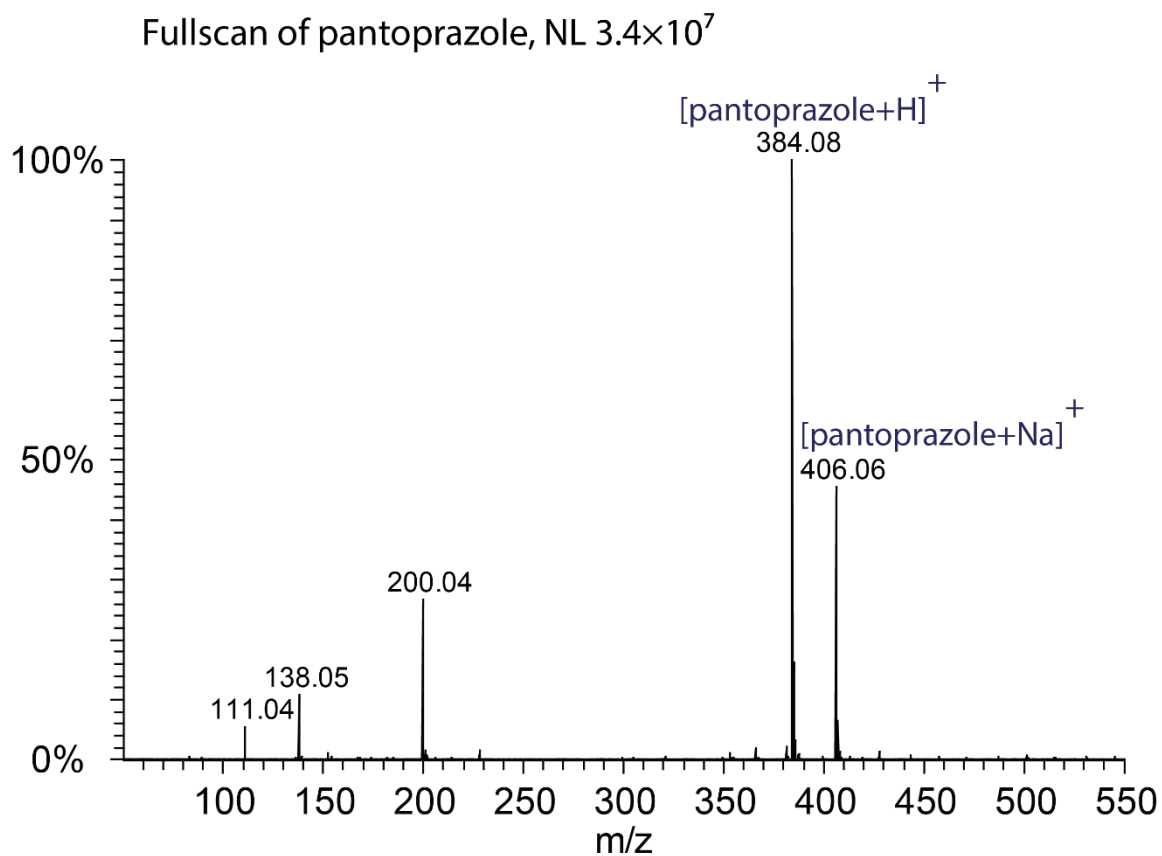


Figure 54 Full-scan spectrum of a pantoprazole tablet (top) and CAD spectrum of the protonated precursor (bottom).

### 2.14.2 Analysis of Skin and Surfaces

Analyzing skin and surface samples for organic compound residues is an important aspect of forensic chemistry. To assess the skin for organic compound residues, an area of approximately 1 x 2 cm on a fingertip was sampled with a prewetted swab by circular motions for 30 seconds using the swab tip only. The generation and stability of the spray were not affected by the skin matrix. A peak at  $m/z$  192.14 was selected for CAD experiments, with the resulting spectrum illustrated in Figure 55 (top). Based on the precursor mass and the fragmentation pattern, panthenol was identified, originating from a hand cream used by the test person.

The proposed fragmentation pattern of panthenol is shown in Figure 55 (top). The fragmentation pathway is characterized by multiple dehydration steps. The most abundant fragment ion at  $m/z$  188.09 resulted from the dehydration of the hydroxyl group adjacent to the protonated amide. In this charge migration fragmentation, the proton is transferred to the hydroxyl group, resulting in the neutral loss of water and the formation of a positively charged carbon. This mechanism is supported by the absence of ions resulting from amide bond cleavage, indicating that dehydration by neutral loss of water is favored. The positive charge proposedly migrates to the carbon adjacent to the amide bond. The peaks at  $m/z$  170.09 and  $m/z$  152.09 are proposed to be the result of two further dehydration steps. The skin matrix and small particles originating from dander, dirt and dust did not interfere with the analysis.

To test for residues of organic compounds on surfaces, a watch glass was sampled by following a similar procedure. The full-scan mass spectrum displayed an abundant peak at  $m/z$  192.14 (shown in Figure 55 at the bottom). Matching precursor and fragment ions with the pesticide library resulted in the identification of diethyltoluamide (DEET), an insect repellent [244,245]. CAD experiments on DEET yielded fragment ions of  $m/z$  100.08, exhibiting minor intensity, and  $m/z$  119.05, displaying high intensity. Both fragment ions are proposed to comprise an acylium moiety incorporating either the dimethylamine ( $m/z$  100.08) or methylbenzene group ( $m/z$  119.05).

DEET became detectable on the glass of the wristwatch, as the wearer frequently applied DEET during summertime to prevent insect bites and stings. Despite regular cleansing of the watch with warm water and soap, DEET was detected at a high intensity.

The high sensitivity of swab spray mass spectrometry, coupled along with the rapid and non-destructive sampling on surfaces, including skin and personal items, underlines its potential for forensic applications. The detection of drugs and explosives

or other crime-related organic compounds could be accomplished in a very short time frame. In-situ analysis, when combined with a mobile mass spectrometer, could drastically enhance the capabilities of forensic chemistry in crime investigations.

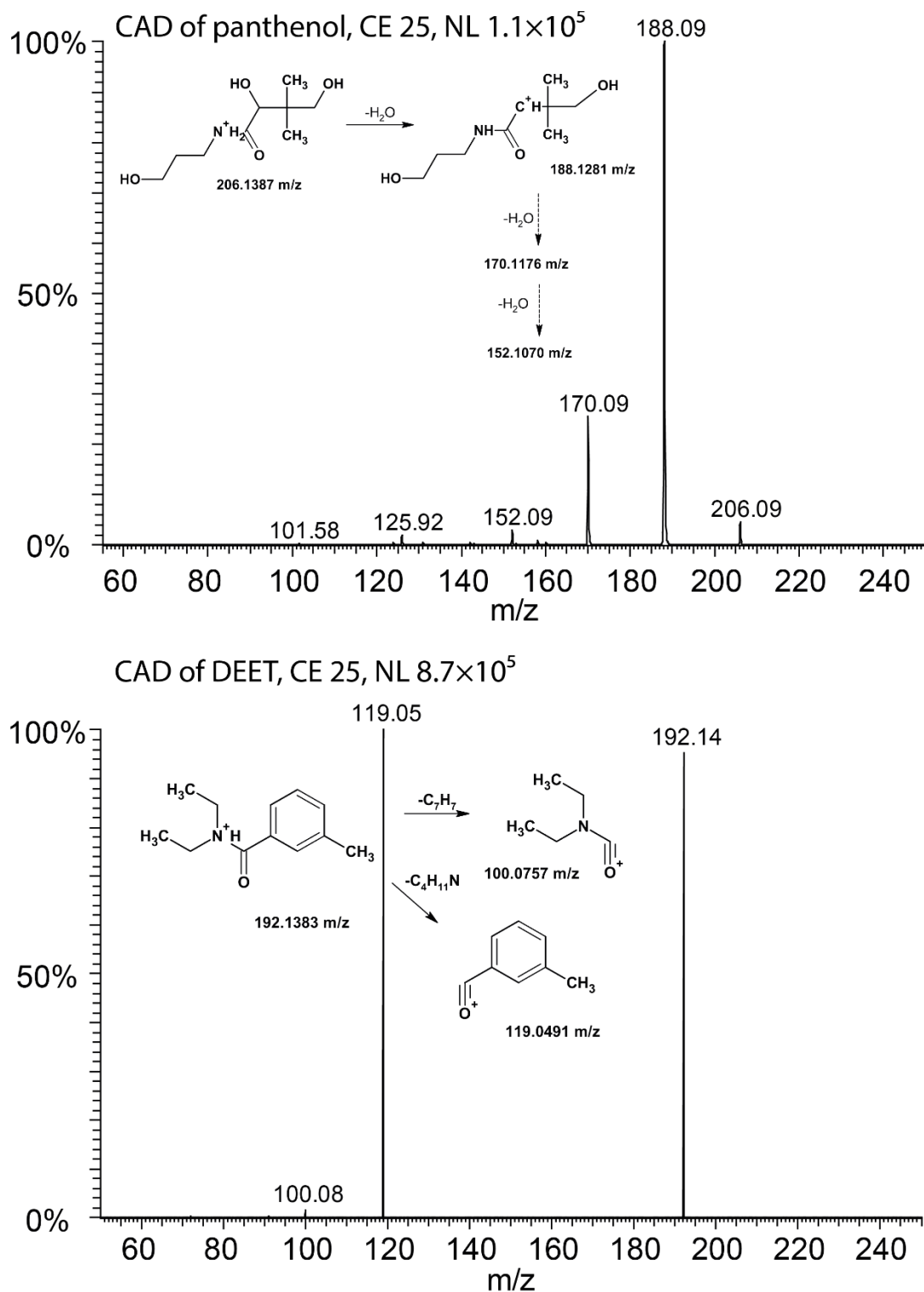


Figure 55 CAD spectrum of panthenol (top) and DEET (bottom).



### 2.14.3 Analysis of Ballpoint Ink

For the identification and differentiation of ballpoint ink on disputed documents, thin layer chromatography (TLC) or optical methods are frequently applied to confirm or disprove fraudulent document alterations. Mass spectrometry-based approaches, such as laser desorption ionization (LDI), MALDI, DART, field desorption (FD), and DESI have been demonstrated to provide superior differentiation capabilities through identification of ink compounds compared to conventional methods, while concurrently minimizing sample destruction [246,247].

To evaluate the efficacy of swab spray mass spectrometry in identifying ballpoint ink, a pre-moistened swab was drawn across a one-centimeter line of ballpoint ink (provided by the Department of Chemistry, Biochemistry, and Pharmaceutical Sciences at the University of Bern). The initial sample uptake proved to be minimal, resulting in a spectrum of low abundance. Multiple samplings were necessary for producing a spectrum of high abundance. However, this process also led to increased document degradation. The obtained full-scan spectrum is illustrated in Figure 57 at the top. A series of peaks with a mass difference of 14.02 Da was observed, beginning at  $m/z$  372.24, and continuing with  $m/z$  358.23,  $m/z$  344.21, and  $m/z$  330.20. The peak at  $m/z$  372.24 likely corresponded to basic violet 3 (shown in Figure 56, also known as methyl violet 10B). Another series of peaks with the same mass differences was visible, starting at  $m/z$  470.26, and continuing with  $m/z$  456.24, and  $m/z$  442.23. The peak at  $m/z$  470.26 likely corresponded to basic blue B (illustrated in Figure 56, also known as Victoria blue B).

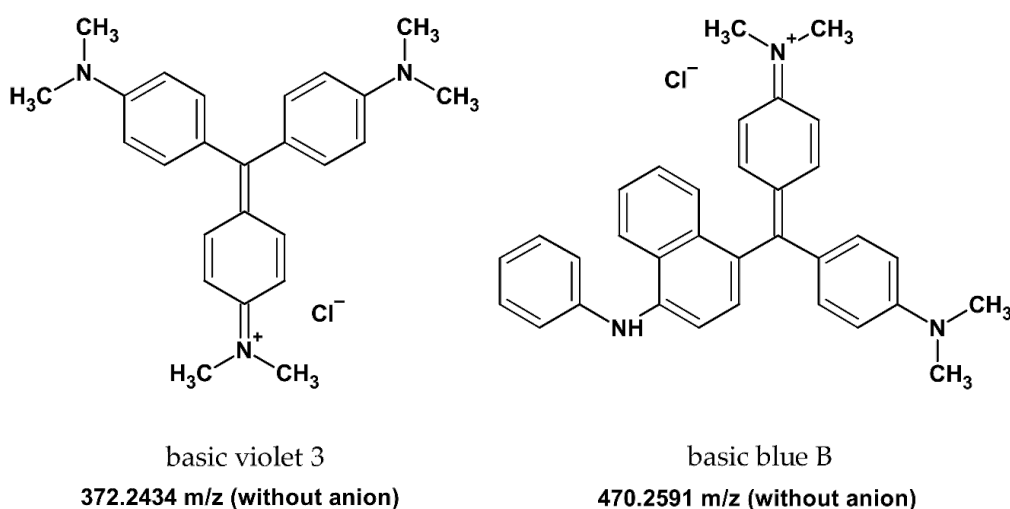


Figure 56 Chemical structure of basic violet 3 (left) and basic blue B (right).

Both inks exhibited a series of peaks with a mass difference of 14.02 Da, which corresponds to a CH<sub>2</sub> moiety. The loss of up to two CH<sub>2</sub> groups in basic blue 3 and the loss of one CH<sub>2</sub> group in basic blue B was attributed to in-source decomposition during LDI of the ink [247]. In contrast to literature findings, the first series of peaks at  $m/z$  358.23,  $m/z$  344.21, and 330.20 were likely attributed to methyl violet 6B, methyl violet 2B, and new Fuchsine, respectively. The second series of peak could not be attributed to any known dyes.

For structural verification, CAD was performed on basic violet 3 (precursor  $m/z$  372.26). The obtained fragment ion spectrum is illustrated in Figure 57 at the bottom. A relatively high normalized collision energy of 45 was applied. Numerous fragment ions were proposed and are illustrated in Figure 58. The loss of a methane at the positively charged amine leads to the formation of a double bond between the remaining CH<sub>2</sub> group and the amine, resulting in an ion with  $m/z$  of 356.21. This ion was observed as the dominant fragment ion. Subsequent fragmentation involves the homolytic abstraction of a N,N-dimethylaniline group, resulting in the formation of a fragment ion with a  $m/z$  of 236.13. The loss of a  $\cdot\text{CH}_3$  group, along with the homolysis of a hydrogen atom from the remaining CH<sub>2</sub> $\cdot$  moiety, leads to the formation of an ion with an  $m/z$  of 357.22. Comparable abstraction mechanisms of alkane moieties from a positively charged amine were observed in the fragmentation of xanthene dyes [248]. The homolytic dissociation of a dimethylamine moiety yields the fragment ion appearing at  $m/z$  328.19, successive cleavage of another dimethylamine moiety produces a product ion of  $m/z$  284.14.

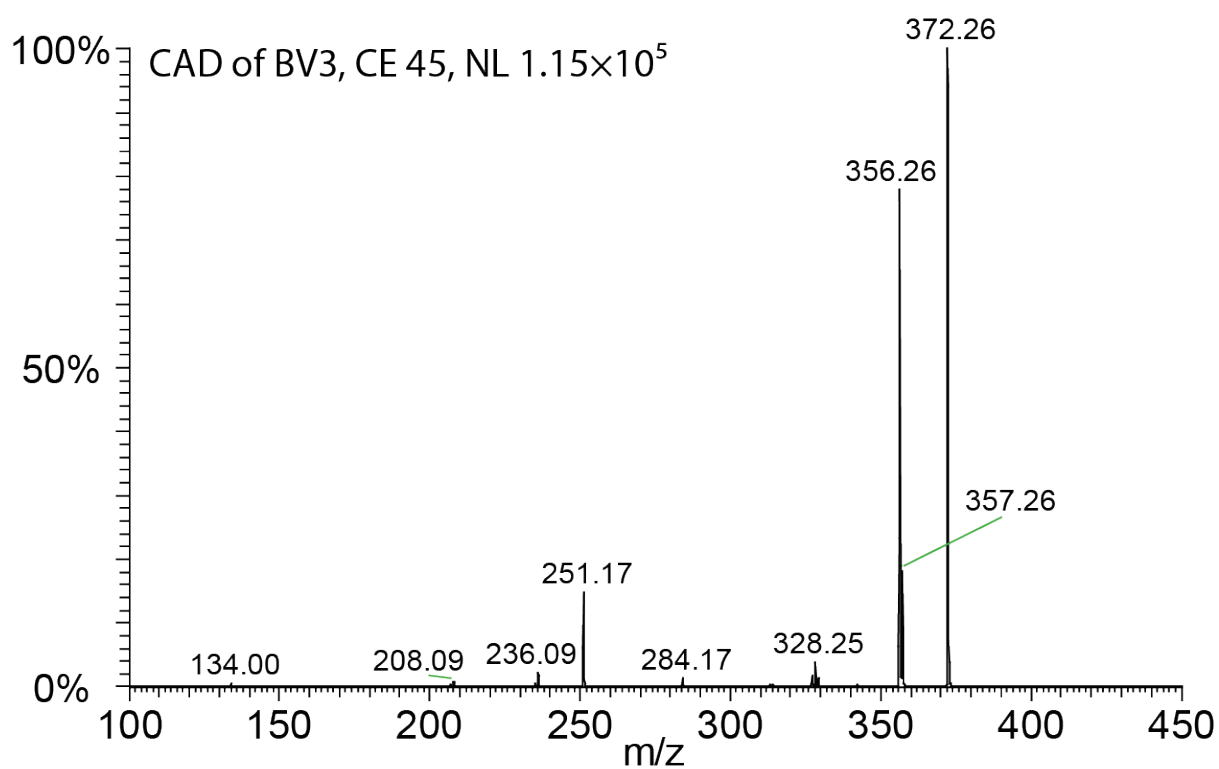
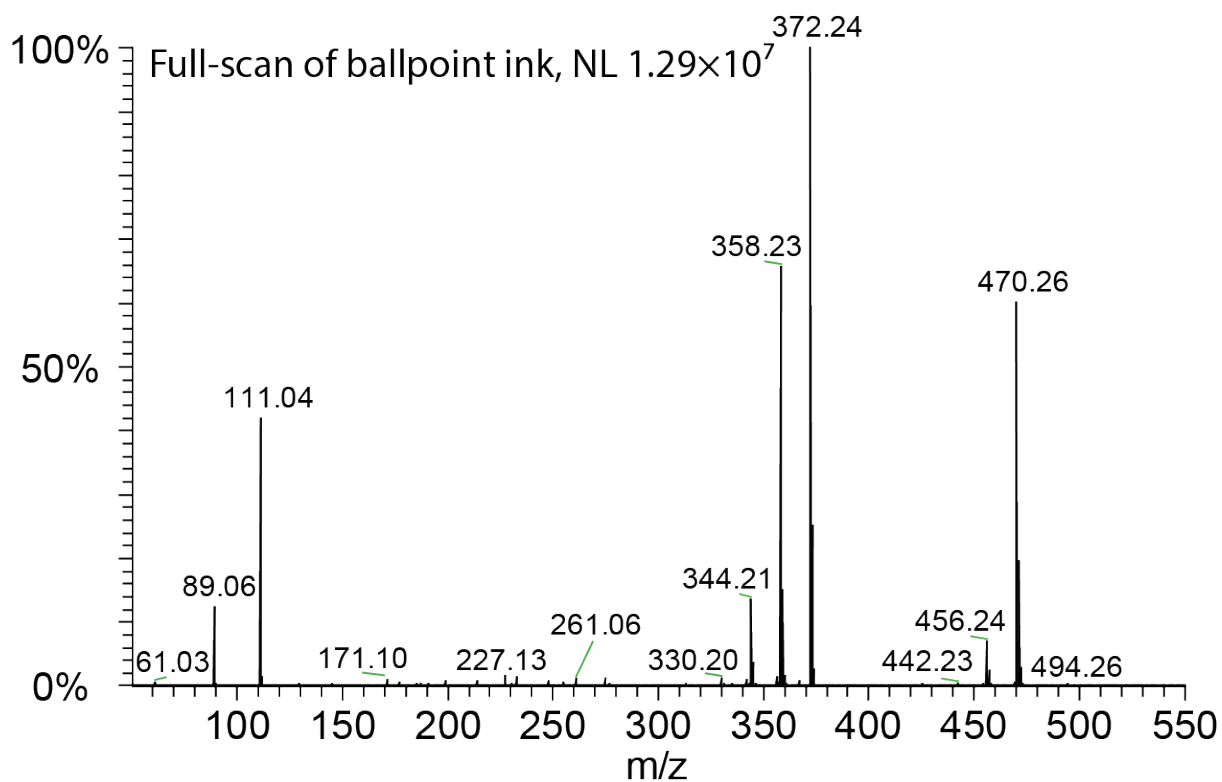


Figure 57 Full-scan spectrum of ballpoint ink (top) and CAD spectrum of basic violet 3 (bottom).

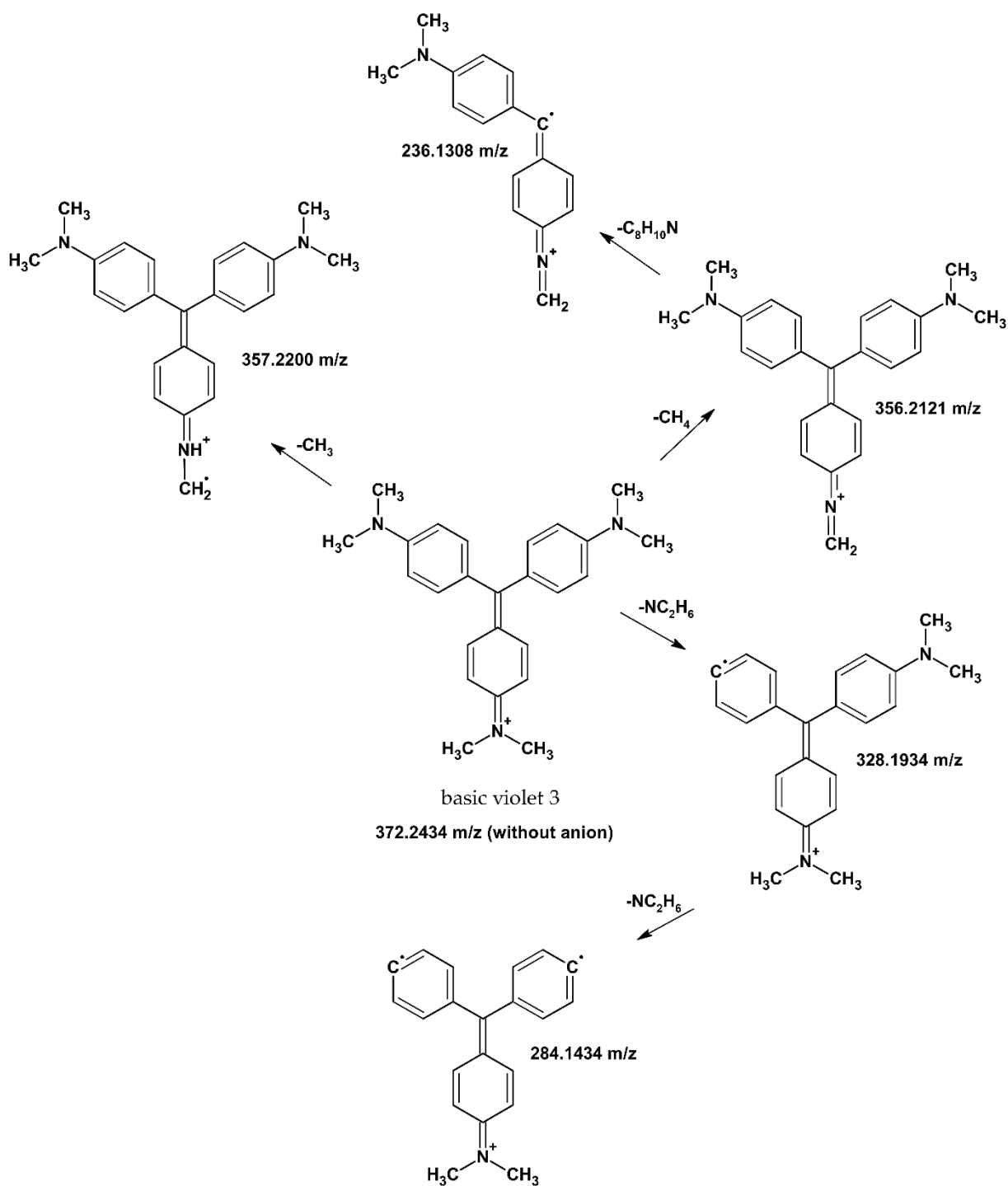


Figure 58 Proposed fragmentation pattern of basic violet 3.

To compare the findings from swab spray analysis with conventional mass spectrometry, the ink was analyzed using reverse phase LC-MS. The extracted ion current of basic violet 3 ( $m/z$  372.24, at 8.87 min), methyl violet 6B ( $m/z$  358.23, at 8.23 min), methyl violet 2b ( $m/z$  344.21, at 7.64 min), new Fuchsine ( $m/z$  330.20, at 7.07 min), and basic blue B ( $m/z$  470.26, at 9.73 min) is illustrated in Figure 59. For each absent  $\text{CH}_2$  group (mass difference of 14.02 Da) an approximate difference in elution time of 0.5 minute was observed.

- A ● XIC Tinte, +TOF MS (50 - 2000): 372.240 +/- 0.025 Da, Gaussian smoothed (2.0 points)  
 B ● XIC Tinte, +TOF MS (50 - 2000): 358.230 +/- 0.025 Da, Gaussian smoothed (2.0 points)  
 C ● XIC Tinte, +TOF MS (50 - 2000): 344.210 +/- 0.025 Da, Gaussian smoothed (2.0 points)  
 D ● XIC Tinte, +TOF MS (50 - 2000): 330.200 +/- 0.025 Da, Gaussian smoothed (2.0 points)  
 E ● XIC Tinte, +TOF MS (50 - 2000): 470.260 +/- 0.025 Da, Gaussian smoothed (2.0 points)  
 F ● XIC Tinte, +TOF MS (50 - 2000): 456.240 +/- 0.025 Da, Gaussian smoothed (2.0 points)  
 G ● XIC Tinte, +TOF MS (50 - 2000): 442.230 +/- 0.025 Da, Gaussian smoothed (2.0 points)

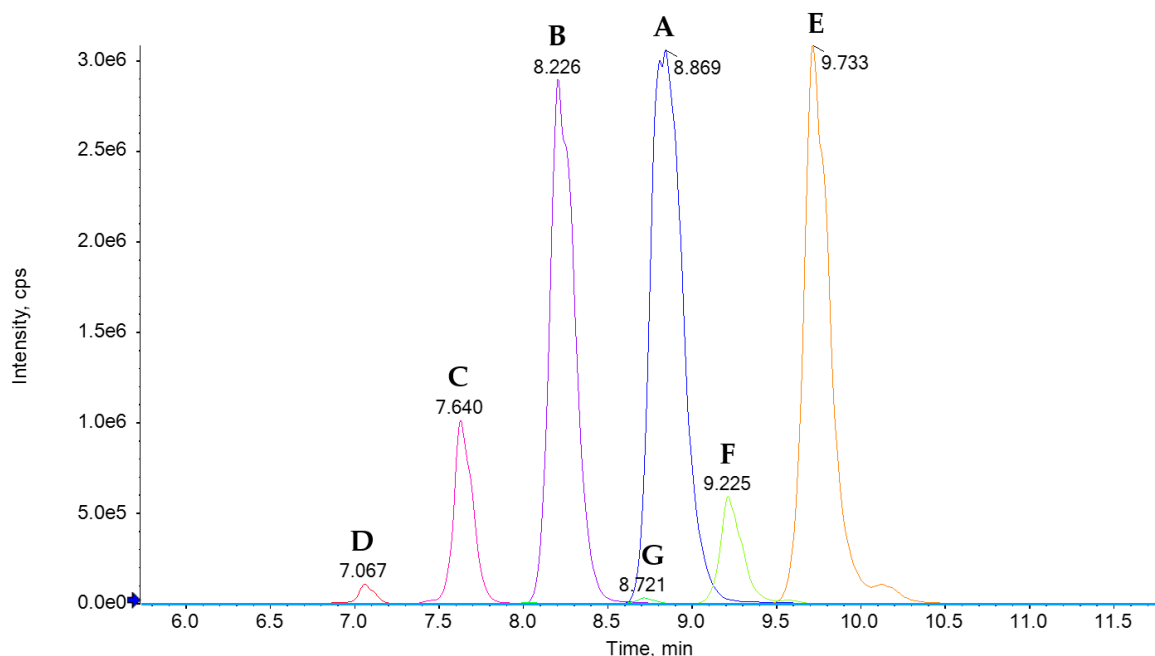


Figure 59 Extracted ion current of basic blue B and basic violet 3, including their series of peaks with a mass difference of 12.04 Da.

The swab spray-based ball point ink analysis worked successfully, enabling the identification of inks by full-scan and CAD. Swab spray mass spectrometry experiments demonstrated that ballpoint ink comprises a mixture of various dyes. However, swab document ink sampling has limited utility in forensic applications due to the degree of document destruction, which ideally should be minimized. Other mass spectrometry-based methods such as LDI or DESI are likely to offer less sample destruction while providing similar capabilities.

### 2.15 Analyte Carryover Effects

In the context of swab spray mass spectrometry, carryover refers to the persistence of a specific analyte signal following the replacement of a swab. In the analysis of pesticides on food products, the carryover of pesticides proved to be non-problematic. However, sample carryover was observed after the disposal of substantial quantities (several hundred micrograms) of reference materials directly onto the swab, especially when numerous repetitive experiments were performed, such as for obtaining the calibration curve of boscalid. To remove carryover signals, the ion sweep cone, ion transfer capillary, and the lower segment of the solvent capillary—those components in direct contact with the swab or the spray plume—were disassembled and cleansed by ultrasonication in methanol for 15 minutes, effectively removing contaminants.

The rather large spray plume generated by the swab spray ion source resulted in sample deposition on the ion sweep cone. It is possible that thermal desorption of analyte molecules, in conjunction with electrospray ionization, contributed to the observed carryover signals. Alternatively, the electrospray plume itself may have facilitated the desorption of deposited molecules through mechanisms like those observed in DESI. The initial hypothesis assumed that the lower segment of the solvent capillary, being in direct contact with the swab, was the primary reason for carryover effects. However, subsequent experimentation, which is described herein, revealed that sample depletion on the ion sweep cone is predominantly accountable for the occurrence of carryover.

An amount of 100 ng of fluorescein, which exhibits thermal stability up to 300°C, was directly deposited to the swab tip, followed by the recording of a full-scan spectrum, as depicted in Figure 60 (top). Compounds that are not stable up to 250 °C may undergo thermal decomposition as the ion transfer capillary temperature was set to 250 °C. The proton adduct of fluorescein was visible at  $m/z$  333.08, occurring as the most abundant peak in the spectrum. A new swab was mounted and a blank background spectrum was recorded, shown in Figure 60 (middle). The peak of fluorescein ( $m/z$  333.08) was no longer as abundant as before. Subsequently, the same swab was used to wipe the outside of the mass spectrometer inlet encompassing the ion sweep cone and front part of the ion transfer capillary. To facilitate sampling, the heated components were dismounted and allowed to cool in the air. Afterwards, a full-scan spectrum was recorded, as presented in Figure 60 (bottom). The proton adduct of fluorescein re-emerged in high intensity at  $m/z$  333.08, providing evidence that sample depletion occurred at the ion sweep cone and inlet.

Inefficient ion transmission from the electrospray plume to the mass spectrometer can result in carryover signals, but also reduces sensitivity. The optimization of ion transmission is a crucial aspect in every ESI source to ensure high ion transmission efficiency [249–251]. In 2005, an attempt was made to enhance ion transmission by compression of the electrospray plume using a hemispherically-shaped electrostatic lens at atmospheric pressure in nanoelectrospray. However, this attempt was unsuccessful, possibly due to an impeded ionization process, as the increased ion density can decrease the desolvation rate [226]. Recently, focusing the electrospray plume by addition of a dielectric layer around the mass spectrometer's inlet demonstrated a moderate signal enhancement [252].

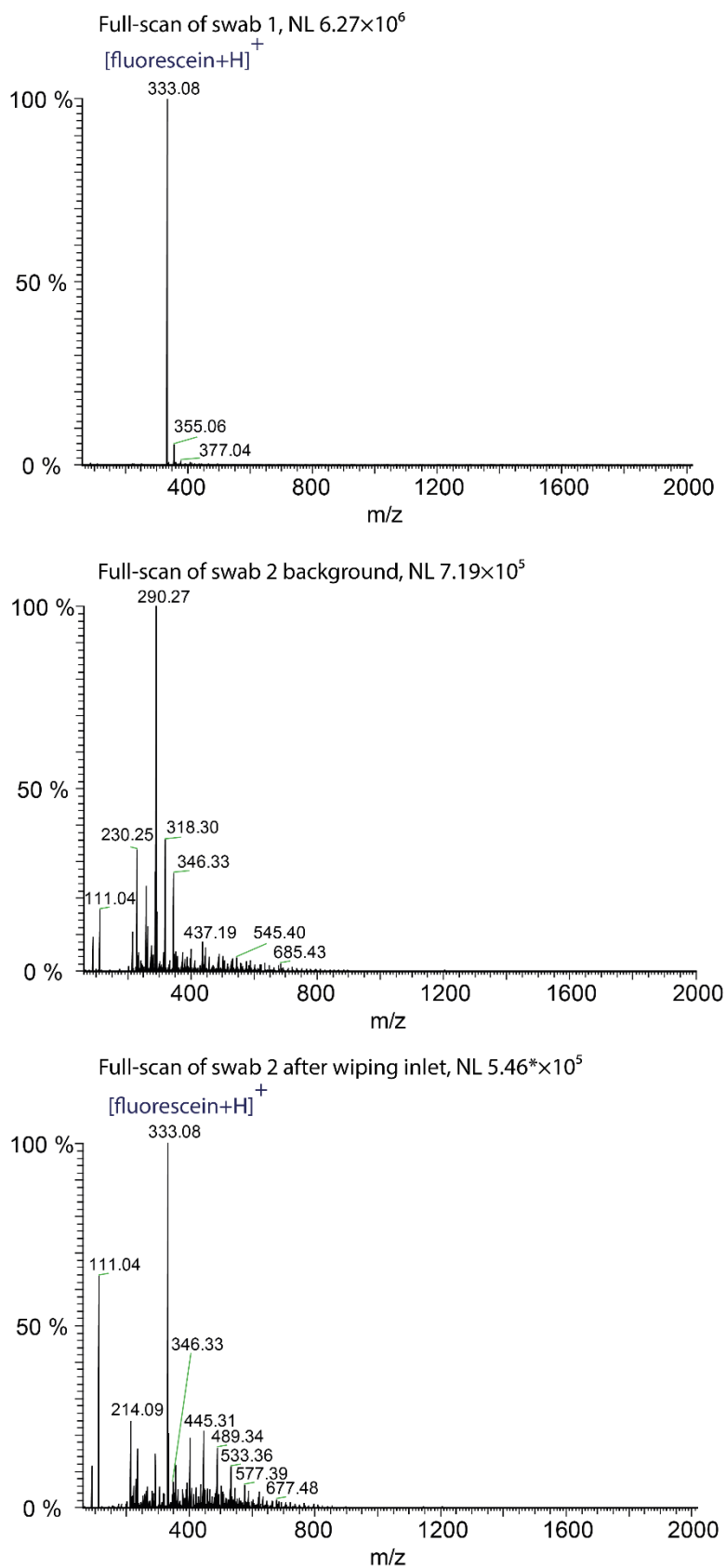


Figure 60 Full-scan spectra obtained after the deposition of fluorescein directly to the swab head (top), after mounting a new swab (middle), and after wiping the ion sweep cone and inlet (bottom).



## 2.16 Analysis of Mycotoxins

Mycotoxins are secondary metabolites produced by fungi, which are not essential for fungal growth or reproduction. They can exert toxic effects on humans and animals through contact, inhalation, and particularly through ingestion. Consequently, analyzing food and feed to prevent toxic effects, including carcinogenicity, cytotoxicity, teratogenicity, immunotoxicity, neurotoxicity, hepatotoxicity, nephrotoxicity, as well as reproductive and developmental toxicity, is of paramount importance [253–259]. Mycotoxins are predominantly produced by fungi belonging to the genera *Aspergillus*, *Fusarium*, and *Penicillium*. The molecular weights of most mycotoxins fall within the range of several hundred Daltons [260]. Currently, the primary methods employed for mycotoxin monitoring are LC-MS, LC-MS/MS, GC-MS, and GC-MS/MS, which involve laborious sample preparation [261–270]. Only a limited number of applications utilized ambient ionization techniques for mycotoxin detection, which included DART and LAESI imaging [271–276].

For the application of swab spray mass spectrometry in mycotoxin detection, the procedure previously utilized for pesticide residue analysis in fruit was employed. To search for mycotoxin precursor ions in the full-scan spectrum, an Excel list was created, incorporating data on 474 mycotoxins [277], including their proton, ammonium, and sodium adducts.

In the initial series of experiments, several molded food samples were analyzed without detection of mycotoxins. This absence could be attributed to either suppression of mycotoxins by matrix effects or their actual absence in the tested samples. Subsequently, in the second phase, three fungal cultures, including *Aspergillus niger* van Tieghem 16888 (Figure 62 (a)), *Aspergillus ochraceus* DSM 824 (Figure 62 (b)), and *Penicillium verrucosum* DSM 12639 (an Ochratoxin positive strain, Figure 62 (c)), were purchased and cultivated on Sabouraud dextrose agar for five days at 25 °C. For analysis, the cultivated fungi were sampled with a gentle swab touch. The analysis of *Aspergillus niger* van Tieghem 16888 revealed an intense peak at  $m/z$  223.18 corresponding to the protonated nigragillin (a secondary metabolite alkaloid), presented in Figure 61. Structural confirmation was achieved through MS<sup>2</sup> experiments, whereas the fragmentation pathway of nigragillin predominately involved the cleavage of the amide bond. Furthermore, desertorin C, lichexanthone, and anhydrofusarubin were detected in low quantities. The precursor ions were identified using full-scan data, and CAD experiments were employed for structural verification. Possibly due to the very dry and brittle texture of *Penicillium verrucosum*

DSM 12639 and *Aspergillus ochraceus* DSM 824, the swab spray analysis did not reveal any mycotoxins. In conclusion, the analysis of mycotoxins via swab spray mass spectrometry poses notable challenges, primarily due to the varying textures that can impede analyte extraction and further by matrix effects.

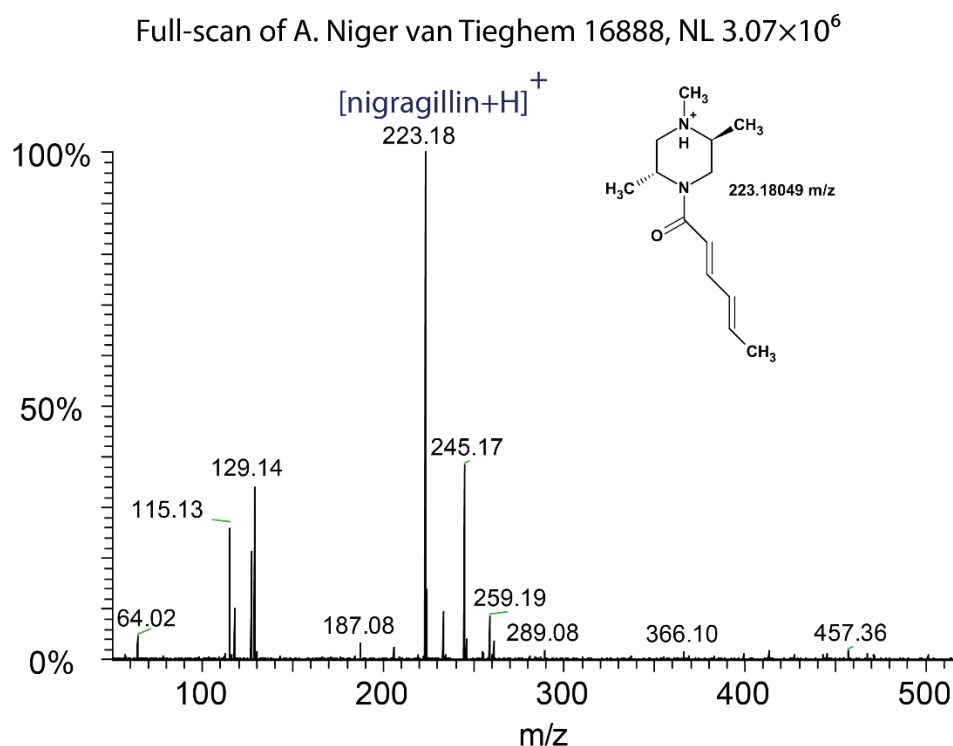


Figure 61 Full-scan spectrum obtained from sampling *Aspergillus niger* van Tieghem 16888 after five days of cultivation.

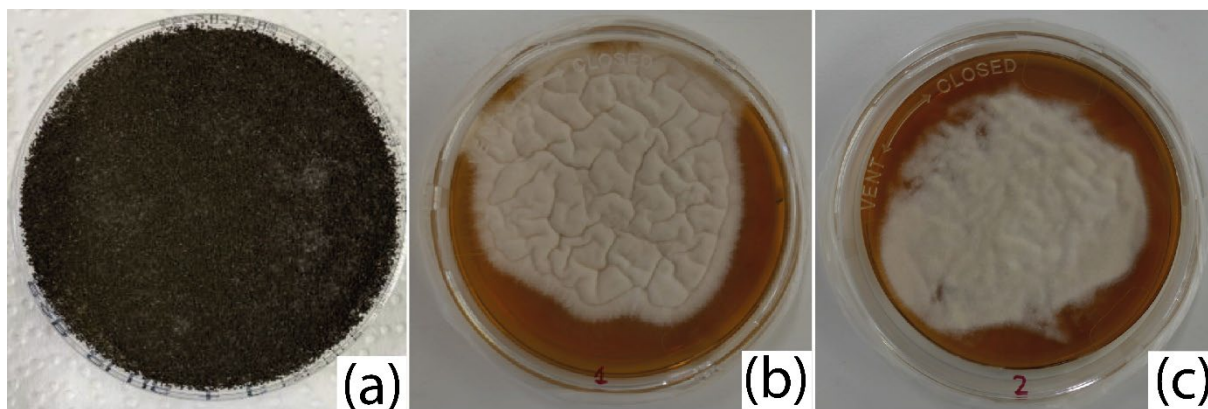


Figure 62 Fungi cultures in Sabouraud dextrose agar after five days of cultivation: *Aspergillus niger* van Tieghem 16888 (a), *Aspergillus ochraceus* DSM 824 (b), and *Penicillium verrucosum* DSM 12639 (c).

## 3 Experimental

### 3.1 Experimental Data

#### 3.1.1 General Settings for Mass Spectrometry and Methods

*Figure 63 A Schematic presentation of the LTQ Orbitrap Velos mass spectrometer can be found in reference [278].*

A schematic presentation of the employed Thermo Fisher Scientific LTQ Orbitrap Velos is given in Figure 63. The S-lens, a radio frequency device, captures and focuses the ions that are generated in the swab spray ion source [279]. The square quadrupole and octopole further help in focusing and transferring the obtained ion beam. The unique dual pressure linear ion trap design enables the decoupling of ion manipulation and detection. The high-pressure cell allows ion increased ion trapping and fragmentation efficiency. While the low-pressure cell increases the mass resolution [280]. Unless otherwise stated, following mass spectrometry settings were applied for experimentation. The mass spectrometer was operated in the positive ionization mode and full-scan spectra were recorded in the range of  $m/z$  50–2000 with a mass resolution of 30,000 ( $m/\Delta m$  @  $m/z$  400). To prevent thermal degradation of labile compounds the ion transfer capillary temperature was kept at 250 °C. The LTQ ion trap was used for tandem mass spectrometric experiments with a precursor selection window of  $m/z$  1,

helium as the collision gas in combination with an ion activation time of 10 ms. For acquisition of MS/MS data, the normalized collision energy was increased stepwise until appropriate fragmentation of the precursor occurred, whereas collision energy values are provided in the related CAD spectrum. The swab was kept at a distance of 7 mm to the ion sweep cone serving as the counter electrode. The solvent capillary was applied on the lower end of the swab head as described in the corresponding section (Section 2.6). The continuous solvent supply of EtOAc/MeOH (70/30, *v/v*) with 0.1% formic acid modifier and 1 ppm of salicylanilide was kept constant at a rate of 45  $\mu\text{L}/\text{min}$ . For instrument control and data acquisition, the Thermo Scientific Xcalibur 2.2 (Thermo Fisher Scientific, Reinach, Switzerland) software was used. Copan 160C swabs, prewashed in EtOAc, were used in all experiments unless otherwise stated. Glass vials in combination with silanized inserts were used for the preparation of stock solutions.

### 3.1.2 Chemicals and Materials

MeOH, EtOAc, ACN, 2-propanol (all Supelco Lichrosolv® hypergrade for LC-MS), and toluene (HPLC grade, 99.9%) were purchased from Merck/Sigma-Aldrich (Buchs, Switzerland). Acetone (HPLC grade, HiPerSolv Chromanorm®) and trichloromethane (Chromasolv™ plus for HPLC, 99.8%, Honeywell Specialty Chemicals (Seelze, Germany)) were purchased from VWR International (Dietikon, Switzerland).

Formic acid (LC-MS grade, LiChropur™), salicylanilide (99%), fluorescein (free acid), octylamine (99%), quinine (anhydrous,  $\geq 98.0\%$ ), boscalid (PESTANAL®, analytical standard), imazalil (PESTANAL®, analytical standard), thiabendazole (PESTANAL®, analytical standard), sodium acetate (anhydrous, ReagentPlus®,  $\geq 99.0\%$ ), ammonium acetate (HPLC grade, LiChropur™), organophosphorus reference mixture solution (2000  $\mu\text{g}/\text{mL}$  in dichloromethane (per compound), including dimethoate, disulfoton, famphur, parathion, parathion-methyl, phorate, sulfotep, thionazin, and triethyl thiophosphate), triazine reference mixture solution (100  $\mu\text{g}/\text{mL}$  in MeOH (per compound), including ametryn, atrazine, prometon, prometryn, propazine, simazine, and terbutryn) were purchased from Merck/Sigma-Aldrich (Buchs, Switzerland).

Glass vials and silanized inserts were purchased from BGB Analytik AG (Böckten, Switzerland). Sabouraud-Dextrose-Agar plates with vents were purchased from Merck/Sigma-Aldrich (Buchs, Switzerland).

### 3.1.3 Analyte Extraction

A solution with 1 mg/mL fluorescein (free acid) was prepared in MeOH. 4  $\mu$ L of the solution was used for visualization of the extraction. To enhance visualization, a 365 nm UV light source was placed on top of the ion source housing.

Stock solutions of octylamine, quinine, and thiabendazole were prepared in a concentration of 1 mg/mL using MeOH. 10  $\mu$ L of the stock solutions were diluted and mixed together to obtain a solution with a concentration of 0.025 mg/mL per compound. 4  $\mu$ L of the solution was directly applied to the swab. The tested solvent combinations included MeOH/H<sub>2</sub>O (90/10, *v/v*), EtOAc, MeOH (70/30, *v/v*), and ACN, all solvents included 0.1% formic acid as modifier and 1 ppm of salicylanilide as suppression marker. The solvent was supplied at a flow rate of 45  $\mu$ L/min.

### 3.1.4 Adduct Formation

To investigate sodium adduct formation, 4  $\mu$ L of a MeOH solution that contained thiabendazole, imazalil, and boscalid reference material, each at a concentration of 0.025 mg/mL, was applied to the swab head. Either 10  $\mu$ L of a 0.1 M sodium acetate solution or 0.1 M ammonium acetate solution in MeOH was added directly to the swab head. The solvent combination EtOAc/MeOH (70/30, *v/v*) and MeOH, both with 0.1% formic acid modifier, and 1 ppm of suppression marker (salicylanilide), were chosen.

### 3.1.5 Triazine Mixture

10  $\mu$ L of the triazine reference mixture solution (100  $\mu$ g/mL in MeOH) were diluted with MeOH to obtain a concentration of 25 ng/ $\mu$ L per compound. 4  $\mu$ L of the solution were directly applied to the swab head by pipette, which yields a mass of 100 ng per triazine compound. EtOAc/MeOH (70/30, *v/v*) with 0.1% formic acid was used as spray solvent for both Copan 160C and IT38040 polyester swabs.

### 3.1.6 Organophosphorus Mixture

10  $\mu$ L of the organophosphorus reference mixture solution (2000  $\mu$ g/mL in dichloromethane), were diluted with MeOH to a concentration of 25 ng/ $\mu$ L per compound. 4  $\mu$ L of the solution were directly applied to the swab head by pipette, which yields a mass of 100 ng per compound. Tested spray solvents included chloroform/MeOH (80/20, *v/v*), EtOAc/MeOH (70/30, *v/v*), acetone, ACN, MeOH, were tested in combination with Copan 160C and IT38040 polyester swabs.

### 3.1.7 Residual Pesticide Analysis of Strawberry

Approximately 1 gram of a strawberry (harvested in Switzerland and purchased from a local supermarket) was homogenized with a mortar and pestle and diluted with 10 mL of MeOH/H<sub>2</sub>O (50/50, *v/v*). The solution was ultrasonicated for one hour at 45 °C. 1 mL of the solution was transferred into an Eppendorf tube and centrifuged at 12100 g for 1 minute. The supernatant was filtrated using Millex®-LH (Merck, Buchs, Switzerland) syringe driven filters (pore size 0.45 µm and 4 mm diameter) and transferred into a glass vial and put in the autosampler rack.

The liquid chromatography was based on a luna omega polar reverse phase C18 from Phenomenex (Phenomenex Inc., Torrance, United States) with a dimension of 2.1 x 100 mm and a particle size of 2.1 µm. The autosampler injection volume was set to 5 µL. The liquid chromatography was based on a gradient starting at 10% acetonitrile/90% water running to 90% acetonitrile/10% water in 15 minutes at a flow rate of 0.3 mL/min. Both eluents included 0.1% formic acid as modifier. The column temperature was kept at 40 °C. Ion source settings on the Sciex X500B (AB Sciex, Baden, Switzerland) included ion source gas 1+2 50 psi, curtain gas 35 psi, ion source gas temperature 400 °C, electric potential +5.5 kV. For data acquisition, the IDA mode for small molecules was employed, including a declustering potential of 80 V, a collision energy of 35 V in combination with a collision energy spread of 10 V, and a TOF acquisition range of 50-2000 Da.

### 3.1.8 Simulated Forensic Applications

All experiments included continuous solvent supply at a flow rate of 45 µL/min. The spray solvent consisted of EtOAc/MeOH (70/30, *v/v*), including 0.1% formic acid modifier and 1 ppm of salicylanilide.

For LC-MS analysis of ballpoint ink, an IT38040 polyester swab (Ideal-Tek, Balerna, Switzerland) was colored and held for one minute in a glass vial containing 100 µL MeOH to dissolve the ink. Afterwards, 2 µL of the solution were injected by the autosampler for LC-MS analysis. The similar LC-MS method as priorly used for the analysis of pesticide residues in strawberries was applied.

### 3.1.9 Sample Carryover Effects

A stock solution with 0.1 mg/mL fluorescein (free acid) was prepared in MeOH. The solution was diluted by a factor of four, yielding a solution with a concentration of

0.025 mg/mL. Then, 4 µL of the solution was directly applied to the swab tip using a pipette.

### **3.1.10 Analysis of Mycotoxins**

Fungi culture *aspergillus niger* van Tieghem 16888 was purchased from American Type Culture Collection (ATCC) (Manassas, Virginia, United States). *Aspergillus ochraceus* DSM 824 and *Penicillium verrucosum* DSM 12639 were purchased from the Leibniz Institute DSMZ (Braunschweig, Germany). To rehydrate the freeze-dried pellets, a liquid medium containing 3% malt extract and 0.3% soya peptone in distilled water was used for a period of 30 minutes. Afterwards, fungi cultures were incubated on Sabouraud-Dextrose-Agar plates. The vent position was set to open for aerobic growing conditions. The plates were stored at 25 °C.





## 4 Conclusions

The advent of ambient ionization techniques presents new opportunities alongside with new challenges. Ambient ionization techniques can significantly reduce analysis time in combination with facilitated sample preparation and further enable in-situ mass spectrometry. Over the past two decades, the number of ambient ionization techniques and their fields of application have rapidly expanded. Swab spray mass spectrometry, a more recent development, merges sample collection and direct ion generation to facilitate the analysis of manifold surfaces for organic compound residues. The swab spray ion source and swab materials, including spray solvents, have to be evaluated carefully to achieve high spray stability and minimize background interference.

This work demonstrates the importance of the solvent's relative permittivity as a key parameter influencing the formation of electrospray in swab spray ionization. Results revealed that the generation of a short jet at the tip of the Taylor cone is essential to achieve high ion yield. It was observed that solvents with a high relative permittivity result in a short jet and solvents with intermediate relative permittivity exhibit a long jet, which is detrimental to the generation of abundant ion signal. Additionally, a dripping pulsation mode, which fails to generate ions, was observed for solvents with very low relative permittivity. However, experiments demonstrated, that the relative permittivity of solvent combinations can be enhanced by the addition of methanol, resulting in a short jet with increased ion yield.

The evaluation of swab materials indicated that prewashed rayon swabs exhibited superior spray stability, reproducibility, and background level if combined with the appropriate spray solvent. Additionally, the aluminum handle of the selected swabs enables easy application of the electric potential. To maintain high reproducibility, it is essential to precisely control ion source parameters such as flow rate, electric potential, solvent capillary position, and distance to the counter electrode. Furthermore, it was found that reproducibility is influenced by both, variations in swab geometry and swab background originating from swab head material.

The optimized swab spray set-up was successfully applied to the qualitative and semi-quantitative analysis of pesticide residues on fruit. Various pesticides on fruit were

identified based on their mass, isotopic pattern, and fragmentation pattern obtained by CAD. Matching MS<sup>2</sup> spectra with libraries simplified identification. Nevertheless, elucidating fragmentation mechanisms is often necessary for comprehensive analysis, as fragment ion spectra are influenced by the instrumentation used. Sampling on fruit and leaves with heterogenous textures presented no significant challenge for sample uptake when prewetted swabs were used. While qualitative acquisition has not been affected by fruit matrix effects, they can influence the accuracy of quantitative results. To minimize sodium adduct formation in favor of the proton adducts, the use of an ethyl acetate/methanol solvent composition, including 0.1% formic acid, as the spray solvent, has been proven beneficial, allowing to focus on the proton adducts only for quantitative analysis. Moreover, the efficacy of analyzing compound residues on skin and personal items was successfully corroborated.

Conclusively, the presented swab spray mass spectrometry ion source enabled quick and accurate detection of organic compound residues on surfaces without the need for sample preparation. The findings obtained contribute to the advancement of electrospray-based ambient ionization techniques in future developments.

## 5 Outlook

Undoubtedly, swab spray mass spectrometry has demonstrated considerable advantages over conventional laboratory-based methods for the analysis of surfaces. The straightforward sampling and the omitted requirement for laborious sample preparation result in a considerable reduction of the overall analysis time. The availability of swabs, which offer a clean background and a high electrospray reproducibility, achieved through minimal manufacturing variations, would be extremely beneficial. Further instrumental optimization, such as the evaluation of introducing heater gas into the swab spray ion source to enhance ionization efficiency could increase ion yield. In addition, constructing an automated swab mounting system could drastically improve sample throughput and enhance user-friendliness. Moreover, employing a state-of-the-art mass spectrometer with IDA and DIA acquisition modes, along with automated data analysis, would significantly improve sensitivity, speed, and streamline data processing.

Beside electrospray ionization, dielectric barrier discharge plasma ionization provides a promising avenue in ambient ionization techniques. This ionization method exhibits a high ionization efficiency and ion transfer rate. If combined with thermal desorption or solvent-assisted thermal desorption of analytes from swabs, a highly sensitive and robust swab ion source may result. The incorporation of a CeraPlas<sup>TM</sup> element, which can generate a cold plasma from a single component, might facilitate cold plasma ion source construction.

The miniaturization of mass spectrometers will promote in-situ analysis, enabling the full utilization of swab-based and other ambient ionization techniques across numerous fields of application. Implementing rapid food screening for pesticides at cargo hubs would result in a significant enhancement of food safety. Improved passenger screening at airports can help reduce drug trafficking and increase safety. Homeland security can benefit from real-time detection, enabling the prevention and response to potential chemical and biological threats. Furthermore, applications in medicine, such as point-of-care diagnostics increase the speed of diagnosis, allowing for faster treatment and improved patient outcomes. This includes skin sampling for metabolites, which can aid in identifying various diseases.



## 6 References

1. Watson, J.T.; Sparkman, O.D. *Introduction to Mass Spectrometry*; Wiley, 2007; ISBN 9780470516348.
2. Edmond de Hoffmann, V.S. *Mass Spectrometry: Principles and Applications*; 3rd Edition.; Wiley, 2007;
3. Li, L.; Yang, S.H.; Lemr, K.; Havlicek, V.; Schug, K.A. Continuous Flow-Extractive Desorption Electrospray Ionization: Analysis from “Non-Electrospray Ionization-Friendly” Solvents and Related Mechanism. *Analytica Chimica Acta* **2013**, 769, 84–90, doi:10.1016/j.aca.2013.01.018.
4. Joyce, J.R.; Richards, D.S. Kinetic Control of Protonation in Electrospray Ionization. *Journal of the American Society for Mass Spectrometry* **2011**, 22, 360–368, doi:10.1007/s13361-010-0037-0.
5. Hiraoka, K.; Ariyada, O.; Usmanov, D.T.; Chen, L.C.; Ninomiya, S.; Yoshimura, K.; Takeda, S.; Yu, Z.; Mandal, M.K.; Wada, H.; et al. Probe Electrospray Ionization (PESI) and Its Modified Versions: Dipping PESI (DPESI), Sheath-Flow PESI (SfPESI) and Adjustable SfPESI (Ad-SfPESI). *Mass Spectrometry* **2020**, 9, A0092–A0092, doi:10.5702/massspectrometry.A0092.
6. Banerjee, S.; Mazumdar, S. Electrospray Ionization Mass Spectrometry: A Technique to Access the Information beyond the Molecular Weight of the Analyte. *International Journal of Analytical Chemistry* **2012**, 2012, 1–40, doi:10.1155/2012/282574.
7. Kebarle, P. A Brief Overview of the Present Status of the Mechanisms Involved in Electrospray Mass Spectrometry. *Journal of Mass Spectrometry* **2000**, 35, 804–817, doi:https://doi.org/10.1002/1096-9888(200007)35:7<804::AID-JMS22>3.0.CO;2-Q.
8. Wilm, M. Principles of Electrospray Ionization. *Molecular & Cellular Proteomics* **2011**, 10, M111.009407, doi:10.1074/mcp.M111.009407.
9. Van Berkel, G.J.; Kertesz, V. Using the Electrochemistry of the Electrospray Ion Source. *Analytical Chemistry* **2007**, 79, 5510–5520, doi:10.1021/ac071944a.

10. Boys, B.L.; Kuprowski, M.C.; Noël, J.J.; Konermann, L. Protein Oxidative Modifications During Electrospray Ionization: Solution Phase Electrochemistry or Corona Discharge-Induced Radical Attack? *Analytical Chemistry* **2009**, *81*, 4027–4034, doi:10.1021/ac900243p.
11. Pei, J.; Hsu, C.-C.; Zhang, R.; Wang, Y.; Yu, K.; Huang, G. Unexpected Reduction of Iminoquinone and Quinone Derivatives in Positive Electrospray Ionization Mass Spectrometry and Possible Mechanism Exploration. *Journal of the American Society for Mass Spectrometry* **2017**, *28*, 2454–2461, doi:10.1007/s13361-017-1770-4.
12. Benassi, M.; Wu, C.; Nefliu, M.; Ifa, D.R.; Volný, M.; Cooks, R.G. Redox Transformations in Desorption Electrospray Ionization. *International Journal of Mass Spectrometry* **2009**, *280*, 235–240, doi:10.1016/j.ijms.2008.10.012.
13. Geoffrey Ingram Taylor Disintegration of Water Drops in an Electric Field. *Proceedings of the Royal Society of London* **1964**, *280*, 383–397, doi:10.1098/rspa.1964.0151.
14. Morad, M.R.; Rajabi, A.; Razavi, M.; Sereshkeh, S.R.P. A Very Stable High Throughput Taylor Cone-Jet in Electrohydrodynamics. *Scientific Reports* **2016**, *6*, 38509, doi:10.1038/srep38509.
15. Ismail, A.S.; Yao, J.; Xia, H.H.; Stark, J.P.W. Breakup Length of Electrified Liquid Jets: Scaling Laws and Applications. *Phys. Rev. Appl.* **2018**, *10*, 064010, doi:10.1103/PhysRevApplied.10.064010.
16. Cloupeau, M.; Prunet-Foch, B. Electrohydrodynamic Spraying Functioning Modes: A Critical Review. *Journal of Aerosol Science* **1994**, *25*, 1021–1036, doi:https://doi.org/10.1016/0021-8502(94)90199-6.
17. El-Faramawy, A.; Siu, K.W.M.; Thomson, B.A. Efficiency of Nano-Electrospray Ionization. *Journal of the American Society for Mass Spectrometry* **2005**, *16*, 1702–1707, doi:10.1016/j.jasms.2005.06.011.
18. Tang, K.; Smith, R.D. Theoretical Prediction of Charged Droplet Evaporation and Fission in Electrospray Ionization. *International Journal of Mass Spectrometry* **1999**, *185–187*, 97–105, doi:10.1016/S1387-3806(98)14107-6.
19. Kebarle, P.; Verkerk, U.H. On the Mechanism of Electrospray Ionization Mass Spectrometry (ESIMS). In *Electrospray and MALDI Mass Spectrometry*; 2010; pp. 1–48 ISBN 9780470588901.
20. Tang, K.; Gomez, A. On the Structure of an Electrostatic Spray of Monodisperse Droplets. *Physics of Fluids* **1994**, *6*, 2317–2332, doi:10.1063/1.868182.

21. Wortmann, A.; Kistler-Momotova, A.; Zenobi, R.; Heine, M.C.; Wilhelm, O.; Pratsinis, S.E. Shrinking Droplets in Electrospray Ionization and Their Influence on Chemical Equilibria. *Journal of the American Society for Mass Spectrometry* **2007**, *18*, 385–393, doi:10.1016/j.jasms.2006.10.010.
22. Kebarle, P.; Verkerk, U.H. Electrospray: From Ions in Solution to Ions in the Gas Phase, What We Know Now. *Mass Spectrometry Reviews*, **2009**, *28*, 898–917, doi:10.1002/mas.20247.
23. Teunissen, S.F.; Eberlin, M.N. Transferring Ions from Solution to the Gas Phase: The Two Basic Principles. *Journal of the American Society for Mass Spectrometry* **2017**, *28*, 2255–2261, doi:10.1007/s13361-017-1779-8.
24. Fernández de la Mora, J. The Fluid Dynamics of Taylor Cones. *Annual Review of Fluid Mechanics* **2006**, *39*, 217–243, doi:10.1146/annurev.fluid.39.050905.110159.
25. Kim, H.-H.; Kim, J.-H.; Ogata, A. Time-Resolved High-Speed Camera Observation of Electrospray. *Journal of Aerosol Science* **2011**, *42*, 249–263, doi:10.1016/j.jaerosci.2011.01.007.
26. Nemes, P.; Marginean, I.; Vertes, A. Spraying Mode Effect on Droplet Formation and Ion Chemistry in Electrosprays. *Analytical Chemistry* **2007**, *79*, 3105–3116, doi:10.1021/ac062382i.
27. Jaworek, A.; Krupa, A. Generation and Characteristics of the Precession Mode of Ehd Spraying. *Journal of Aerosol Science* **1996**, *27*, 75–82, doi:https://doi.org/10.1016/0021-8502(95)00528-5.
28. Pongráč, B.; Kim, H.-H.; Negishi, N.; Machala, Z. Influence of Water Conductivity on Particular Electrospray Modes with Dc Corona Discharge — Optical Visualization Approach. *The European Physical Journal D* **2014**, *68*, 224, doi:10.1140/epjd/e2014-50052-4.
29. Castillo-Orozco, E.; Kar, A.; Kumar, R. Electrospray Mode Transition of Microdroplets with Semiconductor Nanoparticle Suspension. *Scientific Reports* **2017**, *7*, 5144, doi:10.1038/s41598-017-05175-6.
30. Budhwani, K.I.; Pekmezi, G.M.; Selim, M.M. Measuring Surface and Interfacial Tension In Situ in Microdripping Mode for Electrohydrodynamic Applications. *Micromachines (Basel)* **2020**, *11*, 687, doi:10.3390/mi11070687.
31. Maheshwari, S.; Chetwani, N.; Chang, H.-C. Alternating Current Electrospraying. *Industrial & Engineering Chemistry Research* **2009**, *48*, 9358–9368, doi:10.1021/ie801841r.

32. Jaworek, A.; Sobczyk, A.T. Electrospraying Route to Nanotechnology: An Overview. *Journal of Electrostatics* **2008**, *66*, 197–219, doi:10.1016/j.elstat.2007.10.001.
33. John Rumble *CRC Handbook of Chemistry and Physics 104th Edition*; 104th ed.; CRC Press : Boca Raton, 2023;
34. Konermann, L.; McAllister, R.G.; Metwally, H. Molecular Dynamics Simulations of the Electrospray Process: Formation of NaCl Clusters via the Charged Residue Mechanism. *The Journal of Physical Chemistry B* **2014**, *118*, 12025–12033, doi:10.1021/jp507635y.
35. Aliyari, E.; Konermann, L. Formation of Gaseous Peptide Ions from Electrospray Droplets: Competition between the Ion Evaporation Mechanism and Charged Residue Mechanism. *Analytical Chemistry* **2022**, *94*, 7713–7721, doi:10.1021/acs.analchem.2c01355.
36. Nguyen, S.; Fenn, J.B. Gas-Phase Ions of Solute Species from Charged Droplets of Solutions. *Proceedings of the National Academy of Sciences* **2007**, *104*, 1111–1117, doi:10.1073/pnas.0609969104.
37. Metwally, H.; McAllister, R.G.; Popa, V.; Konermann, L. Mechanism of Protein Supercharging by Sulfolane and *m*-Nitrobenzyl Alcohol: Molecular Dynamics Simulations of the Electrospray Process. *Analytical Chemistry* **2016**, *88*, 5345–5354, doi:10.1021/acs.analchem.6b00650.
38. Calixte, E.I.; Liyanage, O.T.; Kim, H.J.; Ziperman, E.D.; Pearson, A.J.; Gallagher, E.S. Release of Carbohydrate–Metal Adducts from Electrospray Droplets: Insight into Glycan Ionization by Electrospray. *The Journal of Physical Chemistry B* **2020**, *124*, 479–486, doi:10.1021/acs.jpcc.9b10369.
39. Duez, Q.; Metwally, H.; Konermann, L. Electrospray Ionization of Polypropylene Glycol: Rayleigh-Charged Droplets, Competing Pathways, and Charge State-Dependent Conformations. *Analytical Chemistry* **2018**, *90*, 9912–9920, doi:10.1021/acs.analchem.8b02115.
40. Aliyari, E.; Konermann, L. Atomistic Insights into the Formation of Nonspecific Protein Complexes during Electrospray Ionization. *Analytical Chemistry* **2021**, *93*, 12748–12757, doi:10.1021/acs.analchem.1c02836.
41. Metwally, H.; Duez, Q.; Konermann, L. Chain Ejection Model for Electrospray Ionization of Unfolded Proteins: Evidence from Atomistic Simulations and Ion Mobility Spectrometry. *Analytical Chemistry* **2018**, *90*, 10069–10077, doi:10.1021/acs.analchem.8b02926.



- 
42. Sutton, J.M.; Guimaraes, G.J.; Annavarapu, V.; van Dongen, W.D.; Bartlett, M.G. Current State of Oligonucleotide Characterization Using Liquid Chromatography–Mass Spectrometry: Insight into Critical Issues. *Journal of the American Society for Mass Spectrometry* **2020**, *31*, 1775–1782, doi:10.1021/jasms.0c00179.
43. Aliyari, E.; Konermann, L. Formation of Gaseous Proteins via the Ion Evaporation Model (IEM) in Electrospray Mass Spectrometry. *Analytical Chemistry* **2020**, *92*, 10807–10814, doi:10.1021/acs.analchem.0c02290.
44. Iribarne, J. V.; Thomson, B.A. On the Evaporation of Small Ions from Charged Droplets. *Journal of Chemical Physics* **1976**, *64*, 2287–2294, doi:10.1063/1.432536.
45. Konermann, L.; Ahadi, E.; Rodriguez, A.D.; Vahidi, S. Unraveling the Mechanism of Electrospray Ionization. *Analytical Chemistry* **2013**, *85*, 2–9, doi:10.1021/ac302789c.
46. Nguyen, S.; Fenn, J.B. Gas-Phase Ions of Solute Species from Charged Droplets of Solutions. *Proceedings of the National Academy of Sciences* **2007**, *104*, 1111–1117, doi:10.1073/pnas.0609969104.
47. Iavarone, A.T.; Williams, E.R. Mechanism of Charging and Supercharging Molecules in Electrospray Ionization. *Journal of the American Chemical Society* **2003**, *125*, 2319–2327, doi:10.1021/ja021202t.
48. Metwally, H.; Duez, Q.; Konermann, L. Chain Ejection Model for Electrospray Ionization of Unfolded Proteins: Evidence from Atomistic Simulations and Ion Mobility Spectrometry. *Analytical Chemistry* **2018**, *90*, 10069–10077, doi:10.1021/acs.analchem.8b02926.
49. Pimlott, D.J.D.; Konermann, L. Using Covalent Modifications to Distinguish Protein Electrospray Mechanisms: Charged Residue Model (CRM) vs. Chain Ejection Model (CEM). *International Journal of Mass Spectrometry* **2021**, *469*, 116678, doi:10.1016/j.ijms.2021.116678.
50. Oss, M.; Tshepelevitsh, S.; Krueve, A.; Liigand, P.; Liigand, J.; Rebane, R.; Selberg, S.; Ets, K.; Herodes, K.; Leito, I. Quantitative Electrospray Ionization Efficiency Scale: 10 Years After. *Rapid Communications in Mass Spectrometry* **2021**, *35*, doi:10.1002/rcm.9178.
51. Leito, I.; Herodes, K.; Huopolahti, M.; Virro, K.; Künnapas, A.; Krueve, A.; Tanner, R. Towards the Electrospray Ionization Mass Spectrometry Ionization Efficiency Scale of Organic Compounds. *Rapid Communications in Mass Spectrometry* **2008**, *22*, 379–384, doi:10.1002/rcm.3371.
-

52. Kiontke, A.; Oliveira-Birkmeier, A.; Opitz, A.; Birkemeyer, C. Electrospray Ionization Efficiency Is Dependent on Different Molecular Descriptors with Respect to Solvent PH and Instrumental Configuration. *PLoS One* **2016**, *11*, e0167502, doi:10.1371/journal.pone.0167502.
53. Liigand, J.; Laaniste, A.; Kruve, A. PH Effects on Electrospray Ionization Efficiency. *Journal of the American Society for Mass Spectrometry* **2017**, *28*, 461–469, doi:10.1007/s13361-016-1563-1.
54. Kruve, A.; Kaupmees, K.; Liigand, J.; Leito, I. Negative Electrospray Ionization via Deprotonation: Predicting the Ionization Efficiency. *Analytical Chemistry* **2014**, *86*, 4822–4830, doi:10.1021/ac404066v.
55. Liigand, P.; Kaupmees, K.; Haav, K.; Liigand, J.; Leito, I.; Girod, M.; Antoine, R.; Kruve, A. Think Negative: Finding the Best Electrospray Ionization/MS Mode for Your Analyte. *Analytical Chemistry* **2017**, *89*, 5665–5668, doi:10.1021/acs.analchem.7b00096.
56. Kageyama (Kaneshima), A.; Motoyama, A.; Takayama, M. Influence of Solvent Composition and Surface Tension on the Signal Intensity of Amino Acids in Electrospray Ionization Mass Spectrometry. *Mass Spectrometry* **2019**, *8*, A0077–A0077, doi:10.5702/massspectrometry.A0077.
57. Rebane, R.; Kruve, A.; Liigand, J.; Liigand, P.; Gornischeff, A.; Leito, I. Ionization Efficiency Ladders as Tools for Choosing Ionization Mode and Solvent in Liquid Chromatography/Mass Spectrometry. *Rapid Communications in Mass Spectrometry* **2019**, *33*, 1834–1843, doi:10.1002/rcm.8545.
58. Paiga, P.; Silva, L.M.S.; Delerue-Matos, C. Optimization of the Ion Source-Mass Spectrometry Parameters in Non-Steroidal Anti-Inflammatory and Analgesic Pharmaceuticals Analysis by a Design of Experiments Approach. *Journal of the American Society for Mass Spectrometry* **2016**, *27*, 1703–1714, doi:10.1007/s13361-016-1459-0.
59. Muggli, T.; Bühr, C.; Schürch, S. Challenges in the Analysis of Gangliosides by LC-MS. *Chimia (Aarau)* **2022**, *76*, 109, doi:10.2533/chimia.2022.109.
60. Chan, W.-H.; Yau, L.-F.; Meng, X.-Y.; Chan, K.-M.; Jiang, Z.-H.; Wang, J.-R. Robust Quantitation of Gangliosides and Sulfatides in Human Brain Using UHPLC-MRM-MS: Method Development and Application in Alzheimer's Disease. *Talanta* **2023**, *256*, 124264, doi:10.1016/j.talanta.2023.124264.
61. Xie, J.; Guo, Y.; Ma, Y.; Jiang, H.; Zhang, L.; Mao, L.; Zhu, L.; Zheng, Y.; Liu, X. Spontaneous In-Source Fragmentation Reaction Mechanism and Highly

- Sensitive Analysis of Dicofol by Electrospray Ionization Mass Spectrometry. *Molecules* **2023**, *28*, 3765, doi:10.3390/molecules28093765.
62. El-Faramawy, A.; Siu, K.W.M.; Thomson, B.A. Efficiency of Nano-Electrospray Ionization. *Journal of the American Society for Mass Spectrometry* **2005**, *16*, 1702–1707, doi:10.1016/j.jasms.2005.06.011.
63. Graça, G.; Cai, Y.; Lau, C.-H.E.; Vorkas, P.A.; Lewis, M.R.; Want, E.J.; Herrington, D.; Ebbels, T.M.D. Automated Annotation of Untargeted All-Ion Fragmentation LC–MS Metabolomics Data with MetaboAnnotatoR. *Analytical Chemistry* **2022**, *94*, 3446–3455, doi:10.1021/acs.analchem.1c03032.
64. Chen, L.; Lu, W.; Wang, L.; Xing, X.; Chen, Z.; Teng, X.; Zeng, X.; Muscarella, A.D.; Shen, Y.; Cowan, A.; et al. Metabolite Discovery through Global Annotation of Untargeted Metabolomics Data. *Nature Methods* **2021**, *18*, 1377–1385, doi:10.1038/s41592-021-01303-3.
65. Cao, L.; Guler, M.; Tagirdzhanov, A.; Lee, Y.-Y.; Gurevich, A.; Mohimani, H. MolDiscovery: Learning Mass Spectrometry Fragmentation of Small Molecules. *Nature Communications* **2021**, *12*, 3718, doi:10.1038/s41467-021-23986-0.
66. Zhang, P.; Chan, W.; Ang, I.L.; Wei, R.; Lam, M.M.T.; Lei, K.M.K.; Poon, T.C.W. Revisiting Fragmentation Reactions of Protonated  $\alpha$ -Amino Acids by High-Resolution Electrospray Ionization Tandem Mass Spectrometry with Collision-Induced Dissociation. *Scientific Reports* **2019**, *9*, 6453, doi:10.1038/s41598-019-42777-8.
67. Krishnan, Y.; Sharma, N.; Lourderaj, U.; Paranjothy, M. Classical Dynamics Simulations of Dissociation of Protonated Tryptophan in the Gas Phase. *The Journal of Physical Chemistry A* **2017**, *121*, 4389–4396, doi:10.1021/acs.jpca.7b01359.
68. Tóth, K.; Nagy, L.; Mándi, A.; Kuki, Á.; Mézes, M.; Zsuga, M.; Kéki, S. Collision-induced Dissociation of Aflatoxins. *Rapid Communications in Mass Spectrometry* **2013**, *27*, 553–559, doi:10.1002/rcm.6482.
69. Albero, B.; Fernández-Cruz, M.L.; Pérez, R.A. Simultaneous Determination of 15 Mycotoxins in Aquaculture Feed by Liquid Chromatography–Tandem Mass Spectrometry. *Toxins (Basel)* **2022**, *14*, 316, doi:10.3390/toxins14050316.
70. Abreu, D.C.P.; Vargas, E.A.; Oliveira, F.A. da S.; Uetanabaro, A.P.T.; Pires, P.N.; Bazzana, M.J.F.; Saczk, A.A. Study of Co-Occurrence of Mycotoxins in Cocoa Beans in Brazil by Liquid Chromatography-Tandem Mass Spectrometry (LC-MS/MS). *Food Additives & Contaminants: Part A* **2023**, *40*, 1049–1058, doi:10.1080/19440049.2023.2238838.

71. ZHAO, R.; HUANG, Q.; YU, Z.; HAN, Z.; FAN, K.; ZHAO, Z.; NIE, D. Simultaneous Determination of 36 Mycotoxins in Fruits by QuEChERS Coupled with Ultra Performance Liquid Chromatography-Tandem Mass Spectrometry. *Chinese Journal of Chromatography* **2023**, *41*, 760–770, doi:10.3724/SP.J.1123.2022.12010.
72. John, H.; Siegert, M.; Kranawetvogl, A.; Thiermann, H. Collision-induced Mass Spectrometric Fragmentation of Protonated Dimethoate and Omethoate Generated by Electrospray Ionization. *Rapid Communications in Mass Spectrometry* **2019**, *33*, 259–271, doi:10.1002/rcm.8343.
73. Niessen, W.M.A. Group-Specific Fragmentation of Pesticides and Related Compounds in Liquid Chromatography–Tandem Mass Spectrometry. *Journal of Chromatography A* **2010**, *1217*, 4061–4070, doi:10.1016/j.chroma.2009.09.058.
74. Bhattacharyya, A.; Pardeshi, A.; Nerpagar, A.; Banerjee, K. Multiresidue Analysis of Pesticides in Three Indian Soils: Method Development and Validation Using Gas Chromatography Tandem Mass Spectrometry. *Journal of Environmental Science and Health, Part B* **2023**, *58*, 158–194, doi:10.1080/03601234.2023.2175578.
75. Kim, H.; Joo Baek, E.; Kim, Y.-K.; Park, H.; Hye Hur, S.; Kim, J.-E.; Jin Kim, H. Development of a Method for Analysis and Risk Assessment of Residual Pesticides in Ginseng Using Liquid and Gas Chromatography-Tandem Mass Spectrometry. *Food Chem.* **2023**, *427*, 136675, doi:10.1016/j.foodchem.2023.136675.
76. Ding, C.; Ren, P.; Qi, Y.; Yang, Y.; Qin, S. Simultaneous Determination of 54 Pesticides in Proso Millet Using QuEChERS with Liquid Chromatography-Tandem Mass Spectrometry (LC–MS/MS). *Molecules* **2023**, *28*, 6575, doi:10.3390/molecules28186575.
77. Stucki, S.R.; Désiron, C.; Nyakas, A.; Marti, S.; Leumann, C.J.; Schürch, S. Gas-Phase Dissociation of Homo-DNA Oligonucleotides. *Journal of the American Society for Mass Spectrometry* **2013**, *24*, 1997–2006, doi:10.1007/s13361-013-0729-3.
78. Tromp, J.M.; Schürch, S. Gas-Phase Dissociation of Oligoribonucleotides and Their Analogs Studied by Electrospray Ionization Tandem Mass Spectrometry. *Journal of the American Society for Mass Spectrometry* **2005**, *16*, 1262–1268, doi:10.1016/j.jasms.2005.03.024.
79. Zuo, M.-Q.; Sun, R.-X.; Fang, R.-Q.; He, S.-M.; Dong, M.-Q. Characterization of Collision-Induced Dissociation of Deprotonated Peptides of 4–16 Amino Acids

- Using High-Resolution Mass Spectrometry. *International Journal of Mass Spectrometry* **2019**, *445*, 116186, doi:10.1016/j.ijms.2019.116186.
80. Mitchell Wells, J.; McLuckey, S.A. Collision-Induced Dissociation (CID) of Peptides and Proteins. In; 2005; pp. 148–185.
81. Giese, S.H.; Fischer, L.; Rappsilber, J. A Study into the Collision-Induced Dissociation (CID) Behavior of Cross-Linked Peptides. *Molecular & Cellular Proteomics* **2016**, *15*, 1094–1104, doi:10.1074/mcp.M115.049296.
82. Schlosser, A.; Lehmann, W.D. Five-Membered Ring Formation in Unimolecular Reactions of Peptides: A Key Structural Element Controlling Low-Energy Collision-Induced Dissociation of Peptides. *Journal of Mass Spectrometry* **2000**, *35*, 1382–1390, doi:10.1002/1096-9888(200012)35:12<1382::AID-JMS84>3.0.CO;2-6.
83. Steckel, A.; Papp, D.; Uray, K.; Schlosser, G. Collision-Induced Dissociation of Citrullinated Peptide Anions. *Journal of the American Society for Mass Spectrometry* **2023**, *34*, 1569–1575, doi:10.1021/jasms.3c00044.
84. Chowdhury, S.M.; Munske, G.R.; Tang, X.; Bruce, J.E. Collisionally Activated Dissociation and Electron Capture Dissociation of Several Mass Spectrometry-Identifiable Chemical Cross-Linkers. *Analytical Chemistry* **2006**, *78*, 8183–8193, doi:10.1021/ac060789h.
85. Keller, K.M.; Brodbelt, J.S.; Hettich, R.L.; Berkel, G.J. Van Comparison of Sustained Off-resonance Irradiation Collisionally Activated Dissociation and Multipole Storage-assisted Dissociation for Top-down Protein Analysis. *Journal of Mass Spectrometry* **2004**, *39*, 402–411, doi:10.1002/jms.602.
86. Wei, B.; Zenaidee, M.A.; Lantz, C.; Ogorzalek Loo, R.R.; Loo, J.A. Towards Understanding the Formation of Internal Fragments Generated by Collisionally Activated Dissociation for Top-down Mass Spectrometry. *Analytica Chimica Acta* **2022**, *1194*, 339400, doi:10.1016/j.aca.2021.339400.
87. Lantz, C.; Wei, B.; Zhao, B.; Jung, W.; Goring, A.K.; Le, J.; Miller, J.; Loo, R.R.O.; Loo, J.A. Native Top-Down Mass Spectrometry with Collisionally Activated Dissociation Yields Higher-Order Structure Information for Protein Complexes. *Journal of the American Chemical Society* **2022**, *144*, 21826–21830, doi:10.1021/jacs.2c06726.
88. Muggli, T.M.; Schürch, S. Analysis of Pesticide Residues on Fruit Using Swab Spray Ionization Mass Spectrometry. *Molecules* **2023**, *28*, 6611, doi:10.3390/molecules28186611.

89. Phapale, P.; Palmer, A.; Gathungu, R.M.; Kale, D.; Brügger, B.; Alexandrov, T. Public LC-Orbitrap Tandem Mass Spectral Library for Metabolite Identification. *Journal of Proteome Research* **2021**, *20*, 2089–2097, doi:10.1021/acs.jproteome.0c00930.
90. Awasthi, K.; Kootimole, C.N.; Aravind, A.; Prasad, T.S.K. Data-Independent Acquisition Approach to Proteome: A Case Study and a Spectral Library for Mass Spectrometry-Based Investigation of *Mycobacterium Tuberculosis*. *OMICS* **2022**, *26*, 142–150, doi:10.1089/omi.2021.0187.
91. Mayer, P.M.; Poon, C. The Mechanisms of Collisional Activation of Ions in Mass Spectrometry. *Mass Spectrometry Reviews* **2009**, *28*, 608–639, doi:10.1002/mas.20225.
92. Niessen, W.M.A. MS–MS and MS<sub>n</sub>. In *Encyclopedia of Spectroscopy and Spectrometry*; Elsevier, 2017; pp. 936–941.
93. Available Online: [www.thermofisher.com/ch/en/home/industrial/mass-spectrometry/mass-spectrometry-learning-center/mass-spectrometry-technology-overview/dissociation-technique-technology-overview.html](http://www.thermofisher.com/ch/en/home/industrial/mass-spectrometry/mass-spectrometry-learning-center/mass-spectrometry-technology-overview/dissociation-technique-technology-overview.html) (Accessed: 16.01.2024).
94. Available Online: [www.tools.thermofisher.com/content/sfs/brochures/psb104-normalized-collision-energy-technology-en.pdf](http://www.tools.thermofisher.com/content/sfs/brochures/psb104-normalized-collision-energy-technology-en.pdf) (Accessed: 16.01.2024).
95. Kingdon, K.H. A Method for the Neutralization of Electron Space Charge by Positive Ionization at Very Low Gas Pressures. *Physical Review* **1923**, *21*, 408–418, doi:10.1103/PhysRev.21.408.
96. Knight, R.D. Storage of Ions from Laser-Produced Plasmas. *Applied Physics Letters* **1981**, *38*, 221–223, doi:10.1063/1.92315.
97. Eliuk, S.; Makarov, A. Evolution of Orbitrap Mass Spectrometry Instrumentation. *Annual Review of Analytical Chemistry* **2015**, *8*, 61–80, doi:10.1146/annurev-anchem-071114-040325.
98. Makarov, A. Orbitrap Journey: Taming the Ion Rings. *Nature Communications* **2019**, *10*, 3743, doi:10.1038/s41467-019-11748-y.
99. Scigelova, M.; Hornshaw, M.; Giannakopoulos, A.; Makarov, A. Fourier Transform Mass Spectrometry. *Molecular & Cellular Proteomics* **2011**, *10*, M111.009431, doi:10.1074/mcp.M111.009431.
100. Zubarev, R.A.; Makarov, A. Orbitrap Mass Spectrometry. *Analytical Chemistry* **2013**, *85*, 5288–5296, doi:10.1021/ac4001223.

101. Feider, C.L.; Krieger, A.; DeHoog, R.J.; Eberlin, L.S. Ambient Ionization Mass Spectrometry: Recent Developments and Applications. *Analytical Chemistry* **2019**, *91*, 4266–4290, doi:10.1021/acs.analchem.9b00807.
102. Huang, M.-Z.; Cheng, S.-C.; Cho, Y.-T.; Shiea, J. Ambient Ionization Mass Spectrometry: A Tutorial. *Analytica Chimica Acta* **2011**, *702*, 1–15, doi:10.1016/j.aca.2011.06.017.
103. Takáts, Z.; Wiseman, J.M.; Gologan, B.; Cooks, R.G. Mass Spectrometry Sampling Under Ambient Conditions with Desorption Electrospray Ionization. *Science* **2004**, *306*, 471–473, doi:10.1126/science.1104404.
104. Sandström, E.; Vettorazzo, C.; Mackay, C.L.; Troalen, L.G.; Hulme, A.N. Development and Application of Desorption Electrospray Ionization Mass Spectrometry for Historical Dye Analysis. *Analytical Chemistry* **2023**, *95*, 4846–4854, doi:10.1021/acs.analchem.2c03281.
105. Cody, R.B.; Laramée, J.A.; Durst, H.D. Versatile New Ion Source for the Analysis of Materials in Open Air under Ambient Conditions. *Analytical Chemistry* **2005**, *77*, 2297–2302, doi:10.1021/ac050162j.
106. Shiea, J.; Huang, M.-Z.; HSu, H.-J.; Lee, C.-Y.; Yuan, C.-H.; Beech, I.; Sunner, J. Electrospray-Assisted Laser Desorption/Ionization Mass Spectrometry for Direct Ambient Analysis of Solids. *Rapid Communications in Mass Spectrometry* **2005**, *19*, 3701–3704, doi:10.1002/rcm.2243.
107. Chen, H.; Venter, A.; Cooks, R.G. Extractive Electrospray Ionization for Direct Analysis of Undiluted Urine, Milk and Other Complex Mixtures without Sample Preparation. *Chemical Communications* **2006**, 2042, doi:10.1039/b602614a.
108. Haddad, R.; Milagre, H.M.S.; Catharino, R.R.; Eberlin, M.N. Easy Ambient Sonic-Spray Ionization Mass Spectrometry Combined with Thin-Layer Chromatography. *Analytical Chemistry* **2008**, *80*, 2744–2750, doi:10.1021/ac702216q.
109. Haddad, R.; Sparrapan, R.; Eberlin, M.N. Desorption Sonic Spray Ionization for (High) Voltage-Free Ambient Mass Spectrometry. *Rapid Communications in Mass Spectrometry* **2006**, *20*, 2901–2905, doi:10.1002/rcm.2680.
110. Hiraoka, K.; Nishidate, K.; Mori, K.; Asakawa, D.; Suzuki, S. Development of Probe Electrospray Using a Solid Needle. *Rapid Communications in Mass Spectrometry* **2007**, *21*, 3139–3144, doi:10.1002/rcm.3201.
111. Na, N.; Zhao, M.; Zhang, S.; Yang, C.; Zhang, X. Development of a Dielectric Barrier Discharge Ion Source for Ambient Mass Spectrometry. *Journal of the*

- American Society for Mass Spectrometry* **2007**, 18, 1859–1862, doi:10.1016/j.jasms.2007.07.027.
112. Wang, H.; Liu, J.; Cooks, R.G.; Ouyang, Z. Paper Spray for Direct Analysis of Complex Mixtures Using Mass Spectrometry. *Angewandte Chemie International Edition* **2010**, 49, 877–880, doi:10.1002/anie.200906314.
113. McBride, E.M.; Mach, P.M.; Dhummakupt, E.S.; Dowling, S.; Carmany, D.O.; Demond, P.S.; Rizzo, G.; Manicke, N.E.; Glaros, T. Paper Spray Ionization: Applications and Perspectives. *TrAC Trends in Analytical Chemistry* **2019**, 118, 722–730, doi:10.1016/j.trac.2019.06.028.
114. Pirro, V.; Jarmusch, A.K.; Vincenti, M.; Cooks, R.G. Direct Drug Analysis from Oral Fluid Using Medical Swab Touch Spray Mass Spectrometry. *Analytica Chimica Acta* **2015**, 861, 47–54, doi:10.1016/j.aca.2015.01.008.
115. Kanu, A.B. Recent Developments in Sample Preparation Techniques Combined with High-Performance Liquid Chromatography: A Critical Review. *Journal of Chromatography A* **2021**, 1654, 462444, doi:10.1016/j.chroma.2021.462444.
116. Rankin-Turner, S.; Sears, P.; Heaney, L.M. Applications of Ambient Ionization Mass Spectrometry in 2022: An Annual Review. *Analytical Science Advances* **2023**, 4, 133–153, doi:10.1002/ansa.202300004.
117. Shigeeda, W.; Yosihimura, R.; Fujita, Y.; Saiki, H.; Deguchi, H.; Tomoyasu, M.; Kudo, S.; Kaneko, Y.; Kanno, H.; Inoue, Y.; et al. Utility of Mass Spectrometry and Artificial Intelligence for Differentiating Primary Lung Adenocarcinoma and Colorectal Metastatic Pulmonary Tumor. *Thorac. Cancer* **2022**, 13, 202–209, doi:10.1111/1759-7714.14246.
118. Hakoda, H.; Kiritani, S.; Kokudo, T.; Yoshimura, K.; Iwano, T.; Tanimoto, M.; Ishizawa, T.; Arita, J.; Akamatsu, N.; Kaneko, J.; et al. Probe Electrospray Ionization Mass Spectrometry-based Rapid Diagnosis of Liver Tumors. *J. Gastroenterol Hepatol* **2022**, 37, 2182–2188, doi:10.1111/jgh.15976.
119. Wang, Y.; Chen, Z.; Shima, K.; Zhong, D.; Yang, L.; Wang, Q.; Jiang, R.; Dong, J.; Lei, Y.; Li, X.; et al. Rapid Diagnosis of Papillary Thyroid Carcinoma with Machine Learning and Probe Electrospray Ionization Mass Spectrometry. *Journal of Mass Spectrometry* **2022**, 57, doi:10.1002/jms.4831.
120. Ifa, D.R.; Eberlin, L.S. Ambient Ionization Mass Spectrometry for Cancer Diagnosis and Surgical Margin Evaluation. *Clin. Chem.* **2016**, 62, 111–123, doi:10.1373/clinchem.2014.237172.
121. Calligaris, D.; Caragacianu, D.; Liu, X.; Norton, I.; Thompson, C.J.; Richardson, A.L.; Golshan, M.; Easterling, M.L.; Santagata, S.; Dillon, D.A.; et al.



- Application of Desorption Electrospray Ionization Mass Spectrometry Imaging in Breast Cancer Margin Analysis. *Proceedings of the National Academy of Sciences* **2014**, *111*, 15184–15189, doi:10.1073/pnas.1408129111.
122. Banerjee, S.; Zare, R.N.; Tibshirani, R.J.; Kunder, C.A.; Nolley, R.; Fan, R.; Brooks, J.D.; Sonn, G.A. Diagnosis of Prostate Cancer by Desorption Electrospray Ionization Mass Spectrometric Imaging of Small Metabolites and Lipids. *Proceedings of the National Academy of Sciences* **2017**, *114*, 3334–3339, doi:10.1073/pnas.1700677114.
123. Porcari, A.M.; Zhang, J.; Garza, K.Y.; Rodrigues-Peres, R.M.; Lin, J.Q.; Young, J.H.; Tibshirani, R.; Nagi, C.; Paiva, G.R.; Carter, S.A.; et al. Multicenter Study Using Desorption-Electrospray-Ionization-Mass-Spectrometry Imaging for Breast-Cancer Diagnosis. *Analytical Chemistry* **2018**, *90*, 11324–11332, doi:10.1021/acs.analchem.8b01961.
124. Cui, Y.; Ge, L.; Lu, W.; Wang, S.; Li, Y.; Wang, H.; Huang, M.; Xie, H.; Liao, J.; Tao, Y.; et al. Real-Time Profiling and Distinction of Lipids from Different Mammalian Milks Using Rapid Evaporative Ionization Mass Spectrometry Combined with Chemometric Analysis. *Journal of Agricultural and Food Chemistry* **2022**, *70*, 7786–7795, doi:10.1021/acs.jafc.2c01447.
125. Hong, Y.; Birse, N.; Quinn, B.; Montgomery, H.; Wu, D.; Rosas da Silva, G.; van Ruth, S.M.; Elliott, C.T. Identification of Milk from Different Animal and Plant Sources by Desorption Electrospray Ionisation High-Resolution Mass Spectrometry (DESI-MS). *NPJ Sci. Food* **2022**, *6*, 14, doi:10.1038/s41538-022-00129-3.
126. Tata, A.; Massaro, A.; Riuzzi, G.; Lanza, I.; Bragolusi, M.; Negro, A.; Novelli, E.; Piro, R.; Gottardo, F.; Segato, S. Ambient Mass Spectrometry for Rapid Authentication of Milk from Alpine or Lowland Forage. *Scientific Reports* **2022**, *12*, 7360, doi:10.1038/s41598-022-11178-9.
127. Tan, H.R.; Chan, L.Y.; Lee, H.H.; Xu, Y.-Q.; Zhou, W. Rapid Authentication of Chinese Oolong Teas Using Atmospheric Solids Analysis Probe-Mass Spectrometry (ASAP-MS) Combined with Supervised Pattern Recognition Models. *Food Control* **2022**, *134*, 108736, doi:10.1016/j.foodcont.2021.108736.
128. Pitman, C.N.; LaCourse, W.R. Rapid Characterization of Vanilla with Molecular Ionization Desorption Analysis Source (MIDAS) for Mass Spectrometry. *International Journal of Mass Spectrometry* **2022**, *479*, 116888, doi:10.1016/j.ijms.2022.116888.

129. Gerbig, S.; Neese, S.; Penner, A.; Spengler, B.; Schulz, S. Real-Time Food Authentication Using a Miniature Mass Spectrometer. *Analytical Chemistry* **2017**, *89*, 10717–10725, doi:10.1021/acs.analchem.7b01689.
130. Chen, T.-H.; Hsu, H.-Y.; Wu, S.-P. The Detection of Multiple Illicit Street Drugs in Liquid Samples by Direct Analysis in Real Time (DART) Coupled to Q-Orbitrap Tandem Mass Spectrometry. *Forensic Science International* **2016**, *267*, 1–6, doi:10.1016/j.forsciint.2016.07.025.
131. Sisco, E.; Appley, M.G.; Tennyson, S.S.; Moorthy, A.S. Qualitative Analysis of Real Drug Evidence Using DART-MS and the Inverted Library Search Algorithm. *Journal of the American Society for Mass Spectrometry* **2022**, *33*, 1784–1793, doi:10.1021/jasms.2c00166.
132. Kim, A.; Kelly, P.F.; Turner, M.A.; Reynolds, J.C. Development of a Rapid, In-situ Analysis Method Using Sheath-flow Probe Electrospray Ionisation-mass Spectrometry for the Direct Identification of Cocaine Metabolites in Dried Blood Spots. *Rapid Communications in Mass Spectrometry* **2023**, *37*, doi:10.1002/rcm.9422.
133. Rydberg, M.; Dowling, S.; Manicke, N.E. Automated and High-Throughput Urine Drug Screening Using Paper Spray Mass Spectrometry. *J. Anal. Toxicol.* **2023**, *47*, 147–153, doi:10.1093/jat/bkac053.
134. Li, L.; Zhang, T.; Ge, W.; He, X.; Zhang, Y.; Wang, X.; Li, P. Detection of Trace Explosives Using a Novel Sample Introduction and Ionization Method. *Molecules* **2022**, *27*, 4551, doi:10.3390/molecules27144551.
135. Hong, H.; Habib, A.; Bi, L.; Wen, L. Gas Phase Ion-Molecule Reactions of Nitroaromatic Explosive Compounds Studied by Hollow Cathode Discharge Ionization-Mass Spectrometry. *Talanta* **2022**, *236*, 122834, doi:10.1016/j.talanta.2021.122834.
136. Gao, Y.; Chu, F.; Chen, W.; Wang, X.; Pan, Y. Arc-Induced Nitrate Reagent Ion for Analysis of Trace Explosives on Surfaces Using Atmospheric Pressure Arc Desorption/Ionization Mass Spectrometry. *Analytical Chemistry* **2022**, *94*, 5463–5468, doi:10.1021/acs.analchem.1c05650.
137. Forbes, T.P.; Sisco, E. Recent Advances in Ambient Mass Spectrometry of Trace Explosives. *Analyst* **2018**, *143*, 1948–1969, doi:10.1039/C7AN02066J.
138. Garcia-Reyes, J.F.; Harper, J.D.; Salazar, G.A.; Charipar, N.A.; Ouyang, Z.; Cooks, R.G. Detection of Explosives and Related Compounds by Low-Temperature Plasma Ambient Ionization Mass Spectrometry. *Analytical Chemistry* **2011**, *83*, 1084–1092, doi:10.1021/ac1029117.

- 
139. Sun, Q.; Luo, Y.; Wang, Y.; Zhang, Q.; Yang, X. Comparative Analysis of Aged Documents by Desorption Electrospray Ionization–Mass Spectrometry (DESI-MS) Imaging. *w* **2022**, *67*, 2062–2072, doi:10.1111/1556-4029.15071.
140. Jurisch, M.; Vendramini, P.H.; Eberlin, M.N.; Augusti, R. Detection of Handwriting Forgery Made with Erasable Pens Using Desorption Electrospray Mass Spectrometry Imaging. *Journal of the American Society for Mass Spectrometry* **2020**, *31*, 1000–1003, doi:10.1021/jasms.0c00007.
141. Li, M.; Jia, B.; Ding, L.; Hong, F.; Ouyang, Y.; Chen, R.; Zhou, S.; Chen, H.; Fang, X. Document Authentication at Molecular Levels Using Desorption Atmospheric Pressure Chemical Ionization Mass Spectrometry Imaging. *Journal of Mass Spectrometry* **2013**, *48*, 1042–1049, doi:10.1002/jms.3250.
142. Min, K.; Yang, Q.; Zhong, X.; Yan, D.; Luo, W.; Fang, Z.; Xiao, J.; Ma, M.; Chen, B. Rapid Analysis of Anionic and Cationic Surfactants in Water by Paper Spray Mass Spectrometry. *Analytical Methods* **2021**, *13*, 986–995, doi:10.1039/D0AY02215B.
143. He, J.; Wang, W.; Zhang, H.; Yu, K.; Kan, G.; Wang, Y.; Guo, C.; Liu, J.; Jiang, J. High-Sensitive Detection of Fluorene by Ambient Ionization Mass Spectrometry. *New Journal of Chemistry* **2021**, *45*, 10325–10330, doi:10.1039/D1NJ01569A.
144. Jackson, S.; Badu-Tawiah, A.K. Enhanced Thread Spray Mass Spectrometry: A General Method for Direct Pesticide Analysis in Various Complex Matrices. *Analyst* **2021**, *146*, 5592–5600, doi:10.1039/D1AN00651G.
145. Wang, L.; Zhao, P.; Zhang, F.; Li, Y.; Pan, C. Direct Analysis in Real Time Mass Spectrometry for the Rapid Identification of Four Highly Hazardous Pesticides in Agrochemicals. *Rapid Communications in Mass Spectrometry* **2012**, *26*, 1859–1867, doi:10.1002/rcm.6274.
146. Crawford, E.; Musselman, B. Evaluating a Direct Swabbing Method for Screening Pesticides on Fruit and Vegetable Surfaces Using Direct Analysis in Real Time (DART) Coupled to an Exactive Benchtop Orbitrap Mass Spectrometer. *Analytical and Bioanalytical Chemistry* **2012**, *403*, 2807–2812, doi:10.1007/s00216-012-5853-6.
147. Beach, D.G.; Rafuse, C.; Melanson, J.E.; McCarron, P. Rapid Quantitative Screening of Cyanobacteria for Production of Anatoxins Using Direct Analysis in Real Time High-resolution Mass Spectrometry. *Rapid Communications in Mass Spectrometry* **2021**, *35*, doi:10.1002/rcm.8940.
-

148. Hoegg, E.D.; Barinaga, C.J.; Hager, G.J.; Hart, G.L.; Koppenaal, D.W.; Marcus, R.K. Isotope Ratio Characteristics and Sensitivity for Uranium Determinations Using a Liquid Sampling-Atmospheric Pressure Glow Discharge Ion Source Coupled to an Orbitrap Mass Analyzer. *Journal of Analytical Atomic Spectrometry* **2016**, *31*, 2355–2362, doi:10.1039/C6JA00163G.
149. Cheng, S.; Wu, Q.; Xiao, H.; Chen, H. Online Monitoring of Enzymatic Reactions Using Time-Resolved Desorption Electrospray Ionization Mass Spectrometry. *Analytical Chemistry* **2017**, *89*, 2338–2344, doi:10.1021/acs.analchem.6b03975.
150. Phelps, D.L.; Balog, J.; Gildea, L.F.; Bodai, Z.; Savage, A.; El-Bahrawy, M.A.; Speller, A.V.; Rosini, F.; Kudo, H.; McKenzie, J.S.; et al. The Surgical Intelligent Knife Distinguishes Normal, Borderline and Malignant Gynaecological Tissues Using Rapid Evaporative Ionisation Mass Spectrometry (REIMS). *Br. J. Cancer* **2018**, *118*, 1349–1358, doi:10.1038/s41416-018-0048-3.
151. Ambrose, S.; Housden, N.G.; Gupta, K.; Fan, J.; White, P.; Yen, H.; Marcoux, J.; Kleanthous, C.; Hopper, J.T.S.; Robinson, C. V. Native Desorption Electrospray Ionization Liberates Soluble and Membrane Protein Complexes from Surfaces. *Angewandte Chemie International Edition* **2017**, *56*, 14463–14468, doi:10.1002/anie.201704849.
152. Available Online: [www.Epa.Gov/Minimum-Risk-Pesticides/What-Pesticide](http://www.Epa.Gov/Minimum-Risk-Pesticides/What-Pesticide) (Accessed: 11.10.2023).
153. Available Online: [www.Gov.Nl.ca/Ecc/Files/Env-Protection-Pesticides-Business-Manuals-Core-Ch1-Nl-092205.Pdf](http://www.Gov.Nl.ca/Ecc/Files/Env-Protection-Pesticides-Business-Manuals-Core-Ch1-Nl-092205.Pdf) (Accessed: 11.10.2023).
154. Available Online: [www.Epa.Gov/Ingredients-Used-Pesticide-Products/Chemically-Related-Groups-Active-Ingredients](http://www.Epa.Gov/Ingredients-Used-Pesticide-Products/Chemically-Related-Groups-Active-Ingredients) (Accessed: 11.10.2023).
155. Umetsu, N.; Shirai, Y. Development of Novel Pesticides in the 21st Century. *J Pestic Sci* **2020**, *45*, 54–74, doi:10.1584/jpestics.D20-201.
156. Available Online: [www.Extension.Psu.Edu/a-Short-History-of-Pest-Management](http://www.Extension.Psu.Edu/a-Short-History-of-Pest-Management) (Accessed 04.10.2023).
157. *Sustainable Agrochemistry*; Vaz, S., Ed.; Springer International Publishing: Cham, 2019; ISBN 978-3-030-17890-1.
158. Isman, M.B. BOTANICAL INSECTICIDES, DETERRENTS, AND REPELLENTS IN MODERN AGRICULTURE AND AN INCREASINGLY REGULATED WORLD. *Annual Review of Entomology* **2006**, *51*, 45–66, doi:10.1146/annurev.ento.51.110104.151146.

- 
159. Smith, A.E.; Secoy, D.M. A Compendium of Inorganic Substances Used in European Pest Control before 1850. *Journal of Agricultural and Food Chemistry* **1976**, *24*, 1180–1186, doi:10.1021/jf60208a048.
160. *Pesticides in the Diets of Infants and Children*; National Academies Press: Washington, D.C., 1993; ISBN 978-0-309-04875-0.
161. Jarman, W.M.; Ballschmiter, K. From Coal to DDT: The History of the Development of the Pesticide DDT from Synthetic Dyes till Silent Spring. *Endeavour* **2012**, *36*, 131–142, doi:10.1016/j.endeavour.2012.10.003.
162. Available Online: [www.Epa.Gov/Ingredients-Used-Pesticide-Products/Ddt-Brief-History-and-Status](http://www.Epa.Gov/Ingredients-Used-Pesticide-Products/Ddt-Brief-History-and-Status) (Accessed: 04.10.2023).
163. Available Online: [www.Umweltbundesamt.de/Themen/Chemikalien/Persistente-Organische-Schadstoffe-Pop/Ddt#:~:Text=Die%20Herstellung%2C%20das%20Inverkehrbringen%20und,Verordnung%E2%81%A0%20ohne%20Ausnahmen%20gelistet.](http://www.Umweltbundesamt.de/Themen/Chemikalien/Persistente-Organische-Schadstoffe-Pop/Ddt#:~:Text=Die%20Herstellung%2C%20das%20Inverkehrbringen%20und,Verordnung%E2%81%A0%20ohne%20Ausnahmen%20gelistet.) (Accessed: 04.10.2023).
164. Coats, J.R. Mechanisms of Toxic Action and Structure-Activity Relationships for Organochlorine and Synthetic Pyrethroid Insecticides. *Environ Health Perspect* **1990**, *87*, 255–262, doi:10.1289/ehp.9087255.
165. Koshlukova, S.E.; Reed, N.R. Chlordane. In *Encyclopedia of Toxicology*; Elsevier, 2014; pp. 841–845.
166. Pakala, R.S.; Brown, K.N.; Preuss, C. V. *Cholinergic Medications*; 2023;
167. Rosenberg, Y.J.; Garcia, K.; Diener, J.; Gerk, W.; Donahue, S.; Mao, L.; Lees, J.; Jiang, X.; Urban, L.A.; Sullivan, D. The Impact of Solvents on the Toxicity of the Banned Parathion Insecticide. *Chem. Biol. Interact.* **2023**, *382*, 110635, doi:10.1016/j.cbi.2023.110635.
168. Mesnage, R.; Antoniou, M.N. Roundup Ready! Glyphosate and the Current Controversy Over the World's Leading Herbicide. In *Encyclopedia of the Anthropocene*; Elsevier, 2018; pp. 149–153.
169. Dill, G.M.; Sammons, R.D.; Feng, P.C.C.; Kohn, F.; Kretzmer, K.; Mehrsheikh, A.; Bleeke, M.; Honegger, J.L.; Farmer, D.; Wright, D.; et al. Glyphosate: Discovery, Development, Applications, and Properties. In *Glyphosate Resistance in Crops and Weeds*; Wiley, 2010; pp. 1–33.
170. Klátyik, S.; Simon, G.; Oláh, M.; Mesnage, R.; Antoniou, M.N.; Zaller, J.G.; Székács, A. Terrestrial Ecotoxicity of Glyphosate, Its Formulations, and Co-

- Formulants: Evidence from 2010–2023. *Environ. Sci. Eur.* **2023**, *35*, 51, doi:10.1186/s12302-023-00758-9.
171. Bouillaud, F. Inhibition of Succinate Dehydrogenase by Pesticides (SDHIs) and Energy Metabolism. *International Journal of Molecular Sciences* **2023**, *24*, 4045, doi:10.3390/ijms24044045.
172. Yamashita, M.; Fraaije, B. Non-target Site SDHI Resistance Is Present as Standing Genetic Variation in Field Populations of *Zymoseptoria Tritici*. *Pest Management Science*. **2018**, *74*, 672–681, doi:10.1002/ps.4761.
173. d'Hose, D.; Isenborghs, P.; Brusa, D.; Jordan, B.F.; Gallez, B. The Short-Term Exposure to SDHI Fungicides Boscalid and Bixafen Induces a Mitochondrial Dysfunction in Selective Human Cell Lines. *Molecules* **2021**, *26*, 5842, doi:10.3390/molecules26195842.
174. Yanicostas, C.; Soussi-Yanicostas, N. SDHI Fungicide Toxicity and Associated Adverse Outcome Pathways: What Can Zebrafish Tell Us? *International Journal of Molecular Sciences* **2021**, *22*, 12362, doi:10.3390/ijms222212362.
175. Carbone, M.; Mathieu, B.; Vandensande, Y.; Gallez, B. Impact of Exposure to Pyraclostrobin and to a Pyraclostrobin/Boscalid Mixture on the Mitochondrial Function of Human Hepatocytes. *Molecules* **2023**, *28*, 7013, doi:10.3390/molecules28207013.
176. Duarte Hospital, C.; Tête, A.; Debizet, K.; Imler, J.; Tomkiewicz-Raulet, C.; Blanc, E.B.; Barouki, R.; Coumoul, X.; Bortoli, S. SDHI Fungicides: An Example of Mitotoxic Pesticides Targeting the Succinate Dehydrogenase Complex. *Environment International* **2023**, *180*, 108219, doi:10.1016/j.envint.2023.108219.
177. Vielba-Fernández, A.; Polonio, Á.; Ruiz-Jiménez, L.; de Vicente, A.; Pérez-García, A.; Fernández-Ortuño, D. Resistance to the SDHI Fungicides Boscalid and Fluopyram in *Podosphaera Xanthii* Populations from Commercial Cucurbit Fields in Spain. *Journal of Fungi* **2021**, *7*, 733, doi:10.3390/jof7090733.
178. Pscheidt, J.W.; Heckert, S.; Cluskey, S.A. Evaluation of Quinone Outside and Succinate Dehydrogenase Inhibitors for Effectiveness Against Eastern Filbert Blight of Hazelnut. *Plant Disease*. **2017**, *101*, 1868–1873, doi:10.1094/PDIS-02-17-0224-RE.
179. Li, H.; Nuckols, T.A.; Harris, D.; Stevenson, K.L.; Brewer, M.T. Differences in Fungicide Resistance Profiles and Multiple Resistance to a Quinone-outside Inhibitor (QoI), Two Succinate Dehydrogenase Inhibitors (SDHI), and a Demethylation Inhibitor (DMI) for Two *Stagonosporopsis* Species Causing

- Gummy Stem Blight of Cucurbits. *Pest Management Science* **2019**, 75, 3093–3101, doi:10.1002/ps.5426.
180. MATSUO, N. Discovery and Development of Pyrethroid Insecticides. *Proceedings of the Japan Academy, Series B* **2019**, 95, 378–400, doi:10.2183/pjab.95.027.
181. Houchat, J.-N.; Cartereau, A.; Le Mauff, A.; Taillebois, E.; Thany, S.H. An Overview on the Effect of Neonicotinoid Insecticides on Mammalian Cholinergic Functions through the Activation of Neuronal Nicotinic Acetylcholine Receptors. *International Journal of Environmental Research and Public Health* **2020**, 17, 3222, doi:10.3390/ijerph17093222.
182. Kadala, A.; Charreton, M.; Collet, C. Flubendiamide, the First Phthalic Acid Diamide Insecticide, Impairs Neuronal Calcium Signalling in the Honey Bee's Antennae. *Journal of Insect Physiology* **2020**, 125, 104086, doi:10.1016/j.jinsphys.2020.104086.
183. Jacquet, F.; Jeuffroy, M.-H.; Jouan, J.; Le Cadre, E.; Litrico, I.; Malausa, T.; Reboud, X.; Huyghe, C. Pesticide-Free Agriculture as a New Paradigm for Research. *Agronomy for Sustainable Development* **2022**, 42, 8, doi:10.1007/s13593-021-00742-8.
184. García-Reyes, J.F.; Jackson, A.U.; Molina-Díaz, A.; Cooks, R.G. Desorption Electrospray Ionization Mass Spectrometry for Trace Analysis of Agrochemicals in Food. *Analytical Chemistry* **2009**, 81, 820–829, doi:10.1021/ac802166v.
185. Gerbig, S.; Stern, G.; Brunn, H.E.; Düring, R.-A.; Spengler, B.; Schulz, S. Method Development towards Qualitative and Semi-Quantitative Analysis of Multiple Pesticides from Food Surfaces and Extracts by Desorption Electrospray Ionization Mass Spectrometry as a Preselective Tool for Food Control. *Analytical and Bioanalytical Chemistry* **2017**, 409, 2107–2117, doi:10.1007/s00216-016-0157-x.
186. Berchtold, C.; Müller, V.; Meier, L.; Schmid, S.; Zenobi, R. Direct Detection of Chlorpropham on Potato Skin Using Desorption Electrospray Ionization. *Journal of Mass Spectrometry* **2013**, 48, 587–593, doi:10.1002/jms.3197.
187. Mainero Rocca, L.; Cecca, J.; L'Episcopo, N.; Fabrizi, G. Ambient Mass Spectrometry: Direct Analysis of Dimethoate, Tebuconazole, and Trifloxystrobin on Olive and Vine Leaves by Desorption Electrospray Ionization Interface. *Journal of Mass Spectrometry* **2017**, 52, 709–719, doi:10.1002/jms.3978.

188. Takáts, Z.; Wiseman, J.M.; Cooks, R.G. Ambient Mass Spectrometry Using Desorption Electrospray Ionization (DESI): Instrumentation, Mechanisms and Applications in Forensics, Chemistry, and Biology. *Journal of Mass Spectrometry* **2005**, *40*, 1261–1275, doi:10.1002/jms.922.
189. Zhang, X.-Z.; Li, C.-J.; Chen, S.-S.; Li, X.-J.; Han, H.; Ma, X.-D. Direct Determination of Atrazine Residue on Chinese Cabbage Leaf Using Desorption Electrospray Ionization-Tandem Mass Spectrometry and Its Application for Diagnosing Atrazine Drift Phytotoxicity. *Journal of AOAC International* **2009**, *92*, 1587–1592, doi:10.1093/jaoac/92.5.1587.
190. Pereira, I.; Rodrigues, S.R.M.; de Carvalho, T.C.; Carvalho, V. V.; Lobón, G.S.; Bassane, J.F.P.; Domingos, E.; Romão, W.; Augusti, R.; Vaz, B.G. Rapid Screening of Agrochemicals by Paper Spray Ionization and Leaf Spray Mass Spectrometry: Which Technique Is More Appropriate? *Analytical Methods* **2016**, *8*, 6023–6029, doi:10.1039/C6AY01154C.
191. Reeber, S.L.; Gadi, S.; Huang, S.-B.; Glish, G.L. Direct Analysis of Herbicides by Paper Spray Ionization Mass Spectrometry. *Analytical Methods* **2015**, *7*, 9808–9816, doi:10.1039/C5AY02125A.
192. Moura, A.C.M.; Lago, I.N.; Cardoso, C.F.; dos Reis Nascimento, A.; Pereira, I.; Vaz, B.G. Rapid Monitoring of Pesticides in Tomatoes (*Solanum Lycopersicum* L.) during Pre-Harvest Intervals by Paper Spray Ionization Mass Spectrometry. *Food Chemistry* **2020**, *310*, 125938, doi:10.1016/j.foodchem.2019.125938.
193. Liu, J.; Wang, H.; Manicke, N.E.; Lin, J.-M.; Cooks, R.G.; Ouyang, Z. Development, Characterization, and Application of Paper Spray Ionization. *Analytical Chemistry* **2010**, *82*, 2463–2471, doi:10.1021/ac902854g.
194. Soparawalla, S.; Tadjimukhamedov, F.K.; Wiley, J.S.; Ouyang, Z.; Cooks, R.G. In Situ Analysis of Agrochemical Residues on Fruit Using Ambient Ionization on a Handheld Mass Spectrometer. *Analyst* **2011**, *136*, 4392, doi:10.1039/c1an15493a.
195. Evard, H.; Krueve, A.; Löhmus, R.; Leito, I. Paper Spray Ionization Mass Spectrometry: Study of a Method for Fast-Screening Analysis of Pesticides in Fruits and Vegetables. *Journal of Food Composition and Analysis* **2015**, *41*, 221–225, doi:10.1016/j.jfca.2015.01.010.
196. Wang, Q.; Zheng, Y.; Zhang, X.; Han, X.; Wang, T.; Zhang, Z. A Silica Coated Paper Substrate: Development and Its Application in Paper Spray Mass Spectrometry for Rapid Analysis of Pesticides in Milk. *Analyst* **2015**, *140*, 8048–8056, doi:10.1039/C5AN01823D.



- 
197. Pu, F.; Zhang, W.; Han, C.; Ouyang, Z. Fast Quantitation of Pyrazole Fungicides in Wine by Ambient Ionization Mass Spectrometry. *Analytical Methods* **2017**, *9*, 5058–5064, doi:10.1039/C7AY01534H.
198. Malaj, N.; Ouyang, Z.; Sindona, G.; Cooks, R.G. Analysis of Pesticide Residues by Leaf Spray Mass Spectrometry. *Analytical Methods* **2012**, *4*, 1913, doi:10.1039/c2ay25222h.
199. Pereira, I.; Rodrigues, S.R.M.; de Carvalho, T.C.; Carvalho, V. V.; Lobón, G.S.; Bassane, J.F.P.; Domingos, E.; Romão, W.; Augusti, R.; Vaz, B.G. Rapid Screening of Agrochemicals by Paper Spray Ionization and Leaf Spray Mass Spectrometry: Which Technique Is More Appropriate? *Analytical Methods* **2016**, *8*, 6023–6029, doi:10.1039/C6AY01154C.
200. Jarmusch, A.K.; Pirro, V.; Kerian, K.S.; Cooks, R.G. Detection of Strep Throat Causing Bacterium Directly from Medical Swabs by Touch Spray-Mass Spectrometry. *Analyst* **2014**, *139*, 4785–4789, doi:10.1039/C4AN00959B.
201. Yang, B.; Wang, F.; Yang, X.; Zou, W.; Wang, J.; Zou, Y.; Liu, F.; Liu, H.; Huang, O. Medical Swab Touch Spray-Mass Spectrometry for Newborn Screening of Nicotine and Cotinine in Meconium. *Journal of Mass Spectrometry* **2016**, *51*, 1237–1242, doi:10.1002/jms.3892.
202. Fedick, P.W.; Bain, R.M. Swab Touch Spray Mass Spectrometry for Rapid Analysis of Organic Gunshot Residue from Human Hand and Various Surfaces Using Commercial and Fieldable Mass Spectrometry Systems. *Forensic Chemistry* **2017**, *5*, 53–57, doi:10.1016/j.forc.2017.06.005.
203. Pirro, V.; Llor, R.S.; Jarmusch, A.K.; Alfaro, C.M.; Cohen-Gadol, A.A.; Hattab, E.M.; Cooks, R.G. Analysis of Human Gliomas by Swab Touch Spray-Mass Spectrometry: Applications to Intraoperative Assessment of Surgical Margins and Presence of Oncometabolites. *Analyst* **2017**, *142*, 4058–4066, doi:10.1039/C7AN01334E.
204. Bain, R.M.; Fedick, P.W.; Dilger, J.M.; Cooks, R.G. Analysis of Residual Explosives by Swab Touch Spray Ionization Mass Spectrometry. *Propellants, Explosives, Pyrotechnics* **2018**, *43*, 1139–1144, doi:10.1002/prop.201800122.
205. Jarmusch, A.K.; Pirro, V.; Logsdon, D.L.; Cooks, R.G. Direct Ion Generation from Swabs. *Talanta* **2018**, *184*, 356–363, doi:10.1016/j.talanta.2018.02.105.
206. Morato, N.M.; Pirro, V.; Fedick, P.W.; Cooks, R.G. Quantitative Swab Touch Spray Mass Spectrometry for Oral Fluid Drug Testing. *Analytical Chemistry* **2019**, *91*, 7450–7457, doi:10.1021/acs.analchem.9b01637.
-

207. PhD Thesis of Fedick, P.W. Ambient Ionization Mass Spectrometry: Advances in Monitoring Clandestine Activities, Supporting the Warfighter, and Chemical Laboratory Education Redevelopment., Purdue University Graduate School, 2019.
208. Costa, C.; van Es, E.M.; Sears, P.; Bunch, J.; Palitsin, V.; Cooper, H.; Bailey, M.J. Exploring a Route to a Selective and Sensitive Portable System for Explosive Detection– Swab Spray Ionisation Coupled to of High-Field Assisted Waveform Ion Mobility Spectrometry (FAIMS). *Forensic Science International* **2019**, *1*, 214–220, doi:10.1016/j.fsisyn.2019.07.009.
209. Muggli, T.M.; Schürch, S. Influence of Solvent Relative Permittivity in Swab Spray Mass Spectrometry. *Molecules* **2024**, *29*, 4274, doi:10.3390/molecules29174274.
210. Pape, J.; Vikse, K.L.; Janusson, E.; Taylor, N.; McIndoe, J.S. Solvent Effects on Surface Activity of Aggregate Ions in Electrospray Ionization. *International Journal of Mass Spectrometry* **2014**, *373*, 66–71, doi:10.1016/j.ijms.2014.09.009.
211. Li, L.; Li, W.; Hu, B. Electrostatic Field-Induced Tip-electrospray Ionization Mass Spectrometry for Direct Analysis of Raw Food Materials. *Journal of Mass Spectrometry* **2019**, *54*, 73–80, doi:10.1002/jms.4309.
212. Thinius, M.; Polaczek, C.; Langner, M.; Bräkling, S.; Haack, A.; Kersten, H.; Benter, T. Charge Retention/Charge Depletion in ESI-MS: Experimental Evidence. *Journal of the American Society for Mass Spectrometry* **2020**, *31*, 773–784, doi:10.1021/jasms.9b00044.
213. Liigand, J.; Kruve, A.; Liigand, P.; Laaniste, A.; Girod, M.; Antoine, R.; Leito, I. Transferability of the Electrospray Ionization Efficiency Scale between Different Instruments. *Journal of the American Society for Mass Spectrometry* **2015**, *26*, 1923–1930, doi:10.1007/s13361-015-1219-6.
214. Liigand, J.; Laaniste, A.; Kruve, A. PH Effects on Electrospray Ionization Efficiency. *Journal of the American Society for Mass Spectrometry* **2017**, *28*, 461–469, doi:10.1007/s13361-016-1563-1.
215. Oss, M.; Kruve, A.; Herodes, K.; Leito, I. Electrospray Ionization Efficiency Scale of Organic Compounds. *Analytical Chemistry* **2010**, *82*, 2865–2872, doi:10.1021/ac902856t.
216. Kiontke, A.; Oliveira-Birkmeier, A.; Opitz, A.; Birkemeyer, C. Electrospray Ionization Efficiency Is Dependent on Different Molecular Descriptors with Respect to Solvent PH and Instrumental Configuration. *PLoS One* **2016**, *11*, e0167502, doi:10.1371/journal.pone.0167502.

- 
217. Kageyama (Kaneshima), A.; Motoyama, A.; Takayama, M. Influence of Solvent Composition and Surface Tension on the Signal Intensity of Amino Acids in Electrospray Ionization Mass Spectrometry. *Mass Spectrometry* **2019**, *8*, A0077–A0077, doi:10.5702/massspectrometry.A0077.
218. Bieber, S.; Letzel, T.; Kruve, A. Electrospray Ionization Efficiency Predictions and Analytical Standard Free Quantification for SFC/ESI/HRMS. *Journal of the American Society for Mass Spectrometry* **2023**, *34*, 1511–1518, doi:10.1021/jasms.3c00156.
219. Liigand, P.; Liigand, J.; Kaupmees, K.; Kruve, A. 30 Years of Research on ESI/MS Response: Trends, Contradictions and Applications. *Analytica Chimica Acta* **2021**, *1152*, 238117, doi:10.1016/j.aca.2020.11.049.
220. Lopez-Hilfiker, F.D.; Pospisilova, V.; Huang, W.; Kalberer, M.; Mohr, C.; Stefenelli, G.; Thornton, J.A.; Baltensperger, U.; Prevot, A.S.H.; Slowik, J.G. An Extractive Electrospray Ionization Time-of-Flight Mass Spectrometer (EESI-TOF) for Online Measurement of Atmospheric Aerosol Particles. *Atmospheric Measurement Techniques* **2019**, *12*, 4867–4886, doi:10.5194/amt-12-4867-2019.
221. Schmidt, A.; Karas, M.; Dülcks, T. Effect of Different Solution Flow Rates on Analyte Ion Signals in Nano-ESI MS, or: When Does ESI Turn into Nano-ESI? *Journal of the American Society for Mass Spectrometry* **2003**, *14*, 492–500, doi:10.1016/S1044-0305(03)00128-4.
222. Jiang, C.; Li, X.J.; Wang, Y.R.; Ma, L.Y.; Wang, Y.K.; Lu, Y.C.; Yang, H. Assessment of Photodegradation of Herbicide Prometryn in Soil. *Water, Air, & Soil Pollution* **2017**, *228*, 135, doi:10.1007/s11270-017-3307-7.
223. Busman, M.; Sunner, J.; Vogel, C.R. Space-Charge-Dominated Mass Spectrometry Ion Sources: Modeling and Sensitivity. *Journal of the American Society for Mass Spectrometry* **1991**, *2*, 1–10, doi:10.1016/1044-0305(91)80055-C.
224. Marsh, B.M.; Rahman, S.; Benkowski, V.M.; Tichy, S.; Cooks, R.G. Space Charge Compensation in Air by Counterion Flow in 3D Printed Electrode Structure. *International Journal of Mass Spectrometry* **2021**, *468*, 116637, doi:10.1016/j.ijms.2021.116637.
225. Tang, K.; Page, J.S.; Smith, R.D. Charge Competition and the Linear Dynamic Range of Detection in Electrospray Ionization Mass Spectrometry. *Journal of the American Society for Mass Spectrometry* **2004**, *15*, 1416–1423, doi:10.1016/j.jasms.2004.04.034.
226. Thompson, J.W.; Eschelbach, J.W.; Wilburn, R.T.; Jorgenson, J.W. Investigation of Electrospray Ionization and Electrostatic Focusing Devices Using a Three-
-

- Dimensional Electrospray Current Density Profiler. *Journal of the American Society for Mass Spectrometry* **2005**, *16*, 312–323, doi:10.1016/j.jasms.2004.11.012.
227. Bythell, B.J.; Suhai, S.; Somogyi, Á.; Paizs, B. Proton-Driven Amide Bond-Cleavage Pathways of Gas-Phase Peptide Ions Lacking Mobile Protons. *Journal of the American Chemical Society* **2009**, *131*, 14057–14065, doi:10.1021/ja903883z.
228. Fokoue, H.H.; Marques, J. V.; Correia, M. V.; Yamaguchi, L.F.; Qu, X.; Aires-de-Sousa, J.; Scotti, M.T.; Lopes, N.P.; Kato, M.J. Fragmentation Pattern of Amides by EI and HRESI: Study of Protonation Sites Using DFT-3LYP Data. *RSC Advances* **2018**, *8*, 21407–21413, doi:10.1039/C7RA00408G.
229. Sun, M.; Dai, W.; Liu, D.Q. Fragmentation of Aromatic Sulfonamides in Electrospray Ionization Mass Spectrometry: Elimination of SO<sub>2</sub> via Rearrangement. *Journal of Mass Spectrometry* **2008**, *43*, 383–393, doi:10.1002/jms.1335.
230. Schwarzenberg, A.; Ichou, F.; Cole, R.B.; Machuron-Mandard, X.; Junot, C.; Lesage, D.; Tabet, J. Identification Tree Based on Fragmentation Rules for Structure Elucidation of Organophosphorus Esters by Electrospray Mass Spectrometry. *Journal of Mass Spectrometry* **2013**, *48*, 576–586, doi:10.1002/jms.3180.
231. Available Online: [www.sciex.Com/Products/Spectral-Library/Pesticide-Libraries](http://www.sciex.Com/Products/Spectral-Library/Pesticide-Libraries) (Accessed: 18.02.2024).
232. Bonner, R.; Hopfgartner, G. SWATH Data Independent Acquisition Mass Spectrometry for Metabolomics. *TrAC Trends in Analytical Chemistry* **2019**, *120*, 115278, doi:10.1016/j.trac.2018.10.014.
233. Liu, Y.; Hüttenhain, R.; Surinova, S.; Gillet, L.C.; Mouritsen, J.; Brunner, R.; Navarro, P.; Aebersold, R. Quantitative Measurements of N-linked Glycoproteins in Human Plasma by SWATH-MS. *Proteomics* **2013**, *13*, 1247–1256, doi:10.1002/pmic.201200417.
234. Lozano, A.; Ferrer, C.; Fernández-Alba, A.R. Selectivity Enhancement Using Sequential Mass Isolation Window Acquisition with Hybrid Quadrupole Time-of-Flight Mass Spectrometry for Pesticide Residues. *Journal of Chromatography A* **2019**, *1591*, 99–109, doi:10.1016/j.chroma.2019.01.019.
235. Klont, F.; Jahn, S.; Grivet, C.; König, S.; Bonner, R.; Hopfgartner, G. SWATH Data Independent Acquisition Mass Spectrometry for Screening of Xenobiotics in Biological Fluids: Opportunities and Challenges for Data Processing. *Talanta* **2020**, *211*, 120747, doi:10.1016/j.talanta.2020.120747.

- 
236. Wang, J.; Leung, D.; Chow, W.; Chang, J.; Wong, J.W. Target Screening of 105 Veterinary Drug Residues in Milk Using UHPLC/ESI Q-Orbitrap Multiplexing Data Independent Acquisition. *Analytical and Bioanalytical Chemistry* **2018**, *410*, 5373–5389, doi:10.1007/s00216-017-0847-z.
237. Wang, J.; Chow, W.; Chang, J.; Wong, J.W. Development and Validation of a Qualitative Method for Target Screening of 448 Pesticide Residues in Fruits and Vegetables Using UHPLC/ESI Q-Orbitrap Based on Data-Independent Acquisition and Compound Database. *Journal of Agricultural and Food Chemistry* **2017**, *65*, 473–493, doi:10.1021/acs.jafc.6b05034.
238. Wang, J.; Chow, W.; Wong, J.W.; Leung, D.; Chang, J.; Li, M. Non-Target Data Acquisition for Target Analysis (NDATA) of 845 Pesticide Residues in Fruits and Vegetables Using UHPLC/ESI Q-Orbitrap. *Analytical and Bioanalytical Chemistry* **2019**, *411*, 1421–1431, doi:10.1007/s00216-019-01581-z.
239. Zomer, P.; Mol, H.G.J. Simultaneous Quantitative Determination, Identification and Qualitative Screening of Pesticides in Fruits and Vegetables Using LC-Q-Orbitrap™-MS. *Food Additives & Contaminants: Part A* **2015**, *32*, 1628–1636, doi:10.1080/19440049.2015.1085652.
240. Krueve, A.; Kaupmees, K.; Liigand, J.; Oss, M.; Leito, I. Sodium Adduct Formation Efficiency in ESI Source. *Journal of Mass Spectrometry* **2013**, *48*, 695–702, doi:10.1002/jms.3218.
241. Hua, Y.; Jenke, D. Increasing the Sensitivity of an LC-MS Method for Screening Material Extracts for Organic Extractables via Mobile Phase Optimization. *Journal of Chromatographic Science* **2012**, *50*, 213–227, doi:10.1093/chromsci/bmr049.
242. Konermann, L.; Liu, Z.; Haidar, Y.; Willans, M.J.; Bainbridge, N.A. On the Chemistry of Aqueous Ammonium Acetate Droplets during Native Electrospray Ionization Mass Spectrometry. *Analytical Chemistry* **2023**, *95*, 13957–13966, doi:10.1021/acs.analchem.3c02546.
243. Wang, L.; Chen, L.; Yao, Y.; Shen, H.; Xu, Y. A Mechanism Study on the (+)-ESI-TOF/HRMS Fragmentation of Some PPI Prazoles and Their Related Substances. *Molecules* **2023**, *28*, 5852, doi:10.3390/molecules28155852.
244. Swale, D.R.; Bloomquist, J.R. Is DEET a Dangerous Neurotoxicant? *Pest Management Science* **2019**, *75*, 2068–2070, doi:10.1002/ps.5476.
245. DeGennaro, M. The Mysterious Multi-Modal Repellency of DEET. *Fly (Austin)* **2015**, *9*, 45–51, doi:10.1080/19336934.2015.1079360.
-

246. Weyermann, C.; Marquis, R.; Mazzella, W.; Spengler, B. Differentiation of Blue Ballpoint Pen Inks by Laser Desorption Ionization Mass Spectrometry and High-Performance Thin-Layer Chromatography. *Journal of Forensic Sciences* **2007**, *52*, 216–220, doi:10.1111/j.1556-4029.2006.00303.x.
247. Gallidabino, M.; Weyermann, C.; Marquis, R. Differentiation of Blue Ballpoint Pen Inks by Positive and Negative Mode LDI-MS. *Forensic Science International* **2011**, *204*, 169–178, doi:10.1016/j.forsciint.2010.05.027.
248. Peters, J.; Grotemeyer, J. Fragmentation of Xanthene Dyes by Laser Activation and Collision-induced Dissociation on a High-resolution Fourier Transform Ion Cyclotron Resonance Mass Spectrometer. *Rapid Communications in Mass Spectrometry* **2011**, *25*, 1169–1172, doi:10.1002/rcm.4972.
249. Cox, J.T.; Marginean, I.; Smith, R.D.; Tang, K. On the Ionization and Ion Transmission Efficiencies of Different ESI-MS Interfaces. *Journal of the American Society for Mass Spectrometry* **2015**, *26*, 55–62, doi:10.1007/s13361-014-0998-5.
250. Page, J.S.; Kelly, R.T.; Tang, K.; Smith, R.D. Ionization and Transmission Efficiency in an Electrospray Ionization—Mass Spectrometry Interface. *Journal of the American Society for Mass Spectrometry* **2007**, *18*, 1582–1590, doi:10.1016/j.jasms.2007.05.018.
251. Yan, Y.; Schmitt, L.; Khramchenkova, A.; Lengyel, J. Ion Transmission in an Electrospray Ionization-mass Spectrometry Interface Using an S-lens. *Journal of Mass Spectrometry* **2023**, *58*, doi:10.1002/jms.4955.
252. Chua, Z.Q.; Prabhu, G.R.D.; Wang, Y.-W.; Raju, C.M.; Buchowiecki, K.; Ochirov, O.; Elpa, D.P.; Urban, P.L. Moderate Signal Enhancement in Electrospray Ionization Mass Spectrometry by Focusing Electrospray Plume with a Dielectric Layer around the Mass Spectrometer's Orifice. *Molecules* **2024**, *29*, 316, doi:10.3390/molecules29020316.
253. Sun, Y.; Song, Y.; Long, M.; Yang, S. Immunotoxicity of Three Environmental Mycotoxins and Their Risks of Increasing Pathogen Infections. *Toxins (Basel)* **2023**, *15*, 187, doi:10.3390/toxins15030187.
254. Paterson, R.R.M.; Lima, N. Toxicology of Mycotoxins. In; 2010; pp. 31–63.
255. Skrzydlewski, P.; Twarużek, M.; Grajewski, J. Cytotoxicity of Mycotoxins and Their Combinations on Different Cell Lines: A Review. *Toxins (Basel)* **2022**, *14*, 244, doi:10.3390/toxins14040244.
256. Ülger, T.G.; Uçar, A.; Çakıroğlu, F.P.; Yilmaz, S. Genotoxic Effects of Mycotoxins. *Toxicon* **2020**, *185*, 104–113, doi:10.1016/j.toxicon.2020.07.004.

- 
257. Perincherry, L.; Lalak-Kańczugowska, J.; Stępień, Ł. Fusarium-Produced Mycotoxins in Plant-Pathogen Interactions. *Toxins (Basel)* **2019**, *11*, 664, doi:10.3390/toxins11110664.
258. Santos Pereira, C.; C. Cunha, S.; Fernandes, J.O. Prevalent Mycotoxins in Animal Feed: Occurrence and Analytical Methods. *Toxins (Basel)* **2019**, *11*, 290, doi:10.3390/toxins11050290.
259. Pleadin, J.; Frece, J.; Markov, K. Mycotoxins in Food and Feed. In; 2019; pp. 297–345.
260. Alshannaq, A.; Yu, J.-H. Occurrence, Toxicity, and Analysis of Major Mycotoxins in Food. *International Journal of Environmental Research and Public Health* **2017**, *14*, 632, doi:10.3390/ijerph14060632.
261. Chen, M.; Liu, W.; Xiang, P.; Xu, L.; Tang, Y.; Kong, R.; Yang, S.; Yan, H.; Di, B. Development of an LC-MS/MS Method for the Determination of Multiple Mycotoxins in Human Urine. *Food Additives & Contaminants: Part A* **2023**, *40*, 917–927, doi:10.1080/19440049.2023.2222842.
262. Warth, B.; Sulyok, M.; Krska, R. LC-MS/MS-Based Multibiomarker Approaches for the Assessment of Human Exposure to Mycotoxins. *Analytical and Bioanalytical Chemistry* **2013**, *405*, 5687–5695, doi:10.1007/s00216-013-7011-1.
263. Xia, L.; Rasheed, H.; Routledge, M.N.; Wu, H.; Gong, Y.Y. Super-Sensitive LC-MS Analyses of Exposure Biomarkers for Multiple Mycotoxins in a Rural Pakistan Population. *Toxins (Basel)* **2022**, *14*, 193, doi:10.3390/toxins14030193.
264. Kappenberg, A.; Juraschek, L.M. Development of a LC-MS/MS Method for the Simultaneous Determination of the Mycotoxins Deoxynivalenol (DON) and Zearalenone (ZEA) in Soil Matrix. *Toxins (Basel)* **2021**, *13*, 470, doi:10.3390/toxins13070470.
265. Lauwers, M.; De Baere, S.; Letor, B.; Rychlik, M.; Croubels, S.; Devreese, M. Multi LC-MS/MS and LC-HRMS Methods for Determination of 24 Mycotoxins Including Major Phase I and II Biomarker Metabolites in Biological Matrices from Pigs and Broiler Chickens. *Toxins (Basel)* **2019**, *11*, 171, doi:10.3390/toxins11030171.
266. Gámiz-Gracia, L.; García-Campaña, A.M.; Arroyo-Manzanares, N. Application of LC-MS/MS in the Mycotoxins Studies. *Toxins (Basel)* **2020**, *12*, 272, doi:10.3390/toxins12040272.
267. Niknejad, F.; Escrivá, L.; Adel Rad, K.B.; Khoshnia, M.; Barba, F.J.; Berrada, H. Biomonitoring of Multiple Mycotoxins in Urine by GC-MS/MS: A Pilot Study
-

- on Patients with Esophageal Cancer in Golestan Province, Northeastern Iran. *Toxins (Basel)* **2021**, *13*, 243, doi:10.3390/toxins13040243.
268. Bloom, E.; Bal, K.; Nyman, E.; Larsson, L. Optimizing a GC-MS Method for Screening of Stachybotrysmycotoxins in Indoor Environments. *Journal of Environmental Monitoring* **2007**, *9*, 151–156, doi:10.1039/B613853E.
269. Rodríguez-Carrasco, Y.; Moltó, J.C.; Mañes, J.; Berrada, H. Development of a GC–MS/MS Strategy to Determine 15 Mycotoxins and Metabolites in Human Urine. *Talanta* **2014**, *128*, 125–131, doi:10.1016/j.talanta.2014.04.072.
270. Rodríguez-Carrasco, Y.; Moltó, J.C.; Mañes, J.; Berrada, H. Development of Microextraction Techniques in Combination with GC-MS/MS for the Determination of Mycotoxins and Metabolites in Human Urine. *Journal of Separation Science* **2017**, *40*, 1572–1582, doi:10.1002/jssc.201601131.
271. da Silva Lima, G.; Franco dos Santos, G.; Ramalho, R.R.F.; de Aguiar, D.V.A.; Roque, J.V.; Maciel, L.I.L.; Simas, R.C.; Pereira, I.; Vaz, B.G. Laser Ablation Electrospray Ionization Mass Spectrometry Imaging as a New Tool for Accessing Patulin Diffusion in Mold-Infected Fruits. *Food Chemistry* **2022**, *373*, 131490, doi:10.1016/j.foodchem.2021.131490.
272. Maragos, C.M. Application of Ambient Ionization Mass Spectrometry to Detect the Mycotoxin Roquefortine C in Blue Cheese. *Food Analytical Methods* **2022**, *15*, 751–760, doi:10.1007/s12161-021-02165-3.
273. Maragos, C.M. Detection of T-2 Toxin in Wheat and Maize with a Portable Mass Spectrometer. *Toxins (Basel)* **2023**, *15*, 222, doi:10.3390/toxins15030222.
274. Vaclavik, L.; Zachariasova, M.; Hrbek, V.; Hajslova, J. Analysis of Multiple Mycotoxins in Cereals under Ambient Conditions Using Direct Analysis in Real Time (DART) Ionization Coupled to High Resolution Mass Spectrometry. *Talanta* **2010**, *82*, 1950–1957, doi:10.1016/j.talanta.2010.08.029.
275. Maragos, C.M.; Busman, M. Rapid and Advanced Tools for Mycotoxin Analysis: A Review. *Food Additives & Contaminants: Part A* **2010**, *27*, 688–700, doi:10.1080/19440040903515934.
276. Busman, M. Quantitation of Mycotoxins Using Direct Analysis in Real Time Mass Spectrometry (DART-MS). *Journal of AOAC International* **2018**, *101*, 643–646, doi:10.5740/jaoacint.17-0338.
277. Nielsen, K. Fungal Metabolite Screening: Database of 474 Mycotoxins and Fungal Metabolites for Dereplication by Standardised Liquid Chromatography–UV–Mass Spectrometry Methodology. *Journal of Chromatography A* **2003**, *1002*, 111–136, doi:10.1016/S0021-9673(03)00490-4.



278. Available Online: [www.Tools.Thermofisher.Com/Content/Sfs/Manuals/Man-125-0580-LTQ-Orbitrap-Velos-Hardware-Man1250580-A-EN.Pdf](http://www.Tools.Thermofisher.Com/Content/Sfs/Manuals/Man-125-0580-LTQ-Orbitrap-Velos-Hardware-Man1250580-A-EN.Pdf) (Accessed: 28.09.2024).
279. Available Online: [www.Assets.Thermofisher.Com/TFS-Assets/CMD/Specification-Sheets/PS-30223-LC-MS-Q-Exactive-Orbitrap-PS30223-EN.Pdf](http://www.Assets.Thermofisher.Com/TFS-Assets/CMD/Specification-Sheets/PS-30223-LC-MS-Q-Exactive-Orbitrap-PS30223-EN.Pdf) (Accessed: 20.09.2024).
280. Available Online: [www.Tools.Thermofisher.Com/Content/Sfs/Brochures/PSB-127-Dual-Pressure-Linear-Ion-Trap-Technology.Pdf](http://www.Tools.Thermofisher.Com/Content/Sfs/Brochures/PSB-127-Dual-Pressure-Linear-Ion-Trap-Technology.Pdf) (Accessed: 25.09.2024).